

VIDEO TECHNIQUES IN THE FEEDBACK CONTROL
OF AN ELECTROMECHANICAL CONTINUUM

by

JOHN LAWRENCE DRESSLER

S.B., Massachusetts Institute of Technology
(1964)

S.M., Massachusetts Institute of Technology
(1966)

E.E., Massachusetts Institute of Technology
(1967)

SUBMITTED IN PARTIAL FULFILLMENT OF THE
REQUIREMENTS FOR THE DEGREE OF
DOCTOR OF SCIENCE

at the

MASSACHUSETTS INSTITUTE OF TECHNOLOGY

August, 1971 (i.e. Feb 1972)

Signature of Author --

Department of Electrical Engineering, September

Certified by

Thesis Supervisor

Accepted by

Chairman, Departmental Committee on Graduate Students



VIDEO TECHNIQUES IN THE FEEDBACK CONTROL
OF AN ELECTROMECHANICAL CONTINUUM

by

John Lawrence Dressler

Submitted to the Department of Electrical Engineering
on September 3, 1971, in partial fulfillment of
the requirements for the degree of Doctor of Science

ABSTRACT

The feedback control of continuum systems with dimensions large compared to potentially unstable wavelengths requires a large number of spatially distributed feedback sensors and drivers. The multiplicity of signals to be amplified and processed suggests the use of computers or other discrete time devices which handle signals on a "time-sharing" basis. Typically, scanning techniques are envisioned to sense and drive, thus introducing to an analytical representation discreteness in both time and space. A general method, based on the Fourier superposition of wavetrains, is developed to describe infinite continuum systems with discrete spatial and temporal feedback. Dynamics are represented by a generalization of the dispersion equation, with Z transforms used to provide closed-form expressions if the discreteness is in space or in time only. The Bers-Briggs criterion is generalized to differentiate between absolute instabilities and amplifying waves with the discrete feedback.

The quasi-one-dimensional model used to illustrate analytical techniques represents typical systems found using electron beams and plasmas, particularly the dynamics of the Z - θ hydromagnetic pinch. An experiment is used to demonstrate temporally and spatially discrete feedback control of the Rayleigh-Taylor instability.

THIS IS SUPERVISOR:....James.R..Melcher.....

TITLE: Professor of Electrical Engineering

Acknowledgement

I would like to express my gratitude to Professor James R. Melcher for his guidance and encouragement throughout this thesis. It would have been impossible without his advice and suggestions. Thanks are also due to Professors Gerald L. Wilson and Richard J. Briggs, each of whom provided active interest, many helpful suggestions, and was available for consultations. Construction of the cathode ray tube was overseen by Professor Charles K. Crawford, and the vacuum system was built with the help of Professor Charles R. Hendricks.

Thanks go to the U.S. Atomic Energy Commission for financial assistance throughout the doctoral program, and to Mr. Harold Atlas for his aid in constructing the experimental apparatus. Mrs. E. M. Holmes is to be commended for her diligence in typing. Mr. Robert F. Perret ably taught me the rewards of honesty and hard work.

TABLE OF CONTENTS

	<u>Page No.</u>
ABSTRACT	2
ACKNOWLEDGEMENTS	3
LIST OF FIGURES	10
CHAPTER I. INTRODUCTION	17
1.1 Background and Scope	17
1.2 Review of Previous Work	19
1.3 Overview	23
The Electrically Stressed String	28
The Fourier-Laplace Transform	32
Outline	33
CHAPTER II. TEMPORALLY SAMPLED FEEDBACK	36
2.1 Introduction	36
2.2 Description of the System	37
2.3 Transforms of Temporally Sampled Signals	41
Detection Scheme: Temporal Sampling	41
Single-Sided Z Transforms	43
Inverse Z Transform: Laurent Expansion	48
Inverse Z Transform: Complex Integral Formula	49
2.4 Open-Loop Discrete Temporal Transfer Function	50
Sample-and-Hold Filter	50
Sampled Transfer Functions	50

TABLE OF CONTENTS (Continued)

2.5	Closed-Loop System	58
	Transfer Function with Feedback	58
	Z-K Closed-Loop Dispersion Equation	58
	Stability Criterion	60
	An Upper Bound on Gain	61
	Results of the Stability Analysis	62
2.6	Summary	64
CHAPTER III.	DISCRETE SPATIAL FEEDBACK FOR AN INFINITE SYSTEM	66
3.1	Introduction	66
3.2	Description of the System	67
3.3	Transforms of Spatially Sampled Signals	71
	Detection Scheme: Spatial Sampling	71
	Double-Sided Z Transforms: D Transforms	72
	Equivalence of Double-and Single-Sided Transforms	79
	Inverse D Transforms	82
	Ambiguity of Inverse D Transforms	84
3.4	Open-Loop Transfer Function	84
	The Electrode as a Spatial Sample-and-Hold Filter	84
	Transfer Function of a Spatially Discrete System	85
	Evaluation of Open-Loop Transfer Function	90
3.5	Closed-Loop System	94
	Closed-Loop Transfer Function	94
	D-S Dispersion Relation	94
	Comparison of Z Transforms and Wave-train Analysis	96
	Stability Criterion for the S-D Dispersion Equation	102
	Results of Stability Analysis	103

TABLE OF CONTENTS (Continued)

3.6	Summary	108
CHAPTER IV.	SPATIALLY-SAMPLED SYSTEM WITH BOUNDARIES	109
4.1	Introduction	109
4.2	Generation of Closed-Loop Modes for a System Described by a Matrix	110
4.3	Generation of Closed-Loop Modes from Open- Loop Modes	115
	Normal Mode Description of the Finite String	116
	Closed-Loop Transfer Functions	118
4.4	Generation of Closed-Loop Modes from the Z Transform of the Unbounded System	124
	Boundaries Create Eigenvalues and Zeros	125
	Transfer Function of a Spatially-Continuous System with Longitudinal Boundaries	126
	Continuous Spatial Feedback for a Bounded System	129
	Transfer Function of a Spatially Discrete System with Boundaries	131
	Discrete Spatial Feedback for a Bounded System	136
4.5	Determination of the System Stability from the Closed-Loop Modes	142
4.6	Summary	144

TABLE OF CONTENTS (Continued)

CHAPTER V. CRITERIA FOR IDENTIFYING AMPLIFYING WAVES AND ABSOLUTE INSTABILITIES ON A SPATIALLY DISCRETE SYSTEM	146
5.1 Introduction	146
5.2 Stability Criterion for the Spatially-Sampled, Time-Independent System	150
5.3 Development of Modified Bers-Briggs Criteria for Spatially Sampled Systems	154
Green's Function Formalism	154
LaPlace Transform of the Response	157
Branch Lines of $\hat{\xi}(n,S)$	159
Analytical Continuation of $\hat{\xi}(n,S)$	160
Distinguishing Between Amplifying and Evanescent Waves	162
Branch Poles of $\hat{\xi}(n,S)$	165
Criterion for Determining the Presence of Absolute Instabilities	167
Criterion for Determining the Presence of a Convective-Absolute Instability	168
5.4 An Example: The Convecting String	172
The Stationary String: An Absolute Instability	176
A Resistive-Wall Interaction: Convective Instability	179
The Perpendicularly Stressed Water Jet: Convective Instability	180
The Perpendicularly Stressed Water Jet: Convective-Absolute Instability	186

TABLE OF CONTENTS (Continued)

5.5	Summary	189
CHAPTER VI. DISCRETE SPATIAL-DISCRETE TEMPORAL CONTINUUM		
	FEEDBACK	193
6.1	Introduction	193
6.2	Spatially and Temporally Sampled Signals	197
	Detection Scheme: Spatial and Temporal Sampling	197
	Transform of the Sampling Function	198
	Transform of the Space-and-Time-Sampled Deflection	202
6.3	The Open-Loop Transfer Function	205
	The Electrode as a Spatial and Temporal Sample-and-Hold Filter	205
	Transfer Function of a Spatially Discrete System	207
	Evaluation of the Spatially and Temporally Discrete Transfer Function	211
6.4	Closed-Loop System	213
	Closed-Loop Transfer Function	213
	The D-S and K-Z Dispersion Equations	215
	Stability Criterion	216
	Results of the Stability Analysis	217
6.5	Summary	224
CHAPTER VII EXPERIMENTS		
7.1	Introduction	227
7.2	Apparatus	228
	The Continuum Instability	228

TABLE OF CONTENTS (Continued)

The Cathode Ray Tube Amplifier and Switching Network	231
The Spatial Sampling System	235
The Synchronizing Network	237
7.3 Operation of the Apparatus	238
Experimental Results	238
Explanation of the Results	239
CHAPTER VIII SUMMARY AND SUGGESTIONS FOR FURTHER RESEARCH	244
8.1 Summary	244
8.2 Suggestions for Further Research	250
Removing the Long-Wave Limit	250
Average Deflection Feedback	253
Extension to Two-Dimensional Surfaces	255
Suggestions for Experimental Work	255
REFERENCES	258

LIST OF FIGURES

<u>Figure No.</u>	<u>Title</u>	<u>Page No.</u>
1.1	A continuum feedback control system where each segment is controlled by an independent feedback loop.	23
1.2	Disturbances with a wavelength equal to two sensor spacings cannot be detected.	24
1.3	A continuum feedback control system where one time-multiplexed amplifier controls each segment of the continuum.	26
1.4	The string is stretched along the x-axis between two electrodes at a bias potential of V_0 volts.	29
2.1	The driving voltage at a fixed point as a function of time.	39
2.2	The driving voltage as a function of x for several periods of time.	40
2.3	The time-sampled output is an array of impulse sheets.	42
2.4	The temporally sampled output is produced by multiplying the deflection by a spatial impulse train.	44
2.5	Contour integral for finding the transform of the sampled function.	46
2.6	The temporally discrete force is generated by driving a sample-and-hold filter with an impulse train.	51
2.7	The electrodes, string, and sensors are a system which accepts a time-sampled input and produces a time-sampled output.	53

List of Figures (continued)

2.8	Block diagram of the temporally discrete open-loop system.	54
2.9	Contour integral for finding the transfer function $G(K,Z)$.	56
2.10	Servo-loop representation of the temporally discrete system with feedback.	59
2.11	Conditions for stability of the string with discrete spatial feedback.	63
3.1	The unbounded electrically-stressed string, driven by a spatially discrete force.	68
3.2	The segmented electrode applies a spatially discrete voltage to the string.	70
3.3	The spatially-sampled output is produced by multiplying the deflection by a spatial impulse train.	73
3.4	Possible contours of integration for the transform of a spatially-sampled function.	77
3.5	The impulse train which produces the transform given in Eq. (3.24).	81
3.6	A spatial impulse is applied to the electrode segment to produce a spatially constant force.	86
3.7	The spatially discrete driving force is generated by driving the sample-and-hold filter by an impulse train.	87

List of Figures (continued)

- 3.8 The electrode segments, string, and sensors are a system which accepts a spatially-sampled input and produces a spatially sampled output. 88
- 3.9 The electrodes, string, and sensors can be represented by a discrete transfer function. 91
- 3.10 Possible contours of integration for finding $G_1(D,S)$. 93
- 3.11 Servo-loop representation of the spatially sampled string with feedback. 95
- 3.12 The servo-loop representation of the spatially discrete string which is obtained from the wave-train analysis. 101
- 3.13 A partial root-locus plot for the string with spatially discrete feedback and no damping. 104
- 3.14 A partial root-locus plot for the string with discrete spatial feedback and damping. The damping reduces the tendency for the string to become overstable. 105
- 3.15 The region of stable operation for the spatially discrete system as determined from the S-D dispersion equation. 106
- 4.1 A system which is spatially sampled in two locations and driven by two forcers can be represented by a system of two coupled inputs and outputs. 112
- 4.2 A cross-sectional view of the bounded string with a finite number of spatially discrete drivers. 117

List of Figures (continued)

- 4.3 The normal modes $\Xi_1, \Xi_3, \Xi_5, \Xi_7, \dots$ of the spatially continuous bounded string can be combined to generate one normal mode of the bounded string with two-station feedback. 120
- 4.4 The normal modes $\Xi_2, \Xi_6, \Xi_{10}, \dots$ of the spatially continuous bounded string can be combined to generate the second normal mode of the bounded string with two-station feedback. 121
- 4.5 The bounded string with spatially continuous feedback can be represented by an infinite number of servo loops. The transfer function in the servo loop is the transfer function of the infinite string evaluated at the eigenvalues k_n . 123
- 4.6 A cross-sectional view of the bounded string with two feedback electrodes. 132
- 4.7 The bounded string with spatially discrete feedback can be represented by a finite number of servo loops. The transfer function in the servo loop is the spatially discrete transfer function of the unbounded string evaluated at the eigenvalues D_p . 139

List of figures (continued)

- 5.1 The three types of instability that can be observed on a spatially discrete continuum system. 147
- 5.2 The region of conversion and the contours for inversion of the two discrete transforms. 152
- 5.3 The contour integral for finding the spatially discrete response, $\hat{\xi}(n,S)$, in the source-free region. 158
- 5.4 The mechanism for finding the branch lines of $\hat{\xi}(n,S)$. 159
- 5.5 The deformed contour used to find $\tilde{\xi}(n,S)$, the analytical continuation of $\hat{\xi}(n,S)$. 161
- 5.6 The method for distinguishing between amplifying and evanescent waves on a spatially discrete system. 163
- 5.7 Mechanism for finding the branch poles of $\tilde{\xi}(n,S)$. 166
- 5.8 The contour of integration for finding the time response when $\tilde{\xi}(n,S)$ has a branch pole. 167
- 5.9 The method for determining the existence of a convective-absolute instability. 169
- 5.10 The modified Bers-Briggs plot for the stationary string. The string is absolutely unstable for $6.0 < \omega_R < 6.5$. 177
- 5.11 The modified Bers-Briggs plot for convecting string with stationary damping. The string is convectively unstable. 181
- 5.12 The modified Bers-Briggs plot for the water jet with discrete spatial feedback. The jet is convectively unstable. 184

List of figures (continued)

- 5.13 A root-locus plot of S for the jet with D set to zero.
The jet has the convective absolute instability when the gain approaches 140. 190
- 5.14 A modified Bers-Briggs plot for the jet showing the existence of the convective absolute instability. 191
- 5.15 The regions of stable and unstable for the water jet as determined from the S - D dispersion equation. The types of instabilities are identified by using the modified Bers-Briggs criteria. 192
- 6.1 The string is driven by an electrode structure which produces a spatially and temporally discrete force. 195
- 6.2 The discrete temporal voltage supplied to a driving electrode. 196
- 6.3 The detected signal is produced by multiplying the continuous signal by an impulse array. 198
- 6.4 The electrode segment accepts an impulse at the sampling time and produces a constant force in both space and time. 206
- 6.5 The force applied to the string is produced by driving the spatial and temporal sample-and-hold filter with an impulse array. 208
- 6.6 The electrode segments, string, and sensors are a system which accepts a spatially and temporally sampled input and produces a spatially and temporally sampled output. 209

List of figures (continued)

6.7	A servo-loop representation of the string with spatially and temporally discrete feedback.	214
6.8	The region of stable operation for the spatially and temporally discrete system with a scanning length of one.	219
6.9	A stability plot for the spatially and temporally discrete system, showing the effect of increasing the sampling rate.	220
6.10	The region of stable operation for the spatially and temporally discrete system for a scanning length of two.	223
7.1	A breakdown drawing of the tank showing the strip electrodes which apply a spatially discrete voltage to the liquid-air interface.	230
7.2	A schematic drawing showing the connections of the CRT to the control electrodes and the level detectors.	232
7.3	The output of the level detector exhibits hysteresis.	236
7.4	The liquid surface goes unstable with the liquid falling under one electrode and rising under the remaining electrodes.	240
8.1	The discontinuity in the video signal determines the location of the liquid-air interface.	256

CHAPTER I

INTRODUCTION

1.1 Background and Scope

The waving of a flag in the breeze, the generating of waves on the ocean by the wind, the breaking up of a jet of water, and the falling of water from a glass turned upside down are all common examples of continuum instabilities. Many similar instabilities occur in the fields of boundary layers, thermonuclear machines, magnetohydrodynamic channel flows and levitation and orientation of liquids by magnetic or electric fields. Often, these instabilities are undesirable, and a means of eliminating them is needed.

One method of stabilizing a continuous medium is by coupling to a passive structure. One example of this method is to hold a piece of paper across the mouth of a glass of water. When the glass is inverted, the paper will be held in place by the ambient air pressure and the water will not fall from the glass. The paper, a passive medium, has coupled to the surface of the water and made it stable. A second example is the stabilization of the boundary layer of an object moving through water. Kramer and Benjamin have found that if the object is covered with an elastic covering, the disturbances in the boundary layer will be damped, and under certain conditions, the flow can remain laminar. The result is less drag as the object moves through the water.

A third example is the stabilization of a plasma by coupling the magnetic field to a conducting wall, and by coupling to the plasma surface by a passive network. The former is explained by Rose and Clark (pages

258-270) and the latter by Carlye.

For many situations, a suitable method of controlling instabilities by coupling to a passive continuum has not been found. The other possibility is that stability can be achieved by coupling to an active structure, that is, by the use of a continuum feedback control system. The continuum feedback control system must detect the disturbances on the continuous medium, and then apply the proper restoring force by drawing on "external" sources of energy.

A continuum control system adds another dimension to conventional control theory. In a conventional, or lumped-parameter control system, the variables are functions only of time. In the continuum, or distributed-parameter control system, the variables are functions of time and of one or more spatial parameters. The lumped-parameter control system must control perturbations only in time; the continuum feedback system must, ideally, control perturbations of variables at every point in space that the variable is defined.

Fortunately, it is not necessary to detect or to drive every point on a continuum in order to stabilize it. The experiment of placing a piece of paper over the mouth of a water glass can be repeated with a piece of screen substituted for the paper; the coupling of the screen to the liquid surface can be sufficient to stabilize that surface. This experiment illustrates the fact that it is possible to stabilize the entire surface by coupling to only certain points of the surface.

Because of the practical difficulties of developing a feedback control that couples to every point on the unstable surface, continuum

feedback control has developed on a discrete spatial basis. The active control systems that have been built have measured deflections only at discrete points, and have applied restoring forces to segments of the surface. This discrete spatial approach will be continued in this thesis, and the added complexity of discrete time control will be considered.

1.2 Review of Previous Work

Continuum feedback control has been developed to some degree in at least three areas. In industry, continuum control has been used to improve distillation tower operation and chemical and nuclear reactor operation. Continuum feedback control has also been used to stabilize electromechanical systems, such as liquids stressed by electric fields, and electron beams. The third area is the stabilization of a confined plasma for the purpose of power generation.

The use of continuum feedback control has been studied for the control of chemical processes by Gould, Desalu, Schlaepfer and Murry. The control of a nuclear reactor has been studied by Weiberg. This type of process is usually dominated by transport and diffusion.

Because of the boundary conditions which are imposed on the nuclear or chemical reactor by the influx and effluent, the mathematics of the process requires an infinite number of spatial eigenfunctions. The method used by Murry for the control of a reactor was to detect and to feed back only to a certain number of these spatial modes. The information from sensors was processed to find the amplitudes of these specific modes. The actuators were then driven in such a way that only the proper modes would be affected. The purpose of this work was to increase the damping of the most significant modes of the system so that disturbances

would damp faster. The problems that were analyzed are the inexact determination of the modes with a finite number of sensors and the ability to drive only specific modes. Desalu extended Murry's method, and generated the control function to maximize profit for a regenerative chemical process.

The problem of stabilizing a continuum electromechanical system with discrete spatial feedback has been analyzed by Melcher (1965, 1966), Crowley (1967), Jefferis, and others. Jefferis has analyzed the prevention of the buckling instability on an axially-compressed beam. Crowley has analyzed the control of a convective kink instability on a water jet that was stressed by an electric field. The deflection of the jet was sensed at discrete points in space and a restoring force applied to segments of the jet. This problem is of interest because the control system made possible the generation of absolute instabilities along with the natural convective instabilities of the system. Melcher has stabilized a conducting "membrane" stressed by an electric field and also a liquid surface stressed by an electric field. In both cases, stability was achieved by applying a constant force to segments of the liquid or membrane surface.

Recently, the efforts to generate power from a fusion reaction have generated interest in the area of continuum feedback control. The devices which have been built to contain a thermonuclear plasma have met with many instability problems. One group of these instabilities appears as fluid type motion of the plasma surface. A possible method of controlling such instabilities is to use a distributed feedback control system to couple to the plasma surface. If the proper electromechanical

interaction can be achieved, the disturbances on the plasma surface could be prevented from growing.

The use of continuum feedback control for stabilizing a plasma had been suggested by Melcher (1966). The idea did not receive much interest until Arsenin, Zilkov and Chuyanov succeeded in stabilizing fluid instabilities in a simple mirror machine. The success of their experiment led to attempts by Parker and Thomassen to achieve similar results. Parker and Thomassen found that they could couple to a certain unstable mode, but not all of the unstable modes. After these early efforts, many experiments were conducted to apply feedback to plasma instabilities. These experiments were reported at the Symposium on Feedback and Dynamic Control of Plasmas, at Princeton University.

In addition to the use of feedback to stabilize a continuum system, a large amount of work has been done to apply optimal control to distributed systems. A comprehensive list of papers, reports, and books which deal with this subject has been compiled by Robinson. The experiments done on the electromechanical continua and on the plasmas can be put into a class of control systems represented by Figure 1.1. The system being controlled is represented by the string stretched between two rigid supports. The string displacement is detected at discrete points and a feedback force applied to a segment of the surface. There is a separate feedback loop for each segment of the surface. This type of apparatus, therefore, uses one sensor for each feedback electrode.

This approach is different from the chemical reactor controls, where the output from all sensors is processed and the processor generates a signal for each actuator. The number of sensors and actuators used on a

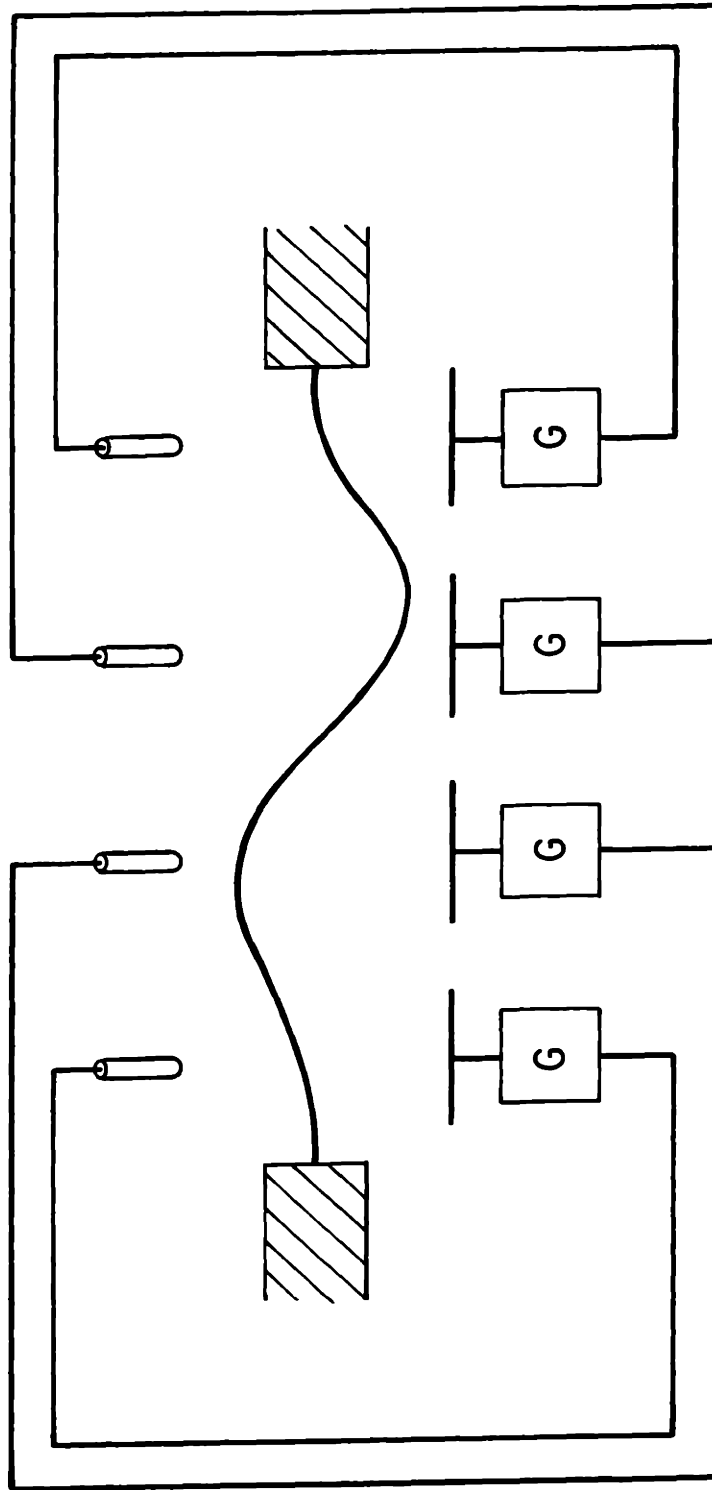


Figure 1.1.1 A continuum feedback control system where each segment of the continuum is controlled by an independent feedback loop.

chemical reactor are not necessarily equal.

The successes and failures of the experiments with plasma demonstrated a result that was obtained by Melcher (1966) in an earlier experiment. He found that the continuum system must be sampled in space at a spatial frequency at least twice that of the unstable waves. The feedback apparatus used by Melcher, or by the plasma experimenters, used sensors to measure periodically the disturbances on the continuum. If the distance between the sampling points is one half the wavelength of the disturbance, then this disturbance cannot be detected by the control system; this is illustrated by Figure 1.2.

The fact is, of course, a consequence of the sampling theorem, better known in the context of time functions. This theorem states that, in order to retain all of the original information of a signal after sampling, the sampling rate must be at least twice as fast as the highest frequency in the original signal. In continuum feedback schemes, only the information on the unstable wavelengths is of concern. Therefore, the spatial sampling must occur at least twice the spatial frequency of the unstable modes.

1.3 Overview

For many continuum systems, the extent of the volume to be controlled is large, and the wavelength of the instability is small. If one were trying to control the liquid coating applied to a sheet of paper in a modern paper coater, he would be controlling essentially a surface in a system ten feet wide, with an unstable (Taylor) wavelength of one-half inch. The limitations imposed by the sampling theorem would require an

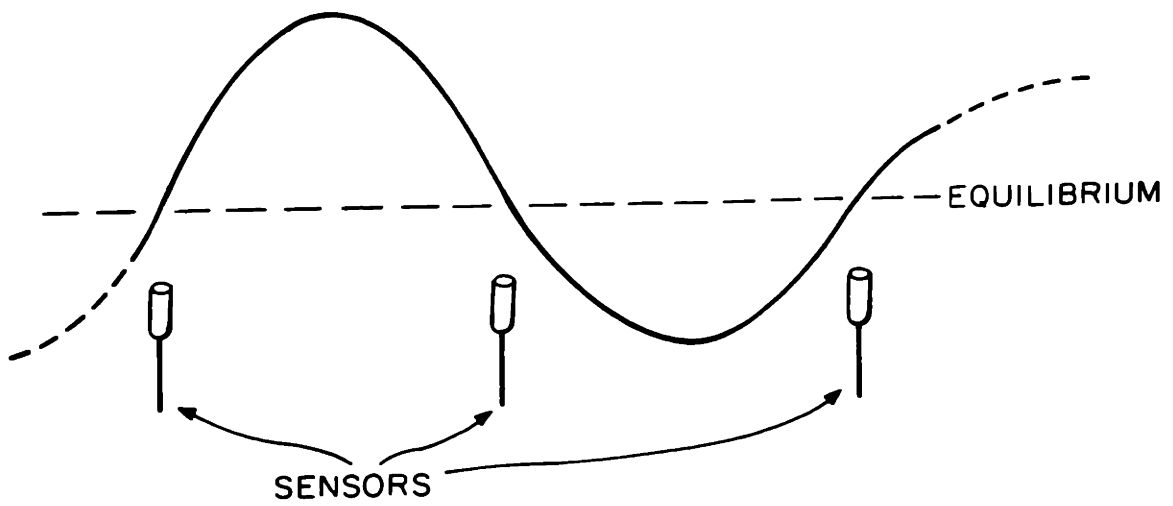


Figure 1.2 Disturbances with a wavelength of two sensor spacings cannot be detected.

array of 24,000 sensors and feedback actuators for each foot of length of the paper. If the control system were built to stabilize a large-scale thermonuclear reactor, a huge number of feedback loops might also be required. It is probably unrealistic to consider having thousands of individual feedback loops; the cost would be enormous and acceptable reliability would be hard to achieve. One method of eliminating some of the hardware requirements would be to use a time-multiplexing scheme, which is illustrated in Figure 1.3. In this system, one wideband feedback amplifier is used by all the feedback loops. The amplifier input is connected to one of the displacement detectors by the scanning system, and the amplifier is connected to proper feedback electrodes by the switching network. While the time-multiplexing will reduce the quantity of equipment needed, it complicates the theoretical prediction of the system dynamics. The equipment needed is also more complex, because a scanning and switching network are needed.

The analysis of a continuum system with discrete spatial and discrete temporal feedback has been done by Thomas. He has analyzed the control of a membrane stretched between two rigid supports and stressed on both sides by electrical fields. To describe the membrane deflections, Thomas used a normal mode expansion. Unfortunately, as the number of feedback stations increases, his method of analysis grows more complicated; for large systems, this method becomes unwieldy. The reason for this complexity is that, as the number of feedback stations increases, the number of normal modes necessary to describe the system also increases.

In his paper, Melcher (1966) shows that, as the number of stations is increased, the effect of the boundaries on the system becomes less

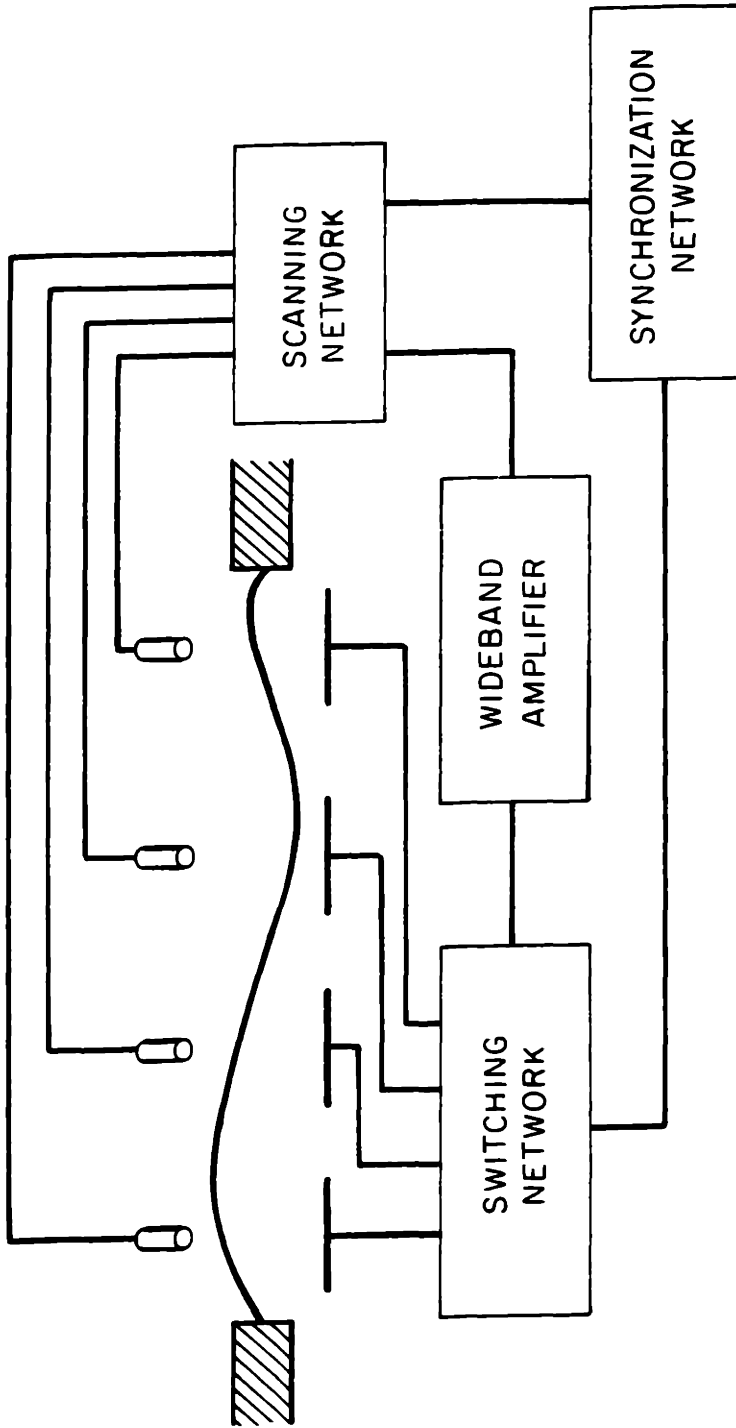


Figure 1.3 A continuum feedback control system where one time-multiplexed amplifier controls each segment of the continuum

important. He analyzed a continuous time system with normal modes and also with a Fourier-transform technique. The normal mode expansion included the effects of the boundaries, but the Fourier-transform analysis considered the system to be infinitely long, with no boundaries. The results of the analysis indicated that the boundaries may be ignored in estimating the limitations of the feedback after the number of feedback stations is four or more. Therefore, if a large system is to be analyzed, there is no need to use a normal mode expansion, with its resultant complexity. The Fourier-transform technique will provide adequate results.

Ignoring the boundary conditions simplifies the discrete-space, continuous-time analysis, and also provides sufficient accuracy. It is likely that ignoring boundary conditions for the discrete-time, discrete-space problem will also simplify the analysis. This thesis will therefore be directed toward generating a discrete-space, discrete-time theory which ignores system boundary conditions. The development of this theory is a 'next step' to be taken in continuum feedback control theory.

The topics that will be developed for the thesis are explained in the following sections. The basic method of analysis will be the Z transform, which is better known for its application to time-sampled signals. This technique is developed for time-sampled systems, space-sampled systems, and finally for time- and space-sampled systems.

Techniques are related to the prototype model described in the next section. It should be emphasized that they are applicable to a wide range of continuum control problems. In the following chapters, the general class of situations that can be represented following the approach

exemplified will be pointed out.

The Electrically Stressed String

The continuum system used extensively as a case study in this thesis is shown in Figure 1.4. A string of density per unit length R is stretched along the x -axis with a longitudinal tension of γ . The string is maintained at ground potential, and is moving at a velocity of u along the x axis. The variable $\xi(x,t)$ represents the deflection of the string from its equilibrium position.

There are two mechanisms for damping the deflections of the string. There is damping because the string is not perfectly elastic, and also damping due to the material between the string and the electrodes. The damping in the string can be considered as moving with the string, thus it will have a different effect than that in the surrounding stationary material.

There is an electrode above the string, and another below the string. These electrodes are at a bias of V_0 volts with respect to the string. In addition to the bias voltage, there is a small driving voltage, $v_d(x,t)$ added to the top electrode and subtracted from the bottom one. It is assumed that the deflections of the string are small compared to the distance d , and also that the wavelengths are long compared to d . With these assumptions, the electric field will be almost entirely in the y direction. This y -directed field is:

$$E_y = V_0 \pm v_d(x,t)/(d \mp \xi) \quad (1.1)$$

where the top sign gives the field above the string and the bottom sign gives the field below the string.

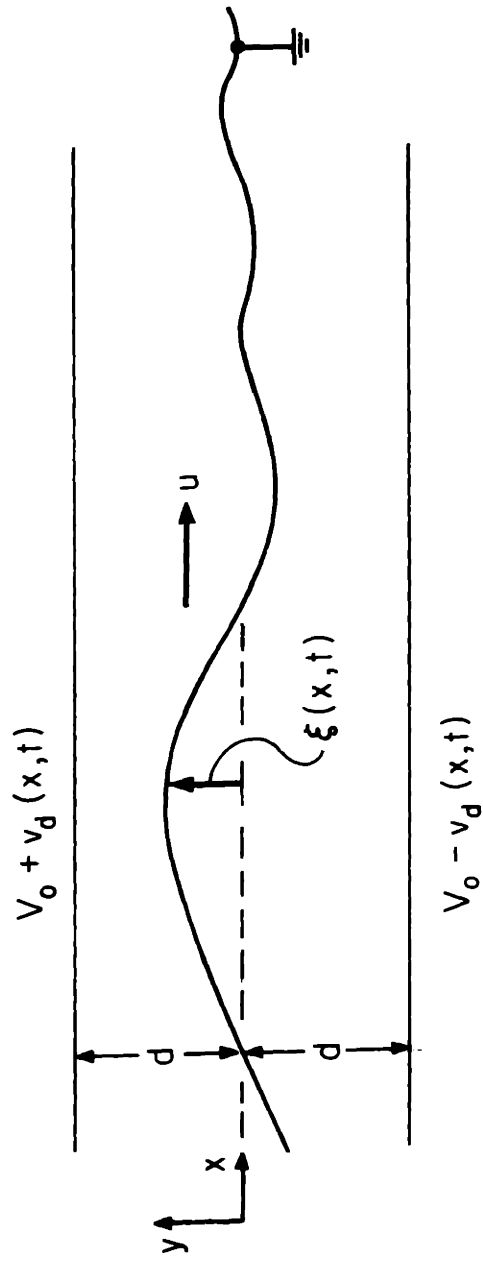


Figure 1.4 The string is stretched along the x -axis between two electrodes at a bias potential of V_0 volts.

From the Maxwell stress tensor, the force in the +y direction can be found at each point on the string.

$$f_y = \frac{1}{2} \epsilon_0 E_+^2 - \frac{1}{2} \epsilon_0 E_-^2 \quad (1.2)$$

By using Eq. (1.1), the force can be linearized to

$$f_y(x,t) = \frac{2\epsilon_0 V_0^2}{d^3} \xi(x,t) + \frac{2\epsilon_0 V_0 v_d(x,t)}{d^2} \quad (1.3)$$

The equation of motion considering damping is derived in Morse and Feshbach (Chapter 2), and also in Shortley and Williams (Chapter 19). If the forces due to the electric fields and the effects of convection are added to the equation of motion, the result is

$$R \frac{D^2 \xi}{D^2 t} = \gamma \frac{\partial^2 \xi}{\partial x^2} - \alpha' \frac{D\xi}{Dt} - \beta' \frac{\partial \xi}{\partial t} + \frac{2\epsilon_0 V_0^2 \xi}{d^3} + \frac{2\epsilon_0 V_0 v_d}{d^2} \quad (1.4)$$

where α' is the damping coefficient due to internal damping, and β' is the damping due to the external stationary medium; D/Dt is the substantive derivative defined as

$$\frac{D}{Dt} = \left(\frac{\partial}{\partial t} + u \frac{\partial}{\partial x} \right) \quad (1.5)$$

Equation (1.4) can be rearranged to obtain a more general form:

$$\frac{1}{v_p^2} \frac{D^2}{Dt^2} \xi = \frac{\partial^2 \xi}{\partial x^2} - \alpha \frac{D\xi}{Dt} - \beta \frac{\partial \xi}{\partial t} + k_c^2 \xi + g v_d \quad (1.6)$$

where

$$v_p = \sqrt{\frac{Y}{R}} \quad (1.7a)$$

$$\alpha = \frac{\alpha'}{\gamma} \quad (1.7b)$$

$$\beta = \frac{\beta'}{\gamma} \quad (1.7c)$$

$$k_c^2 = \frac{2\epsilon_o V_o^2}{\gamma d^3} \quad (1.7d)$$

$$g = \frac{2\epsilon_o V_o}{\gamma d^2} \quad (1.7e)$$

The string model has been picked because it is mathematically similar to many systems which are of practical importance.

The equation of the string, as it is presented in Eq. (1.6), can represent many physical situations. If the deflection ξ is considered to be a rotational disturbance on a long structure (Woodson and Melcher, Problem 11.12), the equation describes rotational waves. Similarly, the equation can describe systems which have compressional waves (Woodson and Melcher, Chapter 11).

When the velocity u is less than the phase velocity v_p , the equation models a convecting process such as a paper web moving through a paper machine. For cases where u is greater than v_p , the equation can model a jet of liquid (Crowley). When the tension is allowed to approach zero, an electron beam is modeled by Eq. (1.6) (Woodson and Melcher, Chapter 10).

The force generated by the bias voltage on the electrodes, $k_c^2 \xi$, has the appearance of a negative spring constant. When the string is perturbed from its equilibrium, this force acts to make the deflection grow. If this term is large enough, the deflection will be statically unstable. This equation does not describe strictly mathematically certain instabilities such as Rayleigh-Taylor instability in a fluid or plasma. However, because this equation does exhibit static instabilities which are similar to the Rayleigh-Taylor type of instability, the string model can

give some insight into the Rayleigh-Taylor instability.

The last term in Eq. (1.6), $g v_d(x,t)$, represents a way to drive the string. If the string is unstable because of a resistive wall or a large negative spring constant, the driving term provides a way to control the instability. The ability to control these instabilities is useful for improving electron beams and for containing a thermonuclear plasma.

The Fourier-LaPlace Transform

The variables used to describe the system are considered to have a LaPlace transform in time and a Fourier transform in space. For example, the displacement of the string, ξ , is related to its transform Ξ by the relations

$$\Xi(K,S) = \int_{-\infty}^{+\infty} \int_{-\infty}^{+\infty} \xi(x,t) e^{-jKx} e^{-St} dx dt \quad (1.8)$$

$$\xi(x,t) = \frac{1}{(2\pi)^2 j} \int_{-j\infty+\sigma}^{+j\infty+\sigma} \int_{-\infty}^{+\infty} \Xi(K,S) e^{jKx} e^{St} dK dS \quad (1.9)$$

There are occasions when the transform of a function is taken only in space or time; in these instances, the transform of the variable will be defined by

$$\hat{\xi}(x,S) = \int_{-\infty}^{+\infty} \xi(x,t) e^{-St} dt \quad (1.10)$$

$$\xi(x,t) = \frac{1}{2\pi j} \int_{-j\infty+\sigma}^{+j\infty+\sigma} \hat{\xi}(x,S) e^{St} dS \quad (1.11)$$

and

$$\hat{\xi}(K,t) = \int_{-\infty}^{+\infty} \xi(x,t) e^{-jKx} dx \quad (1.12)$$

$$\xi(x,t) = \frac{1}{2\pi} \int_{-\infty}^{+\infty} \hat{\xi}(K,t) e^{jKx} dK \quad (1.13)$$

The procedure is to use the capital letter to designate the transform in both space and time, and to use the symbol $\hat{}$ to designate the transform of either space or time. The parameter list is used to resolve the ambiguity whenever the symbol $\hat{}$ is used.

Outline

The Z transform (Jury, Chapter 1) provides the basis for analyzing sampled data control systems. With this transform, transfer functions and servo-loops may be generated. The Z transform technique has commonly been used only on lumped-parameter systems with temporally discrete signals.

In Chapter II, the Z transform is used to describe a continuum with discrete temporal feedback. The infinite string is driven by a control signal that is spatially continuous, but can be adjusted only at discrete points in time. This topic is presented to introduce Z transforms to continuum systems in the usual context of temporally discrete signals. A dispersion equation is derived in terms of the continuous wavenumber K and the discrete frequency Z . An analysis is made to determine the effect of the system's parameters on the stability of the string.

In Chapter III, the infinite string is driven by a control signal that is temporally continuous and spatially discrete. Z transform theory is used to describe the discrete spatial nature of this system. The discrete spatial wavenumber D is defined, and a dispersion equation in terms of D and the continuous frequency S is derived. A stability analysis is

made with the dispersion equation.

Many continuum feedback systems have only a few feedback stations and it is not realistic to consider these systems to be infinite in the longitudinal directions. The effects caused by the boundaries on the longitudinal axis of these systems must be considered. When these boundaries are applied, the system can no longer support modes for any value of D . The allowed modes on the system can occur for only a few eigenvalues of D . In Chapter IV, a method is presented for finding the eigenvalues of D , and the corresponding eigenmodes for a discrete spatial system with longitudinal boundaries.

A stability criterion for spatially discrete systems with convection is developed in Chapter V. For spatially continuous systems, the Bers-Briggs criterion can be used to determine whether a wave is amplifying or evanescent, and whether an absolute instability is present. This criterion is modified so that the same determinations can be made for a spatially discrete system. The convecting string with discrete spatial feedback is used to illustrate the modified Bers-Briggs criterion.

The stabilization of the infinite string by a control system that is discrete in both space and time is studied in Chapter VI. The dispersion equation is found either in terms of Z and K , or in terms of S and D . This dispersion equation is studied to find the values of parameters which give stable operation.

Chapter VII is used to describe an experiment in which a continuum is stabilized by a spatially and temporally sampled control system. A layer of liquid is supported against gravity by air pressure. The control

system is used to prevent the Rayleigh-Taylor instability from developing at the liquid-air interface.

The results of the thesis are summarized in Chapter VIII. This chapter will also show the general applicability of the techniques in this thesis to other continuum feedback systems. The procedure for extending the idea of a discrete spatial wavenumber to three-dimensional systems will be discussed, and suggestions for further research are made.

CHAPTER II

TEMPORALLY SAMPLED FEEDBACK

2.1 Introduction

It was explained in Chapter 1 that continuum feedback control systems which have been realized are spatially discrete systems. When these systems are large compared to the wavelengths which are to be controlled, a large number of feedback sensors and drivers is required. The multiplicity of signals to be generated and processed can require a large amount of hardware, such as amplifiers and filters. In the experimental portion of this thesis, the hardware requirements are reduced by generating the feedback signals with one amplifier and a time-sharing technique. The time-sharing technique makes this system spatially and temporally discrete.

The topic considered in this chapter is the stabilization of a continuum by means of a discrete time control system. The discrete spatial nature of the feedback will be ignored in this chapter, and the feedback driving and sensing signals will be considered as continuous functions of space. This type of system can be used to model a continuum system which has adequate spatial resolution, but does not have good temporal resolution. An example of a system in this class is a television system with a slow sweep rate. The television can provide good spatial resolution of a stationary object. However, when the object is moving, the temporal changes in the image cannot be followed by the television system, and a blurred image results. If this television system were somehow used in a control system, the spatial discreteness could be ignored, but the temporal discreteness would have to be considered.

The principal reason for analyzing this system of discrete temporal, continuous spatial feedback is to introduce Z-transform theory, which is

commonly used to describe discrete time-lumped parameter systems. After their introduction in this chapter, Z transforms will be used to analyze discrete spatial, continuous temporal systems, and then discrete spatial, discrete temporal systems.

Most of the material presented in this chapter about Z transforms can be found in Jury (Chapter 1). The only significant change that has been made is that the variables are functions of both space and time. Jury considers only variables that are functions of time.

Continuous spatial discrete temporal feedback has been studied before by Thomas (1966) for the case of a string with fixed ends. In his analysis, the deflections of the string were represented by a series of normal modes. The problem will now be analyzed for the case of a string whose boundaries are at infinity, and whose deflections can be described by a Fourier integral instead of a Fourier series. It is not easier, mathematically or conceptually, to analyze the case of an infinite string than to analyze that of a string with longitudinal boundaries. However, when the complication of spatial discreteness is added in the later chapters, infinite systems are found to be much easier to analyze than finite systems. Since this chapter is to serve as a basis for the topics treated later, the infinite string is studied here.

2.2 Description of the System

The continuum, which will be stabilized, is the string of Chapter I with damping and no convection. The equation of motion for this serves as a case study in exemplifying a general approach, and is

$$\frac{1}{v_p^2} \frac{\partial^2 \xi(x,t)}{\partial t^2} = \frac{\partial^2 \xi(x,t)}{\partial x^2} - \beta \frac{\partial \xi(x,t)}{\partial t} + k_c^2 \xi(x,t) + g v_d(x,t) \quad (2.1)$$

The driving voltage, $v_d(x,t)$, can be adjusted continuously in space, but it can only be changed at the discrete times $t = 0, T, 2T, \dots$. The form in time of this voltage is shown in Figure 2.1 for a particular point in space and the form in space is shown in Figure 2.2 for several points in time.

This forcing voltage is the type that is usually generated by a control system that includes a computer. The computer updates the driving force at discrete points in time, and holds it constant between these discrete times. In a realistic system, the computer probably could not update the driving signal at each point in space at essentially the same time. The complications caused by the signal not being changed at the same time at every point in space are beyond the scope of this chapter and will be treated in Chapter VI.

The transfer function which relates the deflection of the string to the driving voltage may be found by taking the Laplace transform in time and the Fourier transform in space of Eq. (2.1) to obtain:

$$\Xi(k,s) \left[\frac{1}{v_p^2} s^2 + k^2 + \beta s - k_c^2 \right] = g V_d(k,s) \quad (2.2)$$

It is convenient to normalize the length of time, T , to one. This is accomplished with the following dimensionless variables:

$$S = sT \quad (2.3a)$$

$$\delta = \beta v_p^2 T \quad (2.3b)$$

$$K = kT v_p \quad (2.3c)$$

$$N = k_c^2 v_p^2 T^2 \quad (2.3d)$$

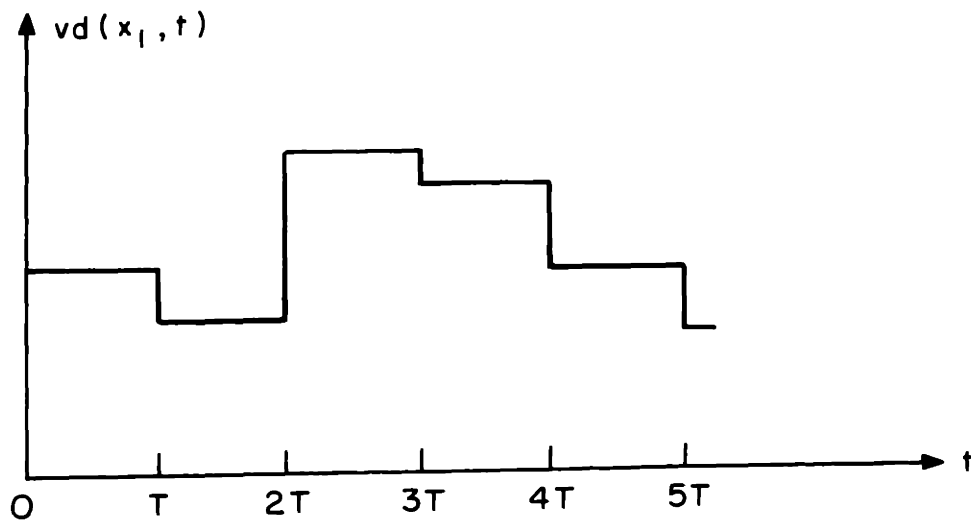


Figure 2.1 The driving voltage at a fixed point
as a function of time

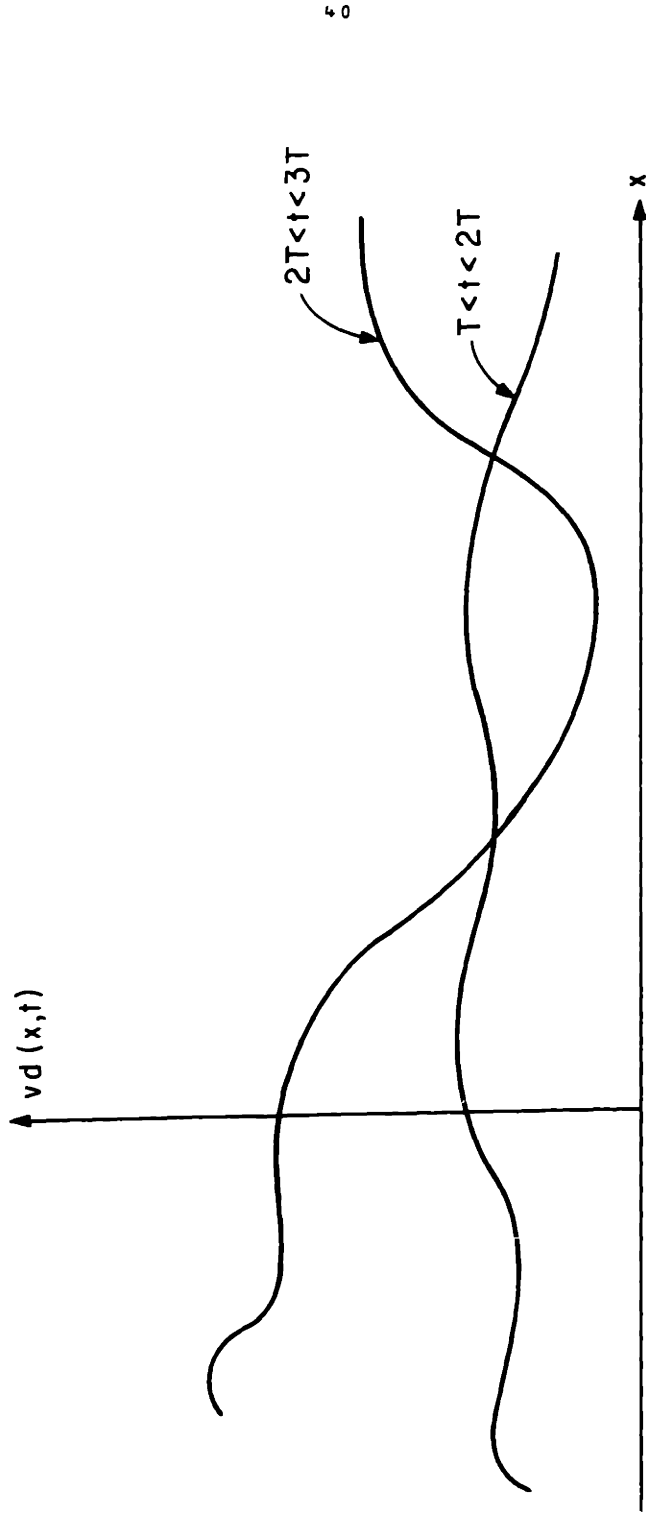


Figure 2.2 The driving voltage as a function of x for several periods of time

$$f(x,t) = v_p^2 T^2 g v_d(x,t) \quad (2.3e)$$

The transformed equation can now be written as:

$$\Xi(K,S) = \frac{1}{S^2 + \delta S + K^2 - N} F(K,S) \quad (2.4)$$

and the transfer function for the string is:

$$H(K,S) = \frac{1}{S^2 + \delta S + K^2 - N} \quad (2.5)$$

The control scheme used in this system measures or "samples" the deflection of the string at discrete instants in time. A restoring force proportional to this measured signal is then generated in an attempt to drive the deflections to zero. The system is complicated, because $f(x,t)$ is the discrete temporal function shown in Figures 2.1 and 2.2, and its transform, $F(K,S)$ is not easily found. Z transforms are used in the following sections to overcome the analytical difficulties caused by the temporal discreteness.

2.3 Transforms of Temporally Sampled Signals

Detection Scheme: Temporal Sampling

The detection scheme incorporated in the control system measures or "samples" the string's deflection at the regularly spaced sampling instants in time. Between the sampling times, the detector is producing no information about the deflection of the string, and therefore the sampled deflection is zero for this period of time. This sampled value of the deflection can be thought of as impulse sheets, parallel to the x axis, and spaced at regular intervals along the t axis. The locations of these impulse sheets on the t axis are the sampling times. The

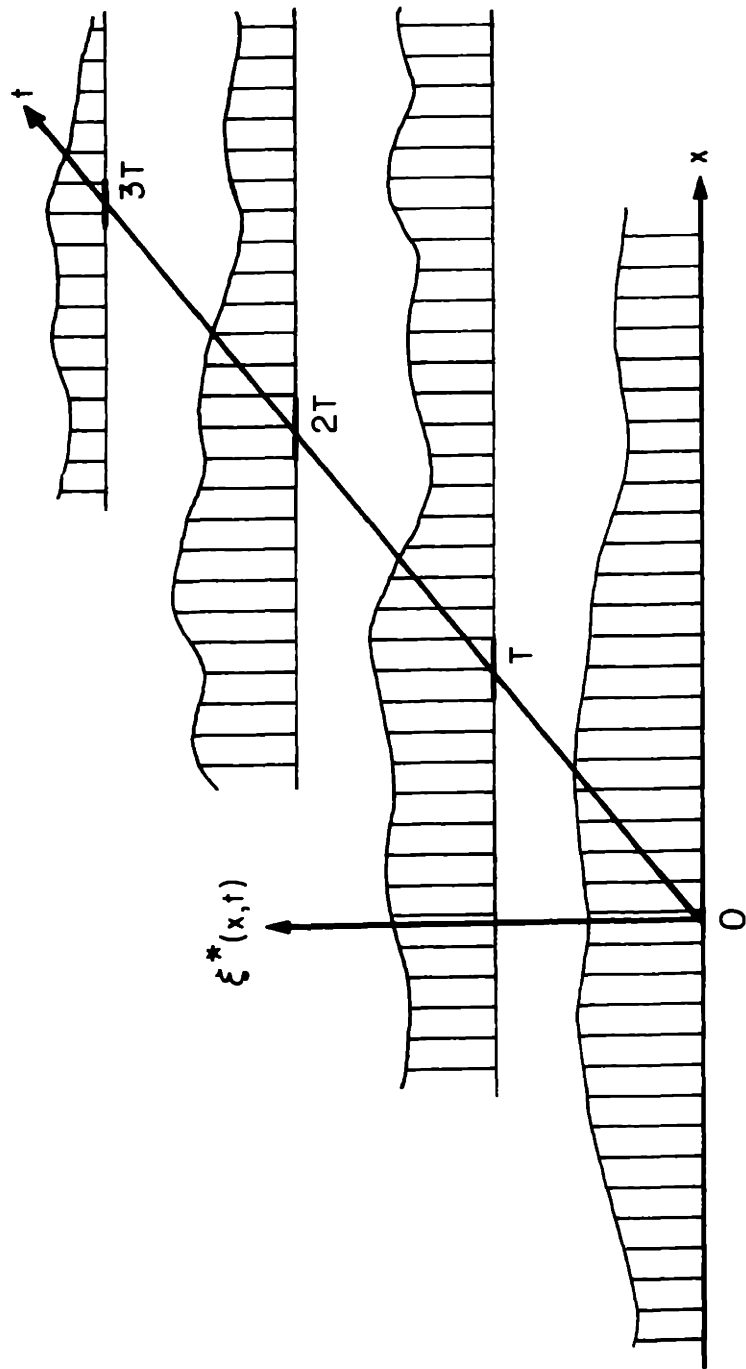


Figure 2.3 The time-sampled output is an array of impulse sheets.

amplitude of the impulse sheets along the x axis represents the amplitude of the string's deflection at the sampling time. These impulse sheets are shown in Figure 2.3.

The sampled deflection, ξ^* , can be written as a product of the deflection and a train of impulse sheets:

$$\xi^*(x,t) = \xi(x,t) \sum_{n=0}^{n=+\infty} u_0(t-nT) \quad (2.6)$$

The lower limit of the summation is zero, because the system is considered to be at rest for $t < 0$. This sampling process can be represented by the network in Figure 2.4. The system deflection and an impulse train $i^*(t)$, (the sampling function), are multiplied together to produce the sampled deflection (sampled function).

Single-Sided Z Transforms

The Fourier-LaPlace transform of the time-sampled deflection can be found by two different methods. The first method shown here uses complex integration to get the transform. The second method is of less general applicability, and involves finding the sum of an infinite series.

If two functions are multiplied together, the Fourier-LaPlace transform of the product is the convolution in K and S space of the two original transforms. If the original signal is considered to be zero for t less than zero, then the sampling function needs to be a series of impulse sheets along the positive t axis. The Fourier-LaPlace transform of the sampling function, with T normalized to one, is given for

$$|e^{-S}| < 1 \text{ by}$$

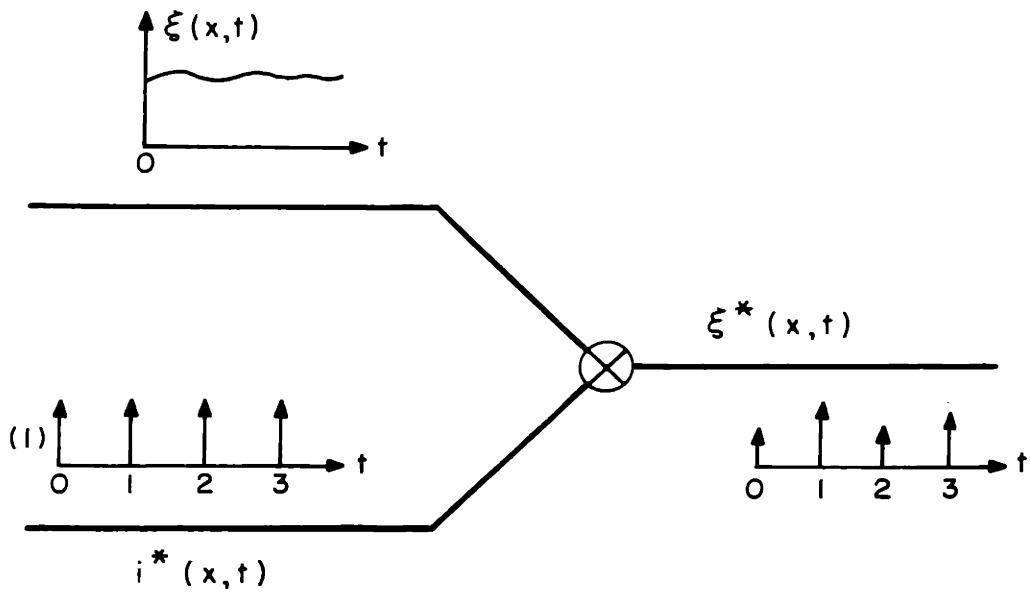


Figure 2.4 The temporally sampled output is produced by multiplying the deflection by a spatial impulse train.

$$I^*(K,S) = \frac{1}{1 - e^{-S}} \quad (2.7)$$

The transform of the sampled function is the convolution in K and S space of the transforms of the displacement and the sampling function. That is

$$\Xi^*(K,S) = \Xi(K,S) \otimes I^*(K,S) \quad (2.8)$$

where \otimes represents the convolution.

Writing out this convolution integral, realizing that the convolution in K space can be ignored because the sampling function is constant in X and its transform is an impulse in K space, gives

$$\Xi^*(K,S) = \frac{1}{2\pi j} \int_{\sigma - j\infty}^{\sigma + j\infty} \Xi(K,P) \left[\frac{1}{1 - e^{-(S-P)}} \right] dP \quad (2.9)$$

This integral is illustrated in Figure 2.5. If the integral is performed on Path C_1 , the only poles enclosed are those of the sampling function.

The result is

$$\Xi^*(K,S) = \sum_{n=-\infty}^{\infty} \Xi(K,S - 2n\pi) \quad (2.10)$$

This type of function will result in a dispersion relation for the system which will be an infinite series, and calculations for stability will be cumbersome.

If the number of poles of $\Xi(K,P)$ is finite, then a closed form of the transform can be obtained by using contour C_2 . The result is

$$\Xi^*(K,S) = \sum_{\text{Poles of } \Xi} \text{Residues} \left[\Xi(K,P) \frac{1}{1 - e^{-(S-P)}} \right] - \frac{1}{2} \hat{\xi}(K,0_+) \quad (2.11)$$

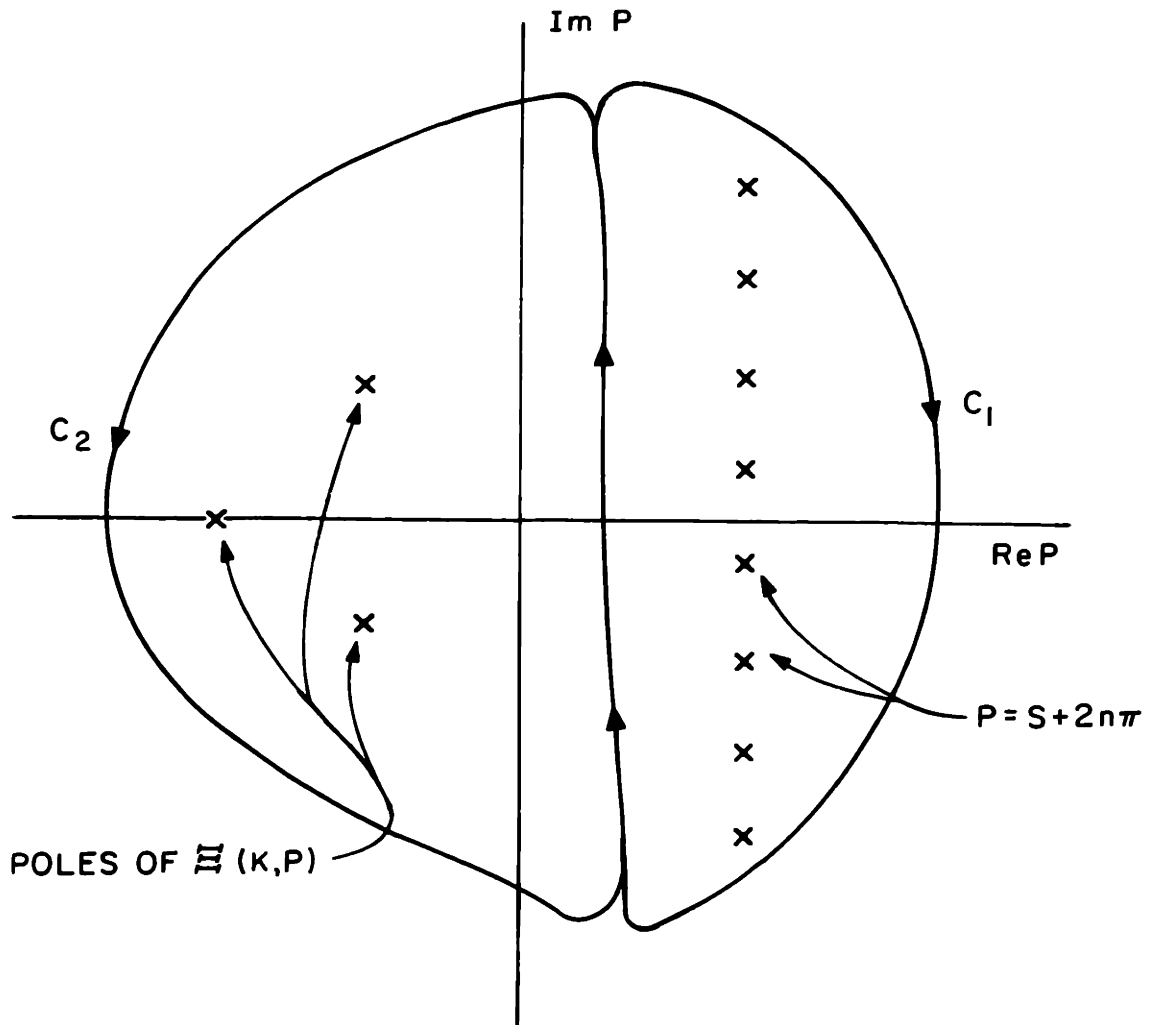


Figure 2.5 Contour integral for finding the transform of the sampled function

The term $1/2 \hat{\xi}(K, 0_+)$ is the Fourier transform in space of the deflection at $t = 0_+$. This term results only when the function being sampled has a step at $t = 0$. The sampling impulse at $t = 0$ will detect only one-half of the value of the step. The summation term includes the whole value of the step and therefore a correction factor must be added. Mathematically, this term occurs because the integral along C_2 is not zero.

The discrete temporal frequency is now defined as

$$Z = e^{-S} \quad (2.12)$$

If this variable is substituted into Eq. (2.11), the transform of the sampled function is obtained in the form

$$\Xi^*(K, S) = \Xi(K, Z) \quad (2.13)$$

which is known as the Z transform.

A second method for finding the transform of the sampled function is available when the deflection, $\xi(x, t)$, is separable into a function of x and a function of t . When the deflection is separable, it and its transform can be written as:

$$\xi(x, t) = \psi(x) \phi(t) \quad (2.14)$$

$$\Xi(K, S) = \Psi(K) \Phi(S) \quad (2.15)$$

Equation (2.6) can then be rewritten as:

$$\xi^*(x, t) = \psi(x) \sum_{n=0}^{\infty} \phi(n) u_0(t-n) - \frac{1}{2} \psi(x) \phi(0_+) u_0(t) \quad (2.16)$$

The last term on the right is introduced for the cases where $\xi(x, t)$ is discontinuous in a step manner at $t = 0$. When this step is multiplied

by the impulse at $t = 0$, the result is an impulse which has an amplitude of one-half of the step. The impulse at $t = 0$ in the summation has an area equal to the step at zero, so the last term is added as a correction factor.

Taking the Fourier-Laplace transform of Eq. (2.16) gives

$$\Xi^*(K, S) = \Psi(K) \sum_{n=0}^{+\infty} \phi(n) e^{-nS} - \frac{1}{2} \Psi(K) \phi(0_+) \quad (2.17)$$

By using the discrete temporal frequency Z from Eq. (2.12), Eq. (2.17) is made into a power series of Z .

$$\Xi^*(K, S) = \Psi(K) \sum_{n=0}^{+\infty} \phi(n) Z^n - \frac{1}{2} \Psi(K) \phi(0_+) \quad (2.18)$$

For most functions of ϕ , the power series will converge for a range of values of Z . This allows the transform of the sampled function, $\Xi^*(K, S)$ to be written in a closed form known as the Z transform:

$$\Xi(K, Z) = \Psi(K) \Phi(Z) \quad (2.19)$$

Inverse Z Transforms: Laurent Expansion

There are two convenient ways of recovering the time-sampled signal from the Z transform. Both of these methods involve finding the coefficients of the series representation of the Z transform. The first method is to expand the Z transform into a power series; this is the reverse of the steps taken between Eqns. (2.18) and (2.19).

$$\Xi(K, Z) = \Psi(K) \left[\frac{1}{2} \phi(0) + \phi(1)Z + \phi(2)Z^2 + \dots \right] \quad (2.20)$$

The coefficients in this series represent the amplitudes at the sampling times. For complicated functions, this method is not convenient, except

for the terms with low values of n .

Inverse Z Transform: Complex Integral Formula

In many cases, it is not easy to expand the Z transform into a series to recover the original function. A simpler method of finding $\phi(n)$, which is the coefficient of Z^n in the expansion, is to use Cauchy's integral formula, which is

$$\oint_{\Gamma} z^K dz = \begin{cases} 2\pi j & K = -1 \\ 0 & K \neq -1 \end{cases} \quad (2.21)$$

where Γ is a contour that encloses the origin.

If $\phi(Z)$ is multiplied by $Z^{-(n+1)}$, then the series expansion of $Z^{-(n+1)} \phi(Z)$ is

$$Z^{-(n+1)} \phi(Z) \rightarrow \dots + \frac{\phi(n-1)}{Z^2} + \frac{\phi(n)}{Z} + \phi(n+1) + Z\phi(n+2) + \dots \quad (2.22)$$

If each term in this series is integrated on a contour around $Z = 0$ on which $\phi(Z)$ is analytic, the only term which may have a non-zero result is the Z^{-1} term. Therefore,

$$\oint_{\Gamma} Z^{-(n+1)} \phi(Z) dZ = 2\pi j \phi(n) \quad (2.23)$$

Rearrangement gives

$$\phi(n) = \frac{1}{2\pi j} \oint_{\Gamma} Z^{-(n+1)} \phi(Z) dZ = \sum \text{Residues of } \phi(Z) Z^{-(n+1)} \quad (2.24)$$

This formula is probably the most useful method of recovering the

spatially sampled signal from the Z transform. It is illustrated here for the situation where ξ is separable into a function of x and a function of t . This restriction is used only because it makes the derivation of the inverse transform easier. In general, the inverse transform is

$$\hat{\xi}(K,n) = \frac{1}{2\pi j} \int_{\Gamma} z^{-(n+1)} \Xi(K,Z) dZ \quad (2.25)$$

where $\hat{\xi}(K,n)$ is the Fourier transform in space of the deflection at the normalized sampling time, n . The contour Γ of this integral is made to enclose the origin, but it must not enclose any of the poles of $\Xi(K,Z)$. The reason for this choice of contour can be seen from Eq. (2.18). The series of Eq. (2.18) will converge for values of $|Z|$ less than the inverse growth rate of the sampled function. This region of convergence includes the origin and the region out to the first pole of $\Xi(K,Z)$. The contour Γ is constrained to be in this region of convergence.

2.4 Open-Loop Discrete Temporal Transfer Function

Sample and Hold Filter

The force, applied to the string by the electrode, is constant for an interval of time T . This electrode and its associated electronics is called a "sample and hold filter"; it is shown in Figure 2.6. The electrode system is driven by an impulse train, and each impulse produces a pulse whose height is the area of the impulse. The duration of the pulse is the sampling time, or the time between input pulses. The output is the discrete time force which is applied to the string.

Sampled Transfer Function

The string with the driving electrodes can be thought of as a system, $G(K,S)$, which receives a time-sampled input, $u^*(x,t)$, and produces an

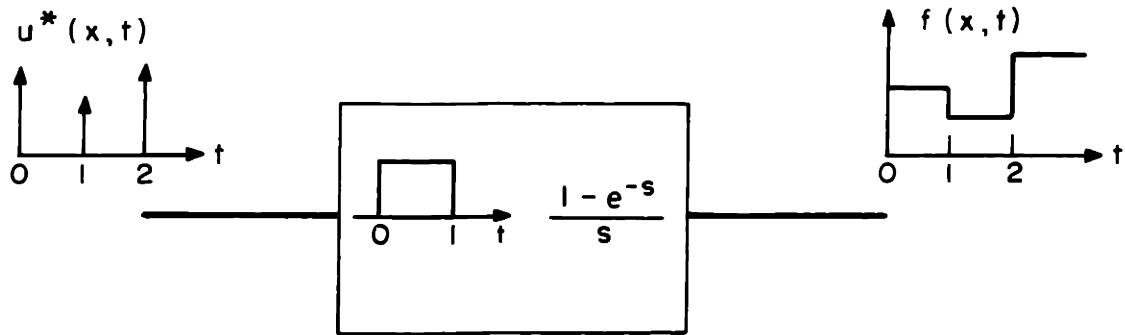


Figure 2.6 The temporally discrete force is generated by driving a sample-and-hold filter with an impulse train.

output, $\xi(x,t)$, which is continuous in space and time. It is important to keep in mind that it is not the continuous deflection $\xi(x,t)$ that is being controlled. The control system knows only the measured value of the deflection $\xi^*(x,t)$ and this is the quantity that is controlled. A diagram representing the system from sampled input to sampled output is shown in Figure 2.7.

From the theory of sampled data control systems, it can be shown that a simple relation exists between the Laplace transforms $U^*(K,S)$ and $\Xi^*(K,S)$. This can be found by noting that

$$\Xi(K,S) = U^*(K,S)G(K,S) \quad (2.26)$$

When the output is sampled, the result, using Eq. (2.10), is

$$\Xi^*(K,S) = \sum_{n=-\infty}^{+\infty} U^*(K,S-2n\pi)G(K,S-2n\pi) \quad (2.27)$$

From Eq. (2.10), it can also be seen that

$$U^*(K,S) = \sum_{n=-\infty}^{+\infty} U(K,S-2n\pi) \quad (2.28)$$

This allows $U^*(K,S-2n\pi)$ to be factored from Eq. (2.27) to give

$$\Xi^*(K,S) = U^*(K,S) G^*(K,S) \quad (2.29)$$

where $G^*(K,S)$ is the sampled value of the impulse response of the string and associated electrodes and circuits.

By rewriting Eq. (2.29) in the Z-form of Eq. (2.19), the system of Figure 2.7 can now be represented by Figure 2.8. The system has been broken down to a system function, $G(K,Z)$, which takes the time-sampled

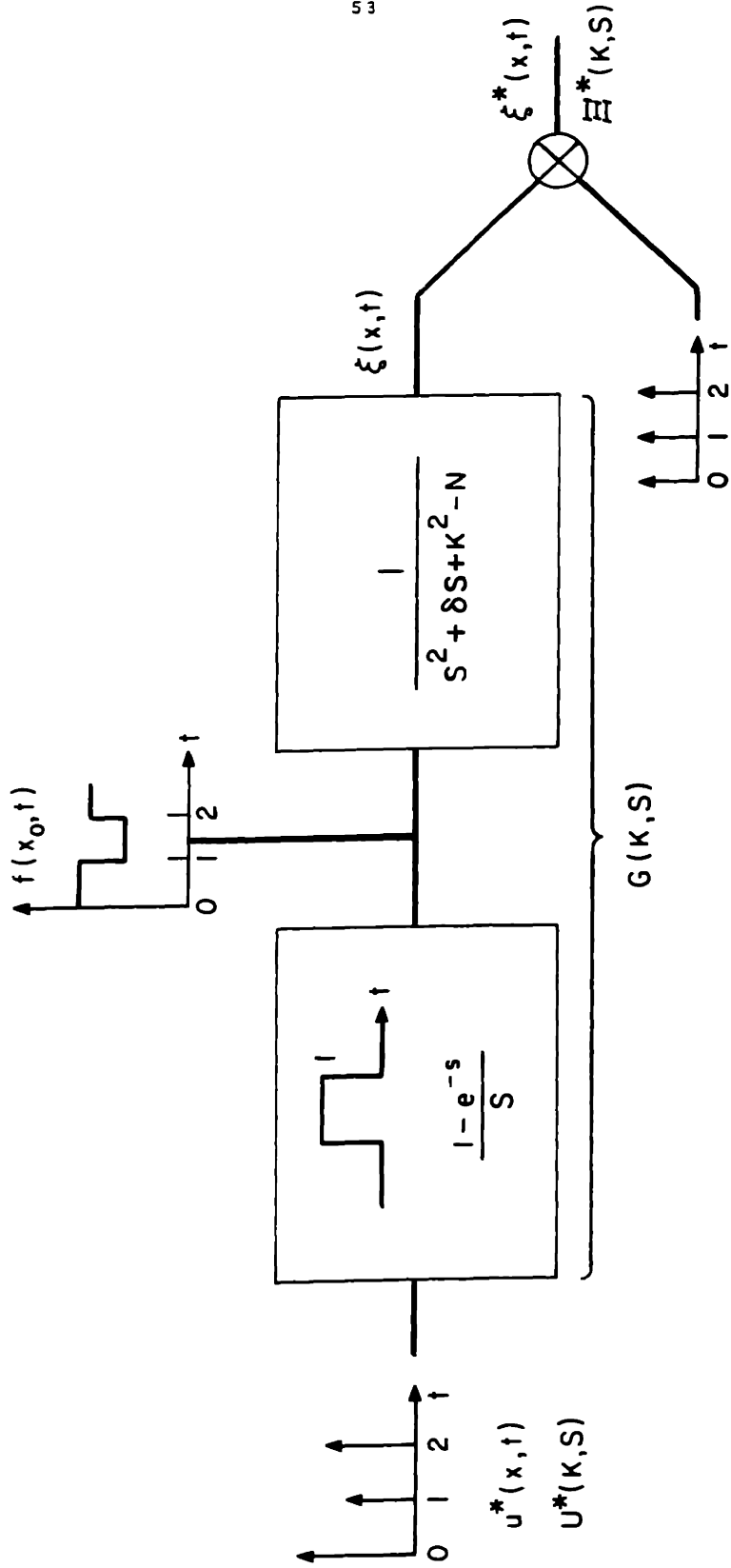


Figure 2.7 The electrodes, string, and sensors are a system which accepts a time-sampled input and produces a time-sampled output.

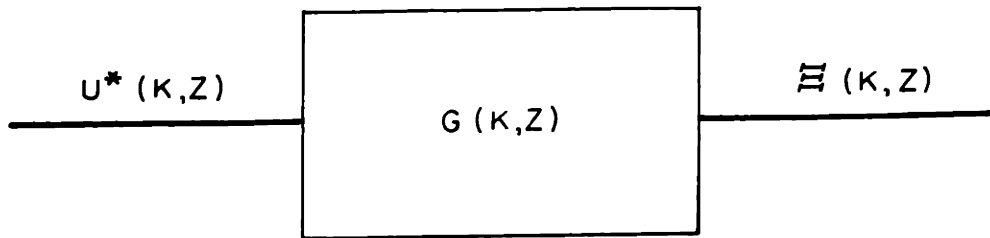


Figure 2.8 Block diagram of the temporally discrete open-loop system

signal $U^*(K,S)$ and produces a time-sampled output $\Xi(K,Z)$. The problem now is to determine $G(K,Z)$ from $G(K,S)$.

The transfer function of the open-loop system is the product of the transfer functions of the sample and hold filter and of the string.

$$G(K,S) = \underbrace{\left(\frac{1-e^{-S}}{S} \right)}_{\text{Sample and hold filter}} \underbrace{\left(\frac{1}{S^2 + \delta S + K^2 - N} \right)}_{\text{String}} \quad (2.30)$$

The sampled response of this filter can be found from Eq. (2.9). With Eqns. (2.30) and (2.13), Eq. (2.9) becomes

$$G(K,Z) = \frac{1}{2\pi j} \int_{\sigma-j\infty}^{\sigma+j\infty} \frac{(1 - e^{-P}) dP}{(P^2 + \delta P + K^2 - N) P [1 - e^{-(S-P)}]} \quad (2.31)$$

The poles of this integral are shown in Figure 2.9.

There are two paths by which the integral can be closed. Path II encircles an infinite number of poles, and is therefore not used. If contour I is used, a problem arises because of the term e^{-P} in the numerator of the integrand. This term goes to infinity for large values of imaginary P and the integral does not converge. This problem can be overcome by realizing that e^{-P} represents a delay of the generated wave. Since the deflection is sampled, the delays of the sampled signal must all be multiples of one sampling period. If an integer delay is factored from the delayed term, the integral becomes

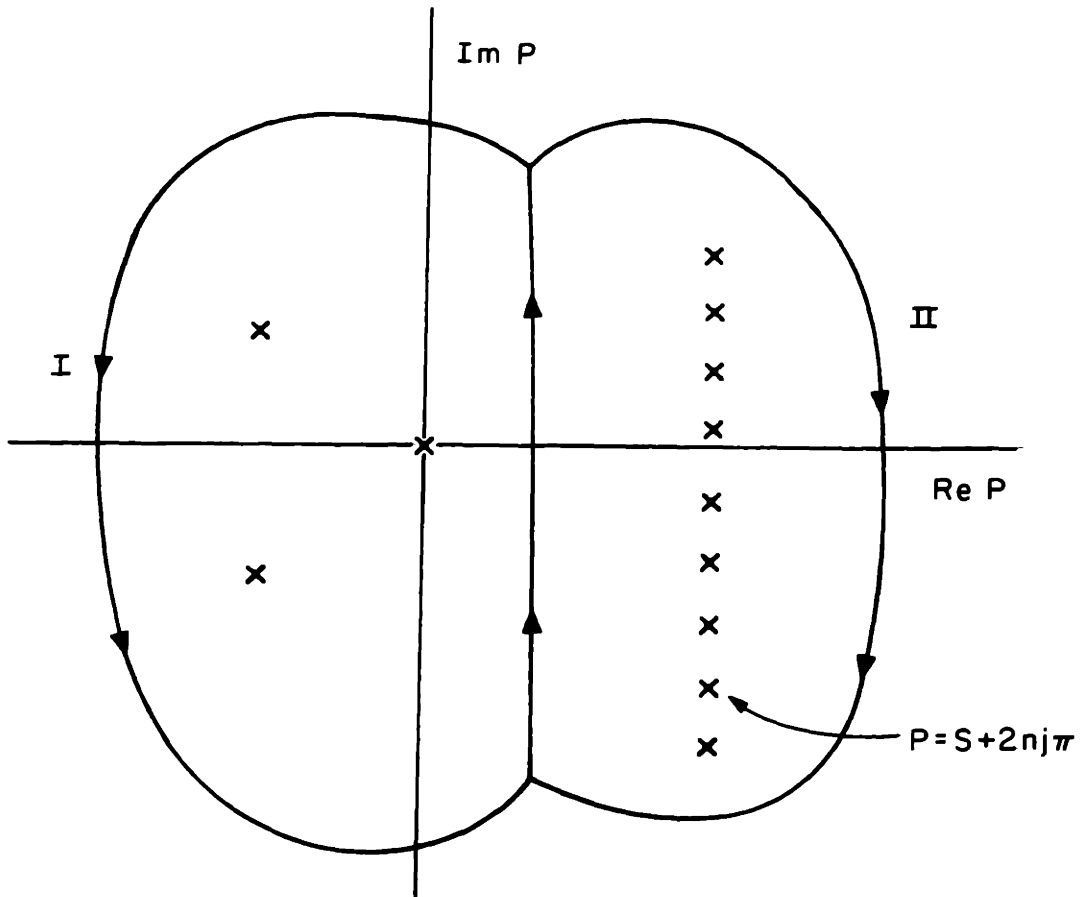


Figure 2.9 Contour integral for finding the transfer function $G(K,Z)$

$$G(K, Z) = \frac{1-e^{-S}}{2\pi j} \int_{\sigma-j\infty}^{\sigma+j\infty} \frac{dP}{(P^2 + \delta P + K^2 - N)P[1-e^{-(S-P)}]} \quad (2.32)$$

This integral has three poles which have the following residues:

$$2\pi j \cdot \text{Residue } (P=0) = \frac{1}{K^2 - N} \quad (2.33)$$

$$2\pi j \cdot \text{Residue } \{P = -\delta/2 - [(\delta/2)^2 - K^2 + N]^{1/2}\} =$$

$$\frac{1 - e^{-S}}{(-\delta/2 - W)(-2W)[1 - e^{-(\delta/2+W)} e^{-S}]} \quad (2.34)$$

$$2\pi j \cdot \text{Residue } \{P = -\delta/2 + [(\delta/2)^2 - K^2 + N]^{1/2}\} =$$

$$\frac{1 - e^{-S}}{(-\delta/2 + W)(2W)[1 - e^{-(\delta/2 - W)} e^{-S}]} \quad (2.35)$$

$$\text{where } W = [(\delta/2)^2 - K^2 + N]^{1/2} \quad (2.36)$$

The total Z transform of the system, which relates the discrete input signal to the time-sampled displacement, is then

$$G(K, Z) = \frac{(1-Z) \{ -2W + Ze^{-\delta/2} [-\delta/2(e^W - e^{-W}) + W(e^W + e^{-W})] \}}{(K^2 - N)(2W)[1 - Ze^{-\delta/2}(e^W + e^{-W}) + e^{-\delta} Z^2]}$$

$$+ \frac{2W[1 - Ze^{-\delta/2}(e^W + e^{-W}) + e^{-\delta} Z^2]}{(K^2 - N)(2W)[1 - Ze^{-\delta/2}(e^W + e^{-W}) + e^{-\delta} Z^2]} \quad (2.37)$$

2.5 Closed-Loop System

Transfer Function with Feedback

For this case study, the following feedback scheme is used. The sampled deflection is amplified and the negative of the resulting signal is applied to the driving electrodes. The system could probably be stabilized better if the feedback loop contained additional filters. However, this chapter serves only to introduce the techniques for analyzing discrete temporal feedback, and therefore only the simplest feedback is considered.

With this feedback the entire system can be represented by the servo-loop of Figure 2.10. The transfer function for this closed-loop system can be written as

$$\frac{\Xi(K,Z)}{U(K,Z)} = \frac{G(K,Z)}{1 + AG(K,Z)} \quad (2.38)$$

Z-K Closed-Loop Dispersion Equation

The discrete natural frequencies of the system, that is, the frequencies at which there may be a response with no drive, can be found by setting the denominator of the transfer function to zero.

$$1 + AG(K,Z) = 0 \quad (2.39)$$

With Eq. (2.37), Eq. (2.39) may be rewritten as

$$\begin{aligned} & (K^2 - N + A)(2W)[1 - Ze^{-\delta/2}(e^W + e^{-W}) + Z^2e^{-\delta}] \\ & + A(1-Z) \{-2W + Ze^{-\delta/2}[-\delta/2(e^W - e^{-W}) + W(e^W + e^{-W})]\} = 0 \end{aligned} \quad (2.40)$$

Equation (2.40) is the Z-K dispersion equation for the closed-loop system. With this equation, the discrete temporal frequencies, Z, can be

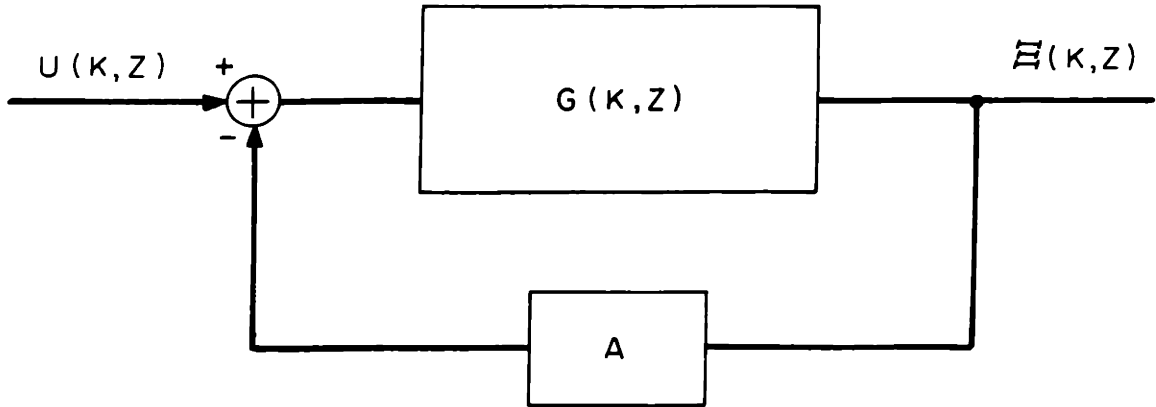


Figure 2.10 Servo-loop representation of the temporally discrete system with feedback

found in terms of the wavenumber, K . It is interesting to note that this dispersion equation is a second-order polynomial in Z and that the original continuous time-transfer function, Eq. (2.4), was second order in S . The use of the Z transform has allowed a dispersion equation to be found for the case of discrete time feedback which is not much more complicated than the dispersion equation for a continuous time system.

Stability Criterion

The stability criterion for this dispersion relation can be easily obtained by several methods. The first method is to use the normal criterion for an ω - k dispersion equation. If an ω - k dispersion relation gives a value of ω with a negative imaginary value (positive real value for S) for a real value of k , then the system is unstable. From the definition of Z , Eq. (2.12) shows that a negative imaginary value of ω will generate a value of Z whose magnitude is less than one. The stability criterion that is used with Eq. (2.40) is to require that

$$|Z| \geq 1 \tag{2.41}$$

for stable operation.

Another method of deriving this same criterion is to use Eq. (2.18), which expresses the Z transform as the sum of an infinite series. If the sum of this series has a pole at a value of Z , the magnitude of which is less than one, then the coefficients of the high order terms of Z in the expanded series must be greater than one. This corresponds to a function that is growing in time and is unstable.

An Upper Bound on Gain

It is possible for this discrete time control system to drive certain modes unstable. If the sampling rate, or the rate at which the feedback force changes, is close to one-half the frequency of a certain mode, then the control system can pump energy into this mode. This mode would be overstable and characterized by growing oscillations unless some damping were added to drain energy from the mode.

A good guess for the mode that the system will first drive overstable is the mode whose complex natural frequency with no gain is twice the sampling frequency. Since the sampling time has been normalized to one, this means the complex part of S should be

$$S = j\pi \quad (2.42)$$

Using the transfer function of the undamped system, Eq. (2.5), the wavenumber which corresponds to this complex frequency is

$$K^2 = (\delta/2)^2 + \pi^2 + N \quad (2.43)$$

With this wavenumber, the value of W becomes

$$W = j\pi \quad (2.44)$$

and the dispersion equation, (2.40), reduces to

$$Z \{e^{-\delta/2} [(\delta/2)^2 + \pi^2 + A] + A\} + (\delta/2)^2 + \pi^2 = 0 \quad (2.45)$$

From the stability criterion that was stated in the previous section, the point of impending instability occurs when

$$|Z| = 1 \quad (2.46)$$

Since all the terms in Eq. (2.45) are real, Eq. (2.46) can be changed to

$$Z = \pm 1 \quad (2.47)$$

The most restrictive case for stability results when the minus sign (-) is used. To satisfy the condition that the magnitude of Z be greater than one, close to the point of $Z = -1$, the following upper bound on the gain is derived from Eq. (2.45):

$$A \leq \frac{[\pi^2 + (\delta/2)^2][1 - e^{-\delta/2}]}{(1 + e^{-\delta/2})} \quad (2.48)$$

The significance of this upper bound on the gain is that it goes to zero as the damping goes to zero. This means that with no damping, the discrete temporal nature of the feedback will always make the system unstable. This fact should be expected, due to the nature of the continuous string. Since any wavenumber K is allowed to exist on the string, then all imaginary values of S can also occur. It is reasonable to assume that the discrete nature of the feedback will cause some modes to be driven. Since there are no boundaries to eliminate some of the modes, then the potentially overstable modes will exist and will be excited.

Results of the Stability Analysis

The dispersion equation, (2.40), can be analyzed on the computer to find the values of gain which would give stable operation for different values of N , δ , and K . The results are shown in Figure 2.11.

It is found that the value of gain, A , must be larger than N for the system to be stable. Along the line $A = N$, the value of Z is $+1$. This

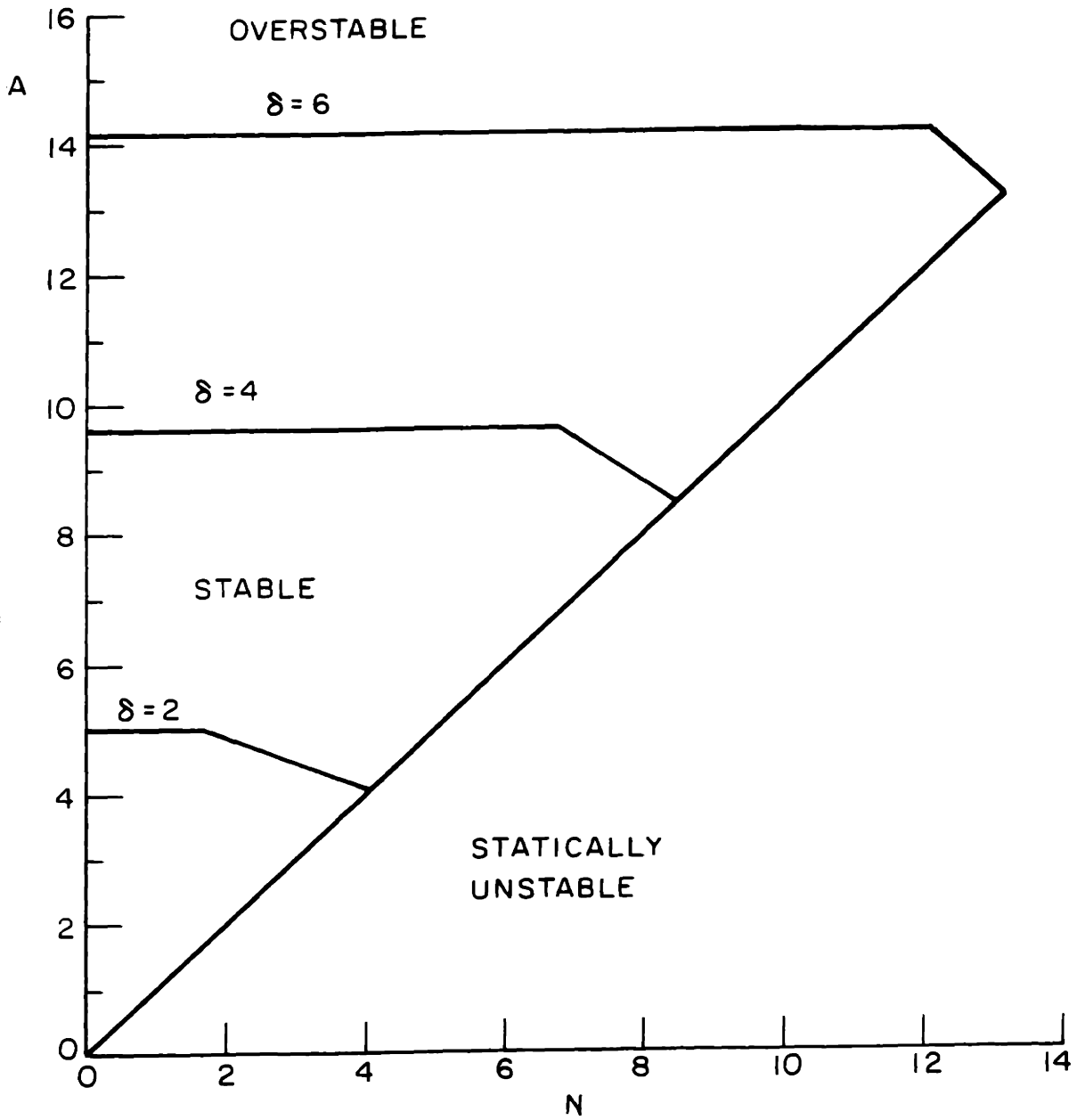


Figure 2.11 Conditions for stability of the string
with discrete temporal feedback

corresponds to an impending static instability.

Along the top boundary of the stable regions, the value of Z is -1 . This corresponds to an impending overstability, or to growing oscillations. It should be noted that this value of Z is the same value that was picked in the section titled "An Upper Bound on Gain" as the most likely to be unstable for high values of gain.

At the top right-hand corner of the stable regions, an instability occurs which is neither purely static or oscillatory. This instability is probably some combination of the two instabilities that have been mentioned. It is significant that the upper bound in gain in Figure 2.11 is less than the value predicted in Eq. (2.47). This should be expected, because there was no guarantee that the derived upper bound was a least upper bound. The significance of (2.47) is not that it gives the least upper bound for stable gain, but that it shows the system is unstable with no damping.

2.6 Summary

The Z transform, which has been used to describe discrete time, lumped-parameter systems, can be applied to discrete time, continuum systems. With Z transforms, a time-sampled continuum can be described by a closed-form transfer function in terms of the wavenumber, K , and the discrete temporal frequency, Z .

When discrete time, spatially continuous feedback is applied to the continuum, a closed-loop transfer function can be generated by use of conventional servo theory. A dispersion equation in terms of Z and K is obtained in closed form from the poles of the closed-loop transfer

function. The stability of the closed-loop system can be determined from this dispersion equation.

The case of the string with discrete temporal feedback was analyzed in detail. It was found that increasing the feedback gain could stabilize the system, but that too much gain drives the string overstable. The maximum gain that can be used before overstableness resulted depended on the damping applied to the string. When there is no damping, any non-zero gain drives the string overstable. This overstableness occurs because there is a wavenumber which corresponds to oscillations at twice the sampling frequency. The control system pumps this mode, and the system becomes overstable.

CHAPTER III

DISCRETE SPATIAL FEEDBACK FOR AN INFINITE SYSTEM3.1 Introduction

At the present time, spatial resolution is a serious limitation for continuum feedback control systems. The spatially discrete nature of the feedback is a restriction because it is almost impossible to make feedback drivers or sensors that can independently drive or detect each point of a continuum. The electrodes which are used to drive electromechanical systems must be a certain finite size. They will, therefore, drive a section of the continuum, rather than one point. In industrial applications, such as chemical reactors, the number of locations for valves or other controls is limited to a few discrete points on the reactor. Sensors are similarly restricted. In electromechanical systems and in chemical processes, important parameters can be measured at only a few discrete points.

In this chapter, the spatially discrete system which will be controlled is the stationary string stressed by an electric field. The feedback force is applied by electrodes of finite size, and the deflection is sampled at the center of each electrode. The same system has been studied previously by Melcher (May, 1965). His analysis uses a Fourier transform technique to describe the deflections of the membrane. This method considers the continuous displacements of the string as the output of the system. The dispersion equation which he derives is an infinite series in ω and k . This dispersion equation must be truncated before the stability of the system can be determined.

The approach that is used in this chapter is to use Z transforms to describe the spatially discrete nature of the system. Using this technique,

the output of the system is considered to be the measured or 'sampled' value of the displacement. The information about the displacement between the sampling points is ignored. This approach is physically closely related to the actual system, since the control system tries to stabilize the sampled displacement; the displacement between the sampling points is unknown to the control system. Z transforms also generate a closed-form transfer function relating the sampled output to the driving voltage. With these transfer functions, servo-loop diagrams (which are an aid for the analysis) can be made.

3.2 Description of the System

As a case study, the unbounded string, with damping and no convection, is analyzed in detail in this chapter. The equation of motion for this case is

$$\frac{1}{v_p^2} \frac{\partial^2 \xi(x,t)}{\partial t^2} = \frac{\partial^2 \xi(x,t)}{\partial x^2} - \beta \frac{\partial \xi(x,t)}{\partial t} + k_c^2 \xi(x,t) + g v_d(x,t) \quad (3.1)$$

It is explained in Chapter I that this equation has wide applicability. With the proper values for the coefficients, it can describe such phenomena as electron beam instabilities or hydromagnetic instabilities in a plasma column. The results obtained in this chapter should also have wide applicability; with only small modifications, the techniques presented here for stabilizing the string can be used for many other situations.

Figure 3.1 shows a physically realizable method of adding the driving voltage to the bias voltage. The bias electrodes are divided into segments of length L . Each segment is driven by a source, V_{dn} , which adds the driving or control voltages to the bias voltage on the

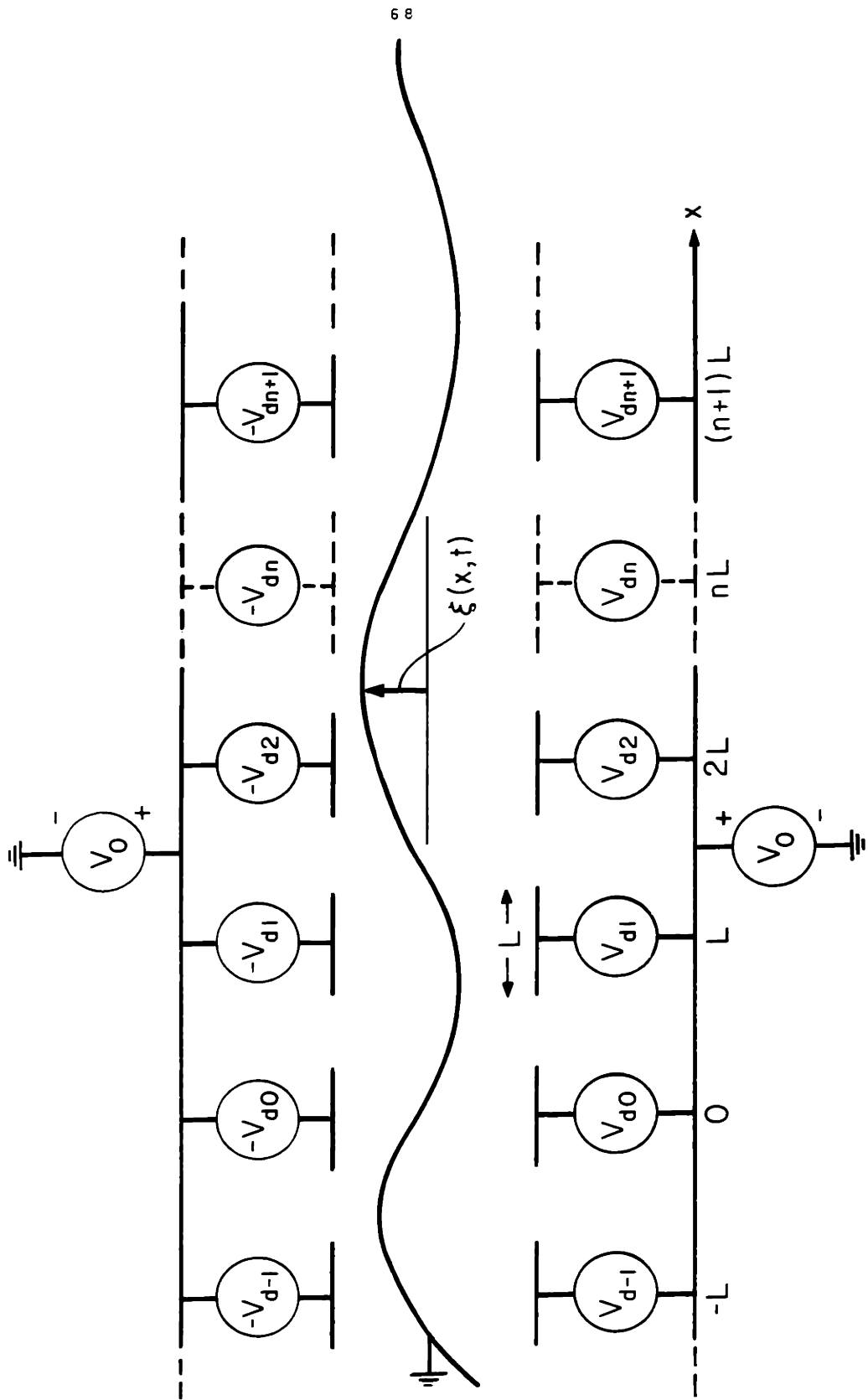


Figure 3.1 The unbounded electrically-stressed string, driven by a spatially discrete force

electrode segment.

Since the voltage on each electrode segment is a constant, the same force is applied to each point of the string adjacent to the electrode segment. The control voltage is, therefore, constant for the regions $(2n - 1)L/2 < x < (2n + 1)L/2$. A picture of the driving voltage that is produced by the electrode structure is shown in Figure 3.2. The transfer function which relates the deflection of the string to the driving force may be found by taking the Fourier transform in space and the Laplace transform in time of Eq. (3.1) to obtain

$$\Xi(k,s) \left[\frac{1}{v_p} 2s^2 + k^2 + \beta s - k_c^2 \right] = g v_d(k,s) \quad (3.2)$$

It is mathematically convenient to normalize the length of an electrode to one by defining the following dimensionless variables:

$$S = \frac{Ls}{v_p} \quad (3.3a)$$

$$K = kL \quad (3.3b)$$

$$\delta = \beta v_p L \quad (3.3c)$$

$$N = k_c^2 L^2 \quad (3.3d)$$

$$f(x,t) = L^2 g v_d(x,t) \quad (3.3e)$$

The transformed equation may now be written as

$$\Xi(K,S) = \frac{1}{S^2 + \delta S + K^2 - N} F(K,S) \quad (3.4)$$

and the transfer function for the string is

$$H(K,S) = \frac{1}{S^2 + \delta S + K^2 - N} \quad (3.5)$$

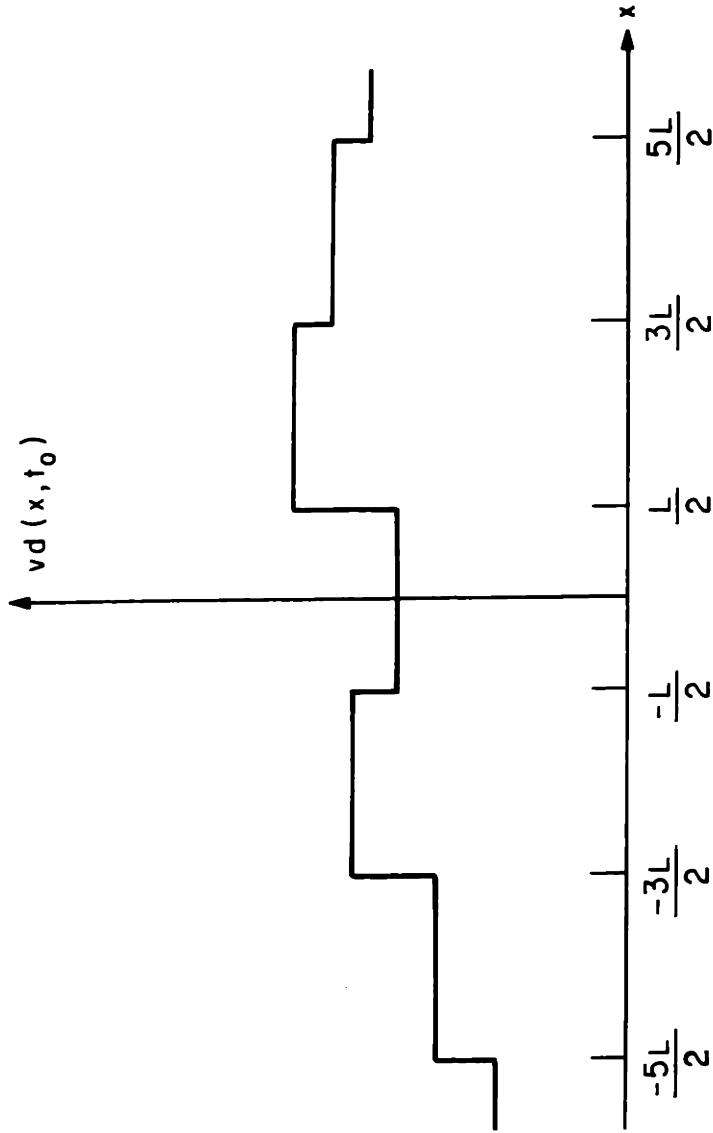


Figure 3.2 The segmented electrode applies a spatially discrete voltage to the string.

The control scheme used for this system measures the deflection of the string at the center of each electrode. A restoring force is then generated to drive the sampled deflection to zero. This control scheme may be thought of as 'spatially sampling' the deflection and feeding this signal back to the string by means of a 'spatial filter', the driving electrodes. Some other sampling schemes may be easier to implement on a real system and could provide better control than the scheme studied here. For example, Melcher and Warren (November 1966), measured the average deflection of a fluid surface by measuring the capacitance between the fluid and the driving electrode. However, when the average deflection is sampled, the system is mathematically more complicated than when the deflection is sampled. Since the purpose of this chapter is only to illustrate the techniques for analyzing discrete spatial feedback, the mathematically simplest case is studied.

The system is complicated because the driving force $f(x,t)$ is spatially discrete and its transform, $F(K,S)$, is not simple to find. The method of generating a closed-loop transfer function from the open-loop function in Eq. (3.4) is not obvious. In the following sections, Z transforms will be used to overcome these difficulties.

3.3 Transforms of Spatially Sampled Signals

Detection Scheme: Spatial Sampling

The detection scheme incorporated in this system measures or 'spatially samples' the string's deflection at the center of each electrode; that is, at the points $x = 0, \pm 1, \pm 2, \dots$. The measuring circuit does not obtain any information about the string between the sampling points, and therefore the sampled deflection is zero for these regions. This

sampled deflection can be thought of as impulse sheets, parallel to the t axis and spaced at regular intervals along the x axis. These impulse sheets are located at the sampling points on the x axis. The variation of the amplitude along the t axis gives the amplitude of the deflection as a function of time at the sampling points.

The spatially-sampled deflection, ξ^* , can be written as a product of the deflection and a train of impulse sheets:

$$\xi^*(x,t) = \xi(x,t) \sum_{n=-\infty}^{+\infty} u_0(x-n) \quad (3.6)$$

The limits of this summation are different from those of the summation in Eq. (2.6). Causality does not apply to waves traveling in space and a disturbance can travel in the negative x direction as well as in the positive x direction.

The process of generating the spatially-sampled signal can be represented by the network shown in Figure 3.3. The spatially continuous output is multiplied by an impulse train $i^*(x)$, to produce the spatially-sampled signal.

Double-Sided Z Transforms: D Transforms

When the Fourier-LaPlace transform of a spatially sampled signal is calculated, it must be remembered that a disturbance can propagate either to the left or right on the x axis. This complication does not appear in Chapter II when time sampling was considered, because disturbances can travel only forward in time.

The method of generating the transform by means of a Laurent series illustrates the problems of the double-sided transform. For example,

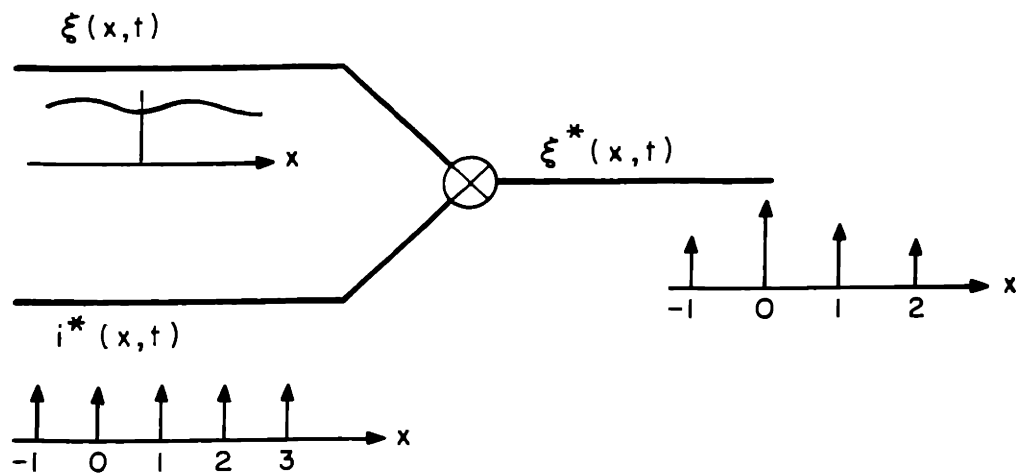


Figure 3.3 The spatially-sampled output is produced by multiplying the deflection by a spatial impulse train.

take the case in which the disturbance can be broken up into a function of t and a function of x . For this case, the deflection and its transform can be written as

$$\xi(x,t) = \psi(x) \phi(t) \quad (3.7)$$

$$\Xi(K,S) = \Psi(K) \Phi(S) \quad (3.8)$$

Equation (3.6) can be rewritten as

$$\xi^*(x,t) = \phi(t) \sum_{n=-\infty}^{\infty} \psi(x) u_0(x-n) \quad (3.9)$$

The transform of Eq. (3.9) can be seen to be

$$\Xi^*(K,S) = \Phi(S) \sum_{n=-\infty}^{\infty} \psi(n) e^{-jKn} \quad (3.10)$$

The discrete spatial wavenumber, D , is now defined as

$$D = e^{-jK} \quad (3.11)$$

and Eq. (3.10) becomes a Laurent series in terms of D . This series is broken up into two series: one in positive powers of D , one in negative powers of D .

$$\Xi^*(K,S) = \Phi(S) \left[\sum_{n=-\infty}^{-1} \psi(n) D^n + \sum_{n=+1}^{\infty} \psi(n) D^n + \psi(0) \right] \quad (3.12)$$

These two series in (3.12) will probably converge for various values of D . The problem which may happen is that no value of D exists which allows both of the series of Eq. (3.12) to converge, and a closed-form of the equation does not exist. An example of this situation is when the spatial function $\psi(n)$ increases in both directions away from the origin.

The problem caused by the series of Eq. (3.12) not converging when the disturbances grow in space as one moves away from the origin will be covered in Chapter V. For this chapter, this problem will be ruled out by physical considerations. It is known that non-convecting systems like the string do not support amplifying waves or waves that grow in space. Therefore, Eq. (3.12) is assumed to converge for some value of D to give

$$\Xi(D,S) = \Phi(S) \Psi(D) \quad (3.13)$$

which is the transform of the spatially-discrete function in terms of the discrete spatial wavenumber D , and the continuous temporal frequency S .

A second method of generating the transform of the spatially-sampled function is to use the method of convolution in the K - S plane. This method is similar to that used in Chapter II, but the fact that the disturbances can travel either direction on the x axis makes the problem more difficult.

The Fourier-LaPlace transform of the disturbance on the string can usually be broken up by a partial fraction expansion into two terms; one term represents the disturbance which travels to the left, the other represents the disturbance traveling to the right.

$$\Xi(K,S) = \Xi_+(K,S) + \Xi_-(K,S) \quad (3.14)$$

The part of the disturbance that travels on the positive x axis will be sampled by an impulse train that starts at zero and exists on the positive x axis. That part of the disturbance that travels on the negative x axis will be sampled by an impulse train that exists on the negative x axis.

Since the sampling process is the same as multiplying the continuous deflection by an array of impulses in space, the transform of the sampled function can be found by convolving the transforms of the continuous function and the impulse train.

$$\Xi^*(K,S) = \Xi_+(K,S) \otimes I_+(K,S) + \Xi_-(K,S) \otimes I_-(K,S) \quad (3.15)$$

where
$$I_+(K,S) = \frac{1}{1 - e^{-jK}} u_0(S) \quad (3.16)$$

and

$$I_-(K,S) = \frac{1}{1 - e^{jK}} u_0(S) \quad (3.17)$$

are the transforms of the sampling function on the positive x axis and negative x axis, respectively.

Writing out the convolution integrals of Eq. (3.15) gives

$$\begin{aligned} \Xi^*(K,S) = & \frac{1}{2\pi} \int_{-\infty}^{+\infty} \Xi_+(Q,S) \left[\frac{1}{1 - e^{-j(K-Q)}} \right] dQ \\ & + \frac{1}{2\pi} \int_{-\infty}^{+\infty} \Xi_-(Q,S) \left[\frac{1}{1 - e^{+j(K-Q)}} \right] dQ \end{aligned} \quad (3.18)$$

The first of these integrals is represented in Figure 3.4a and the second in Figure 3.4b. If these integrals are both performed on the paths labeled C_1 , an infinite number of poles of the sampling function are enclosed.

The result is

$$\Xi^*(K,S) = \sum_{n=-\infty}^{+\infty} [\Xi_+(K - 2n\pi, S) + \Xi_-(K - 2n\pi, S)] \quad (3.19)$$

This is the form of the transform for the sampled displacement which was

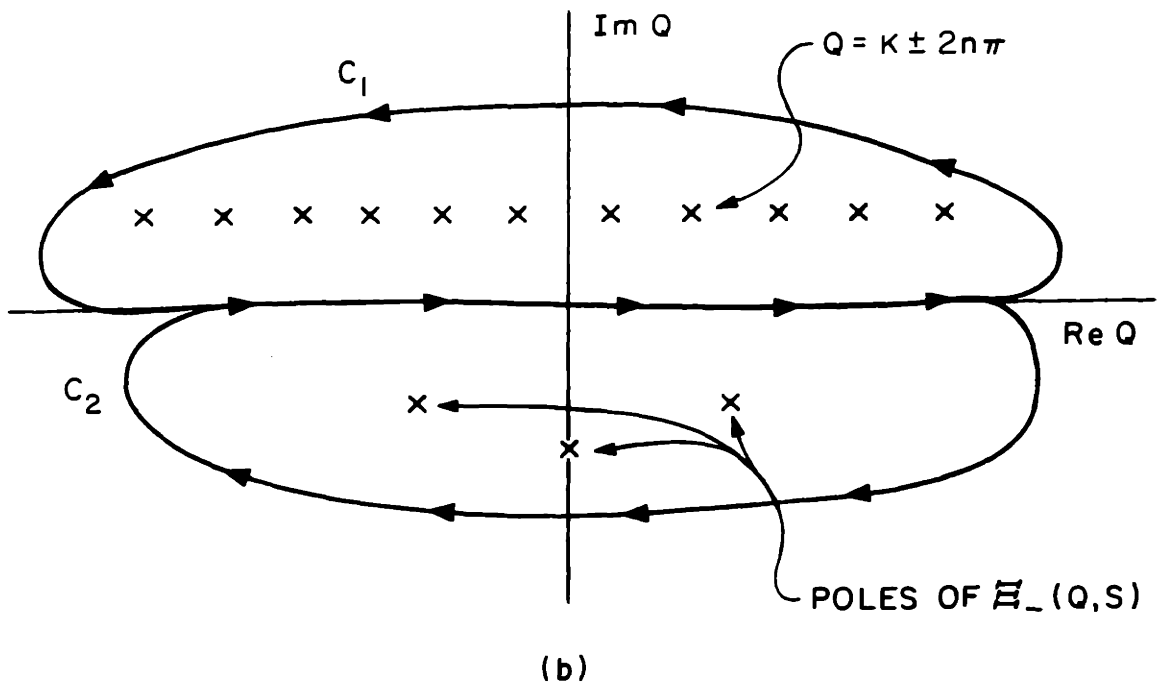
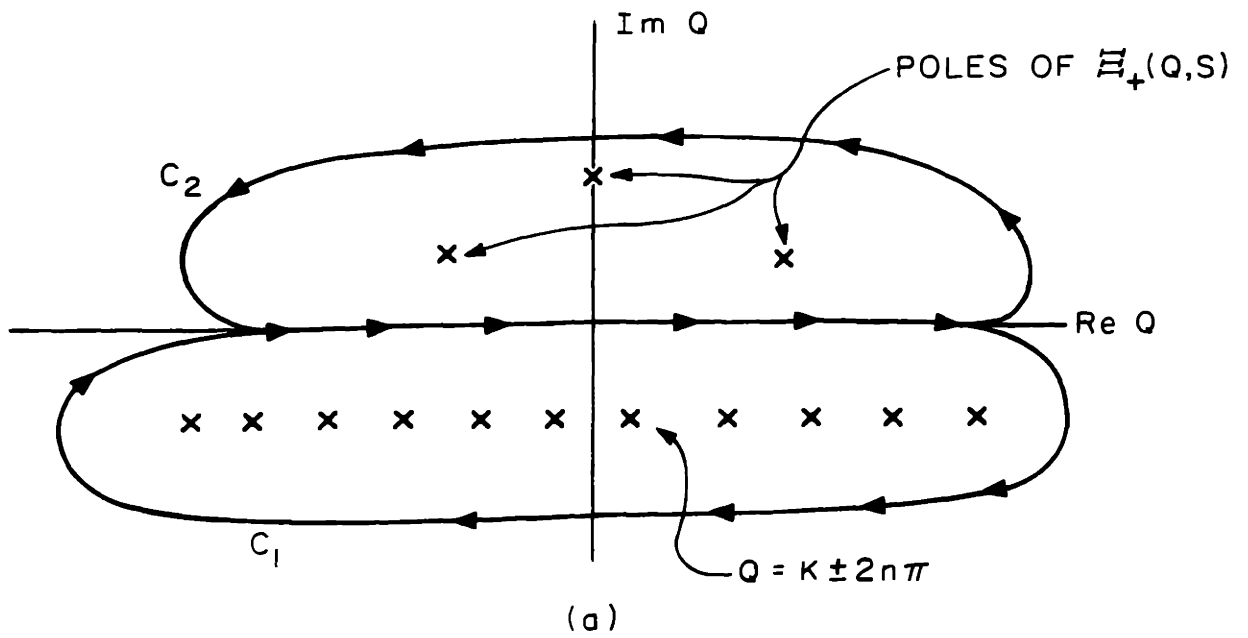


Figure 3.4 Possible contours of integration for the transform of a spatially-sampled function

used by Melcher (May, 1965). It results in a dispersion equation for the system which is an infinite series, and calculations for stability are cumbersome.

If the number of poles of Ξ_+ and Ξ_- are finite, then a closed-form expression for $\Xi^*(K,S)$ can be obtained. Integrating around the contours C_2 gives

$$\begin{aligned} \Xi(K,S) = & \sum_{\text{Poles of } \Xi_+} \text{Residues} \left(\Xi_+(Q,S) \frac{1}{1 - e^{-j(K-Q)}} \right) - \frac{1}{2} \xi_+(0,S) \\ & - \sum_{\text{Poles of } \Xi_-} \text{Residues} \left(\Xi_-(Q,S) \frac{1}{1 - e^{j(K-Q)}} \right) - \frac{1}{2} \xi_-(0,S) \quad (3.20) \end{aligned}$$

The two terms $\hat{\xi}_+(0,S)$ and $\hat{\xi}_-(0,S)$ represent the LaPlace transform of the value of the two waves at $x = 0$. Whenever the disturbances traveling to the left or right have a step discontinuity at $x = 0$, the value of the integral on the semicircular path, C_2 , is not zero, but is equal to one-half of the jump at $x = 0$. Physically, these terms appear because the sampling pulse at zero will detect only one-half of the value of the step.

This form of the transform of the sampled function is the Z transform. By using the discrete spatial wavenumber D , which is defined in Eq. (3.11), Eq. (3.20) can be rewritten as

$$\Xi^*(K,S) = \Xi(D,S) \quad (3.21)$$

The transform of the spatially-sampled function has now been obtained in closed form in terms of the continuous temporal frequency S , and of the discrete spatial wavenumber D .

Equivalence of Double- and Single-Sided Transforms

In the previous section, it was assumed that the Fourier-LaPlace transform of a function could be broken up into two terms, one representing the wave traveling to the left, the second representing the wave traveling to the right. In cases where convection is present and amplifying or evanescent waves may occur, it is difficult to decide whether a certain root of the transform corresponds to a left- or right-traveling wave. To make the separation called for in (3.14) properly, it is necessary to use the Bers-Briggs criterion (Briggs, Chapter 2).

Fortunately, a simpler method of obtaining the double-sided discrete transform is available. If all disturbances are assumed to travel to the right, and the single-sided discrete transform is computed, the proper mathematical form of the double-sided discrete transform is obtained. The problem with this method is that the region of analyticity of the resulting transform is not known, and the transform cannot be inverted to achieve the spatial functions.

To show that the same discrete transform is arrived at if a left-traveling wave is assumed to travel to the right, the following method is used. Assume that a disturbance which travels to the left is launched on some system. From Eq. (3.18), the discrete transform of this disturbance is obtained from the transform of the disturbance's impulse response by

$$\Xi^*(K,S) = \frac{1}{2\pi} \int_{-\infty}^{+\infty} \Xi_L(Q,S) \left[\frac{1}{1 - e^{j(K-Q)}} \right] dQ \quad (3.22)$$

This integral is closed on the right, to enclose only the poles of $\Xi_L(Q,S)$.

The result is

$$\Xi^*(K,S) = - \sum_{\text{Poles of } \Xi_L} \text{Residue} \left[\frac{\Xi_L(Q,S)}{1 - e^{j(K-Q)}} \right] - \frac{1}{2} \hat{\xi}_L(0,S) \quad (3.23)$$

The right side of (3.23) may be rearranged to give:

$$\begin{aligned} & - \sum_{\text{Poles of } \Xi_L} \text{Residue} \left[\frac{\Xi_L(Q,S)}{1 - e^{j(K-Q)}} \right] - \frac{1}{2} \hat{\xi}_L(0,S) \\ &= \sum_{\text{Poles of } \Xi_L} \text{Residue} \left[\frac{\Xi_L(Q,S) e^{-j(K-Q)}}{1 - e^{-j(K-Q)}} \right] - \frac{1}{2} \hat{\xi}_L(0,S) \end{aligned} \quad (3.24)$$

The summation on the right side of Eq. (3.24) is the transform that results if Ξ_L represents a right-traveling wave which is sampled by an impulse train whose impulse at zero is missing. That is the impulse train shown in Figure 3.5. The information in a right-traveling wave at $x = 0$ is not detected by this sampling function. One half of the value of the disturbance at the origin is, therefore, missed by this sampling function.

The value of $\xi(0,t)$, which results from assuming $\Xi_L(K,S)$ represents a wave traveling to the left, is the negative of the value of $\xi(0,t)$ which results if $\Xi_L(K,S)$ represents a wave traveling to the right. That is

$$\frac{1}{2} \hat{\xi}_L(0,S) = - \frac{1}{2} \hat{\xi}_R(0,S) \quad (3.25)$$

where $\hat{\xi}_R(0,S)$ is the value at zero of the right-traveling wave. Equation (3.25) allows the right side of (3.24) to be changed to

$$\begin{aligned} & \sum_{\text{Poles of } \Xi_L} \text{Residues} \left[\frac{\Xi_L(Q,S) e^{-j(K-Q)}}{1 - e^{-j(K-Q)}} \right] - \frac{1}{2} \hat{\xi}_L(0,S) \\ &= \sum_{\text{Poles of } \Xi_L} \text{Residues} \left[\frac{\Xi_L(Q,S) e^{-j(K-Q)}}{1 - e^{-j(K-Q)}} \right] + \hat{\xi}_R(0,S) - \frac{1}{2} \hat{\xi}_R(0,S) \end{aligned} \quad (3.26)$$

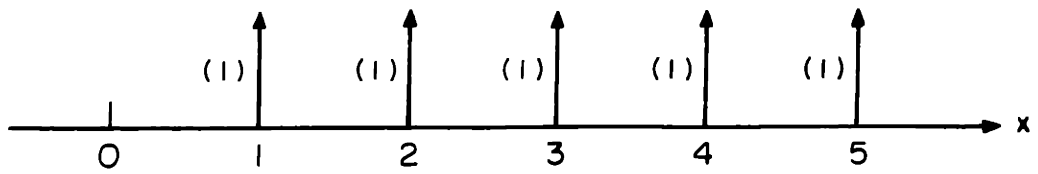


Figure 3.5 The impulse train which produces the transform given in Eq. (3.24)

The term $\hat{\xi}_R(0,S)$ can be incorporated into the summation; then, Eq. (3.23) becomes

$$\Xi^*(K,S) = \sum_{\text{Poles of } \Xi_L} \text{Residues} \left[\frac{\Xi_L(Q,S)}{1 - e^{-j(K-Q)}} \right] - \frac{1}{2} \hat{\xi}_R(0) \quad (3.27)$$

Comparison of Eq. (3.27) with (3.20) shows that the discrete transform of the left-traveling wave represented by Ξ_L can be juggled into the same form which results if Ξ_L represents a right-traveling wave. This result is very important for finding the transform of a sampled function that may be traveling either in the positive or negative x direction. What it means is that the transform of the discrete function may be found from the transform of the continuous function by using the formula

$$\Xi^*(K,S) = \frac{1}{2\pi} \int_{-\infty}^{+\infty} \frac{\Xi(Q,S) dQ}{1 - e^{-j(K-Q)}} \quad (3.28)$$

This simplifies finding the discrete transforms, because it is not necessary to break up the transform of the continuous function, as was done in Eq.(3.14). By convolving the transform of the continuous function with the transform of an impulse train that exists only for $x \geq 0$, the correct discrete transform will be obtained.

Inverse D Transform

There are two convenient methods of recovering the spatially sampled signal from its D transform. The first is to expand the transform into a Laurent series in terms of D. This is the reverse of the step taken in Eqs. (3.12) and (3.13).

$$\Xi(D,S) = \Phi(S) \sum_{n=-\infty}^{+\infty} \psi(n) D^n \quad (3.29)$$

The individual terms in this expansion represent the amplitude of the function at the sampling points. For complicated functions, this method is not convenient, except for low values of n .

The second method for recovering the spatially-sampled function is to use Cauchy's integral formula. This method allows a coefficient of any power of D in the Laurent expansion to be found without actually making the expansion. Cauchy's formula says that

$$\oint_{\Gamma} D^k dD = \begin{cases} 2\pi j & k = -1 \\ 0 & k \neq -1 \end{cases} \quad (3.30)$$

If the expansion of $\Xi(D,S)$ is multiplied by $D^{-(n+1)}$, the result is:

$$D^{-(n+1)} \Xi(D,S) = \Phi(S) \left[\dots \frac{\psi(n-1)}{D^2} + \frac{\psi(n)}{D} + \psi(n+1) + D\psi(n+2) + \dots \right] \quad (3.31)$$

If this series is integrated about $D = 0$ on a contour on which $\Psi(D)$ is analytic, the result is

$$\oint_{\Gamma} D^{-(n+1)} \Xi(D,S) dD = 2\pi j \Phi(S) \psi(n) \quad (3.32)$$

Rearrangement gives

$$\Phi(S) \psi(n) = \frac{1}{2\pi j} \oint_{\Gamma} D^{-(n+1)} \Xi(D,S) dD \quad (3.33)$$

or

$$\Phi(S) \psi(n) = \sum \text{Residues of } \frac{\Xi(D,S)}{D^{n+1}} \text{ inside } \Gamma \quad (3.34)$$

This derivation assumed that the deflection was separable. This restriction was made only to make the derivation easier to understand. The more general inverse transform can be written as

$$\hat{\xi}(n, S) = \frac{1}{2\pi j} \oint_{\Gamma} D^{-(n+1)} \Xi(D, S) dD \quad (3.35)$$

where $\hat{\xi}(n, S)$ is the LaPlace transform in time of the spatially sampled signal at $x = n$.

Ambiguity of Inverse D Transforms

A problem occurs when either of the two methods is used to recover the original spatial function from a double-sided transform. This problem is: the region of analyticity of the transform must be known to invert the transform properly. The Laurent expansion in Eq. (3.29) is not unique, and the number of poles enclosed in Eq. (3.35) by Γ is not known unless the analytical region is specified.

A modified form of the Bers-Briggs criterion is presented in Chapter V. With this criterion, the region of analyticity for the double-sided transforms can be determined, and the transforms can be inverted. For the case of no convection that is studied in this chapter, the modified Bers-Briggs criterion shows that the region of analyticity includes the real K axis. When the transform is analytic for real K , the value of Γ for Eq. (3.35) is the unit circle, and the region of analyticity for the Laurent expansion of Eq. (3.29) is the unit circle. With this information the stability of the non-convecting system studied in this chapter may be determined. When convection is present, finding the proper contour for Γ is difficult, because amplifying waves may possibly exist. This problem is studied in detail in Chapter V.

3.4 Open-Loop Transfer Function

The Electrode as a Spatial Sample-and-Hold Filter

The electrode segment, which drives the string, applies a constant force to the adjacent section of the string and no force to the remainder of the string. This electrode, with its attached wire, may be thought of as a spatial network which takes a signal that exists at only one point on the x axis, the connecting wire, and spreads it out over the length of the electrode segment. This network is the spatial equivalent to the sample-and hold filter which was used in Chapter II, and is illustrated in Figure 3.6.

The signal on the wire is considered to be a spatial impulse whose area is proportional to the voltage on the wire. The filter produces a voltage pulse of a fixed width on the x axis, the amplitude of which is proportional to the impulse area. The force applied to the entire string may be generated by this network if it is driven by a spatial impulse train. The area of each impulse corresponds to the signal fed to each electrode segment by a wire. The resultant output is the force $f(x,t)$, applied to the string. This process is illustrated in Figure 3.7.

Transfer Function of a Spatially Discrete System

The string, with its driving electrodes, can be thought of as a system which accepts a spatially discrete input, and produces an output that is continuous in space and time. The control system does not see the continuous deflection, however; it sees only the measured or 'spatially sampled' value of the deflection. The system, as seen by the control system, is illustrated in Fig. 3.8. The signals on the wires connected to the electrode segments are pictured as the impulse train $u^*(x,t)$. The electrode segments are driven by this impulse train, and produce the spatially discrete forcing function, $f(x,t)$. This function drives the

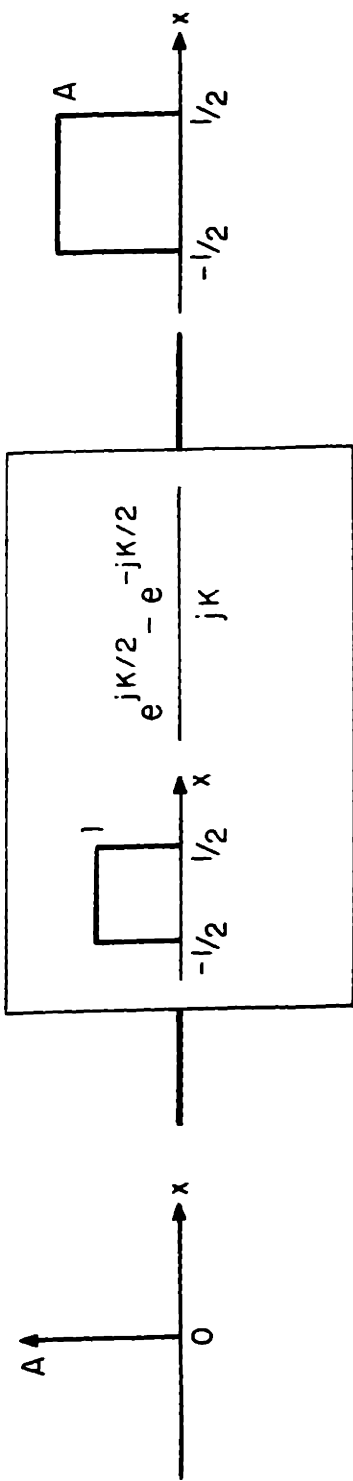


Figure 3.6 A spatial impulse is applied to the electrode segment to produce a spatially constant force.

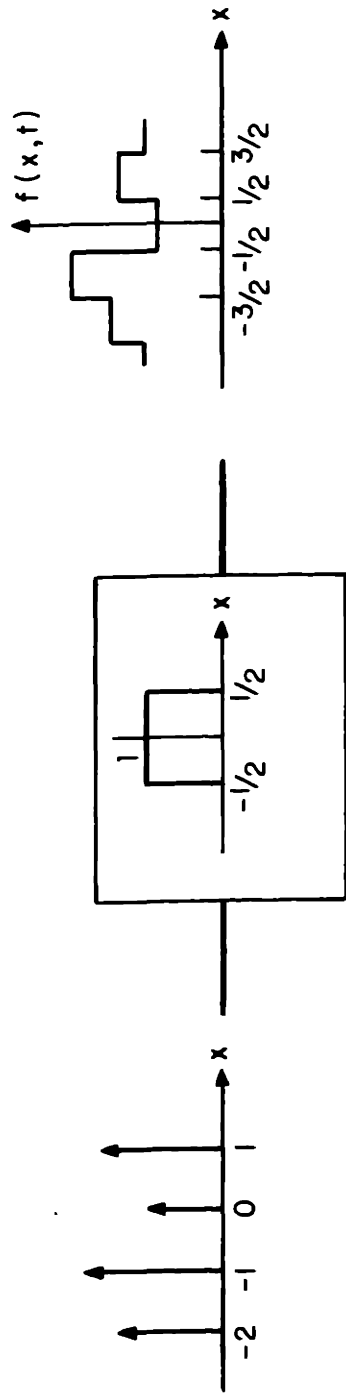


Figure 3.7 The spatially discrete driving force is generated by driving the sample-and-hold filter by an impulse train.

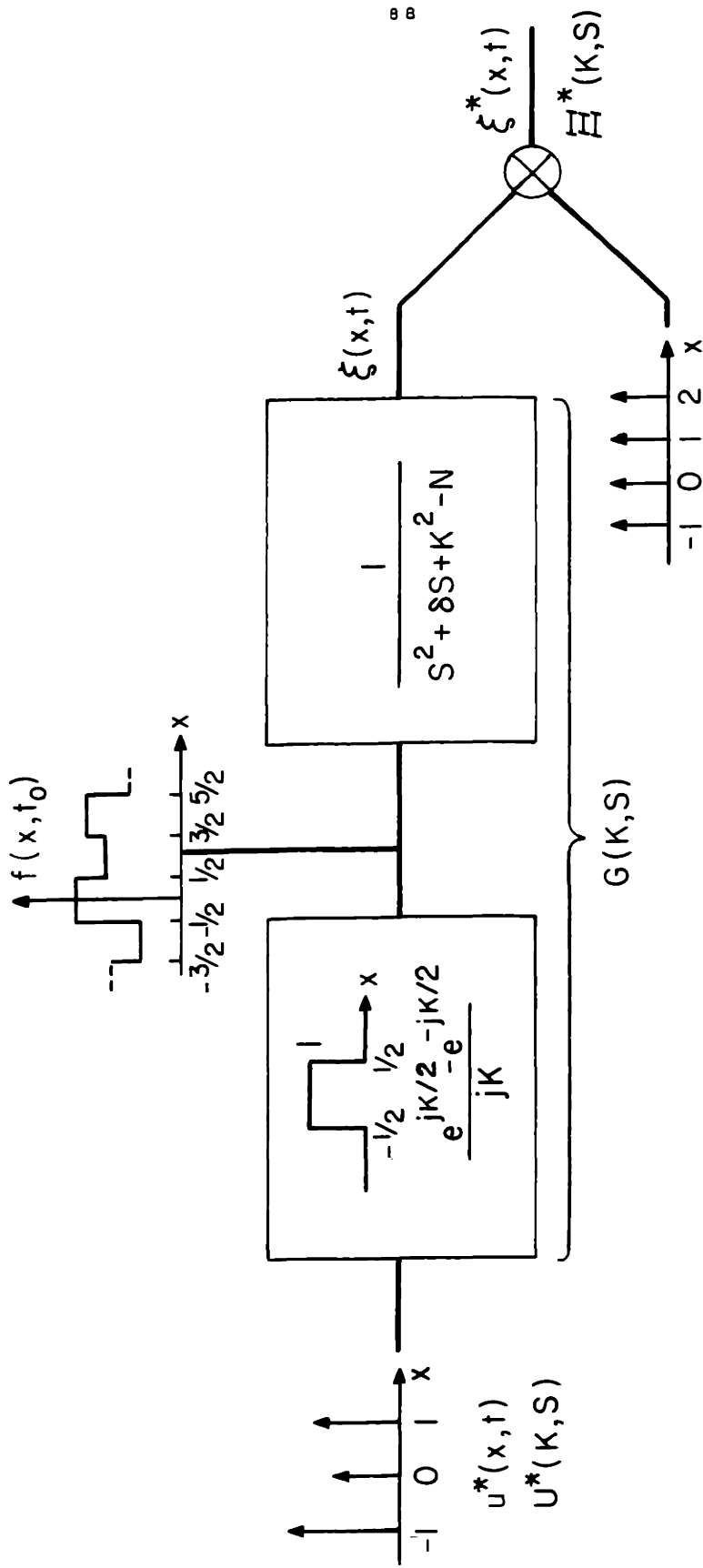


Figure 3.8 The electrode segments, string, and sensors are a system which accepts a spatially-sampled input and produces a spatially-sampled output.

string to produce the spatially continuous deflection $\xi(x,t)$. The detection system then measures the deflection at regular intervals, to produce the spatially discrete output $\xi^*(x,t)$.

It is convenient to have a transfer function that relates the discrete output to the discrete input. This transfer function can be found by finding the transform of the continuous output in terms of the transform of the input:

$$\Xi(K,S) = U^*(K,S)G(K,S) \quad (3.36)$$

By using Eq. (3.19), the transform of the spatially sampled output is found to be

$$\Xi^*(K,S) = \sum_{n=-\infty}^{+\infty} U^*(K + 2n\pi, S) G(K + 2n\pi, S) \quad (3.37)$$

Since $U^*(K,S)$ represents a sampled function, Eq. (3.19) can be used to get

$$U^*(K,S) = \sum_{n=-\infty}^{+\infty} U(K + 2n\pi, S) \quad (3.38)$$

Equation (3.38) shows that $U^*(K,S)$ is periodic in K with a period of 2π .

Therefore,

$$U^*(K + 2n\pi, S) = U^*(K, S) \quad (3.39)$$

and (3.37) can be written as

$$\Xi^*(K,S) = U^*(K,S) \sum_{n=-\infty}^{+\infty} G(K + 2n\pi, S) \quad (3.40)$$

From Eq. (3.40), the transfer function relating the spatially discrete input and output is the transform of the spatially sampled response

of the system to an impulse at $x = 0$. From Eqs. (3.19) and (3.28), this discrete transfer function is

$$G^*(K,S) = G(D,S) = \frac{1}{2\pi} \int_{-\infty}^{+\infty} \frac{G(Q,S)dQ}{1-e^{-j(K-Q)}} \quad (3.41)$$

With the discrete transfer function, $G(D,S)$, Figure 3.8 can be condensed to the simple open-loop system shown in Figure 3.9.

Evaluation of Open-Loop Transfer Function

The continuous transfer function, $G(K,S)$, is the product of the transfer functions of the electrodes and the string

$$G(K,S) = \underbrace{\frac{e^{jK/2} - e^{-jK/2}}{jK}}_{\text{electrodes}} \underbrace{\frac{1}{S^2 + \delta S + K^2 - N}}_{\text{string}} \quad (3.42)$$

A partial fraction expansion of $G(K,S)$ gives

$$G(K,S) = \frac{e^{jK/2} - e^{-jK/2}}{j} \left[\frac{-1}{\frac{2(S^2 + \delta S - N)}{K + j(S^2 + \delta S - N)^{1/2}} + \frac{-1}{\frac{2(S^2 + \delta S - N)}{K - j(S^2 + \delta S - N)^{1/2}}} \right] + \frac{1}{K(S^2 + \delta S - N)} \quad (3.43)$$

When Eq. (3.41) is used to find the discrete transfer function, a problem arises that must be solved by a physical argument. This problem is illustrated by the convolution of the first term on the right of Eq. (3.43)

$$G_1^*(K,S) = \frac{-1}{2\pi} \int \frac{e^{jQ/2} - e^{-jQ/2}}{2j(S^2 + \delta S - N)} \frac{dQ}{[Q + j(S^2 + \delta S - N)^{1/2}][1 - e^{-j(K-Q)}]} \quad (3.44)$$

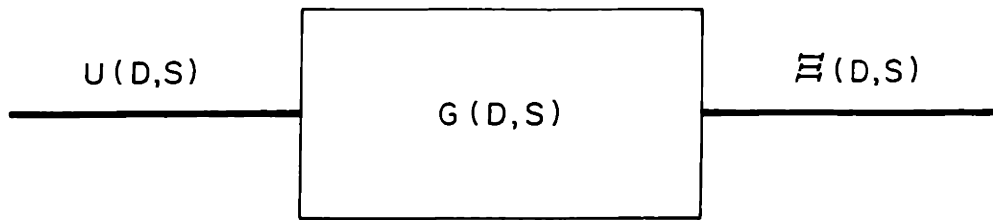


Figure 3.9 The electrodes, string, and sensors can be represented by a discrete transfer function.

Path I is the desired path of integration in Figure 3.10 because there is a finite number of poles encircled and a closed-form solution is obtained for the integral. However, the term $e^{-jQ/2}$ goes to infinity for large, imaginary values of Q , and this integral blows up. This problem can be overcome by realizing that $e^{-jQ/2}$ represents a delay in the generated wave. Since the wave is sampled, any delay will cause delays in the sampled function of at least one sampling period. By removing an integer delay from the sampling term, the integral is changed to

$$G_1^*(K, S) = \frac{-(1-e^{-jK})}{2\pi} \int_{-\infty}^{+\infty} \frac{e^{jQ/2} dQ}{2j(S^2 + \delta S - N) [Q + j(S^2 + \delta S - N)^{1/2}] [1 - e^{-j(K-Q)}]} \quad (3.45)$$

Closing this integral on Path I of Figure 3.10, and using the discrete wavenumber D gives

$$G_1(D, S) = \frac{-(1-D) e^{\frac{1}{2}(S^2 + \delta S - N)^{1/2}}}{2(S^2 + \delta S - N) [1 - De^{(S^2 + \delta S - N)^{1/2}}]} \quad (3.46)$$

The same procedure can be repeated for the other terms of Eq. (3.43), and the discrete transfer function is

$$G(D, S) = \frac{e^{-\frac{1}{2}W}}{2W^2} \left[\frac{(1-D)^2 (1+e^{-W})}{D(1+e^{-2W}) - (D^2 + 1)e^{-W}} \right] + \frac{1}{W^2} \quad (3.47)$$

where

$$W = (S^2 + \delta S - N)^{1/2} \quad (3.48)$$

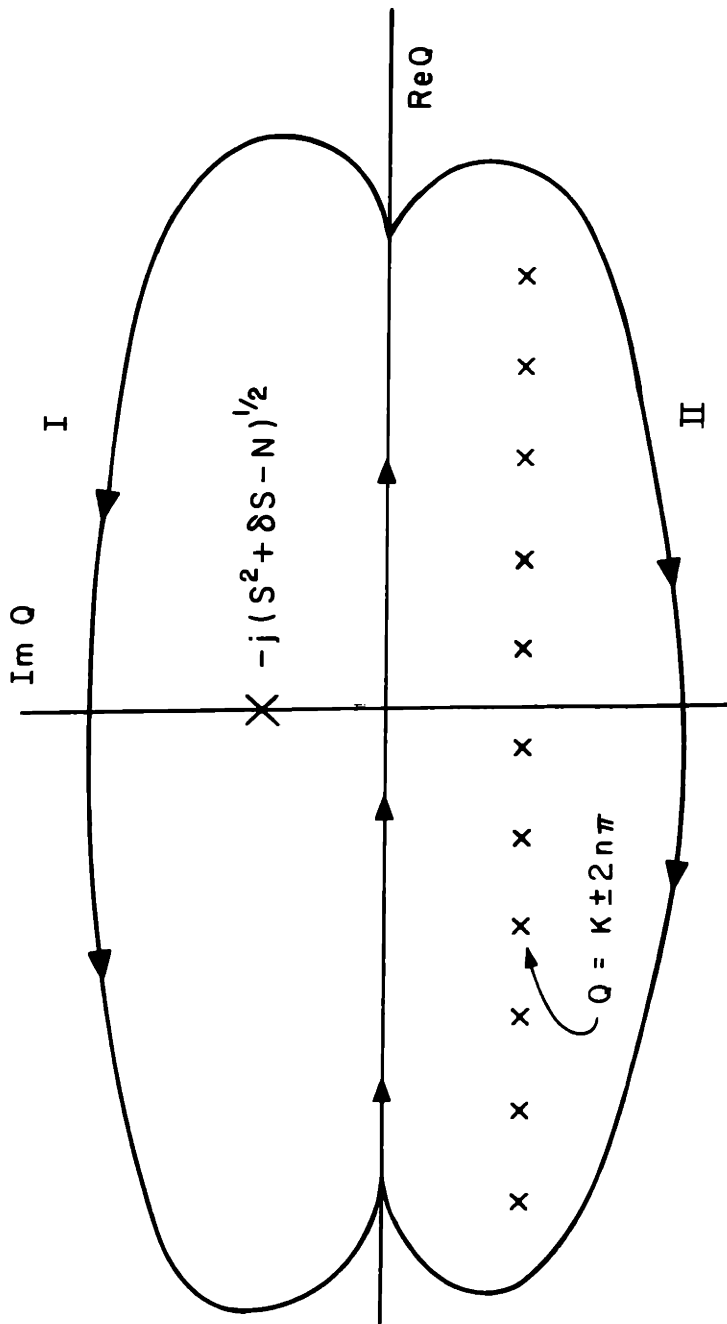


Fig. 3.10 Possible contours of integration for finding $C_1(D.S)$

3.5 Closed-Loop System

Closed-Loop Transfer Function

The purpose of the feedback system is to apply a restoring force to the string that will make all deflections stable. The method of generating the feedback signal used here is to apply a voltage to an electrode segment that is proportional to the displacement at the middle of the electrode. The polarity of the voltage is such that the force tries to drive the displacement to zero. Schematically, this feedback process is illustrated in Figure 3.11. The transfer function of the servo-loop is

$$\frac{\Xi(D,S)}{U(D,S)} = \frac{G(D,S)}{1+AG(D,S)} \quad (3.49)$$

The gain A can have some frequency compensation as in conventional servo theory, and it can also have some compensation dependent on the discrete wavenumber, D. However, this chapter serves only to illustrate the method for analyzing a discrete spatial feedback system, and therefore only the simplest case of constant feedback is considered.

D-S Dispersion Relation

To determine the stability of the closed-loop system, it is necessary to find the natural frequencies of the system. These are found by setting the denominator of the closed-loop function equal to zero. Using Eqs. (3.47) and (3.48), this dispersion relation is found to be

$$2(W^2 + A)[D(1 + e^{-2W}) - (D^2 + 1)e^{-W}] + A[(e^{-\frac{3}{2}W} + e^{-\frac{1}{2}W})(D^2 - 2D + 1)] = 0 \quad (3.50)$$

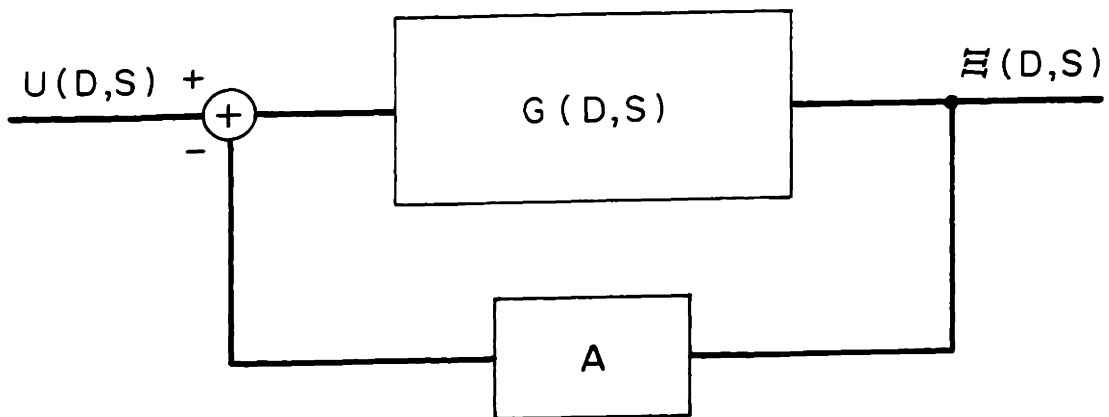


Figure 3.11 Servo-loop representation of the spatially sampled string with feedback

With this dispersion equation, the discrete spatial wavenumbers of a disturbance can be found as a function of the frequency, S . It is important to notice that this equation is second-order in D and that the denominator of the spatially continuous transfer function was of second order in K . The use of Z -transform theory has allowed a dispersion equation to be obtained for a system with discrete spatial feedback which is only slightly more complicated than the dispersion equation for the continuous spatial case.

Comparison of Z Transforms and Wave-train Analysis

Melcher (May 1965) has analyzed this same system by another method, and has achieved a dispersion equation that appears to be different from the dispersion Eq. (3.50). In this section it is shown that Melcher's dispersion equation is merely a different form of the one derived here. The transfer function $G(D,S)$ is expanded into a series of poles of the variable W , which was defined in Eq. (3.48). If this form of the transfer function is used in (3.49), Melcher's dispersion equation is obtained.

The method of expanding a meromorphic function into a series of poles is given by Morse and Feshback (pp. 382 - 385.) By their method, $G(D,W)$ will be made into a series of the form

$$G(D,W) = \text{constant} + \sum_{n=-\infty}^{+\infty} \frac{b_n}{W - a_n} \quad (3.51)$$

By letting W go to zero, the constant can be evaluated, and Eq. (3.51) rewritten as

$$G(D,W) = G(D,W=0) + \sum_{-\infty}^{\infty} \left(\frac{b_n}{W - a_n} + \frac{b_n}{a_n} \right) \quad (3.52)$$

The value of $G(D, W=0)$ can be found by rewriting Eq. (3.47) as

$$G(D, W) = \frac{- (1-D)^2 \cosh(W/2) + (1-De^W)(1-De^{-W})}{W^2 (1 - De^W) (1 - De^{-W})} \quad (3.53)$$

This function is expanded about the point $W = 0$ and terms of second order are retained:

$$G(D, W) = \frac{- (1-D)(1 + W^2/8) + (1-D)^2 - DW^2}{W^2 (1 - D^2)} \quad (3.54)$$

Taking the limit as $W \rightarrow 0$ gives

$$G(D, 0) = \frac{1}{8} + \frac{\cos^2(K/2)}{4 \sin^2(K/2)} \quad (3.55)$$

The function $G(D, W)$ is now broken up into two functions defined as

$$f_1(W) = \frac{- (1 - e^{-jK}) e^{W/2}}{2W^2 (1 - e^{-jK} e^W)} \quad (3.56)$$

$$f_2(W) = \frac{- (1 - e^{-jK}) e^{-W/2}}{2W^2 (1 - e^{-jK} e^{-W})} \quad (3.57)$$

The poles of $f_1(W)$ are at

$$W = jK + 2n\pi j \quad (3.58)$$

and the poles of $f_2(W)$ are at

$$W = -jK - 2m\pi j \quad (3.59)$$

These poles are the values of a_n for Eq. (3.52). When W is close to one of these poles, the functions are approximately equal to

$$f_1(W) = \frac{j \sin(K/2) (-1)^{n+1}}{(K + 2n\pi)^2 (W - jk - 2n\pi j)} \quad (3.60)$$

$\lim_{W \rightarrow a_n}$

$$f_2(W) = \frac{j \sin(K/2) (-1)^m}{(K+2m\pi)^2 (W+jk+2mj\pi)} \quad (3.61)$$

$$\lim W \rightarrow a_n$$

the terms b_n , which are needed for Eq. (3.52), are the residues of the above two functions. With these values for b_n , Eq. (3.52) becomes

$$\begin{aligned} G(D,W) &= \frac{1}{8} + \frac{\cos^2(K/2)}{4 \sin^2(K/2)} + \sum_{n=-\infty}^{+\infty} \left[\frac{j \sin(K/2) (-1)^{n+1}}{(K+2n\pi)^2 (W-jK-2nj\pi)} + \frac{\sin(K/2) (-1)^{n+1}}{(K+2n\pi)^3} \right] \\ &+ \sum_{m=-\infty}^{+\infty} \left[\frac{j \sin(K/2) (-1)^m}{(K+2m\pi)^2 (W+jK+2mj\pi)} - \frac{\sin(K/2) (-1)^m}{(K+2m\pi)^3} \right] \end{aligned} \quad (3.62)$$

The terms of the two summations are combined by letting $n = m$ to give

$$\begin{aligned} G(K,w) &= \frac{1}{8} + \frac{\cos^2(K/2)}{4 \sin^2(K/2)} + \sum_{n=-\infty}^{+\infty} \frac{(-1)^n 2 \sin(K/2)}{(K+2n\pi) [W^2 + (K+2n\pi)^2]} \\ &- \sum_{n=-\infty}^{+\infty} \frac{2 \sin(K/2)^n (-1)^n}{(K+2n\pi)^3} \end{aligned} \quad (3.63)$$

This equation can be simplified if the second summation is put into closed form. Morse and Feshback (pp. 413-414) explain how this is done and the formula is

$$\sum (-1)^n h(n) = - \sum \text{residues of } \pi h(Z) \csc(\pi Z) \text{ at the poles of } h(Z) \quad (3.64)$$

For the series being summed here

$$h(n) = \frac{2 \sin(K/2)}{(2\pi)^3 (K/2\pi + n)^3} \quad (3.65)$$

and $h(Z)$ has a second-order pole at $Z = -K/2\pi$. Plugging Eq. (3.65) back into (3.64) gives

$$\sum_{n=-\infty}^{+\infty} \frac{(-1)^n 2 \sin(K/2)}{(K + 2n\pi)^3} = \frac{1}{8} + \frac{\cos^2(K/2)}{4 \sin^2(K/2)} \quad (3.66)$$

Equation (3.63) can now be simplified to the desired form of $G(D,W)$

$$G(D,W) = \sum_{n=-\infty}^{+\infty} \frac{(-1)^n 2 \sin(K/2)}{(K + 2n\pi) [W^2 + (K + 2n\pi)^2]} \quad (3.67)$$

Now that the transfer function of the spatially-sampled system has been made into an infinite series, Melcher's work must be juggled into the same form. In his paper, Melcher assumes that the spatial deflection of the string is of the form

$$\xi(x) = \sum_{q=-\infty}^{+\infty} A_q e^{j(K+2q\pi)x} + \sum_{q=-\infty}^{+\infty} A_q^* e^{-j(K+2q\pi)x} \quad (3.68)$$

With this solution, he derives an infinite set of equations for the amplitudes A_q .

$$A_q [(K + 2\pi q)^2 + S^2 + \delta S - N] + \frac{2A}{(K + 2\pi q)} \sum_{n=-\infty}^{+\infty} A_n (-1)^n \sin(K/2) \quad (3.69)$$

This equation appears different from the one in Melcher's paper because the length, ℓ , has been normalized to one, the long-wave limit has been used, and damping has been added. If Eq. (3.69) is divided by $(K + 2\pi q)^2 + S^2 + \delta S - N$, and multiplied by $\sin(K/2)(-1)^q$, the result is

$$A_q \sin(K/2)(-1)^q = \frac{-2A \sin(K/2)(-1)^q \sum_{m=-\infty}^{+\infty} A_m \sin(K/2)(-1)^m}{(K+2\pi q)[(S^2 + \delta S - N) + (K+2\pi q)^2]} \quad (3.70)$$

Adding together all of the equations represented by (3.70) gives

$$\sum_{m=-\infty}^{+\infty} A_m \sin(K/2)(-1)^m = \frac{-A \sum_{q=-\infty}^{+\infty} 2 \sin(K/2)(-1)^q \sum_{m=-\infty}^{+\infty} A_m \sin(K/2)(-1)^m}{(K+2\pi q)[(S^2 + \delta S - N) + (K+2\pi q)^2]} \quad (3.71)$$

If the summation $\sum_{m=-\infty}^{+\infty} A_m \sin(K/2)(-1)^m$ is considered to be a variable, Eq. (3.71) represents the servo-loop shown in Figure 3.12.

The open-loop transfer function of Figure 3.12, which has been derived from a wavetrain analysis, is the same as the transfer function given in Eq. (3.67). Therefore, the closed-loop dispersion equations, obtained from Z transforms and wavetrain techniques, are the same. The only difference between the dispersion equations is that the one obtained from the Z transform, Eq. (3.50), is the closed form of the dispersion equation generated by Melcher's wavetrain analysis, Eq. (3.71).

The fact that the wavetrain method and Z transforms give the same dispersion equation raises a question about the two methods. Melcher considered the continuous deflection of the string to be the system output; the Z transform assumes that the sampled deflection was the output of the system. The question that occurs is: where in Melcher's analysis is the information that determines the displacement between the sampling points? The answer is: this information is contained in the set of equations given by Eq. (3.69). With this set of equations, the amplitudes, A_q , of all of the various waves can be found and the deflection at any

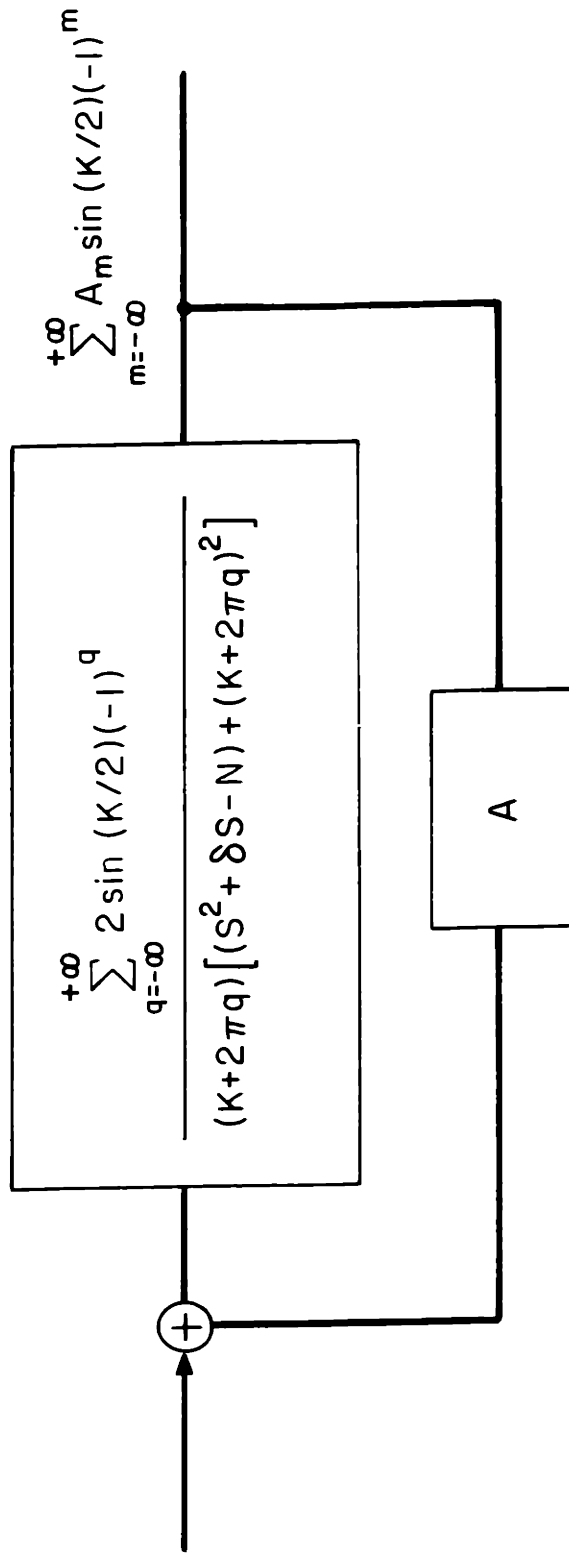


Figure 3.12 The servo-loop representation of the spatially discrete string which is obtained from the wave-train analysis

point in space can be generated. When all of these equations are added together to get Eq. (3.71), the relations between the various amplitudes are destroyed.

Therefore, the fundamental difference between the wavetrain analysis and the Z-transform analysis is the difference between the equations represented by (3.69) and (3.71). Equation (3.71) is the expansion of the Z transform, and there is no way of finding the various amplitudes A_q from this equation. Only the sum of the amplitudes, $\sum A_n \sin(K/2)(-1)^m$, can be found. When the set of Eqs. (3.68) is available, it is possible to determine the amplitudes A_q of the individual waves, and the entire deflection can be obtained.

Stability Criterion for the S-D Dispersion Equation

The stability criterion used with the dispersion equation given in Eq. (3.50) is the same criterion that is used for an $\omega - K$ dispersion equation. In general, the value of S (or ω) is found for all real values of K . If there is a real K for which the corresponding S has a positive real part, the system is unstable.

The discrete spatial frequency D has been defined as e^{-jK} . Thus, all real values of K correspond to all values of D on the unit circle. To determine the stability of the system from Eq. (3.50), the values of S are found for all values of D on the unit circle. If there is a value of D on the circle which gives a value of S with a positive real part, the system is unstable. This criterion actually is the same as solving for S for $0 \leq K \leq 2\pi$. All real values of K are not used. Equation (3.19) shows that the spatial sampling has made the transforms of this system periodic on the

K axis with a period of 2π . Therefore, using all values of K between 0 and 2π is equivalent to using all real values of K.

Results of Stability Analysis

The dispersion equation of the closed-loop system, Eq. (3.50), can be studied to find the values of the parameters which give stable operation. Values of N, δ , and D are picked and a root locus plot of S is constructed as a function of the gain. The values of gain for which the real part of S is not positive can be found on the root locus plot. This process must be repeated for all values of D on the unit circle to find the range of gain which gives stable operation for a given N and δ .

A portion of one of the root locus plots is shown in Figures 3.13. The parameters for this plot are $N = 4$, $D = e^j$ and $\delta = 0$. At zero gain, the system is unstable because there is a root at $S = +1.7$. As the gain is increased, the two roots on the real axis move to the imaginary axis and the string becomes stable. As the gain is increased more, the roots which began at $j4.9$ and $j7.0$ move together. When these two roots meet, they break away from the imaginary axis, and the string becomes overstable. Increasing the gain still more causes these roots to rejoin the imaginary axis and roots farther from the origin to break away from the imaginary axis. Thus, the overstability moves to higher frequencies as the gain is increased.

In Fig. 3.14, the effect of damping is illustrated. This plot has the same parameters as Fig. 3.13, except that the damping has been increased to 1. The roots now tend to move along the line $-\delta/2$ ($-\frac{1}{2}$) instead of the imaginary axis, as they did with no damping. It now takes more gain to force a root across the imaginary axis and to cause an overstability.

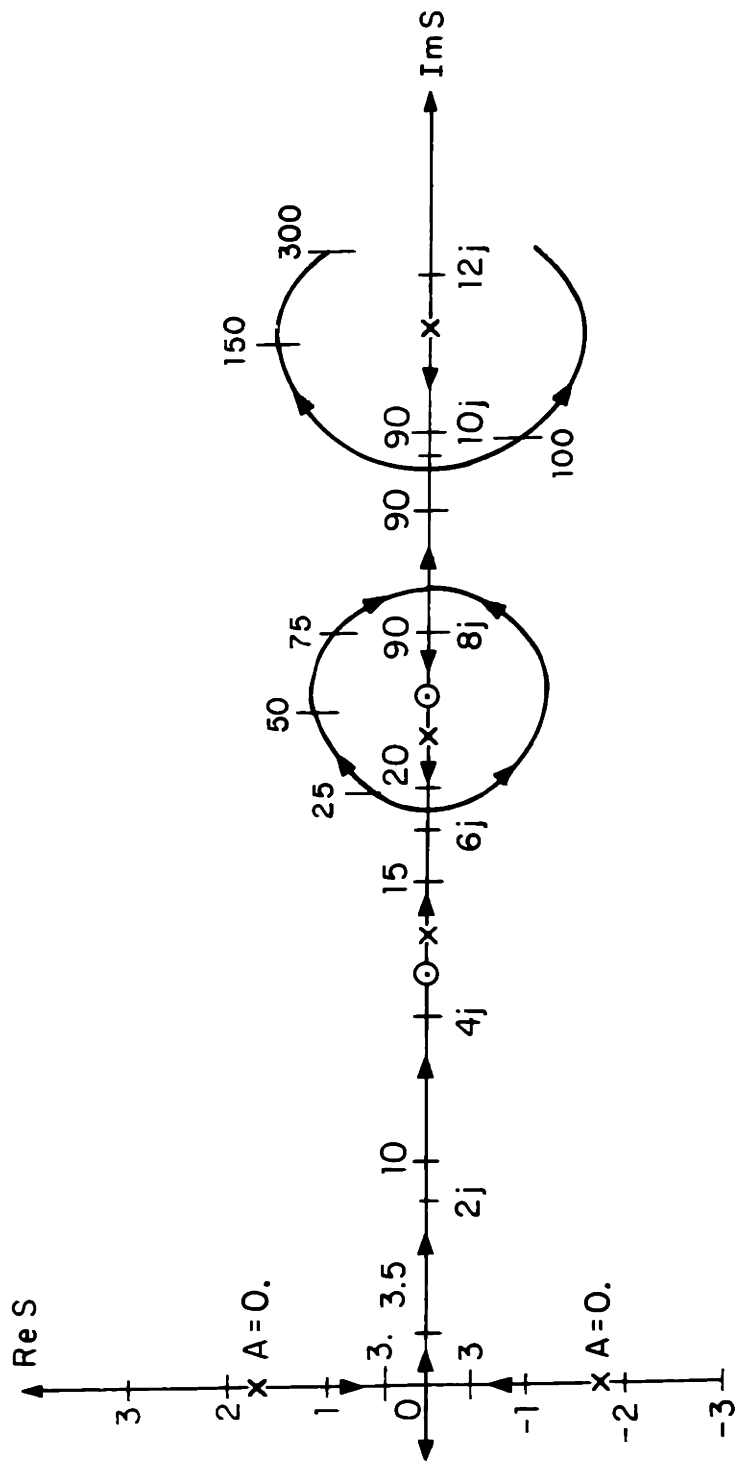


Figure 3.13 A partial root locus plot for the string with spatially discrete feedback and no damping

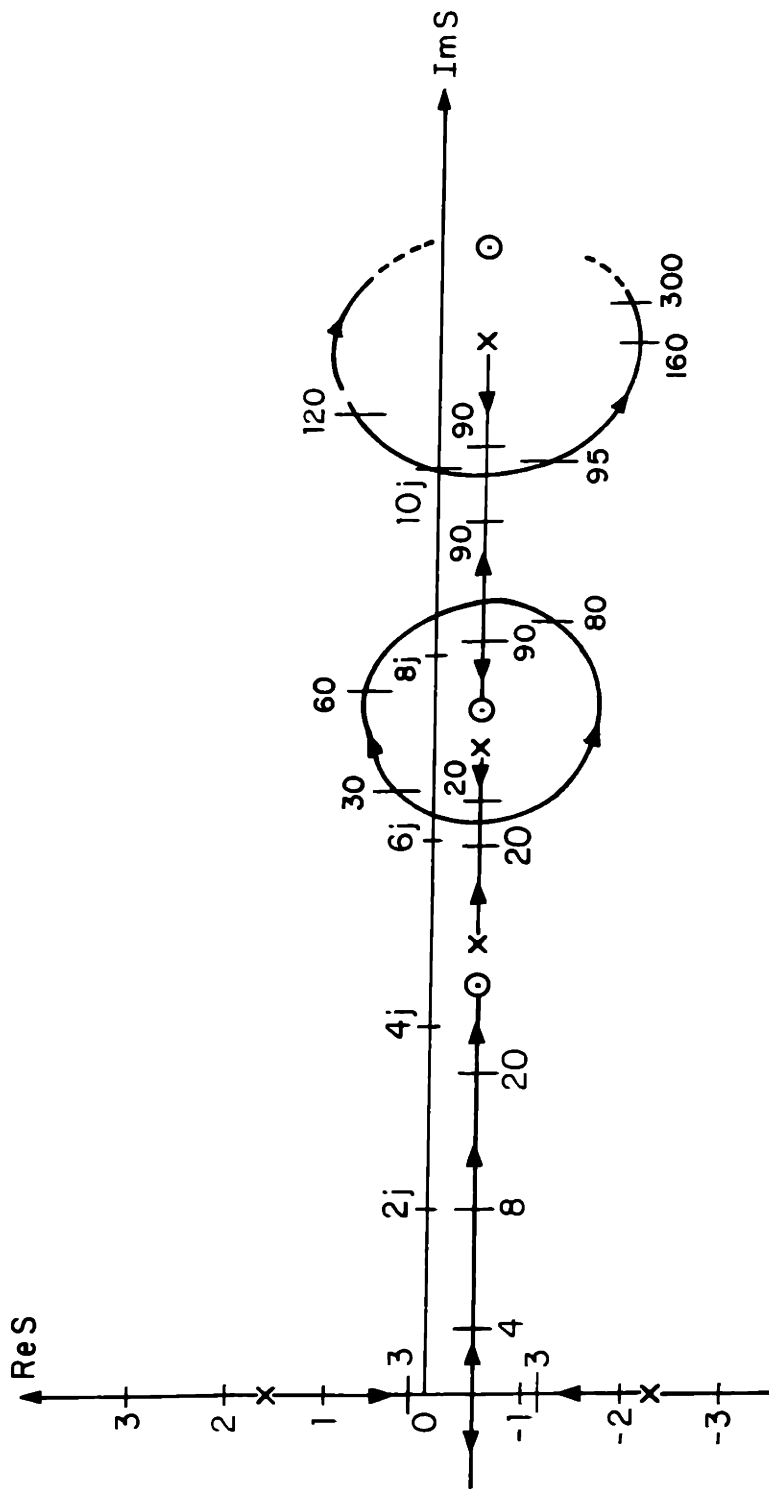


Figure 3.14 A partial root locus plot for the string with discrete spatial feedback and damping. The damping reduces the tendency for the string to become overstable.

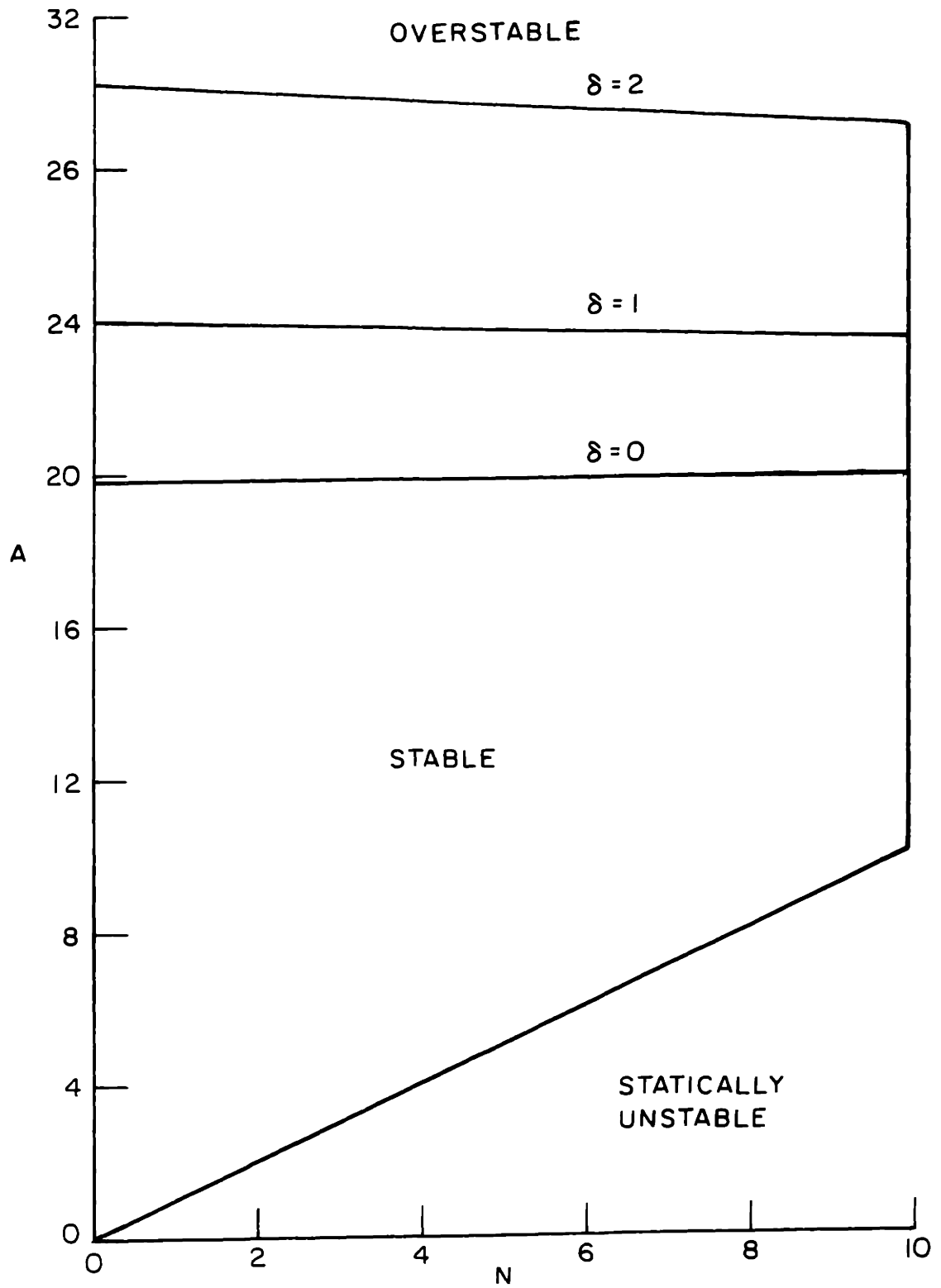


Figure 3.15 The region of stable operation for the spatially discrete system as determined from the S-D dispersion equation

The value of gain needed to stabilize the string by driving the root on the positive S axis to the imaginary S axis is unchanged from the case of no damping.

Thus, the effect of damping is to hinder the onset of overstability. The damping does not change the gain necessary to remove the initial instability.

The region of stable operation in the A - N plane is plotted in Fig. 3.15 for several values of δ . For long wavelength disturbances, there is no restoring force due to surface tension. The only restoring force is the feedback force, and it must be equal to the unstabilizing force for the system to be stable. The lower boundary for the stable region is therefore the line $A = N$. The right-hand limit of the stable region is due to the spatial sampling. For values of N greater than π^2 , the wavelength that is twice the sampling distance is unstable. This wavelength cannot be detected by the sampling system, and thus it cannot be stabilized.

The upper boundary of the stable region is a result of the discrete nature of the feedback. If a disturbance has a wavelength which is shorter than the electrode width, the feedback can pump this mode and drive the system unstable [Thomas, p. 43]. By adding damping to the system, energy can be drained from these modes and the region of stability is increased.

3.6 Summary

The Z transform, which is usually used to describe temporally discrete systems, can be adapted to spatially discrete systems. With this transform, a spatially sampled continuum can be described by a closed-form transfer function in terms of the discrete spatial wave-number, D , and the frequency, S . When spatially discrete feedback is applied to the system, a closed-loop transfer function is generated. The natural frequencies of this transfer function determine the dispersion equation of the system in terms of S and D .

For analyzing spatially discrete systems, the Z transform technique has several advantages over the wave train analysis used by Melcher. The dispersion equation obtained with the Z transforms is a closed form expression in terms of S (or ω) and D . The dispersion equation obtained from the wave train analysis is an infinite series in terms of S and K . To do calculations with Melcher's dispersion equation, the series must be truncated, and there is the possibility of truncation error. The dispersion equation obtained from the Z transform method is in closed form, and there is no possibility of truncation error.

CHAPTER IV

SPATIALLY-SAMPLED SYSTEM WITH BOUNDARIES

4.1 Introduction

Many continuum feedback control schemes have been generated for systems which have only a few feedback sensors and drivers. Typically, a normal mode expansion of the uncontrolled system is used to describe the dynamics of the closed-loop system. One of the advantages of using the normal modes of a system is that they do not influence each other. Consider the case of a string with ends that are fixed at $x = 0$ and $x = L$. The equation of motion for the spatial deflection of this string is:

$$S^2 \xi(x) = \frac{\partial^2}{\partial x^2} \xi(x) \quad (4.1)$$

and the resulting solutions to this equation are the normal modes

$$\phi_n(x) = \sin \frac{n\pi}{L} x \quad (4.2)$$

If this string is driven by a force with the same spatial dependence as one of the normal modes, $\phi_k(x)$, then the resulting disturbance on the string will consist of only this mode; none of the other modes will be excited.

Most drivers or actuators that are applied to distributed systems are not designed to excite only one of the open-loop normal modes. Electrodes which drive a section of a plasma column or a valve on a distillation column will cause changes in many of the open-loop modes. The sensors are also not designed to pick out just one mode, but measure displacements which are combinations of many modes.

Because continuum feedback systems usually cannot distinguish or excite single open-loop modes, the ability of these modes to remain uncoupled is destroyed. With no feedback, there is a dispersion equation of low order for each of the open-loop modes. With feedback, there is a dispersion equation of infinite order for the system of coupled open-loop modes.

A method of eliminating the coupling of modes is to define the set of normal modes for the system with feedback. These closed-loop normal modes are not coupled, and may be easier to manipulate than the open-loop modes. For instance, in Section 3.5, it is shown that Z-transforms lump an infinite number of the Fourier modes into a sum. This sum of Fourier modes may be thought of as a closed-loop mode.

In this chapter, the closed-loop modes are found for a string which has longitudinal boundaries and discrete spatial feedback. These closed-loop modes are derived by several methods; by use of a matrix description of the system, by use of the Fourier normal modes, and by use of the Z-transform. In addition to defining the closed-loop normal modes, these derivations will illustrate the relationships between the various methods of analyzing spatially discrete feedback systems.

4.2 Generation of Closed-Loop Modes for a System Described by a Matrix

Previous studies by Thomas (1966) and Melcher (May 1965) of continuous systems with longitudinal boundaries have considered the spatially continuous distribution of some variable of the continuum as the output and the spatially continuous force generated by the drivers as the input.

The approach used by Gould (Chapter 7) for analyzing the control problem is to consider the several measured deflections of the system as

outputs, and the signals to the drivers as inputs. This approach has the advantage that it seems to reduce the number of dimensions of the system to the number of sampling stations. Instead of writing an equation for each mode of the open loop system, an equation relating each output or measured deflection is written in terms of the various inputs. Using this approach, a system which is sampled at two places would be described by only two equations. A system with feedback, which is sampled at two places, is shown in Figure 4.1. In this system, the outputs are multiplied by a negative gain, and this signal is fed to the corresponding input. Hopefully, this feedback scheme will drive the displacements to zero.

The equation for the outputs of this system, written in matrix form, is:

$$\underline{\xi} = \underline{G} \underline{Y} - \underline{G} \underline{A} \underline{\xi} \quad (4.3)$$

where

$$\underline{\xi} = \begin{bmatrix} \xi_1 \\ \xi_2 \end{bmatrix} ; \quad \underline{Y} = \begin{bmatrix} y_1 \\ y_2 \end{bmatrix} ; \quad \underline{G} = \begin{bmatrix} g_{11} & g_{12} \\ g_{21} & g_{22} \end{bmatrix}$$

and

$$\underline{A} = \begin{bmatrix} a & 0 \\ 0 & a \end{bmatrix}$$

The closed-loop transfer function for the system can be found by rewriting Eq. (4.3) as

$$\underline{\xi} = [\underline{I} + \underline{A} \underline{G}]^{-1} \underline{G} \underline{Y} \quad (4.4)$$

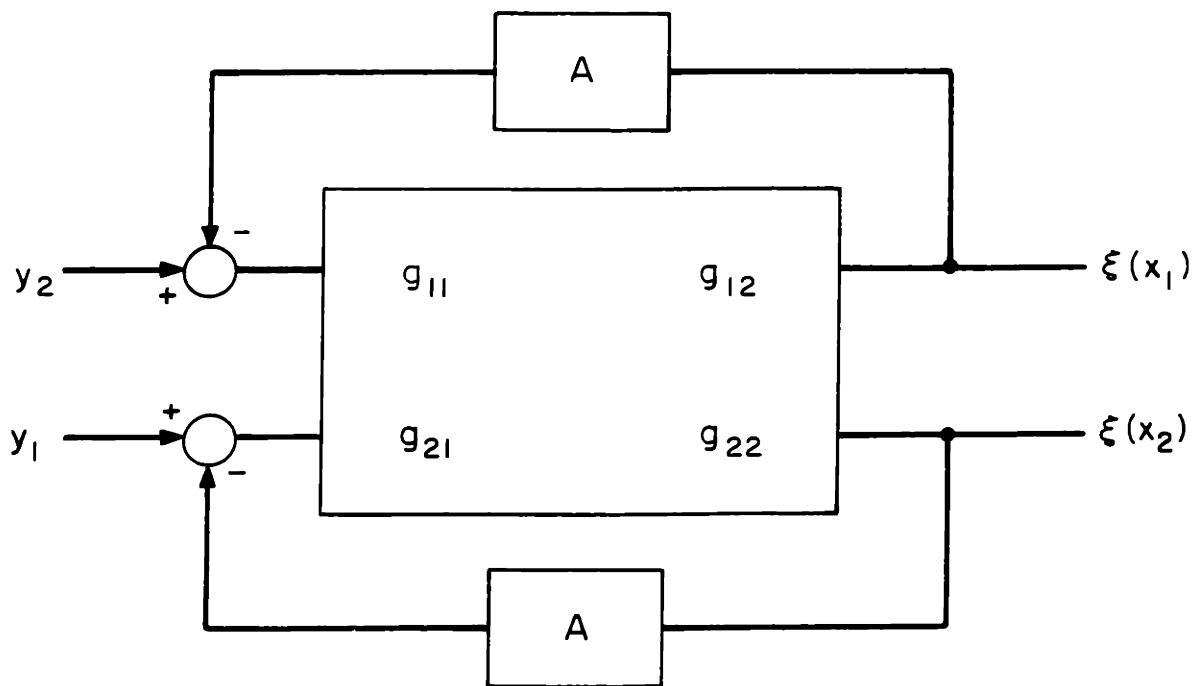


Figure 4.1 A system which is spatially sampled in two locations and driven by two forcers can be represented by a system of two coupled inputs and outputs.

The transfer function for this system will, in general, contain no zero elements. If a transformation could be made so that the off-diagonal terms of the transfer matrix were zero, then the system would become two independent systems. That is, a transformation matrix \underline{T} is desired which will diagonalize the matrix $[\underline{I} + \underline{A} \underline{G}]^{-1} \underline{G}$. If this transformation is found, the system can be described by the equation

$$\begin{bmatrix} \underline{u}_1 \\ \underline{u}_2 \end{bmatrix} = \begin{bmatrix} f_{11} & 0 \\ 0 & f_{22} \end{bmatrix} \begin{bmatrix} \underline{w}_1 \\ \underline{w}_2 \end{bmatrix} \quad (4.5)$$

where the vectors \underline{u} and \underline{w} are found from $\underline{\xi}$ and \underline{Y} by the transformations

$$\underline{w} = \underline{T} \underline{Y} \quad (4.6)$$

$$\underline{u} = \underline{T}^{-1} \underline{\xi} \quad (4.7)$$

and f_{11} and f_{22} are the non-zero diagonal terms of the matrix

$$\underline{F} = \underline{T}^{-1} [\underline{I} + \underline{A} \underline{G}]^{-1} \underline{G} \underline{T} \quad (4.8)$$

The method for finding the transformation matrix \underline{T} can be found in DeRusso (chapter 4) and Hildebrand (chapter 1).

The significance of Eq. (4.5) is that the outputs, u_i , are uncoupled from each other. Instead of being two coupled subsystems, where any drive w_i affects both outputs, the transformed system consists of two uncoupled systems which are described by the equations

$$u_1 = f_{11} w_1 \quad (4.9)$$

$$u_2 = f_{22} w_2 \quad (4.10)$$

For the more general case of n sampling stations, n independent systems of the form

$$u_j = f_{jj} w_j \quad (4.11)$$

are found.

The transformation matrix \underline{T} is significant because it is made from the characteristic vectors of the system. These characteristic vectors define the orthogonal coordinates in the space defined by the sampled output of the system. In the situation where there is no sampling or feedback, the normal modes of the system are sinusoids of the proper frequencies. Since there are an infinite number of points on the continuous system, an infinite number of these normal modes are needed to describe the system. In the situation in which the system is sampled, only a few points on the system are known. This can be thought of as saying that the system has only a few "dimensions". When the modal matrix \underline{T} is found, what is actually found is the orthogonal coordinates, or normal modes of the sampled system. When the equations for the system are written in the uncoupled form, Eq. (4.5), the drive \underline{Y} , and the response $\underline{\xi}$ are broken up into their components along the various normal modes.

As an example, Gould's technique could be applied to the case of the string with discrete spatial feedback. The inputs, y_i , are the signals to the driving electrodes and the outputs, ξ_i are the deflections at the sampling points. The transfer elements, g_{ij} , are the relationships between the drives and the sampled deflections. These transfer elements can be found by the use of Green's functions, which are explained by Morse and Feshbach (chapter 7). Once the transfer elements

have been computed, the process of finding the uncoupled modes of the system is straightforward. Unfortunately, the algebraic manipulations necessary to compute the transfer elements are difficult to perform and it is practically impossible to put the diagonal matrix $\underline{T}^{-1} [\underline{I} + \underline{AG}]^{-1} \underline{G} \underline{T}$ into a usable form.

The purpose of this section is merely to introduce the concept of the closed-loop normal modes as they are described by Gould. Since the analysis of the string is so complicated by Gould's method, it is not considered to be a worthwhile example, and is not presented here. The closed-loop modes for the string are found later in this chapter, by easier methods.

4.3 Generation of Closed-Loop Modes from Open-Loop Modes

In previous studies of the string by Melcher (May 1965) and Thomas (1966), the spatially continuous deflection of the string is considered to be the output of the system. This deflection is described by an infinite number of the open-loop normal modes. Because the deflection of each point of the string can be found by their methods, their analysis must contain much more information than is necessary to find the deflection at only the sampling points. If this extra information can be discarded from the normal mode analysis, then only the information about the sampled deflection would remain. From this remaining information, the closed-loop or sampled normal modes can be found.

This method of finding the closed-loop normal modes gives the same modes that could be obtained from the matrix approach. The advantage of starting with the open-loop normal modes is that the algebraic manipulations are much easier.

Normal-Mode Description of the Finite String

The system studied in this section is the electrically stressed string of finite length whose ends are attached to solid supports. This system is shown in Fig. 4.2. The string is driven by a finite number of electrodes which are of length L . The ends of the string are fastened at the points $x = 0$ and $x = mL$, where m is the number of feedback electrodes. The equation of motion for the string is

$$\frac{1}{v_p^2} \frac{\partial^2 \xi(x,t)}{\partial t^2} = \frac{\partial^2 \xi(x,t)}{\partial x^2} - \beta \frac{\partial \xi(x,t)}{\partial t} + k_c^2 \xi(x,t) + g v_d(x,t) \quad (4.12)$$

where v_d is similar to the spatially-discrete voltage shown in Fig. 3.2.

The length of a driving electrode, L , is normalized to one and the length of the string is normalized to m by the introduction of the following normalized variables:

$$S = \frac{Ls}{v_p} \quad (4.13a)$$

$$N = k_c^2 L^2 \quad (4.13b)$$

$$\delta = \beta v_p L \quad (4.13c)$$

$$M = L^2 g \quad (4.13d)$$

Assuming that the displacement is an infinite sum of the open-loop normal modes,

$$\xi(x,t) = \text{Real} \left(\sum_{n=1}^{\infty} \Xi_n \sin \frac{n\pi x}{m} \right) e^{St} \quad (4.14)$$

allows Eq. (4.12) to be rewritten as

$$\sum_{n=1}^{\infty} \left(\Xi_n \sin \frac{n\pi x}{m} \right) [S^2 + \delta S + \left(\frac{n\pi}{m} \right)^2 - N] = \hat{M} v_d(x) \quad (4.15)$$

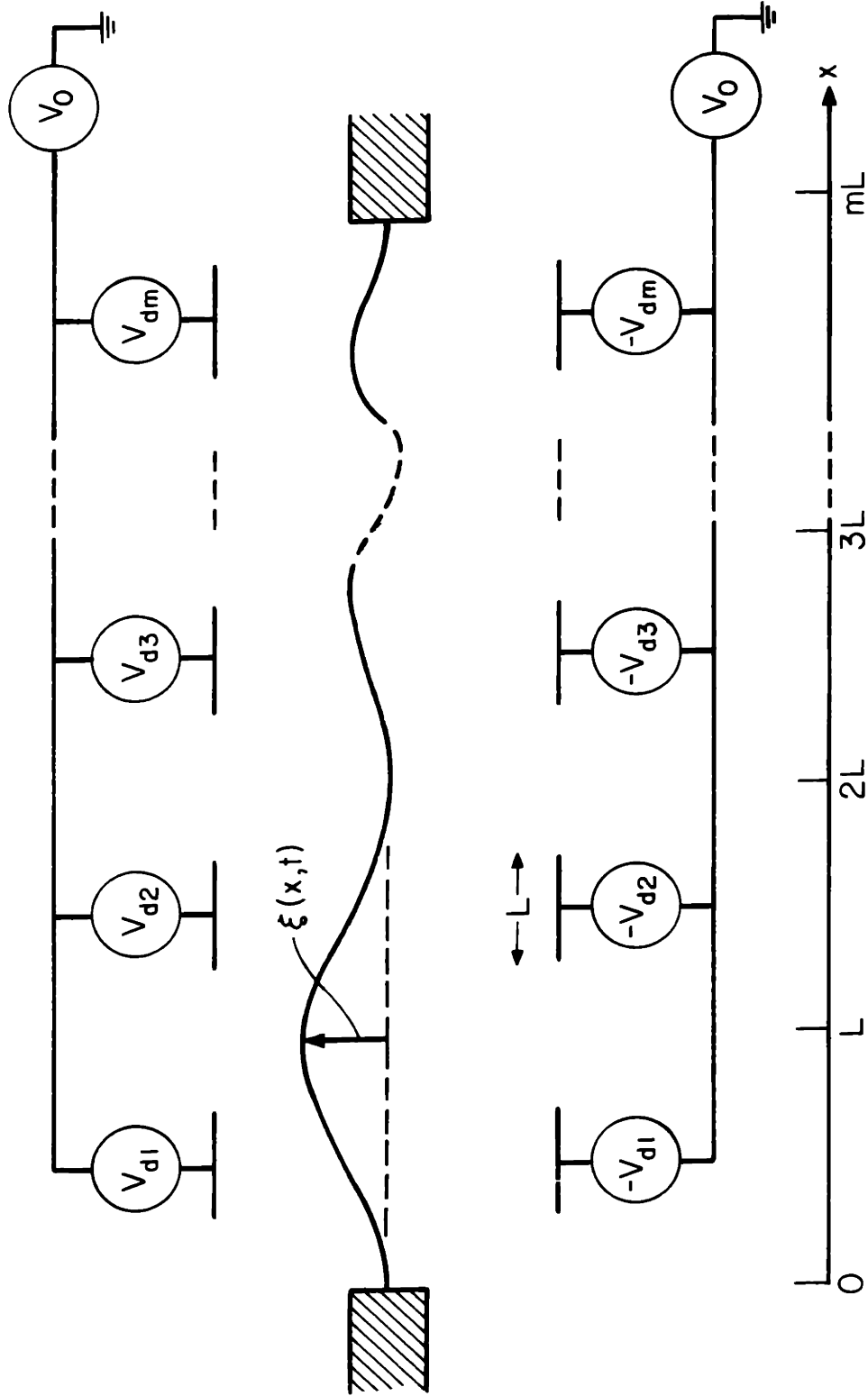


Figure 4.2 A cross-sectional view of the bounded string,

with a finite number of spatially discrete drivers.

When this system is described by its open-loop normal modes, it is not in the matrix form of Eq. (4.3), and the closed-loop normal modes cannot be formed by the method shown in Section 4.2. This problem is overcome in the following section.

Closed-Loop Transfer Functions

As an example, the closed-loop normal modes and their transfer functions will be developed for the case of two feedback stations. The ends of the string are fastened at $x = 0$ and $x = 2$. For this case, one electrode drives the string for $0 < x < 1$, and the other electrode drives $1 < x < 2$. The voltages on the two electrodes are given by $R_e[V_{d1}e^{St}]$ and $R_e[V_{d2}e^{St}]$, respectively.

Multiplying Eq. (4.15) by $\sin n\pi/2$ and integrating from 0 to 2 gives:

$$E_n [S^2 + (\frac{n\pi}{2})^2 + \delta S - N] = \begin{cases} \frac{2M}{n\pi}(V_{d1} + V_{d2}) & n \text{ odd} \\ \frac{4M}{n\pi}(V_{d1} - V_{d2}) & n = 2, 6, 10, \dots \\ 0 & n = 0, 4, 8, \dots \end{cases}$$

(4.16)

This equation shows that, with this electrode structure, it is impossible to drive the modes $n = 0, 4, 8, \dots$. These modes cannot be influenced, and are called "uncontrollable".

The detection scheme that is used here is to sample the displacement at the center of each driving electrode. To drive this displacement to zero, a voltage proportional to the measured displacement and of opposite polarity is applied to each electrode. That is, V_{d1} is proportional to $\xi(1/2, t)$ and V_{d2} is proportional to $\xi(3/2, t)$. In terms of

the open-loop normal modes, the driving voltages are

$$V_{d1} = -G' \left[\frac{\sqrt{2}}{2} (\Xi_1 + \Xi_3 - \Xi_5 - \Xi_7 + \Xi_9 \dots) \right. \\ \left. + (\Xi_2 - \Xi_6 + \Xi_{10} - \Xi_{14} \dots) \right] \quad (4.17)$$

$$V_{d2} = -G' \left[\frac{\sqrt{2}}{2} (\Xi_1 + \Xi_3 - \Xi_5 - \Xi_7 + \Xi_9) \right. \\ \left. - (\Xi_2 - \Xi_6 + \Xi_{10} - \Xi_{14} + \dots) \right] \quad (4.18)$$

where G' is the constant for the feedback gain. Substituting Eqs. (4.17) and (4.18) into (4.16) gives

$$\Xi_n [S^2 + \delta S + \left(\frac{n\pi}{2}\right)^2 - N] = -\frac{2\sqrt{2}A}{n\pi} (\Xi_1 + \Xi_3 - \Xi_5 - \Xi_7 + \dots) \quad (4.19)$$

for n odd, and

$$\Xi_n [S^2 + \delta S + \left(\frac{n\pi}{2}\right)^2 - N] = -\frac{8A}{\pi n} (\Xi_2 - \Xi_6 + \Xi_{10} - \Xi_{14} + \dots) \quad (4.20)$$

for $n = 2, 6, 10, 14, \dots$

where $A = MG'$ (4.21)

These are the same equations that were derived by Melcher (May 1965). The trick now is to get this infinite number of equations representing the open-loop modes into just two equations representing the closed-loop modes. If Eq. (4.19) is divided by the coefficient of Ξ_n , the result is

$$\Xi_n = \frac{-2A}{(S^2 + \delta S + \left(\frac{n\pi}{2}\right)^2 - N)} \frac{\sqrt{2}}{\pi n} (\Xi_1 + \Xi_3 - \Xi_5 - \Xi_7 + \dots) \quad (4.22)$$

for n odd.

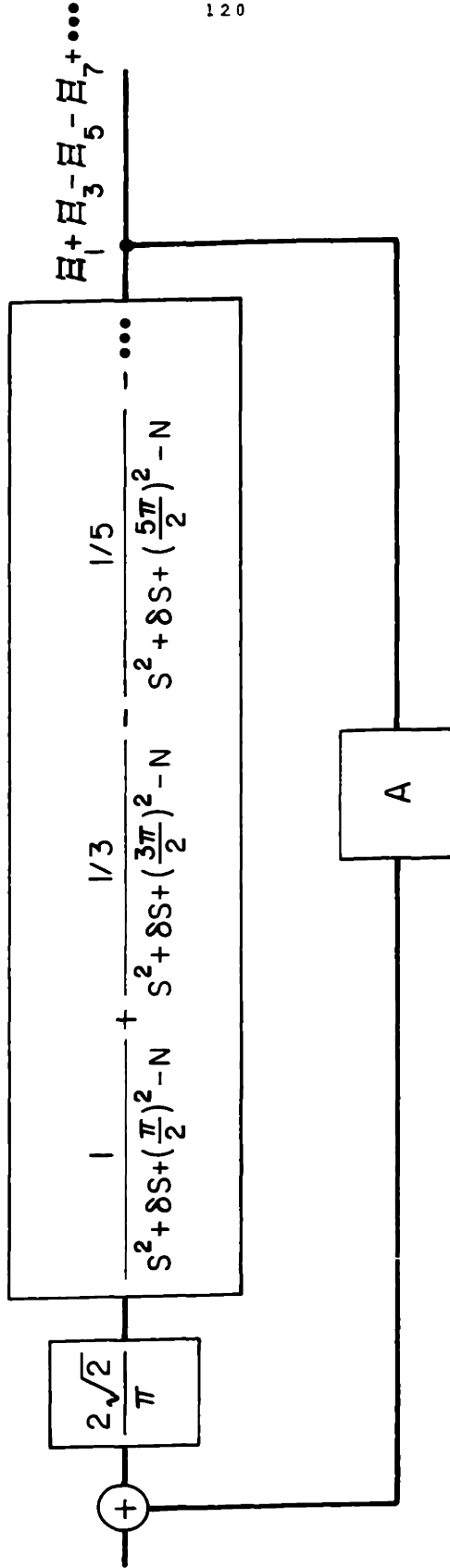


Fig. 4.3 The normal modes $E_1, E_3, E_5, E_7, \dots$ of the spatially continuous bounded string can be combined to generate the first normal mode of the bounded string with two-station feedback.

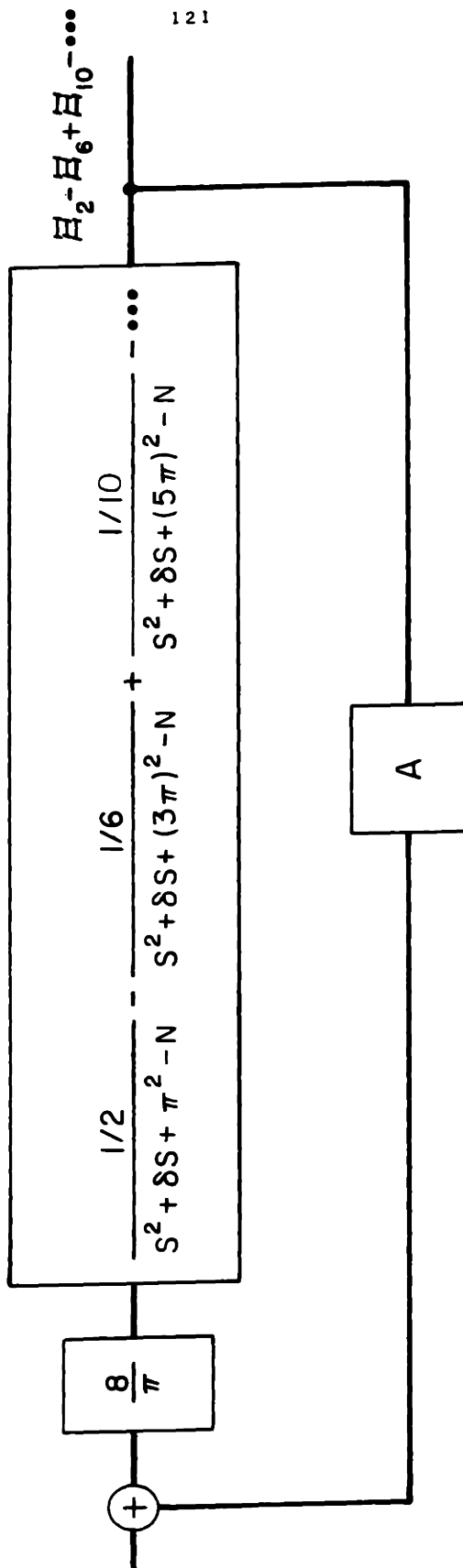


Figure 4.4 The normal modes $E_2, E_6, E_{10} \dots$ of the spatially continuous bounded string can be combined to generate the second normal mode of the bounded string with two-station feedback.

The set of equations represented by (4.22) is now added and subtracted together, to get

$$\begin{aligned}
 & (\Xi_1 + \Xi_3 - \Xi_5 - \Xi_7 + \dots) = \\
 & - \frac{A2\sqrt{2}}{\pi} \left(\frac{1}{S^2 + \delta S + \left(\frac{\pi}{2}\right)^2 - N} + \frac{1/3}{S^2 + \delta S + \left(\frac{3\pi}{2}\right)^2 - N} \right. \\
 & \left. - \frac{1/5}{S^2 + \delta S + \left(\frac{5\pi}{2}\right)^2 - N} - \frac{1/7}{S^2 + \delta S + \left(\frac{7\pi}{2}\right)^2 - N} + \dots \right) \cdot \\
 & (\Xi_1 + \Xi_3 - \Xi_5 - \Xi_7 + \dots) \tag{4.23}
 \end{aligned}$$

The same process can be repeated on the even modes of Eq. (4.20), to obtain:

$$\begin{aligned}
 & (\Xi_2 - \Xi_6 + \Xi_{10} - \Xi_{14} + \Xi_{16} - \dots) = \\
 & - \frac{8A}{\pi} \left(\frac{1/2}{S^2 + \delta S + \left(\frac{2\pi}{2}\right)^2 - N} - \frac{1/6}{S^2 + \delta S + \left(\frac{6\pi}{2}\right)^2 - N} + \right. \\
 & \left. \frac{1/10}{S^2 + \delta S + \left(\frac{10\pi}{2}\right)^2 - N} - \dots \right) \cdot (\Xi_2 - \Xi_6 + \Xi_{10} - \Xi_{14} + \Xi_{16} - \dots) \tag{4.24}
 \end{aligned}$$

If the sums of the normal modes in Eqs. (4.23) and (4.24) are considered to be variables, then these equations can be represented by the servo loops in Figures 4.3 and 4.4.

The system description has been changed from one consisting of an infinite number of open-loop normal modes to one consisting of two independent closed-loop modes. Comparison of the output of the two servo loops with Eqs. (4.17) and (4.18) shows that the two closed-loop modes are proportional to the sum and the difference of the two measured

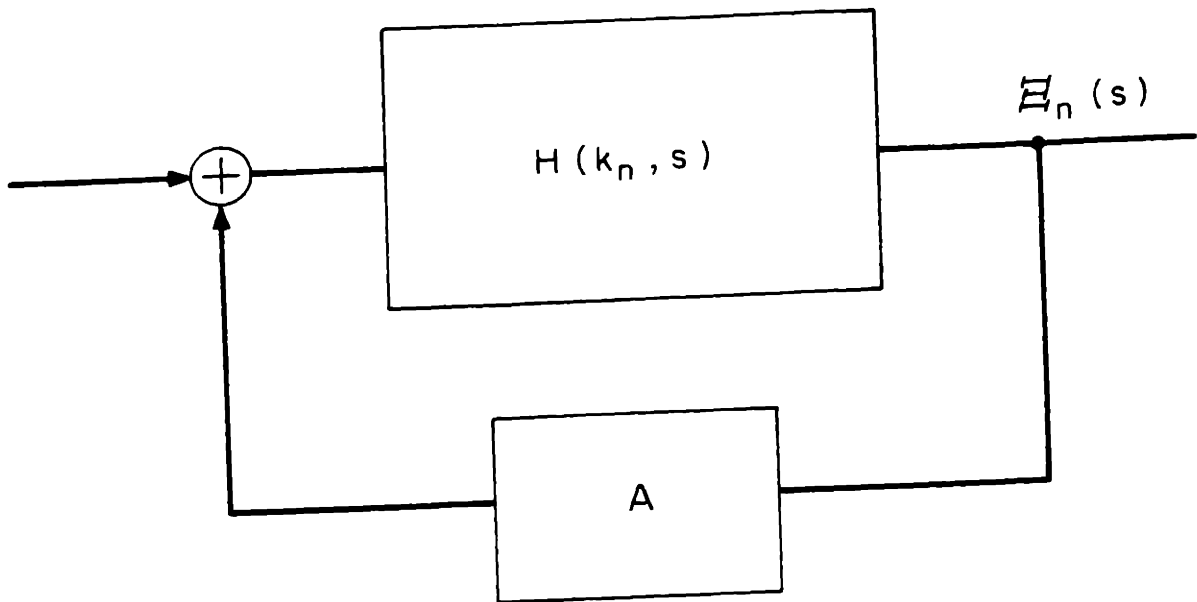


Figure 4.5 The bounded string with spatially continuous feedback can be represented by an infinite number of servo loops. The transfer function in the servo loop is the transfer function of the infinite string evaluated at the eigenvalues k_n .

displacements.

By finding the two closed-loop normal modes which describe the system, the number of equations which describe the system has been reduced from an infinite set to two. This reduction in the number of equations must correspond to a loss of information about the system. The lost information is the value of the string's deflection at any point other than the sampling points.

In Eq. (4.14), the deflection of the string is described as a sum of the open-loop normal modes. If the amplitude of each of these modes is known, the deflection at any point can be constructed. With Eqs. (4.19) and (4.20), these amplitudes can be determined. When the sets of equations represented by Eqs. (4.19) and (4.20) are added together to get Eqs. (4.22) and (4.23), the ability to find the individual amplitudes, E_n , is lost. Only the sums of the amplitudes, shown as the outputs in Figs. 4.3 and 4.4, can be determined. By taking the sum and differences of these two outputs, the deflection at the sampling points can be determined to within a multiplicative constant.

4.4 Generation of Closed-Loop Modes from the Z-Transform of the Unbounded System

When the closed-loop modes are generated from the open-loop modes, the information which determines the value of the deflection between the sampling points is lost. It is shown in Section 3.5 that using Z-transforms corresponds to dropping the information about the deflection between the sampling points. This suggests that there is probably a relationship between the closed-loop normal modes and Z-transforms. This connection is developed and a method of generating the closed-loop modes from

the Z-transform is presented in this section.

Boundaries Create Eigenvalues and Zeros

An infinitely long structure, such as a parallel-plate transmission line or a string, will support waves for any real wavenumber, k . These transmission lines also put no restriction on the phase of a wave; a wave with a spatial variation of $\sin(kx)$ can exist, as well as one with a spatial variation of $\cos(kx)$.

If the transmission line is terminated by a free end, or a short, or if the string is fastened to a rigid support, the wavenumber and the phase of the disturbances are restricted. The wavenumber, k , of a disturbance is restricted to certain eigenvalues and the eigenmodes, the disturbances at the eigenvalues of k , can occur only with certain values of phase. For example, a string fastened at $x = 0$ and $x = L$ will have waves whose spatial distribution is $\sin(kx)$; waves which have a distribution of $\cos(kx)$ cannot exist. The value of k is also fixed at the values $n\pi/L$.

The previous discussion leads to some conclusions about the relationship of the transfer function for an infinite system to the transfer function of a finite system. The first conclusion is that the transfer function for the bounded system must contain zeros that are not in the infinite transfer function. These zeros will insure that no disturbance will exist when a drive with the wrong phase characteristics is applied to the string. The string with the ends pinned at $x = 0$ and $x = L$ will have to have zeros that assure that no waves with a spatial variation of $\cos(kx)$ can exist. The second conclusion is that the transfer function

for the bounded system applies only to the eigenvalues of k . In addition to the proper phase, the waves must also have the proper wavelength to satisfy the boundary conditions. By restricting k to the values $n\pi/L$, the string will have no deflection at $x = 0$ and $x = L$.

Transfer Function of a Spatially-Continuous System with
Longitudinal Boundaries

The method of finding the transfer function for a bounded system from the transfer function of the unbounded system is derived in this section. The system studied here is terminated at the points $x = a$ and $x = b$, so that the disturbances are zero at these boundaries. An example of this situation is a transmission line with the voltage shorted at the ends or a string with the ends attached to a solid support.

This system has spatially continuous feedback. By analyzing this system, the procedures for forcing the proper phase onto the disturbance and for finding the eigenvalues of k can be introduced without the complications of spatial discreteness. This complication is added later.

At a boundary, a reflected wave is generated which interferes with the incident wave and makes the deflection zero. A procedure, illustrated by Morse and Feshback (Chapter 7), for mathematically generating this reflection, is to use the method of images. The reflection or image due to the boundary at $x = b$ is made by flipping the incident wave about the point $x = b$ and multiplying by a minus (-) sign. The incident wave and the reflected wave approach the boundary from opposite sides and with opposite polarities. The two waves meet and the destructive interference at the boundary makes the displacement zero at this point. In

terms of the incident wave, the first reflected wave is

$$\xi_{R_1}(x,t) = -\xi_i(-x-2b,t) \quad (4.25)$$

The second boundary at $x = a$ creates more reflections. An image wave must be set up to cancel not only the incident wave, but also the first reflected wave. This second reflected wave can be written as

$$\xi_{R_2} = -\xi_i(-x-2a,t) - \xi_{R_1}(-x-2a,t) \quad (4.26)$$

Using Eq. (4.25), this second reflection is

$$\xi_{R_2} = -\xi_i(-x-2a,t) + \xi_i(x+2b-2a,t) \quad (4.27)$$

The sum of the original wave plus the two reflections matches the boundary conditions at $x = a$, but the boundary condition at $x = b$ is no longer satisfied. A third reflected wave, ξ_{R_3} , must be generated to cancel ξ_{R_2} at this boundary. The creation of ξ_{R_3} will now necessitate the generation of another reflected wave, ξ_{R_4} , to match the boundary condition at $x = a$. The process is continued indefinitely as an infinite number of reflections are created by the waves bouncing back and forth between the boundaries. The total disturbance on the bounded system can be written as

$$\begin{aligned} \xi(x,t) = & \sum_{n=-\infty}^{\infty} [\xi_i(x+2n(b-a),t)] \\ & - \sum_{n=-\infty}^{\infty} \xi_i[x+2n(b-a)+2b,t] \end{aligned} \quad (4.28)$$

and the transform of the disturbance on the bounded system is

$$\begin{aligned} \bar{\Xi}(k,s) = & [\bar{\Xi}_i(k,s) - e^{-2jkb} \bar{\Xi}_i(-k,s)] \cdot \\ & [1 + e^{2jk(b-a)} + e^{-2jk(b-a)} + e^{4jk(b-a)} + e^{-4jk(b-a)} + \dots] \end{aligned} \quad (4.29)$$

The series in this transform can be recognized as the transform of an impulse train with a period of $2(b-a)$ on the x axis. In Mason and Zimmerman (pp. 242-247), this transform is shown to be

$$1 + e^{2jk(b-a)} + e^{-2jk(b-a)} + e^{4jk(b-a)} + \dots = \frac{\pi}{b-a} \sum_{n=-\infty}^{\infty} u_o(k - \frac{n\pi}{b-a}) \quad (4.30)$$

With Eq. (4.30), the transform of the disturbance on the bounded system in terms of the disturbance on the unbounded system is:

$$\bar{\Xi}(k,s) = [\bar{\Xi}_i(k,s) - e^{-2jkb} \bar{\Xi}_i(-k,s)] \left(\frac{\pi}{b-a} \right) \sum_{n=-\infty}^{\infty} u_o(k - \frac{n\pi}{b-a}) \quad (4.31)$$

If the original disturbance on the unbounded system, $\bar{\Xi}_i$, is written as the product of some drive $U_i(k,s)$, and the transfer function of the unbounded system, $H(k,s)$, the disturbance on the bounded system is

$$\bar{\Xi}(k,s) = [U_i(k,s)H(k,s) - e^{-2jkb} U_i(-k,s)H(-k,s)] \left(\frac{\pi}{b-a} \right) \sum_{n=-\infty}^{\infty} u_o(k - \frac{n\pi}{b-a}) \quad (4.32)$$

This equation shows how the boundaries have affected the transfer function. The impulses at $k = n\pi/(b-a)$ have made the system function apply to only these eigenvalues. There can be no energy at any other wavenumber. The proper phase relationship is forced onto the disturbance by the term in brackets in Eq. (4.32). This can be seen by considering the case in

which the left end of the system is fastened at the origin so that $a = 0$. From normal mode theory, it is known that disturbances on this system are of the form $\sin(kx)$ and are, therefore, odd functions in k space. At the eigenvalues of k , the value of e^{-2jkb} is equal to one, and the term in brackets is the proper odd function of k .

Continuous Spatial Feedback for a Bounded System

The transform of the disturbance, which is given in Eq. (4.32), is not in a familiar form, because it does not appear as the product of a drive and a transfer function. The longitudinal boundaries on the system have forced the disturbance to be a complicated function of the drive and the unbounded transfer function. Fortunately, there are special cases where Eq. (4.32) can be put into the familiar form. Two examples are whenever $U_i(k,s)$ or $H(k,s)$ are even or odd functions of k .

For many systems, the characteristics of a wave are independent of the direction in which the wave is traveling. The string is an example of this kind of system; a wave traveling to the left has the same speed and sees the same impedance as a wave traveling to the right. A system with this property will have a transfer function which is an even function of k . For these systems, the transfer function of the disturbance can be written as

$$\Xi(k,s) = H(k,s) [U_i(k,s) - e^{-2jkb}U_i(-k,s)] \left(\frac{\pi}{b-a}\right) \sum_{n=-\infty}^{\infty} u_o\left(k - \frac{n\pi}{b-a}\right) \quad (4.33)$$

From the form of Eq. (4.31), it is seen that the impulses and the term in brackets on the R.H.S. of (4.33) are the drive that exists on the bounded system. That is,

$$U(k,s) = \frac{\pi}{b-a} [U_i(k,s) - e^{-2jkb} U_i(-k,s)] \sum_{n=-\infty}^{\infty} u_o(k - \frac{n\pi}{b-a}) \quad (4.34)$$

The feedback signal is generated by amplifying the sampled deflection by a negative gain. Therefore, the drive for the bounded system is

$$U(k,s) = -A \bar{\Xi}(k,s) . \quad (4.35)$$

The transform of the deflection on the closed-loop system can be found by substituting Eqs. (4.34) and (4.35) into (4.33), to obtain

$$\bar{\Xi}(k,s) = -AH(k,s) \bar{\Xi}(k,s) . \quad (4.36)$$

Equation (4.36) is of the same form as the equation for the closed-loop response of an unbounded system. The differences between the bounded and unbounded cases are the restrictions applied to $\bar{\Xi}(k,s)$ when longitudinal boundaries are present. Equation (4.31) shows that, when boundaries are present, $\bar{\Xi}(k,s)$ has a value only at the eigenvalues of k . Equation (4.31) also shows that the phase of $\bar{\Xi}(k,s)$ is restricted because the values of $\bar{\Xi}(k,s)$ and $\bar{\Xi}(-k,s)$ are not independent. If the boundaries are removed from the system, the restrictions are removed from $\bar{\Xi}(k,s)$.

From Eq. (4.31), the deflection can be seen to be of the form

$$\bar{\Xi}(k,s) = \sum_{n=-\infty}^{\infty} \bar{\Xi}_n(s) u_o(k - \frac{n\pi}{b-a}) \quad (4.37)$$

Substituting Eq. (4.37) into (4.36) produces the following infinite set of equations:

$$\bar{\Xi}_n(s) = -AH(k_n,s) \bar{\Xi}_n(s) \quad (4.38)$$

where $k_n = \frac{n\pi}{b-a}$.

From this set of equations, an infinite number of servo loops like the one in Figure 4.5 can be drawn.

By using Eq. (4.31) the servo loops for any amplitude $\bar{E}_b(s)$ and the corresponding amplitude $\bar{E}_{-b}(s)$ can be combined. The result is a servo-loop representation for each of the sinusoidal normal modes of the system.

A specific example will not be given for this situation where the feedback force is a continuously variable function of space. This problem has been done by Melcher (May 1965) and Thomas (1966) for the case of the string, and there is no value in repeating it. This section was presented only to illustrate the method of generating the transfer function for a bounded system from the transfer function of an unbounded system. The complexity of discrete spatial feedback was left out to simplify the derivation. The problems caused by discrete spatial feedback are considered in the following sections.

Transfer Function of a Spatially Discrete System with Boundaries

By modifying the technique which we presented earlier in section 4.4, the transfer function of a discrete spatial system with longitudinal boundaries will be derived from the transfer function of the same system without boundaries. The system to be studied here is the string with discrete spatial feedback that was studied in section 4.3. The method that is used is applicable to a string with any number of feedback stations. However, to avoid the complexity of a variable number of feedback stations, the number is set at two in the following derivation. The string with two feedback electrodes is shown in Figure 4.6.

The feedback system samples the deflection at the center of each electrode. Because it is convenient to have the first sample occur at the

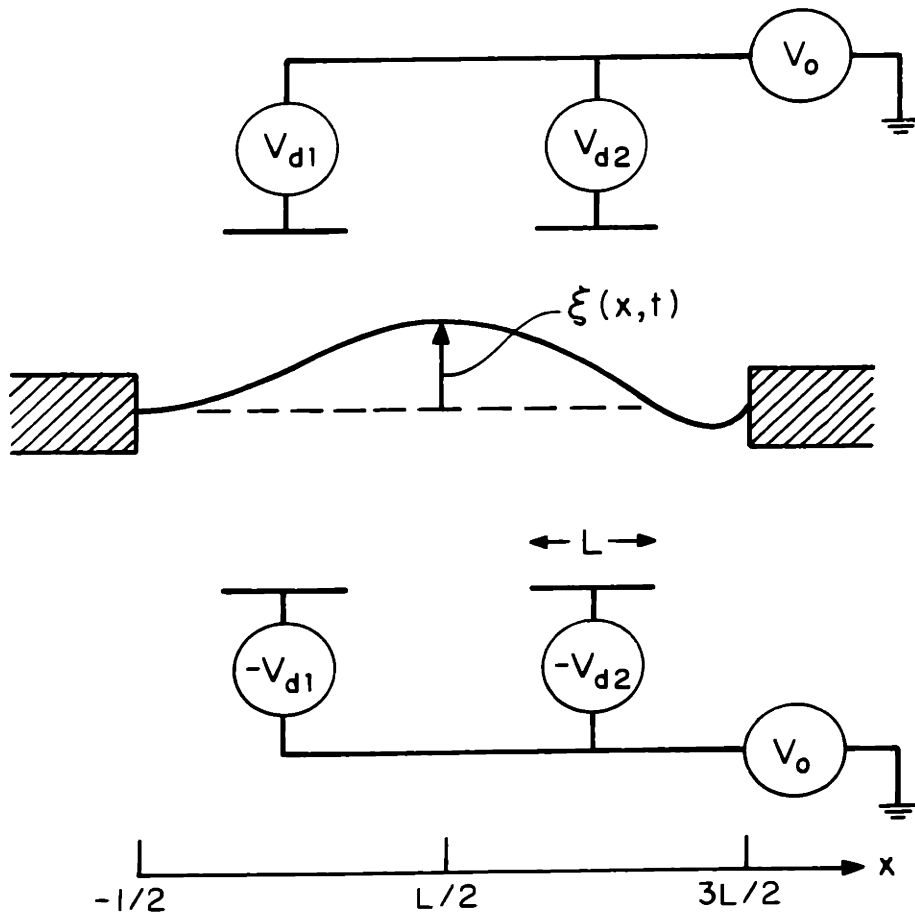


Figure 4.6 A cross-sectional view of the bounded string with two feedback electrodes

origin, the system is located with the left end at $x = -1/2L$.

The transform of the continuous displacement of this system can be obtained from Eq. (4.32). The only modification that must be made is that the drive must now be designated as a sampled function. Using the values $a = -1/2 L$ and $b = 3/2 L$ gives the transform of the displacement as

$$\Xi(k,s) = [U_1^*(k,s)G(k,s) - e^{-3jkL} U_1^*(-k,s)G(-k,s)] \cdot \left(\frac{\pi}{2L}\right) \sum_{n=-\infty}^{+\infty} u_0\left(k - \frac{n\pi}{2L}\right) \quad (4.39)$$

The transfer function for the infinite system, $G(k,s)$ includes the properties of both the driving electrode and the string. $G(k,s)$ is given by Eq. (3.42).

For convenience, the length L is normalized to one by using the definitions in Eqs. (3.3a) through (3.3e). Equation (4.39) can now be written as

$$\Xi(K,S) = [U_1^*(K,S)G(K,S) - e^{-3jK} U_1^*(-K,S)G(-K,S)] \cdot \frac{\pi}{2} \sum_{n=-\infty}^{+\infty} u_0\left(K - \frac{n\pi}{2}\right) \quad (4.40)$$

The next step is to sample the displacement at the points $x = 0, 1, 2, \dots$.

The result is

$$\Xi^*(K,S) = \frac{\pi}{2} [U_1^*(K,S)G(K,S) \sum_{n=-\infty}^{+\infty} u_0\left(K - \frac{n\pi}{2}\right)]^* - \frac{\pi}{2} [U_1^*(-K,S) e^{-3jK} G(-K,S) \sum_{n=-\infty}^{+\infty} u_0\left(K - \frac{n\pi}{2}\right)]^* \quad (4.41)$$

It is shown in Eq. (3.19) that spatial sampling makes a function periodic in K space with a period of 2π . Because the impulse train, the drive, and

the delay e^{-3jK} are already periodic at this rate, the sampling does not affect them. The only term affected by the sampling is $G(K,S)$. Rewriting Eq. (4.41) gives

$$\begin{aligned} \Xi^*(K,S) = & \frac{\pi}{2} U_i^*(K,S)G^*(K,S) \sum_{n=-\infty}^{+\infty} u_o(K - \frac{n\pi}{2}) \\ & - \frac{\pi}{2} U_i^*(-K,S)G^*(-K,S)e^{-3jK} \sum_{n=-\infty}^{+\infty} u_o(K - \frac{n\pi}{2}) \end{aligned} \quad (4.42)$$

The impulse train in Eq. (4.42) is periodic with a period of $\pi/2$. The other terms in the equation have a period of 2π . This means that the terms $U_i^*(K,S)G^*(K,S)$ and $e^{-3jK}U_i^*(-K,S)G^*(-K,S)$ are sampled by the impulse train four times in a period of 2π .

The impulse train in Eq. (4.42) can be factored into a group of four impulses that is repeated with a period of 2π . The result is

$$\begin{aligned} \Xi^*(K,S) = & \frac{\pi}{2} \sum_{n=-\infty}^{+\infty} \sum_{p=1}^4 [U_i^*(K,S)G^*(K,S) - e^{-3jK}U_i^*(-K,S)G^*(-K,S)] \cdot \\ & u_o(K - K_p - 2n\pi) \end{aligned} \quad (4.43)$$

$$\text{where } K_p = \frac{p\pi}{2}, \quad 1 \leq p \leq 4 \quad (4.44)$$

By using the techniques shown in Chapter 3, the periodicity of 2π on the K axis can be removed by writing Eq. (4.43) in the D form. The result is

$$\begin{aligned} \Xi(D,S) = & \frac{\pi}{2} [U_i(D,S)G(D,S) - D^3U_i(D^{-1},S)G(D^{-1},S)] \cdot \\ & \sum_{p=1}^4 u_o(D = D_p) \end{aligned} \quad (4.45)$$

$$\text{where } D_p = e^{-j(p\pi/2)} \quad 1 \leq p \leq 4 \quad (4.46)$$

Equation (4.45) can be generalized for the case of r sampling stations. When there are r sampling stations, the left end of the system is located at $x = -\frac{1}{2}$ and the right end is at $x = r - \frac{1}{2}$. The equation for this case is seen to be

$$\Xi(D, S) = \frac{\pi}{r} \left[U_i(D_p, S)G(D_p, S) - D_p^{2r-1} U_i(D_p^{-1}, S)G(D_p^{-1}, S) \right] \cdot \sum_{p=1}^{2r} u_o(D - D_p) \quad (4.47)$$

$$\text{where } D_p = e^{-jp\pi/r} \quad 1 \leq p \leq 2r \quad (4.48)$$

Equation (4.45) shows the effects that boundaries have on the transform of the deflection. When there were no longitudinal boundaries on the system, the transform was a continuous function on the D axis. When the boundaries are applied, the transform becomes impulses at the eigenvalues of D . The boundaries have also created zeros in the transform of the deflection. The term in brackets in Eq. (4.45) assures that a disturbance with the wrong phase cannot exist on the string.

There is a significant difference between the disturbance on a spatially discrete bounded system and the disturbance on a spatially continuous bounded system. For the spatially continuous system, Eq. (4.31) shows that the number of eigenvalues of K is infinite. For the spatially discrete system, Eq. (4.44) shows that the number of eigenvalues of D is finite. The difference in the number of eigenvalues can be explained by the argument that was presented in Section 4.2. The output of the continuous system is considered to be the continuous deflection of the string. Since there are an infinite number of points on the string, an

infinite number of eigenmodes is needed to describe the deflection. The output of the spatially discrete system is the deflection at a finite number of sampling points. Because the deflection is known at only a few points, only a few eigenmodes are needed to describe the measured output. As the number of sampling points increases, the number of eigenmodes also increases.

Discrete Spatial Feedback for a Bounded System

Similar to the case of a spatially continuous system, the transform of the discrete spatial deflection given by Eq. (4.47) does not appear as the product of a drive and a transfer function. The longitudinal boundaries force the disturbance to be a complicated function of the drive and the unbounded transfer function. This transform can be put in the desired form only when the drive or transfer function have certain forms.

For many systems, the character of a disturbance is independent of the direction of travel. A wave traveling to the left has the same speed, and sees the same impedance, as a wave traveling to the right. A system with this property has a transfer function which is an even function of K . If this system is spatially sampled, the discrete transfer function obeys the relation

$$G(D,S) = G(D^{-1},S) \quad (4.49)$$

The stationary string and its driving electrodes are a system whose transfer function has this property.

When the unbounded transfer function satisfies the condition given by Eq. (4.49), Eq. (4.47) can be written as

$$\Xi(D,S) = G(D,S) \left[\frac{\pi}{r} U_i(D,S) - \frac{\pi}{r} D^{2r-1} U_i(D^{-1},S) \right] \cdot \sum_{p=1}^{2r} u_o(D - D_p) \quad (4.50)$$

From Eqs. (4.31) and (4.47), it can be seen that ^{the} impulses and the term in brackets on the right side of (4.50) are the drive that exists on the bounded system. That is,

$$U(D,S) = \frac{\pi}{r} [U_i(D,S) - D^{2r-1} U_i(D^{-1},S)] \cdot \sum_{p=1}^{2r} u_o(D - D_p) \quad (4.51)$$

The feedback signal for this example is generated by amplifying the sampled deflection by a negative gain. The drive for the bounded system is therefore

$$U(D,S) = -A \Xi(D,S) \quad (4.52)$$

The transform of the deflection on the closed-loop system can be found by substituting Eqs. (4.51) and (4.52) into Eq. (4.50) to obtain

$$\Xi(D,S) = -AG(D,S) \Xi(D,S) \quad (4.53)$$

Equation (4.53) is of the same form as the equation for the closed-loop response of an unbounded system. The differences between the two cases are the restrictions applied to $\Xi(D,S)$ when longitudinal boundaries are present. Equation (4.47) shows that, when boundaries are present, $\Xi(D,S)$ can have a value only at the eigenvalues of D . Equation (4.47) also shows that the phase of $\Xi(D,S)$ and $\Xi(D^{-1},S)$ are not independent. If the boundaries are removed from the system, both of these restrictions are removed from $\Xi(D,S)$.

From Eq. (4.47), the deflection is of the form

$$\Xi(D,S) = \sum_{p=1}^{2r} \Xi_p(S) u_o(D - D_p) \quad (4.54)$$

where

$$D_p = e^{-jp\pi/r}$$

The following set of $2r$ equations is produced by substituting Eq. (4.54) into (4.53) and equating the impulses at the same values of D .

$$\Xi_p(S) = -AG(D_p, S) \Xi_p(S) \quad (4.55)$$

From this set of equations, a set of $2r$ servo-loops like the one in Fig. 4.7 can be drawn. By studying these servo-loops, the stability of each amplitude, Ξ_p , can be determined.

As an example, the transfer functions of the discrete eigenmodes will be derived for the case of the string illustrated in Fig. 4.6. The ends of the string are fastened at $x = -1/2$ and $x = 3/2$ and two feedback electrodes are used to drive it. This is the same example that was considered in § 4.3. In that previous example, the transfer functions are derived from the eigenmodes of the unsampled system. The form of these transfer functions is a series of poles in the K - S plane. For purposes of comparison, it is desirable for the results of the example worked here to also be in the form of a series. Therefore, the series form of $G(D, S)$, given in Eq. (3.67), is used here. If the closed form of $G(D, S)$ were used, the closed form of the transfer function would result.

For the case of two feedback stations ($r = 2$), Eq. (4.48) gives for the eigenvalues of D

$$D_p = e^{-\frac{jp\pi}{2}} \quad p = 1, 2, 3, 4 \quad (4.56)$$

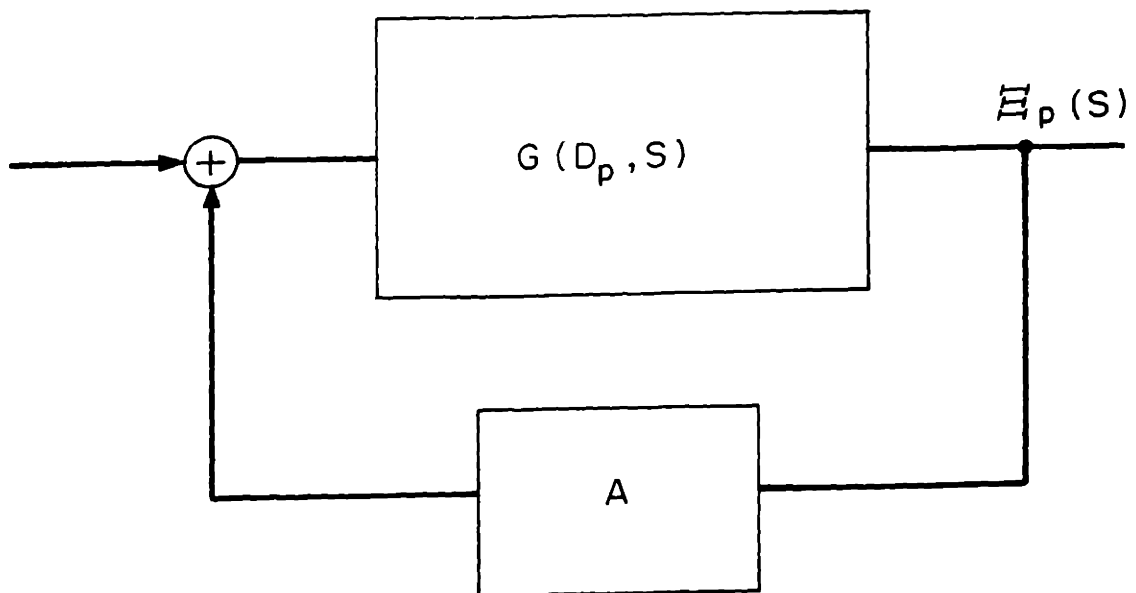


Figure 4.7 The bounded string with spatially discrete feedback can be represented by a finite number of servo loops. The transfer function in the servo loop is the spatially discrete transfer function of the unbounded string evaluated at the eigenvalues D_p .

These values of D_p correspond to the principal values of K

$$K_p = \frac{p}{2} \quad p = 1, 2, 3, 4 \quad (4.57)$$

Substituting the principal values of K from (4.57) into the series form of $G(D, S)$, Eq. (3.67), gives for the discrete transfer functions

$$G(D_p, S) \Big|_{K_p = \frac{\pi}{2}} = \sum_{n=-\infty}^{\infty} \frac{(-1)^n 2 \sin(\pi/4)}{(\pi/2 + 2n\pi) [S^2 + \delta S - N + (\pi/2 + 2n\pi)^2]} \quad (4.58)$$

$$G(D_p, S) \Big|_{K_p = \pi} = \sum_{n=-\infty}^{\infty} \frac{(-1)^n 2 \sin(\pi/2)}{(\pi + 2n\pi) [S^2 + \delta S - N + (\pi + 2n\pi)^2]} \quad (4.59)$$

$$G(D_p, S) \Big|_{K_p = \frac{3\pi}{2}} = \sum_{n=-\infty}^{\infty} \frac{(-1)^n 2 \sin(3\pi/4)}{(3\pi/2 + 2n\pi) [S^2 + \delta S - N + (\frac{3\pi}{2} + 2n\pi)^2]} \quad (4.60)$$

$$G(D_p, S) \Big|_{K_p = 2} = \sum_{n=-\infty}^{\infty} \frac{(-1)^n 2 \sin(\pi)}{(2\pi + 2n\pi) [S^2 + \delta S - N + (2\pi + 2n\pi)^2]} \quad (4.61)$$

The transfer functions given by Eqs. (4.58) and (4.60) are identical, and can be expanded to give

$$G(D_p, S) \Big|_{K_p = \frac{\pi}{2}, \frac{3\pi}{2}} = \frac{2\sqrt{2}}{\pi} \left[\frac{1}{[S^2 + \delta S - N + (\pi/2)^2]} + \frac{1}{3[S^2 + \delta S - N + (\frac{3\pi}{2})^2]} \right. \\ \left. - \frac{1}{5[S^2 + \delta S - N + (\frac{5\pi}{2})^2]} - \dots \right] \quad (4.62)$$

The transfer function given by Eq. (4.59) can be expanded to give

$$G(D_p, S)_{K_p = \pi} = \frac{4}{\pi} \left[\frac{1}{S^2 + \delta S - N + \pi^2} - \frac{1}{3(S^2 + \delta S - N + (3\pi)^2)} + \frac{1}{5[S^2 + \delta S - N + (5\pi)^2]} - \dots \right] \quad (4.63)$$

These transfer functions are the same as the previously derived transfer functions that are shown in Figs. 4.3 and 4.4.

If the transfer function in Eq. (4.61) is expanded, it is found to be zero.

$$G(D_p, S)_{K_p = 2\pi} = 0 \quad (4.64)$$

The reason the transfer functions are equal for the eigenmodes at $K_p = \pi/2$ and $K_p = 3\pi/2$ can be explained by Eq. (4.47). Examination of Eq. (4.47) shows the eigenmode for a given D (or K_p) is related to the eigenmode for the corresponding D_p^{-1} (or K_p). Since the amplitudes of these eigenmodes are not independent, the transfer functions for the two modes must be the same.

This relationship between the two modes is a consequence of the boundaries. It has been pointed out that the boundaries force the deflection to have a certain wavenumber and phase. The proper phase is obtained by making the two modes dependent. This dependence is easily seen by considering a spatially continuous system of length l . Two of the possible modes are $A_1 e^{j\pi x}$ and $A_2 e^{-j\pi x}$. If the system has ends at $x = 0$ and l , then A_1 must equal $-A_2$ and the deflection is of the form $\sin(\pi x)$. If the ends are at $x = \pm \frac{l}{2}$, then A_1 equals A_2 and the deflection is of the form $\cos(\pi x)$.

The transfer function for the eigenmode at $K_p = 2\pi$ is zero. The explanation for this can be found in Eqs. (4.17) and (4.18). When the system is described by the open-loop normal modes, the modes corresponding to $n = 0, 4, 8, 12, \dots$ cannot be detected by the feedback sensors (spatial samples). These modes therefore do not contribute to the sampled output. In Chapter 3, it was shown that the D transform represents a sum of the open loop modes. For the system considered here, the closed-loop eigenmode at $K_p = 2\pi$ ($D_p = 1$) represents a sum of all of the open-loop modes which are not detected by the feedback sensors. This closed-loop mode is also not detectable and its transfer function must be zero.

4.5 Determination of the System Stability from the Closed-Loop Modes

The stability of the closed-loop normal modes can be determined from the transfer functions of these modes. The poles of these functions in the S plane are found as functions of the variables A, N, and δ . The values of these parameters, for which the poles of all of the modes are in the left-half S plane, determine the region of stability in the A, N, δ plane.

A problem that can occur is that the closed-loop modes may be stable but the system is unstable. This happens if the instability is not detected by the control system. A potentially unstable wave which is not detected by the control system is illustrated in Fig. 1.2. If this wave is unstable, the system is unstable. Since the closed-loop modes consider only the deflection measured by the control system, the closed-loop modes can be stable for this case.

It is important that no potential instability be missed when the closed-loop normal modes are used. By carefully deriving the closed-loop modes,

the possible existence of these unobservable modes is revealed. These unobservable modes must be checked for stability along with the closed-loop modes.

In section 4.3, the closed-loop modes are derived from the open-loop modes. This derivation shows that unobservable disturbances are possible. For the case of two feedback stations, Eqs. (4.17) and (4.18) show that the modes $\bar{\epsilon}_4, \bar{\epsilon}_8, \bar{\epsilon}_{12} \dots$ are not observed by the control system.

To insure that the entire system is stable, both of the closed-loop modes and each of the unobserved open-loop modes must be checked for stability.

The existence of unobservable disturbances is also revealed when the closed-loop modes are derived from the Z transform of the unbounded system. For the case of two-station feedback, the transfer function for the eigenvalue $D = 1$ is found to be zero. The numerator of the transfer function is zero because the spatial sampling cannot detect the corresponding eigenmode. A trick which allows this mode to be seen is to ignore the zero in the numerator of the transfer function for $D = 1$. The roots in S of the denominator are then found, and if there are any poles in the right-half S plane, this unobservable mode is unstable.

The region of stability in the A, N, δ plane which can be computed from the closed-loop modes is not given here. This information has been given by Melcher [May, 1965] and there is no need to repeat it in this thesis.

4.6 Summary

In this chapter, three methods for describing a spatially sampled continuum system with boundaries have been compared. These three methods are: the matrix approach used by Gould, the theory of normal modes used by Melcher, and the Z transform.

The matrix approach considers the measured, or "sampled", deflections of the system as the outputs and the signals to the drivers as the inputs. This view of a continuum system results in a model with a finite number of coupled inputs and outputs. By the proper transformation, the normal coordinates of this system can be found. With these normal coordinates, the system can be made into a finite number of independent, single-input, single-output systems.

The Z transform method also considers the sampled deflection as the output. By using Fourier integral techniques, the discrete normal modes of the system are found. These modes are not coupled by the feedback. The total system then can be modeled by a finite sum of uncoupled feedback loops, one for every discrete normal mode. These discrete normal modes are the same as the normal coordinates found by Gould's method.

Melcher has modeled the bounded system by the normal modes of the system without feedback. This analysis considers the continuous deflection of the system as the output. By this approach, the output has an infinite number of degrees of freedom, and therefore an infinite number of modes are required to describe the system. By the proper mathematical manipulations, the information about the deflection between the sampling points can be dropped from Melcher's analysis, which then gives the same closed-loop normal modes that can be obtained from the Z-transform method or from Gould's matrix method.

The easiest method of determining if a spatially discrete system is unstable is to use Gould's method or the Z transform. Both methods provide the same set of independent feedback loops which represent the total system. By checking the stability of each of these loops, the total system stability can be found.

Melcher's normal-mode approach is more complicated than the other two methods, because it provides information about the entire deflection of the string. This method is useful when the deflection at every point of the string must be determined. With any spatially sampled system, there is a chance that the instability is not detected by the control system. With Melcher's normal-mode method and with the Z-transform method, any possible unobservable disturbances are easily identified. These unobserved modes can be checked, and the stability of the entire system can be determined.

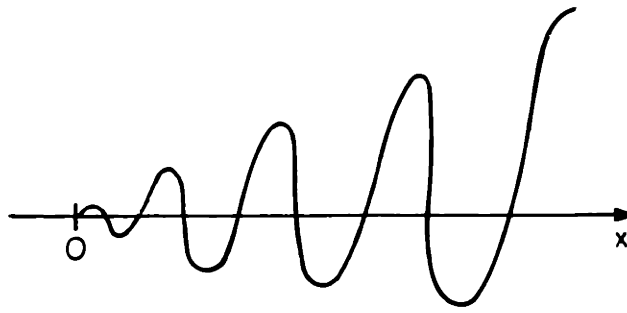
If Green's functions are used to derive a matrix description of the system, it is not apparent how the unobserved disturbances can be detected. Thus, for systems which may contain unobservable instabilities, the Z-transform and modal methods are probably the best methods to use.

CRITERIA FOR IDENTIFYING AMPLIFYING WAVES AND ABSOLUTE INSTABILITIES
ON A SPATIALLY DISCRETE SYSTEM

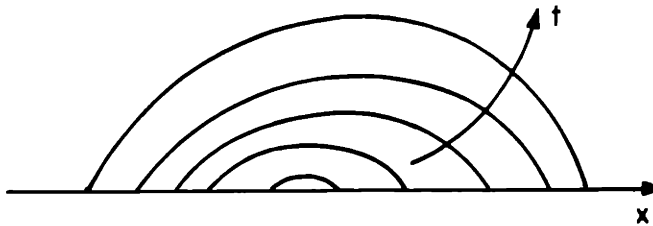
5.1 Introduction

When the stability of a continuum system is being studied, it is sometimes important not only to find out if instabilities are present, but also to determine the type of instability. Twiss (1951), Sturrock (1958) and others have indicated that it is possible for two distinct types of instabilities to be observed on spatially continuous systems of infinite extent: "convective" instabilities and "absolute" instabilities. These two types of instabilities are shown in Figs. 5.1a and 5.1b, respectively. When a system is unstable in the absolute sense, a pulse of finite amplitude and finite spatial extent will have unbounded growth at every point in space. When a system is convectively unstable, a pulse on the system will grow without bound as it moves along the system. The propagation is fast enough so that the pulse moves past any fixed point on the system. Eventually, the amplitude at any fixed point decreases to zero.

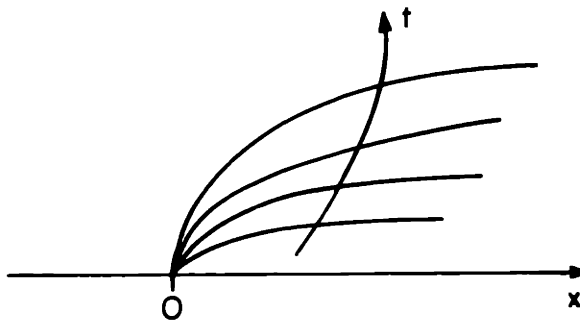
An absolute instability is often undesirable unless an oscillator or self-excited device is desired. A convective instability has practical applications in such devices as a traveling-wave tube. A pulse that is introduced at the input of a traveling-wave tube will grow. The convective nature of the instability causes the growing pulse to be transported along the tube. At the output end of the tube, the pulse is extracted. Due to the growth of the pulse as it traveled through the tube, the output is an amplified replica of the input. It is this, and other applications of



5.1a Convective Instability



5.1b Absolute Instability



5.1c Convective Absolute Instability

Figure 5.1 The three types of instability that can be observed on a spatially discrete continuum system.

convective instabilities that make it important to be able to distinguish between convective and absolute instabilities.

A method of distinguishing between amplifying and evanescent waves, and for detecting the presence of absolute instabilities, has been developed by Bers and Briggs (Oct. 1963). Their criteria are applicable to systems which are time-invariant and uniform in one spatial dimension. This type of system has perturbations of the form $\exp [j(\omega t - kx)]$. The relation between the frequency ω and the wavenumber k is given by the dispersion equation

$$\Delta(\omega, k) = 0 \quad (5.1)$$

When the system is spatially discrete, the problem of determining the type of an instability is more complicated. A spatially discrete system is not uniform in one spatial dimension, and a dispersion equation such as (5.1) does not exist. It is therefore impossible to use the Bers-Briggs stability criteria on a spatially discrete system.

Crowley (1965) has studied a jet of water which was stressed by an electric field. The kink mode is convectively unstable on this system. To control the instability, a spatially discrete feedback system was used. He found this feedback arrangement could stabilize the jet, and it would also cause a type of instability that is not seen on spatially continuous systems. This new type of instability is a mixture of a convective and an absolute instability. It resembles an absolute instability, because a pulse, applied to the system, will create an unbounded response at all points downstream of the point of excitation. The instability resembles a convective instability because the disturbances do not propagate upstream. This instability is illustrated in Fig. 5.1c.

Crowley found that the behavior of the system can be predicted analytically. He formulated stability criteria that require using the method of characteristics to determine the proper boundary conditions for the system. His method is more specialized than the adaptation of the method developed by Bers and Briggs. In Chapter 3, a method is presented for generating a dispersion equation for a spatially discrete system. This dispersion equation is a relation between the complex frequency S and the discrete spatial frequency D , which is of the form

$$\Delta(S,D) = 0 \quad (5.2)$$

A simple stability criterion was also developed to go with the dispersion equation. The system is unstable if, for any value of D with unit magnitude, the dispersion equation gives a value of S with a positive real part. This simple criterion does not give any information about the nature of the instability.

This chapter is concerned with modifying the Bers-Briggs criteria so that they can be applied to spatially discrete systems with dispersion equations like Eq. (5.2). With these new criteria, it is possible to determine if a spatially discrete system is stable, convectively unstable, absolutely unstable, or unstable in the hybrid mode which Crowley observed. For an example the string will be analyzed and the type of the instabilities will be determined. The string, with convection, is described by the same mathematical model as the water jet that was analyzed by Crowley. The results obtained here are therefore compared directly to Crowley's, and a verification of the modified Bers-Briggs criteria is obtained.

5.2 Stability Criterion for a Spatially-Sampled, Time-Independent System

Mason and Zimmerman (pp. 369 - 385) present a method for determining the stability of a time function from the function's Laplace transform. By their criterion, a function which propagates forward in time is unstable if the transform has a pole in the right-half S plane. A function propagating backwards in time is unstable if the transform has a pole in the left-half S plane.

In this section, an equivalent criterion is presented for time-independent spatially-sampled functions which can be described by D transforms. This criterion determines if the function is stable in a spatial sense; that is, does it remain unbounded as x approaches plus or minus infinity? This criterion is not very useful by itself; however, the ideas presented in this section must be understood before the stability criteria for temporal and spatial instabilities can be understood. If more information about Z transforms is needed, a thorough treatment, such as the book by Jury (1964), should be consulted.

The simple stability criteria for spatially sampled signals can be deduced by studying two functions; one function exists for positive values of x and the other for negative values of x ; these are:

$$f_1(x) = \begin{cases} e^{\alpha x} & x \geq 0 \\ 0 & x < 0 \end{cases} \quad (5.3)$$

$$f_2(x) = \begin{cases} e^{\alpha x} & x \leq 0 \\ 0 & x > 0 \end{cases} \quad (5.4)$$

Both of these functions are sampled at unit intervals on the x -axis; the sampled functions are

$$f_1^*(x) = \begin{cases} \sum_{n=1}^{\infty} e^{\alpha x} u_0(x-n) & x > 0 \\ 0 & x < 0 \\ \frac{1}{2} u_0(x) & x = 0 \end{cases} \quad (5.5)$$

$$f_2^*(x) = \begin{cases} \sum_{n=-1}^{-\infty} e^{\alpha x} u_0(x-n) & x < 0 \\ 0 & x > 0 \\ \frac{1}{2} u_0(x) & x = 0 \end{cases} \quad (5.6)$$

The reason that both functions have an impulse of value $1/2$ at the origin is that the sampling impulse at the origin detects only half the value of the step at the origin. A more complete explanation is given in § 3.3.

The LaPlace transforms of the sampled functions are

$$F_1^*(k) = -\frac{1}{2} + \sum_{n=0}^{\infty} e^{\alpha n} e^{-jnk} \quad (5.7)$$

$$F_2^*(k) = -\frac{1}{2} + \sum_{n=0}^{-\infty} e^{\alpha n} e^{-jnk} \quad (5.8)$$

By using the definition of D ,

$$D = e^{-jk} \quad (5.9)$$

the Laplace transforms can be rewritten as

$$F_1(D) = F_1^*(k) = \frac{1}{2} + e^{\alpha}D + e^{2\alpha}D^2 + \dots \quad (5.10)$$

$$F_2(D) = F_2^*(k) = \frac{1}{2} + e^{-\alpha}D^{-1} + e^{-2\alpha}D^{-2} + \dots \quad (5.11)$$

For $|D|$ less than $e^{-\alpha}$, the series of Eq. (5.10) will converge, and for $|D|$ greater than $e^{-\alpha}$, the series of Eq. (5.11) will converge. The sums of these series are

$$F_1(D) = \frac{1/2(1 + e^{\alpha}D)}{(1 - e^{\alpha}D)} \quad \text{for } |D| < e^{-\alpha} \quad (5.12)$$

$$F_2(D) = \frac{-1/2(1 + e^{\alpha}D)}{(1 - e^{\alpha}D)} \quad \text{for } |D| > e^{-\alpha} \quad (5.13)$$

These two transforms are the same except for a minus sign. A pole-zero plot of $F_1(D)$ is shown in Fig. 5.2a, and a pole-zero plot of $F_2(D)$ is shown in Fig. 5.2b. The regions of convergence of these transforms are marked by shading.

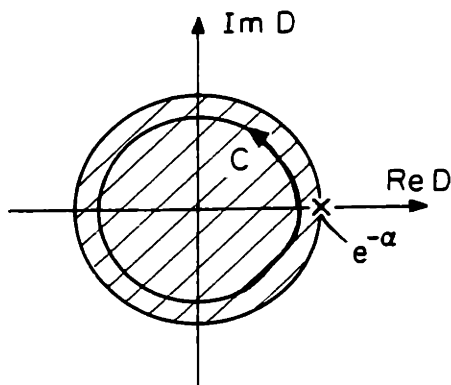


Fig. 5.2a

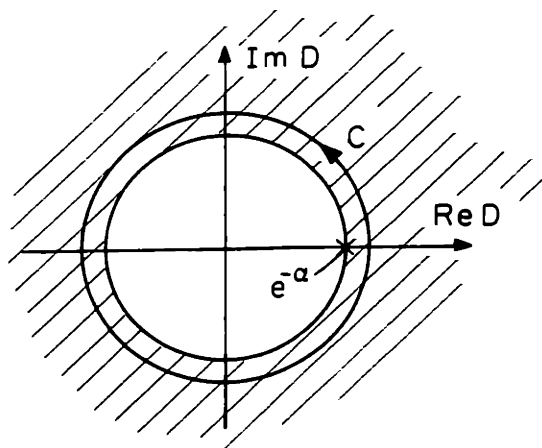


Fig. 5.2b

The formula for recovering the original function from the D transform is derived in §3.3. It is

$$f(n) = \frac{1}{2\pi j} \int_C F(D) D^{-(n+1)} dD \quad (5.14)$$

In Eq. (5.14), the contour C must not only surround the origin, but must also lie in the region of convergence of F(D). Suitable contours for $F_1(D)$ and $F_2(D)$ are shown in Figs. 5.2a and 5.2b.

The criterion for determining the stability of $f_1(n)$ and $f_2(n)$ from their D transforms can be deduced from Figs. 5.2a and b. Then α is greater than 0, the function $f_1(n)$ grows away from the origin, and the function $f_2(n)$ decays away from the origin. In Fig. 5.2, the poles will be inside the unit circle for this case. When α is less than zero, the function $f_1(n)$ decays away from the origin, while $f_2(n)$ grows away from the origin. For this case, the poles in Fig. 5.2 will be outside the unit circle. From these observations, the criterion for spatial stability of a spatially sampled function is:

- 1) If a pole of F(D) is located inside the unit circle ($\alpha > 0$), the function represented by F(D) is unstable if it exists on the positive x- axis. That is, this pole represents an unstable wave if it is outside the contour of integration used in Eq. (5.14).
- 2) If a pole of F(D) is located outside the unit circle ($\alpha < 0$), the function represented by F(D) is unstable if it exists on the negative x- axis. That is, this pole represents an unstable wave if it is inside the contour of integration used in Eq. (5.14).

This criterion considers only spatial instabilities; i.e., disturbances that are unbounded as one moves away from the origin. Time-dependent

instabilities are not taken into consideration. This criterion is therefore useful only for determining the existence of convective instabilities.

The big problem with the stability criterion presented in this section is that the region of convergence for the D transform must be known. When complex systems are studied, the region of convergence of the transforms usually is not known. Also, the possible presence of absolute instabilities makes the criterion inadequate.

In the following section, the Bers-Briggs criteria are modified to provide a useful set of criteria for determining the nature of instabilities on a spatially discrete system. With these new criteria, the problems of determining absolute instabilities and of finding the region of convergence of the D transform are overcome.

5.3 Development of Modified Bers-Briggs Criteria for Spatially

Sampled Systems

The Bers-Briggs criteria have been derived (Briggs, Chapter 2) for a system that is infinitely long in one spatial dimension and uniform in that same dimension. In this section, the equivalent criteria are derived for a system, infinitely long in the x- direction, that is spatially discrete. This spatially discrete system accepts inputs that are impulses in space and produces an output that is also an impulse train. The spatially discrete system is also uniform in a discrete sense. That is, if the position of the input is changed, the only change in the output is a similar change of position.

Green's Function Formalism

The simple criterion for spatial instability developed in the previous section was restricted because it required a knowledge of the region of

convergence of the D transform. This is equivalent to knowing if the original function exists on the positive or negative x- axis. If general criteria are to be developed for determining the types of instabilities, then a method must be found to excite waves and see which direction they travel. The method of exciting these waves in space is an adaptation of a technique used in circuit theory. In circuit theory, it is known that, after the drive to a circuit is turned off, the only signals present on the circuit are at the natural frequencies of the circuit. These responses at the natural frequencies may be thought of as the normal modes in time of the circuit. To excite these modes, the circuit is driven with a short pulse, and the resulting response is a combination of the temporal normal modes.

In a similar manner, the normal modes in space of a distributed system (continuum) can be excited by a pulse in space. In the region of space away from the driving pulse, the only response will be at the "spatial natural frequencies". The spatial natural frequencies determine the normal modes of the system. The source used in this analysis cannot be a pulse, because the discrete system accepts only impulses as inputs. The source used is therefore restricted to be a finite number of impulses located near the origin.

When absolute instabilities are present on a system, some waves grow without limit, and a steady-state response does not exist. If this growth is to be detected, the response must be observed at a finite time after the source is turned on. The source therefore is required to be zero for $t < 0$. By fixing the time the source is turned on, the response outside of the source region may be watched, to see if exponential growth exists.

If a convective instability may be present, it is necessary to watch the steady-state response outside of the source region. If this steady-state response contains any modes which are increasing away from the source region, then these modes are amplifying waves.

The source function which drives the discrete system is of the form

$$s^*(x,t) = f(t) \sum_n b(n) u_0(x-m) \quad (5.15)$$

where $f(t)$ is zero for $t < 0$ and $b(n)$ is zero except for a few values of n close to the origin.

The spatially discrete response of the system due to the drive $s^*(x,t)$ is computed using the spatially discrete Green's function for the system, $g^*(t,n)$. The response is

$$\xi^*(x,t) = \int_{-\infty}^{\infty} \sum_{n=-\infty}^{\infty} g^*(t-t', x-n) s^*(n,t') dt' \quad (5.16)$$

A double-sided Z transform is now performed on the spatial coordinate x , and a Laplace transform is performed with respect to time. The Z transform can be guaranteed to converge for $|D| = 1$ for all finite time because of the finite speed of propagation of any disturbance. The transform of the response is

$$\Xi(D,S) = G(D,S)F(S)B(D) \quad (5.17)$$

The source is considered to be an oscillator operating at a constant frequency. The excitation is therefore of the form

$$f(t) = e^{S_0 t} \quad t > 0 \quad (5.18)$$

and its transform is

$$F(S) = \frac{1}{S - S_0} \quad (5.19)$$

It should be noted that, since the source, $b(n)$, is localized, its transform contains no poles other than at $D = 0$. With Eq. (5.17), the actual response at any of the sampling points is found to be

$$\xi(n, t) = \frac{1}{(2\pi j)^2} \int_{-j\infty + \alpha}^{j\infty + \alpha} \oint_{|D|=1} G(D, S) F(S) B(D) e^{St} \bar{D}^{(n+1)} dD dS \quad (5.20)$$

Equation (5.20) gives the response of the system at any time and place in terms of the transforms of the Green's function and the drive. This is the proper format for investigating the response to see if it grows in time or in space. It is important to notice that outside of the source region, the only poles in D that affect the response are the poles of $G(D, S)$. These poles are at the values of D which satisfy Eq. (5.2), the dispersion equation for the system.

LaPlace Transform of the Response

It is convenient to define a new variable and to write Eq. (5.20) in a different form; let

$$\hat{\xi}(n, S) = \frac{1}{2\pi j} \oint_{|D|=1} G(D, S) B(D) D^{-(n+1)} dD \quad (5.21)$$

This new variable is the LaPlace transform in time of the response at a particular sampling point. In terms of this new variable, the response at a given sampling point is

$$\xi(n, t) = \frac{1}{2\pi j} \int_{-j\infty + \sigma}^{+j\infty + \sigma} \hat{\xi}(n, S) F(S) e^{St} ds \quad (5.22)$$

In order that the causality condition be obeyed, it is necessary for the contour of Eq. (5.22) to be to the right of any singularities of $\hat{\xi}(n, S)$. That is, σ should be larger than the fastest growth rate in time of any unstable wave. A method of finding this value of σ is given in the section on branch lines. For now, it will be assumed that a large enough value of σ has been selected.

From the previous discussion about the spatial limitations of the drive, the response in the source-free region is a sum of the normal modes of the system. That is, the response, $\hat{\xi}(n, S)$, is determined from the poles of the Green's function, $G(D, S)$. These poles are the roots of the dispersion equation, $\Delta(D, S) = 0$, for S on the Laplace contour. The contour integral for $\hat{\xi}(n, S)$ in the source-free region is illustrated in Fig. 5.3.

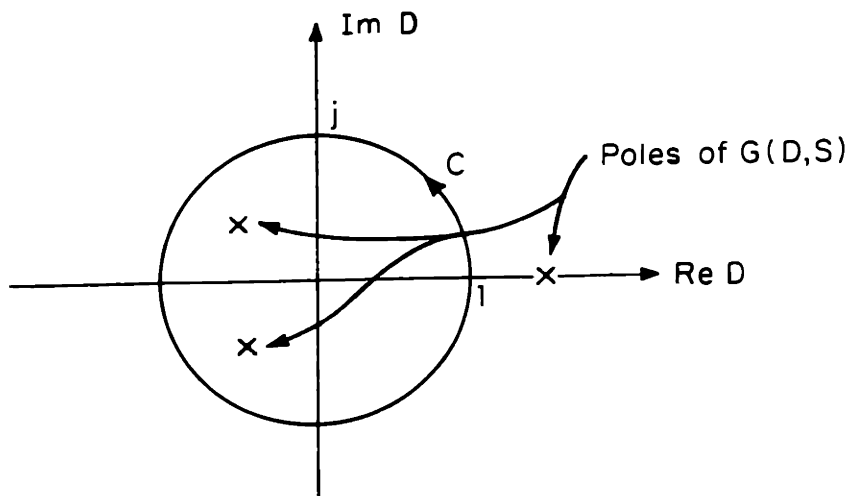


Figure 5.3

The poles inside the contour correspond to normal modes which exist to the left of the source, and the poles outside correspond to normal modes which exist to the right of the source. It is important to notice that the response $\hat{\xi}(n,S)$ consists of modes that all decay away from the source for any S on the Laplace contour.

Branch Lines of $\hat{\xi}(n,S)$

To obey the requirement of causality, it is necessary that the contour of Eq. (5.22) lie to the right of all of the singularities of $\hat{\xi}(n,S)$ in the right-half S plane. One of the two types of singularities that can occur is a branch line. The mechanism for finding these branch lines is shown in Fig. 5.4.

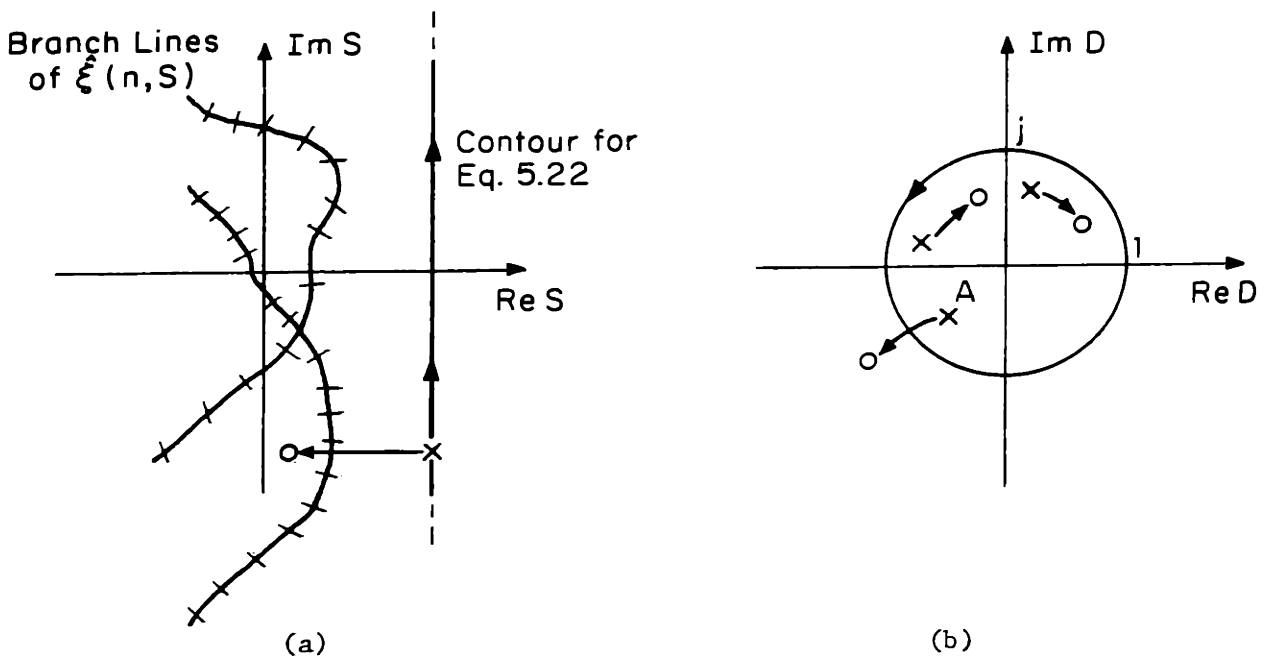


Figure 5.4

In Fig. 5.4a a value of S , marked by an x , is picked in the right-

half plane. The imaginary part of S is held fixed, and the real part is decreased from σ_1 to σ_2 . While the real part of S is changing, the poles of $G(D, S)$ are observed. From Eq. (5.21) and Fig. 5.4, the attentive reader can see that $\hat{\xi}(n, S)$ will be a continuous function of S , unless one of the roots of $G(D, S)$ crosses the unit circle, as illustrated by pole A in Fig. 5.4b. When this occurs, $\hat{\xi}(n, S)$ will jump in value, because the number of poles inside the contour of integration will change.

The loci of all points in the S plane which correspond to roots of $G(D, S)$ on the unit circle in the D plane are branch lines for the function $\hat{\xi}(n, S)$. These branch lines are the lines found by solving the dispersion equation, $\Delta(D, S) = 0$, for all values of D on the unit circle.

If a pole of $G(D, S)$ crosses the unit circle in the D plane for some S in the right-half S plane, then the dispersion equation must give values of S with a positive real part for some value of D with a unit magnitude. The value of σ used on the Laplace contour in Eq. (5.22) must therefore be larger than the maximum growth rate in time obtained from the dispersion equation for a value of D on the unit circle.

Analytical Continuation of $\hat{\xi}(n, S)$

If the integrals of Eqs. (5.21) and (5.22) are evaluated using the proper Laplace contour, the response of the system can be found for all time and space. If only the nature of the instability is desired, it may be unnecessary to perform the integral. With the proper mathematical trick, the desired information can be found without calculating the detailed response. The mathematical technique used to simplify the calculations is to define the analytical continuation of $\hat{\xi}(n, S)$. This technique is described by Hildebrand (Chapter 10) and Morse and Feshbach

(Chapter 4).

The analytical continuation of $\hat{\xi}(n, S)$, designated by $\check{\xi}(n, S)$, is found by redefining $\hat{\xi}(n, S)$ in its integral form as

$$\check{\xi}(n, S) = \frac{1}{2\pi j} \oint_C G(D, S) B(D) D^{-(n+1)} dD \quad (5.23)$$

Instead of being fixed to the unit circle, the contour C of the integral is allowed to deform to contain the same poles as S is moved toward the imaginary axis. The integral is illustrated in Fig. 5.5.

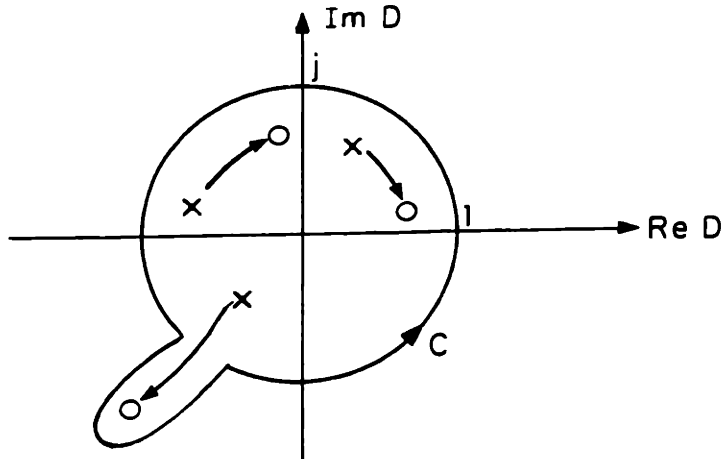


Figure 5.5.

The difference between $\check{\xi}(n, S)$ and $\hat{\xi}(n, S)$ can be seen by comparing the integrals illustrated in Figs. 5.4b and 5.5. As S crosses a branch line in Fig. 5.4a, the contour for $\check{\xi}(n, S)$ is deformed, so that no poles of $G(D, S)$ cross the contour. The value of $\check{\xi}(n, S)$ is therefore continuous as S crosses the branch lines of $\hat{\xi}(n, S)$.

For values of S which are to the right of any singularities of $\hat{\xi}(n, S)$, the values of $\hat{\xi}(n, S)$ and $\check{\xi}(n, S)$ are identical. Therefore,

$\tilde{\xi}(n, S)$ can be substituted for $\hat{\xi}(n, S)$ in Eq. (5.22) and the proper response of the system will still be found.

Distinguishing Between Amplifying and Evanescent Waves

By using the analytical continuation, $\tilde{\xi}(n, S)$, the criterion for distinguishing between amplifying and evanescent waves can be developed. To simplify the following treatment, the assumption is made that there are no singularities of $\hat{\xi}(n, S)$ in the right-half S plane, except for branch lines. The other possible singularity, a branch pole, is considered in the section on absolute instabilities.

The equation for the response of the system, in terms of $\tilde{\xi}(n, S)$, is

$$\xi(n, t) = \frac{1}{2\pi j} \int_{-j\infty + \sigma}^{+j\infty + \sigma} \tilde{\xi}(n, S) F(S) e^{St} dS \quad (5.24)$$

The integrals to find $\xi(n, t)$ and $\tilde{\xi}(n, S)$ are illustrated in Figs. 5.6a and 5.6b., for values of n outside of the source region. The Laplace contour which is to the right of the branch lines of $\hat{\xi}(n, S)$, is illustrated by the dashed line in Fig. 5.6a. The solid contour in Fig. 5.6a represents a contour that can be used to find the response when it is defined in terms of $\tilde{\xi}(n, S)$. This contour is to the right of the singularities of $\tilde{\xi}(n, S)$, and it is also to the right of the pole of $F(S)$.

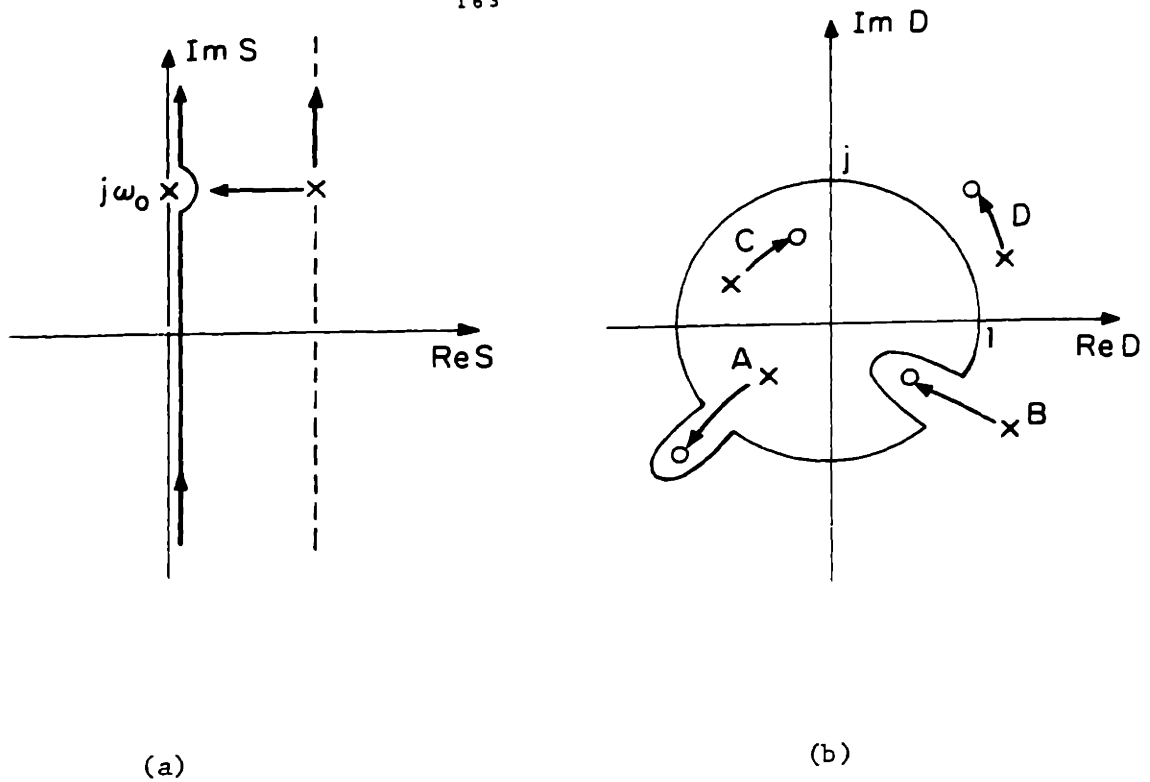


Figure 5.6

The response obtained by using the solid contours illustrated in Fig. 5.6 is the same response that is obtained by using the Laplace contour for the integral in the S plane, and the unit circle for the contour in the D plane. This fact can be seen by moving the contour in the S plane to the right until it coincides with the Laplace contour. The contour in the D plane can now be deformed to the unit circle without changing the enclosed poles. Since no singularities, in either plane, have crossed a contour of integration, the response obtained by either set of contours is the same.

Whenever the value of S is on the Laplace contour, the values of $\hat{\xi}(n, S)$ and $\check{\xi}(n, S)$ are the same. It therefore follows that the response obtained by using Eq. (5.24) and the solid contour shown in Fig. 5.6a is the same as that obtained by using Eq. (5.22) and the Laplace contour.

The use of the analytical continuation of $\tilde{\xi}(n, S)$ has allowed the contour of integration in the S plane to be moved to the imaginary axis. The pole of the driving function at $S = j\omega_0$ prevents the contour from moving farther to the left. The response of the system due to any poles of $\tilde{\xi}(n, S)$ in the left-half S plane will decay with time. Thus, the response of the system for large time will be

$$\lim_{t \rightarrow \infty} \xi(n, t) \approx \tilde{\xi}(n, j\omega_0) e^{j\omega_0 t} \quad (5.25)$$

By using the stability criterion for spatial instabilities developed in § 5.2, it can be determined from Fig. 5.6b if amplifying waves exist on the system. The poles A and C are inside the contour, and correspond to waves traveling in the negative x -direction; the poles B and D are outside the contour, and correspond to waves traveling in the positive x -direction. The pole A is outside the unit circle and represents an amplifying wave that grows as x becomes more negative; B is inside the unit circle and represents an amplifying wave that grows as x becomes more positive. The poles C and D represent waves that decay in the minus and plus x directions, respectively.

The criteria for distinguishing between amplifying and evanescent waves can now be stated. The loci of the values of D , which are found from the dispersion equation, are plotted as S is varied from $j\omega_0 + \sigma$ to $j\omega_0$. If a locus of D crosses the unit circle, then this root corresponds to an amplifying wave at $S = j\omega_0$. If the locus moves from outside of the unit circle to the inside as the real part of S decreases, the wave amplifies in the positive x -direction; if the locus moves from inside

the unit circle to the outside, the wave amplifies in the negative x -direction. Loci which do not cross the unit circle correspond to evanescent waves. This test must be repeated for all real values of ω_0 , and the value of σ must be picked larger than the fastest possible growth rate in time of an unstable wave.

Branch Poles of $\tilde{\xi}(n,S)$

In the development of the criterion for distinguishing between amplifying and evanescent waves, the only type of singularity considered was a branch line. The other possible singularity is a branch pole, which can cause an absolute instability if it is in the right-half S plane. The mechanism for finding the branch poles of $\tilde{\xi}(n,S)$ is illustrated in Fig. 5.7. A value of S , marked by an x , is picked in the right-half S plane at $j\omega_0 + \sigma$. The imaginary part of S is held fixed and the real part is decreased toward zero. The loci of the values of D , which are obtained from the dispersion equation, are plotted as S is varied.

For some values of S , marked by an O in Fig. 5.7a, two poles in the D plane may come together from opposite sides of the contour. The particular value of S for which this occurs is a branch pole of $\tilde{\xi}(n,S)$. At the branch pole, the contour of integration used to find $\tilde{\xi}(n,S)$ is pinched between two poles, and a singularity of $\tilde{\xi}(n,S)$ results. This singularity can be seen by expanding the dispersion equation about the double root at $D = D_2$ to get

$$\Delta(D,S) = \left(\frac{\partial \Delta}{\partial S} \right)_{\substack{j\omega_0 + \sigma_2 \\ D_2}} (S - j\omega_0 - \sigma_2) + \frac{1}{2} \left(\frac{\partial^2 \Delta}{\partial D^2} \right)_{\substack{j\omega_0 + \sigma_2 \\ D_2}} (D - D_2)^2 \quad (5.26)$$

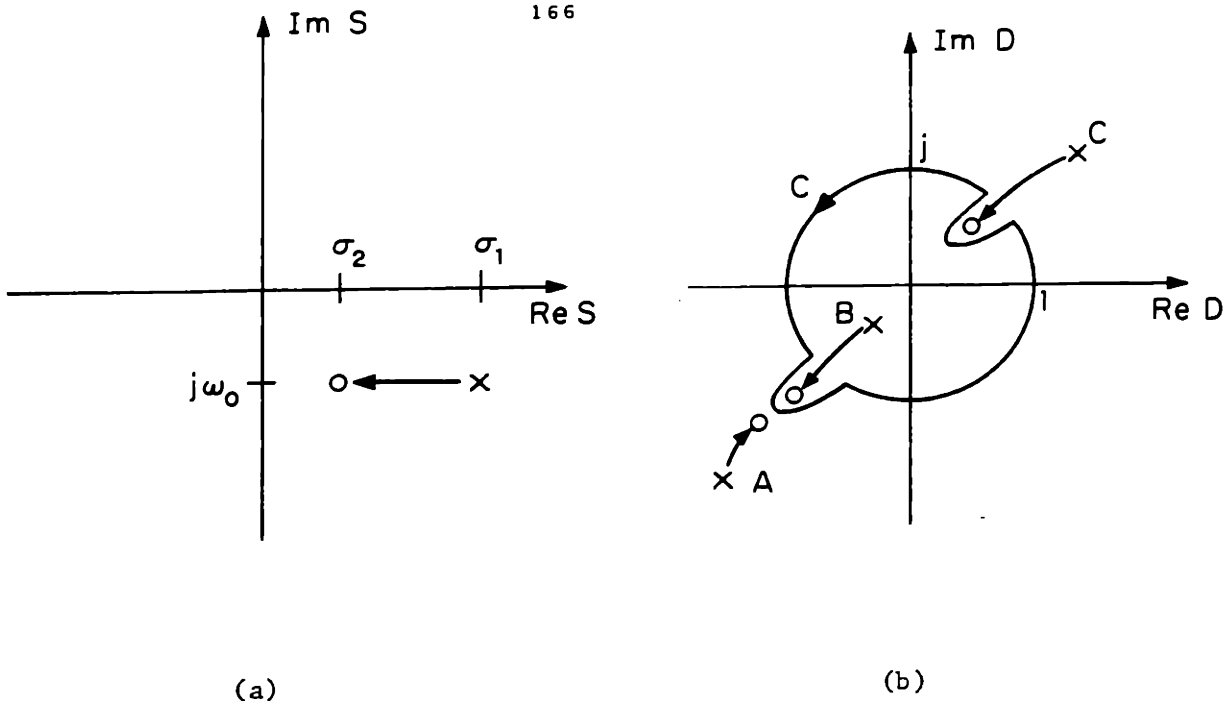


Figure 5.7

The first partial derivative with respect to D is zero, because of the double root of D at D_2 .

Equation (5.26) can be used to find the poles of the Green's function in the D plane as S approaches $j\omega_0 + \sigma_2$. By using these poles in Eq. (5.23), the value of $\tilde{\xi}(n, S)$ is found to be

$$\tilde{\xi}(n, S) \approx \frac{B(D_2)D_2^{-(n+1)}}{\left[2 \left(\frac{\partial \Delta}{\partial S} \right) \left(\frac{\partial^2 \Delta}{\partial D^2} \right) \right]_{D_2}^{1/2} (S - j\omega_0 - \sigma_2)^{1/2}} \quad (5.27)$$

Other poles of the Green's function also make a contribution to $\tilde{\xi}(n, S)$. Their effect was considered in the section on amplifying waves, and is ignored in this section.

Criterion for Determining the Presence of Absolute Instabilities

When the response in time is calculated, the branch pole of $\tilde{\xi}(n, S)$ must be taken into account. The proper contour of integration for Eq. (5.24) is shown in Fig. 5.8.

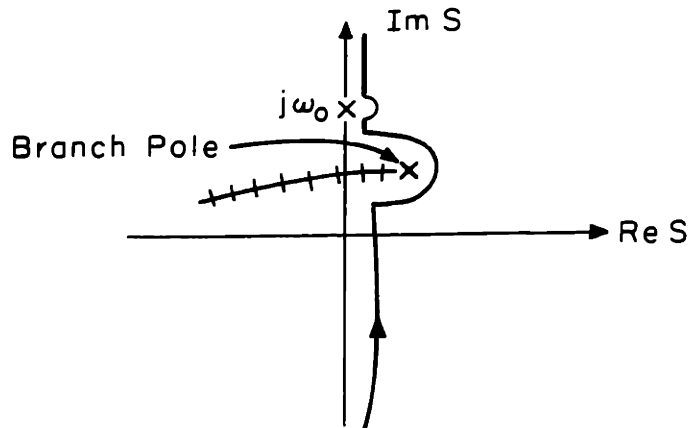


Figure 5.8

To obey the requirement of causality, this contour must lie to the right of the branch pole and the pole of the driving function. The singularity which is the farthest into the right-half plane is the dominant influence as $t \rightarrow \infty$. For the case illustrated in Fig. 5.8, the branch pole is the dominant term, and the response due to this branch pole is

$$\tilde{\xi}(n, t) \approx \frac{B(D_2)F(j\omega_o + \sigma_2)D_2^{-(n+1)}e^{(j\omega_o + \sigma_2)t}}{\left[2\pi j\right] \left[2\left(\frac{\partial \Delta}{\partial S}\right)\left(\frac{\partial^2 \Delta}{\partial D^2}\right)\right]^{1/2}} \int_C \frac{e^{(S - j\omega_o - \sigma_2)t} dS}{(S - j\omega_o - \sigma_2)^{1/2}}$$

$$\approx \frac{B(D_2)F(j\omega_o + \sigma_2)D_2^{-(n+1)}e^{(j\omega_o + \sigma_2)t}}{\left[2\pi j\left(\frac{\partial \Delta}{\partial S}\right)\left(\frac{\partial^2 \Delta}{\partial D^2}\right)\right]^{1/2}} t^{1/2} e^{j\omega_o t + \sigma_2 t} \quad (5.28)$$

$S = j\omega_o + \sigma_2$
 $D = D_2$

The response due to the branch pole is seen to be growing exponentially in time for every value of n . This exponential growth does not occur for every pair of poles of $G(D,S)$ which come together. If two roots start on the same side of the contour in the D plane, they will not pinch the contour between themselves when they meet. This double pole will therefore give only a finite contribution to $\tilde{\xi}(n,S)$ as S approaches the critical value and no exponential growth occurs.

From the previous discussion, the criterion for determining if an absolute instability exists can be stated. As the frequency, S , is varied from $j\omega_0 + \sigma$ to $j\omega_0$, the loci of the values of D , which are the roots of the dispersion equation, are plotted. If two roots, which start on opposite sides of the unit circle, come together, then an absolute instability will exist for that value of S . This test must be repeated for all real values of ω_0 to find the frequency with the fastest growth rate. The initial value of σ that is used must be larger than the largest growth rate obtained from the dispersion equation for a value of D on the unit circle.

Criteria for Determining the Presence of a Convective-Absolute Instability

It has been shown by Crowley that an absolute instability that does not propagate upstream can exist on a spatially discrete system. The system is characterized by an unbounded growth at all sampling points downstream of the initial disturbance. This unbounded response does not occur upstream from the initial disturbance.

The method for determining the existence of this instability is similar to the method used to find absolute instabilities. For an

absolute instability, the poles of the Green's function are observed as the real value of S is decreased. If two poles pinch the contour of integration for $\tilde{\xi}(n,S)$ between themselves, an absolute instability results. The poles of the Green's function are the only singularities in the integral for $\tilde{\xi}(n,S)$ that are watched. The pole in the integrand of Eq. (5.23) due to the term $\bar{D}^{-(n+1)}$ is not considered in the test for an absolute instability.

It is possible, in Eq. (5.23), for a pole of the Green's function to pinch the contour of integration between itself and the pole, due to the term $\bar{D}^{-(n+1)}$ as the real part of S is decreased. Pole A in Fig. 5.9 illustrates this event. When the contour is pinched in this manner, a singularity results in the right-half S plane, and the response of the system is characterized by exponential growth in time.

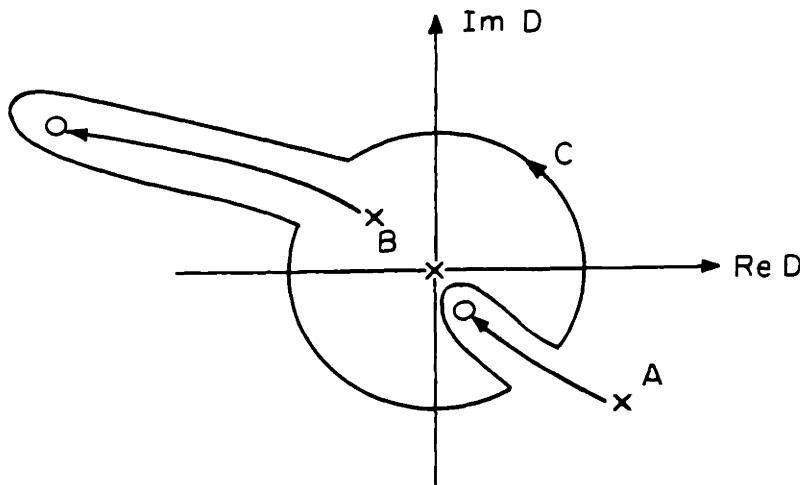


Figure 5.9

From Eq. (5.23) it can be seen that, at the sampling points on the negative x - axis ($n < 1$), the pole due to $D^{-(n+1)}$ will be at infinity and not at the origin. For these values of n , a singularity does not occur in the right-half S plane when the pole A moves to the origin. The exponential growth in time of the disturbance will therefore occur only on the positive x - axis or for $n > 0$.

It is also possible for a system to exhibit exponential temporal growth only on the negative x - axis ($n < 0$). If a pole drags the contour to infinity, then the contour is pinched between this pole of the Green's function and the pole due to $D^{-(n+1)}$. This effect is illustrated by pole B in Fig. 5.9. When the value of n is positive, $D^{-(n+1)}$ is not a pole at infinity. The movement of pole B to infinity as S is moved toward the imaginary axis does not pinch the contour, and does not cause a singularity in the right-half S plane. The movement of the pole B to infinity will therefore create exponential growth in time only on the negative x - axis.

The exponential growth on the positive x - axis can be demonstrated mathematically by expanding the dispersion equation about the root in the D plane that is near zero:

$$\Delta(S,D) \approx \left(\frac{\partial \Delta}{\partial S} \right)_{j\omega_0 - \sigma_2} (S - j\omega_0 - \sigma_2) + \left(\frac{\partial \Delta}{\partial D} \right)_0 (D - 0) \quad (5.29)$$

Using (5.29) as the denominator of the Green's function, the value of $\tilde{\xi}(n,S)$, computed from Eq. (5.23), is

$$\tilde{\xi}(n, S) = \frac{B(0) \left[\left(\frac{\partial \Delta}{\partial D} \right)^n \left(\frac{\partial \Delta}{\partial S} \right)^{-(n+1)} \right]_{D=0}}{(S - j\omega_0 - \sigma_2)^{n+1}} \quad (5.30)$$

This value was computed by considering the pole of $D^{-(n+1)}$ as the only pole inside the contour of integration. The multiple pole at $S = j\omega_0 + \sigma$ will lead to a disturbance of the form

$$\tilde{\xi}(n, t) = \frac{B(0)F(j\omega_0 + \sigma_2)}{n!} \left[\left(\frac{\partial \Delta}{\partial D} \right)^n \left(\frac{\partial \Delta}{\partial S} \right)^{-(n+1)} \right]_{D=0} t^n e^{j\omega_0 t + \sigma_2 t} \quad (5.31)$$

This disturbance is exponentially growing for all positive values of n . For values of n less than zero, the pole at the origin disappears, and there is no exponential growth in time. This same analysis can be repeated for roots of the Green's function which drag the contour to infinity and create exponential growth for all points on the negative x -axis.

The criterion for determining the existence of a convective-absolute instability can be summarized. The frequency S is varied from the value $j\omega_0 = \sigma_1$ to $j\omega_0$, and the loci of the poles of the Green's function are plotted in the D plane. If a pole, which started outside the unit circle, hits the origin, then the system is absolutely unstable on the positive x -axis. If a pole which started on the inside of the unit circle goes to infinity, the system is absolutely unstable on the negative x -axis. This test must be repeated for all real values of ω_0 and the initial value, σ_1 , must be larger than the fastest growth rate obtained from the dispersion equation for values of D on the unit circle.

5.4 An Example: The Convecting String

For an example, the modified Bers-Briggs criterion is applied to the convecting string, described by Eq. (1.4). This example is picked because the convecting string, with spatially discrete feedback, can exhibit the three types of instability which are possible on a spatially discrete system.

The equation of Motion of the string, including damping and convection, is derived in Chapter 1. It is

$$\frac{1}{v^2} \frac{D^2 \xi}{Dt^2} = \frac{\partial^2 \xi}{\partial x^2} - \alpha \frac{D\xi}{Dt} - \beta \frac{\partial \xi}{\partial t} + k_c^2 \xi + g v_d \quad . \quad (5.32)$$

The feedback scheme used in this example is the same spatially discrete system that was studied in Chapter 3. The feedback system is illustrated in Fig. 3.1 and the spatially discrete voltage it produces is shown in Fig. 3.2.

If the convective velocity of the string is set to zero, Eq. (5.32) describes the stationary string which is known to exhibit absolute instabilities. If both damping terms are set to zero in Eq. (5.32), the equation describes the unstable water jet which Crowley has studied. He has shown that the jet can exhibit either the convective instability or the convective absolute instability. When the convecting damping term and the constant k_c are set to zero, the equation describes a system which has a resistive-wall instability. Woodson and Melcher [pp. 608-613] have analyzed this resistive-wall instability, and have shown that it is a convective instability.

Both of the previously mentioned studies have used the method of

characteristics to determine the nature of the instability. By repeating the studies, using the modified Bers-Briggs criterion, the two methods can be compared.

The derivation of the D-S dispersion equation for the convecting string is similar to that of the dispersion equation for the stationary string given in Chapter 3. The only change that is made is the inclusion of the convection term in the equation of motion.

Taking the LaPlace transform in time and the Fourier transform in space of Eq. (5.32) gives

$$\Xi(k,s) \left[\frac{1}{v_p^2} (s + jku)^2 + k^2 + \beta s + \alpha(s + jku) - k_c^2 \right] = gV_d(k,s). \quad (5.33)$$

By defining the following dimensionless variables, the length of a driving electrode, L , is normalized to one.

$$S = sL/v_p \quad (5.34a)$$

$$K = kL \quad (5.34b)$$

$$\delta = \beta v_p L \quad (5.34c)$$

$$\nu = \alpha L v_p \quad (5.34d)$$

$$N = k_c^2 L^2 \quad (5.34e)$$

$$U = u/v_p \quad (5.34f)$$

$$F(K,S) = gL^2 V_d(K,S) \quad (5.34g)$$

With the dimensionless variables, Eq. (5.33) is rewritten to illustrate the transfer function relating the deflections of the string to the driving force.

$$\Xi(K,S) = \frac{F(K,S)}{[S^2 + K^2(1-U^2) + K(2USj + \nu Uj) + \delta S + \nu S - N]} \quad (5.35)$$

It is shown in § 3.4 that the driving force, $F(K,S)$, is generated by driving the electrodes by a spatial impulse train, $U^*(K,S)$. The transfer function between the driving impulses and the string's deflection is the product of the transfer function of the driving electrode and the transfer function of the convecting string. It is

$$G(K,S) = \underbrace{\frac{e^{jK/2} - e^{-jK/2}}{jK}}_{\text{driving electrode}} \underbrace{\frac{1}{[S^2 + K^2(1-U^2) + K(2USj + \nu Uj) + \delta S + \nu S - N]}}_{\substack{\text{convecting} \\ \text{string}}} \quad (5.36)$$

The feedback signal for this example is generated by sampling the deflection of the string at the center of each electrode pair. To find the transfer function relating the measured deflection to the electrode inputs, Eq. (3.28) is used with (5.36) to get

$$G(D,S) = \frac{1 - e^{-jK}}{2\pi j(1-U^2)} \int_{-\infty}^{+\infty} \frac{e^{jQ/2} dQ}{Q(Q + \lambda + jW)(Q + \lambda - jW)(1 - e^{-jK} e^{+jQ})} \quad (5.37)$$

where

$$\lambda = \frac{2UjS + \nu Uj}{2(1-U^2)} \quad (5.38a)$$

$$\text{and } W = \frac{[S^2 + \nu S + \delta S(1-U^2) - N(1-U^2) + (\nu^2 U^2/4)]^{1/2}}{(1-U^2)} \quad (5.38b)$$

The contour for the integral is made to include only poles of $G(K,S)$ and the discrete transfer function is obtained in closed form. The values of the residues at these poles are

$$\text{Residue } (Q=0) = \frac{1}{(\lambda^2 + W^2)(1-D)} \quad (5.39)$$

$$\text{Residue } (Q = -\lambda + jW) = \frac{e^{-j\lambda/2} e^{-W/2}}{(-\lambda + jW)(2jW)(1 - De^{-j\lambda - W})} \quad (5.40)$$

$$\text{Residue } (Q = -\lambda - jW) = \frac{e^{-j\lambda/2} e^{W/2}}{(-\lambda - jW)(-2jW)(1 - De^{-j\lambda + W})} \quad (5.41)$$

The discrete transfer function is $2\pi j$ times the sum of the residues multiplied by the coefficient of the integral in Eq. (5.37), which is

$$\begin{aligned} G(D, S) = & \frac{(1 - D) e^{-j\lambda/2} (+2\lambda) \sinh(W/2) (1 + De^{-j\lambda})}{(1 - U^2) (\lambda^2 + W^2) (2jW) (1 - De^{-j\lambda} e^{-W}) (1 - De^{-j\lambda} e^{+W})} \\ & + \frac{(1 - D) (-2jW) \cosh(W/2) (1 - De^{-j\lambda}) e^{-j\lambda/2}}{(1 - U^2) (\lambda^2 + W^2) (2jW) (1 - De^{-j\lambda} e^{-W}) (1 - De^{-j\lambda} e^{+W})} + \frac{1}{(1 - U^2) (\lambda^2 + W^2)} \end{aligned} \quad (5.42)$$

When the sampled deflection is amplified and fed back to the driving electrodes, the system can be represented by the servo loop shown in Fig. 3.11. The transfer function of the closed-loop system is

$$T(D, S) = \frac{G(D, S)}{1 + AG(D, S)} \quad (5.43)$$

The dispersion equation for the closed-loop system is found by equating the denominator of the closed-loop transfer to zero. Using Eqs. (5.43) and (5.42), this dispersion equation is found to be

$$\begin{aligned} & [(1 - U^2) (W^2 + \lambda^2) + A] (2jW) [1 + D^2 e^{-2j\lambda} - 2De^{-j\lambda} \cosh W] \\ & + A(1 - D) e^{-j\lambda/2} [2\lambda \sinh(W/2) (1 + De^{-j\lambda}) - \\ & 2jW \cosh(W/2) (1 - De^{-j\lambda})] = 0 \end{aligned} \quad (5.44)$$

This is the dispersion equation for the convecting string with discrete spatial feedback. It is a second-order polynomial in terms of the discrete spatial wavenumber, D . To apply the modified Bers-Briggs criteria

to this dispersion equation, the quadratic formula is used to find the two roots in D for any value of S in the right-half plane. Without the complication of spatial discreteness, the string is described by a dispersion equation that is a quadratic function of K . To apply the Bers-Briggs criterion to the dispersion equation of the continuous system, the quadratic formula is used to find the two roots in K for values of S in the right-half plane. It therefore can be seen that, by using the discrete spatial wavenumber D and the modified Bers-Briggs stability criterion, the spatially discrete system can be studied as easily as the continuous system.

The Stationary String: An Absolute Instability

In Chapter III, the stability of the stationary string is analyzed in detail. It is assumed that any instability on the system is an absolute instability. This assumption is made because there is no obvious mechanism for convecting a growing pulse away from its initial position.

The modified Bers-Briggs plot of the stationary string ($U = 0$) for one set of the parameters is shown in Fig. 5.10. The value of gain, A , is 50 and the parameters ν , δ and N are zero. This plot shows that, for some value of S between $j6.0$ and $j6.5$, the two loci, which started on opposite sides of the unit circle, come together. According to the stability criterion, the string is absolutely unstable for this set of parameters. By repeating this test for various values of N , A , and δ , the same region of stability as shown in Fig. 3.15 can be found.

It is of interest to review the numerical procedure used in Chapter III to obtain the stability plot of Fig. 3.15 and compare it with the modified Bers-Briggs method. In Chapter III, the roots of the dispersion

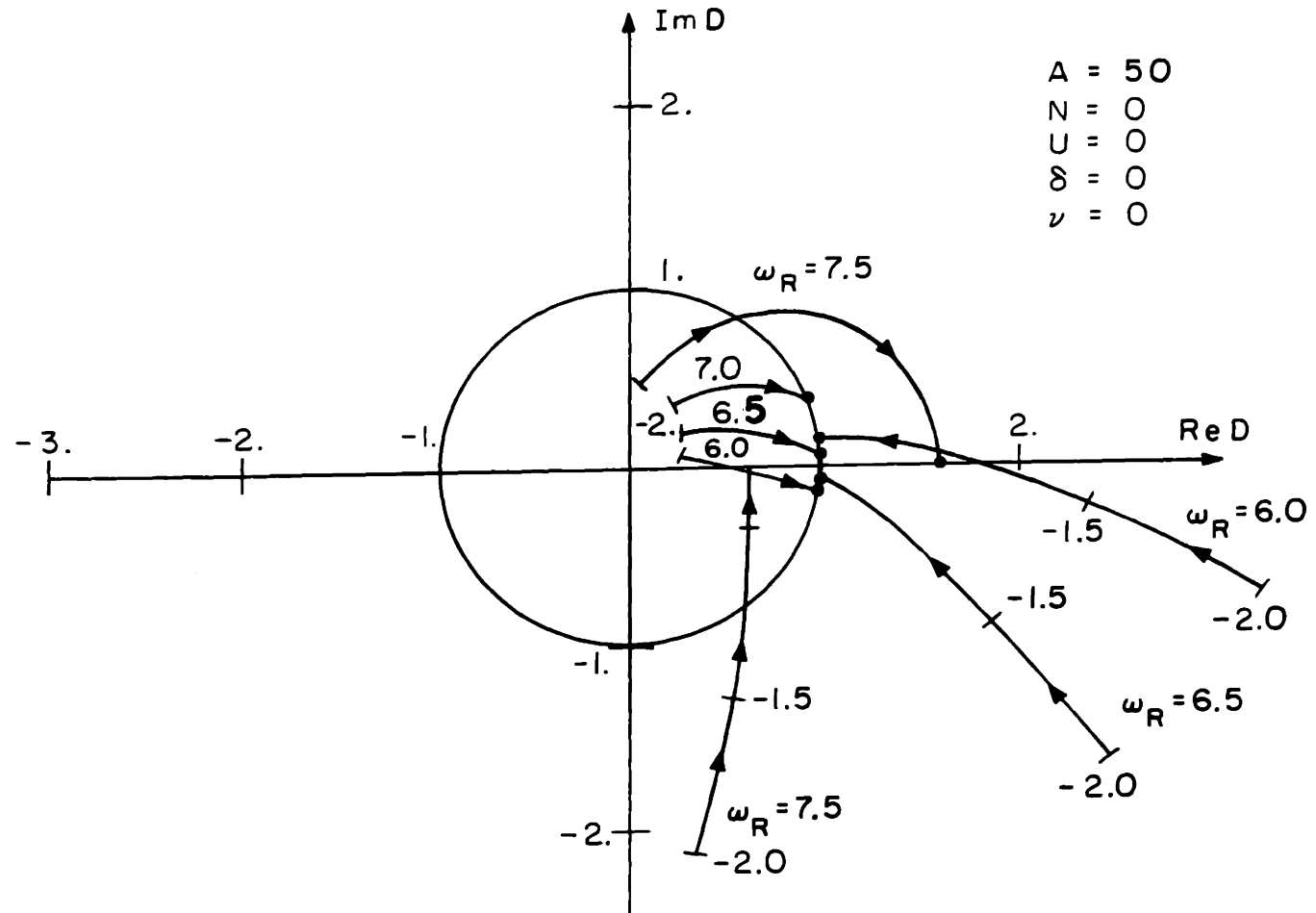


Figure 5.10 The modified Bers-Briggs plot for the stationary string. The string is absolutely unstable for $6.0 < \omega_R < 6.5$.

in S are found for values of D on the unit circle. Since the dispersion equation is transcendental in S , an iterative procedure must be used to find the roots. The process is further complicated because there are an infinite number of roots in S for each value of D . Enough of the roots must be found to assure that there are no overlooked instabilities. The procedure must be repeated for enough values of D on the unit circle to assure that the most unstable value of D has been found.

When the modified Bers-Briggs method is used, the roots of the dispersion equation in D are found for values of S in the right-half plane. The dispersion equation is a quadratic function of D , and the two roots can be found with the quadratic formula. This procedure must be repeated for enough values of S in the right-half plane to assure that all critical frequencies have been investigated.

The advantages of each method can be seen. If the dispersion equation is used to find the frequencies S which result for a given D , then many roots must be found by an iterative procedure. If the discrete wave-number D is found from the dispersion equation for a given value of S , only two roots must be found and the quadratic formula can be used. When D is used as an input parameter in the dispersion equation, representative values are picked from the unit circle. When S is used as an input parameter, representative values must be picked from the entire right-half plane. The result is that, when S is the input parameter to the dispersion equation, finding the roots in D is an easy operation but many values of S must be tried. When D is used as the input parameter, finding the roots in S is difficult, but only a few values of D are tried.

A Resistive Wall Interaction: Convective Instability

Convective instabilities can result when a stream interacts with a stationary structure. An example of an application of this effect is a traveling wave tube. Here, an electron beam is coupled to a stationary transmission line, and an amplifying wave results. The amplifying wave is used to amplify signals in microwave systems. The coupling of an electron beam to a stationary structure can also have undesirable results. The beam in a particle accelerator can couple to the resistance in the accelerator wall, which causes the beam to become unstable and limits the maximum beam current. This effect has been studied by Birdsell, Brewer and Haeff, and by Laslett, Neil and Sessler.

A simplified version of the resistive-wall instability has been studied by Woodson and Melcher [pp. 608-612]. They studied the convective string which is surrounded by a stationary viscous material. The transverse deflections of the string are convectively unstable because of the coupling between the moving string and the stationary damping material. The system which they have studied can be described by Eq. (5.35) if the transverse stress, N , and the convecting damping term, ν , are set to zero. When the velocity, u , is greater than the phase velocity, v_p , the stationary damping causes the string to be unstable.

The consequences of applying spatially discrete feedback to the string to influence the instability can easily be determined. The closed-loop dispersion equation for the system is obtained from Eq. (5.44) by using the proper constants. The stability criteria are then used to determine if there is a value of gain for which the string is stable.

A plot of the loci of the roots of the closed-loop dispersion equation for the string is shown in Fig. 5.11 for the parameter values $A = 4$, $\delta = 2$, and $U = 2$. For large negative values of the imaginary part of ω , the loci are both outside the unit circle. As the imaginary value of ω moves toward zero, some of the loci cross the unit circle; the string is therefore convectively unstable for this set of parameters.

Other values of gain, damping, and velocity can be tested by plotting the loci of the roots of the D-S dispersion equation. If the normalized velocity is greater than one, the result is always the same; the feedback cannot stabilize the string. This result probably occurs because the feedback force is not similar to the unstabilizing force. In Eq. (5.33), the damping is seen to produce a force proportional to the time derivative of the deflection, while the feedback force is proportional to the deflection. The feedback force is sometimes adding to the unstabilizing force and sometimes it is subtracted from it. The final result is that the spatially discrete feedback scheme used here cannot stabilize the resistive-wall instability on the string.

The Perpendicularly Stressed Water Jet: Convective Instability

In his doctoral thesis, Crowley has studied the control of a water jet which was stressed in the transverse direction by an electric field. Because of the applied electric field, the transverse deflections of the jet are convectively unstable. In an attempt to control the instability, a spatially discrete feedback system was used, which sensed the deflection of the jet at several locations and drove the jet by electrodes which applied a constant force to a segment of the jet. With the proper constants

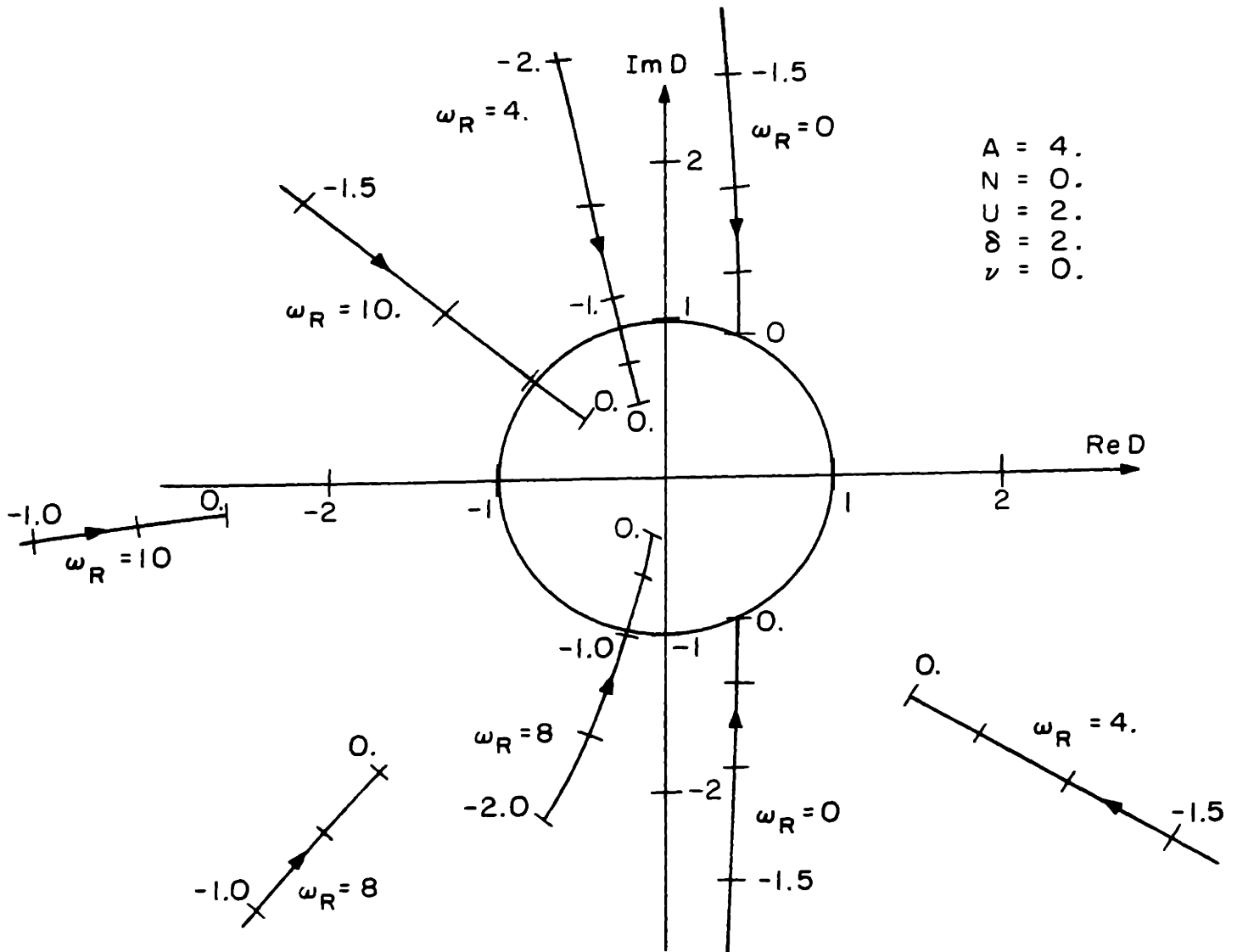


Figure 5.11 The modified Bers-Briggs plot for convecting string with stationary damping. The string is convectively unstable.

the jet's transverse deflections can be described by the same equation that describes transverse deflections of the string, (1.4). The jet has very little damping and thus both damping terms are assumed to be zero. The convective velocity, u , must also be greater than the phase velocity, v_p . If this condition is not satisfied, the liquid jet can not be formed; only blobs of liquid would issue from the nozzle.

The electrode structure used by Crowley to apply the bias electric field and the driving field to the jet is similar to the electrode structure shown in Fig. 3.1. The feedback force applied to the jet is also generated in the same manner as that used in Chapter 3; the deflection of the jet is measured at the center of each driving electrode segment and a proportional voltage is applied to the segment. The closed-loop transfer function for the jet is therefore obtained from the transfer function for the convecting string, Eq. (5.43), by setting the damping terms to zero and requiring the normalized velocity to be greater than one.

The water jet with discrete spatial feedback is studied here for several reasons. This example shows how discrete spatial feedback can be used to influence a system which is convectively unstable. That information may be useful for the design of amplifiers or other devices which use an amplifying wave. This example also illustrates how the modified Bers-Briggs criteria can simplify the analysis of a convecting system. When Crowley studied the water jet, he had to use the method of characteristics to determine the proper boundary conditions for a disturbance and to determine the nature of the instabilities. With the stability criteria presented here, all of the boundary conditions can be deduced from the D-S dispersion equation and there is no need to study the res-

ponse of the system in space and time with a characteristic plot.

Since this example has already been done in detail by Crowley, comparing the results obtained here with his results should provide a check on the validity of the stability criteria.

In Fig. 5.9, it is shown that the stationary string is absolutely unstable when it is stressed by an electric field. The initial excitation of the string excites waves which travel in both directions, and thus, for values of S with a large positive real part, the two loci are on opposite sides of the contour. As the real part of S is decreased, the two loci come together and the contour is pinched between them. An absolute instability therefore exists on the stationary string.

If the string is moved toward the right (+ x direction) at a velocity greater than that of propagation on the string, all of the waves on the string will propagate toward the right. Both the loci in the modified Bers-Briggs plot will then begin outside the unit circle for large positive values of the real part of S . According to the stability criteria, the system cannot support an absolute instability because the contour cannot be pinched between the two loci. However, the string will exhibit a convective instability if either of the two loci crosses the unit circle as the real part of S is decreased.

A plot of the loci for the water jet is shown in Fig. 5.12 for one value of A and N . This plot is generated by the same method used to generate Figs. 5.10 and 5.11. The two roots in D of the dispersion equation are found for a value of S in the right-half plane. The imaginary part of S (real part of ω) is held constant, and the real part of S (negative imaginary ω) is decreased. The loci of the roots of the

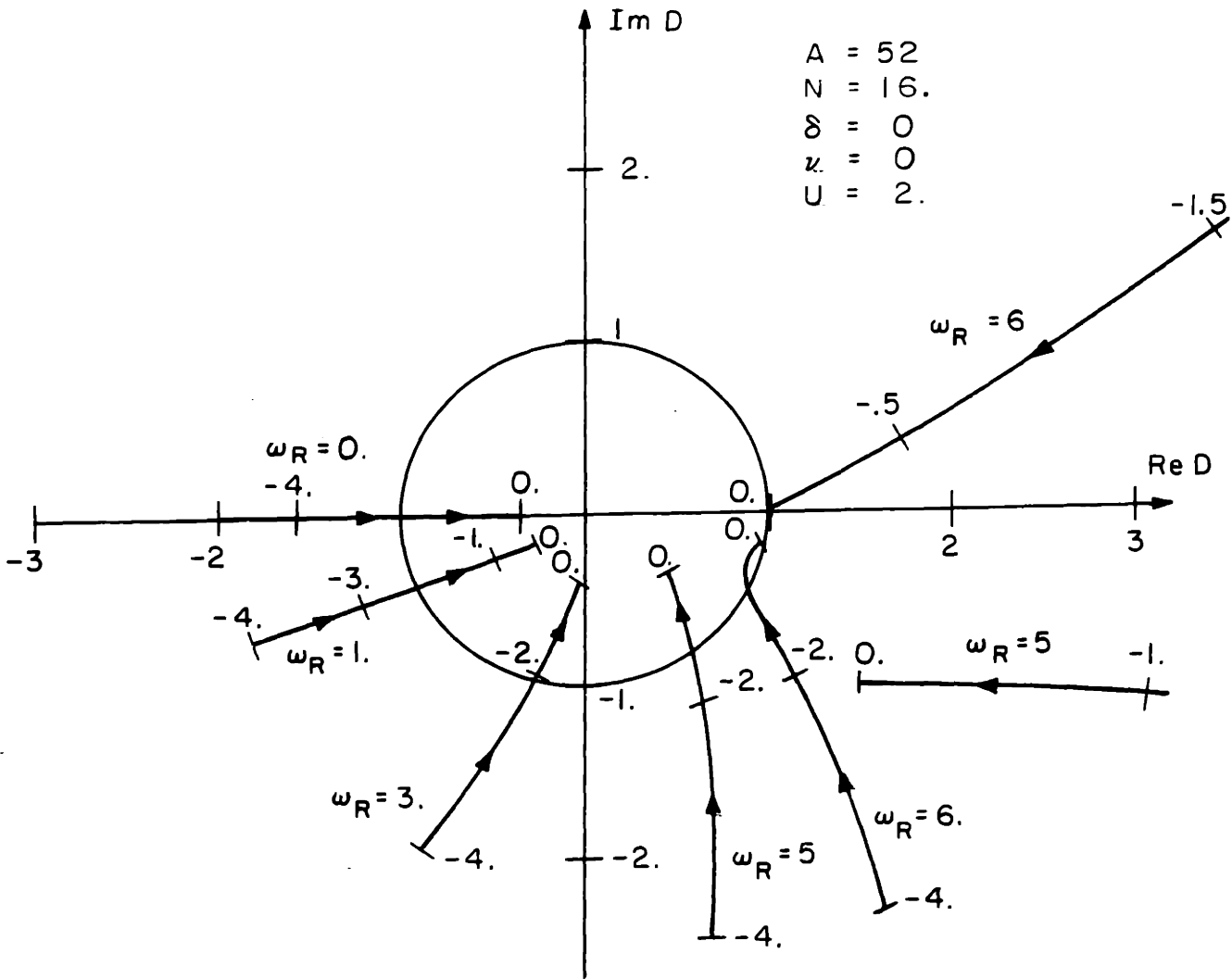


Figure 5.12 The modified Bers-Briggs plot for the water jet with discrete spatial feedback. The jet is convectively unstable.

dispersion equation are plotted for the different values of real S . On these loci, the real value of (ω_R) is given and the points corresponding to various values of imaginary ω are marked.

The plot of the loci shows that for $A = 52$ and $N = 16$, the jet is unstable. Since all disturbances are carried downstream by the jet, both loci are located outside the unit circle for values of ω with a large negative imaginary part (large positive S_R). As the imaginary value of ω approaches zero, the loci move toward the origin. For some values of ω_R , one of the loci crosses the unit circle and thus the system is convectively unstable for disturbances of this frequency.

The other values of A and N can be checked to find the values for which the lateral deflections of the jet are stable. For the other values of the parameters, it is not necessary to plot the loci of D for values of ω in the lower half plane (S in the right-half plane). Figure 5.12 shows that both loci are outside the unit circle when ω has a large negative imaginary part. As the imaginary value of ω is increased, the loci may cross the unit circle. If the jet is unstable for the particular value of gain and electrical stress, one of the loci will end inside the unit circle for a value of ω on the real axis. The stability of the system can thus be determined by finding the two roots in D of the dispersion equation for all real values of ω .

The region of stable operation of the jet in the A - N plane is shown in Fig. 5.15. This region has one significant difference from the stable region of the stationary string. The right-hand boundary

is located at $N = 4\pi^2$, while the boundary for the stable region of the stationary string (Fig. 3.15) is located at $N = \pi^2$. When there is no convection, the right-hand boundary is caused by the inability of the sensors to detect a disturbance whose wavelength is equal to two sampling distances. With convection, the sensors can detect a disturbance of any wavelength, and the boundary is moved farther to the right. The right-hand boundary for the convecting system occurs because the driving electrodes cannot drive a disturbance whose wavelength is equal to the width of the electrode segment.

The stable region of the jet is similar to that of the stationary string in two ways. Line $A = N$ forms most of the lower boundary for the stable region for the jet and the string. The stable region is bounded on the top by an overstability which is caused by the spatially discrete control system.

The results shown in Fig. 5.15 are similar to those obtained by Crowley and confirm that the use of the modified Bers-Briggs criteria is consistent with the use of the method of characteristics.

The Perpendicularly Stressed Water Jet: Convective-Absolute Instability

Crowley has found that with high values of feedback gain, the water jet can exhibit the convective-absolute instability. This is caused by the spatially discrete nature of the feedback sensors and drivers. The sensor measures the deflection of the jet and a force, proportional to the measured signal, is applied to a section of the jet. The applied force is centered around the sensor and thus both

upstream and downstream portions of the jet are affected. The upstream portion of the jet moves past the sensor, and a new signal is generated which causes the jet upstream of the sensor to be driven. If the proper conditions are satisfied, the interaction of the control system and the jet can cause an absolute instability in the region of the electrode and sensor. Because the driving electrode does not affect the jet at the next sensing point upstream, the absolute instability is not transported upstream from the point of excitation. The natural velocity of the jet carries the disturbance downstream. The result is the convective-absolute instability. All points downstream from the original excitation are characterized by unbounded growth.

According to the modified stability criteria for a spatially discrete system, a convective absolute instability will occur when one of the loci of D pinches the contour against the origin for some value of S in the right-half plane. The value of gain (A) necessary to cause this to happen for a given amount of perpendicular stress (N) can be found by the following method. The closed-loop, D - S dispersion equation for the jet is generated by setting the damping terms δ and ν , equal to zero in Eqs. (5.38a) and (5.38b). The value of D in the dispersion equation (5.44) is set equal to zero and the following equation is obtained:

$$(S^2 - N + A) \frac{2j[S^2 - N(1-U^2)]^{1/2}}{(1-U^2)} - 2A_j W \cosh(W/2) = 0 \quad (5.45)$$

The solutions of (5.45) are the values of S for which one value of D in Eq. (5.44) is zero. If the value of S lies in the right-half S plane, then a convective-absolute instability will exist for the corresponding

values of N , U , and A .

Figure 5.13 shows a root-locus plot of one root in S of Eq. (5.45) for $U = 2$ and $N = 4$. As the gain is increased beyond 130, the root moves into the right-half plane. For values of gain large enough to move a root of Eq. (5.45) into the right-half plane, a value of D equal to zero can be found from the dispersion equation for a value of S in the right half plane. The gain necessary to move the root locus in Fig. 5.13 into the right-half plane is thus that necessary to induce the convective-absolute instability.

A stability plot of the loci of the roots of D is given in Fig. 5.14, for the values $A = 87$ and $N = 16$. These values were selected because a root locus plot similar to that of Fig. 5.13 has shown them to be unstable. Both the loci start outside of the unit circle for large negative values of ω_i . As the magnitude of ω_i decreases, the loci move toward the origin, and one of them hits the origin for a value of ω_R between 15 and 16. The incipience of the convective absolute instability for $N = 16$ will consequently occur for a gain, A , slightly less than 87 and for a frequency, ω_R , a little higher than 15.

The region in the A - N plane where the jet exhibits the convective-absolute instability is shown in Fig. 5.15. It can be seen that this region is bordered by the convectively unstable region; the stable region and the region of the convective-absolute instability do not touch. This happens because the loci have to cross the unit circle to get to the origin. For each value of N , there is a value of gain less than the value needed for the convective absolute instability, for which the loci penetrate into the unit circle but do not reach the origin. These values of gain cause the region of convective-absolute

instability to be bounded from below by a region of convective-absolute instability.

The boundary for the convective-absolute instability in Fig. 5.15 is calculated by making root-locus plots, similar to Fig. 5.13, from Eq. (5.45). The loci of the roots of the dispersion equation do not have to be computed. It is necessary, however, to construct one of the plots of the loci of D to insure that the locus which hits the origin starts outside the unit circle for large negative values of the imaginary part of ω .

5.5 Summary

Criteria for determining the existence and type of instabilities on a spatially discrete system are developed in this chapter. These criteria make it possible to determine if the system is stable, or if it exhibits an absolute instability, a convective instability, or a convective-absolute instability.

Bers and Briggs have previously derived stability criteria, which are used to investigate the stability of spatially continuous systems. Their criteria are applied to the ω - k dispersion equation for the system. The criteria presented here are derived by modifying the Bers-Briggs so they can be applied to spatially discrete systems described by an S - D dispersion equation. For an example, the criteria are applied to the string driven by a spatially discrete feedback system. It is shown that, with the proper values of gain, damping, and convection, the string can exhibit any of the three possible types of instability.

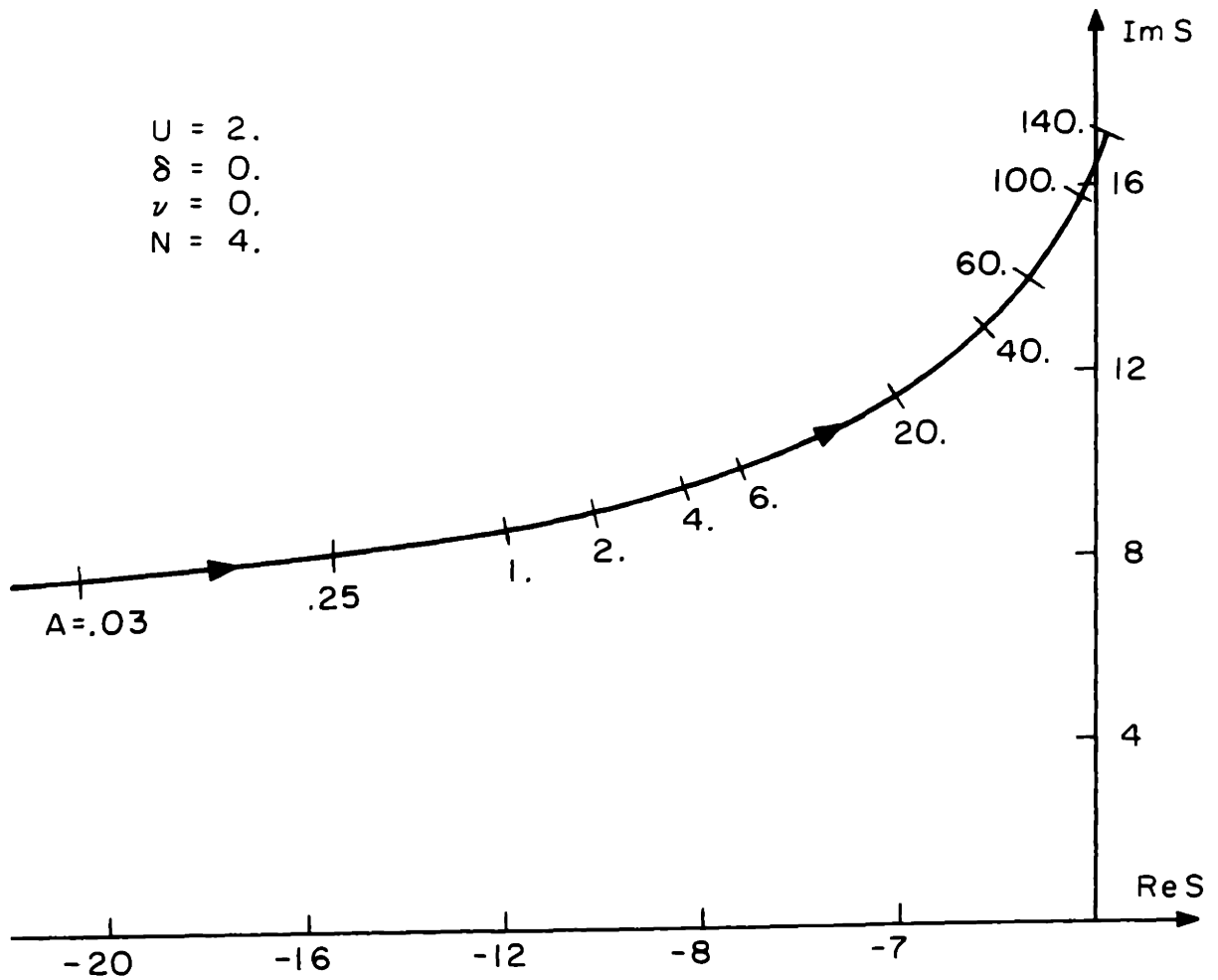


Figure 5.13 A root-locus plot of S for the jet with D set to zero. The jet has the convective absolute instability when the gain approaches 140.

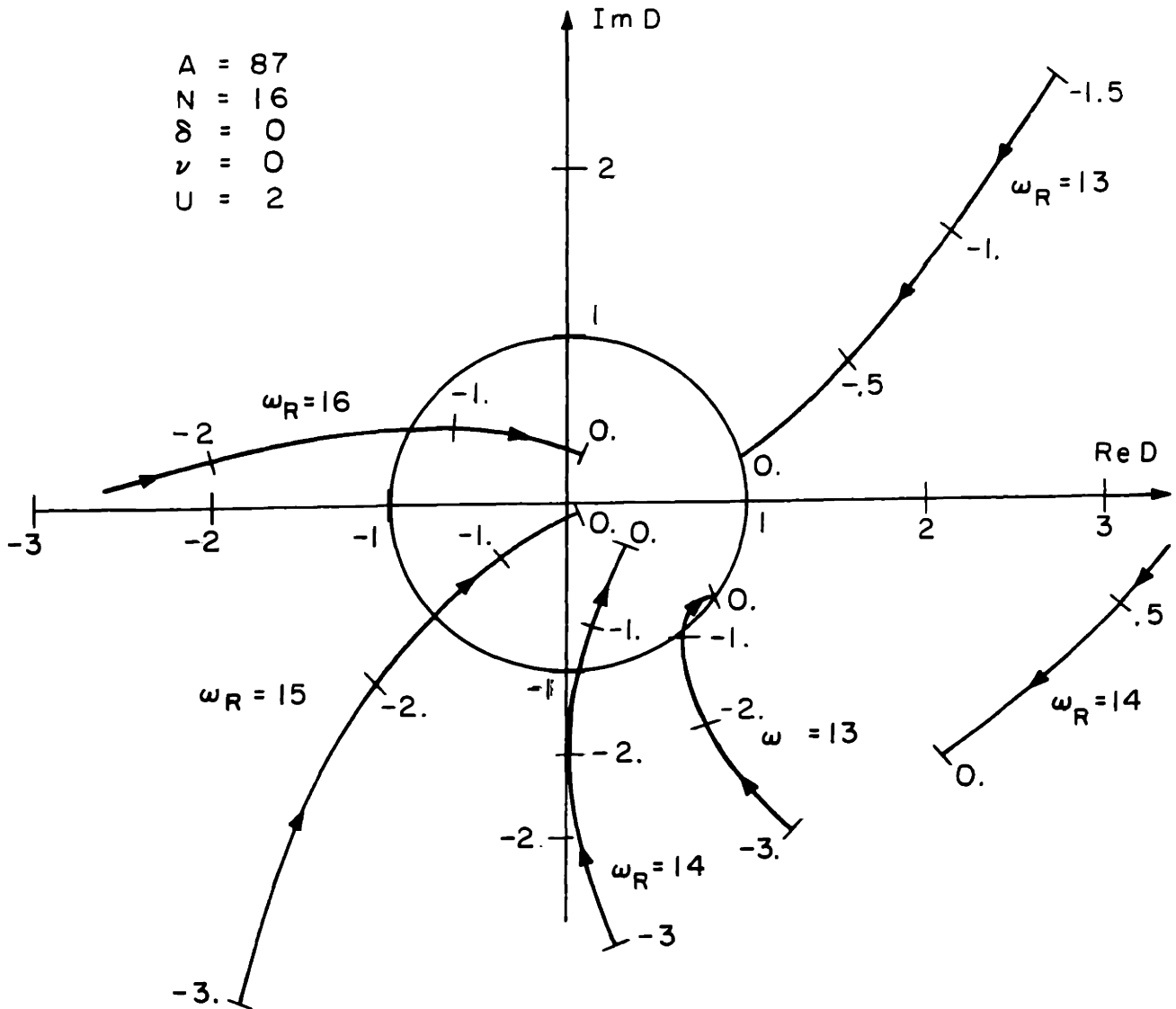


Figure 5.14 A modified Bers-Briggs plot for the jet showing the existence of the convective absolute instability.

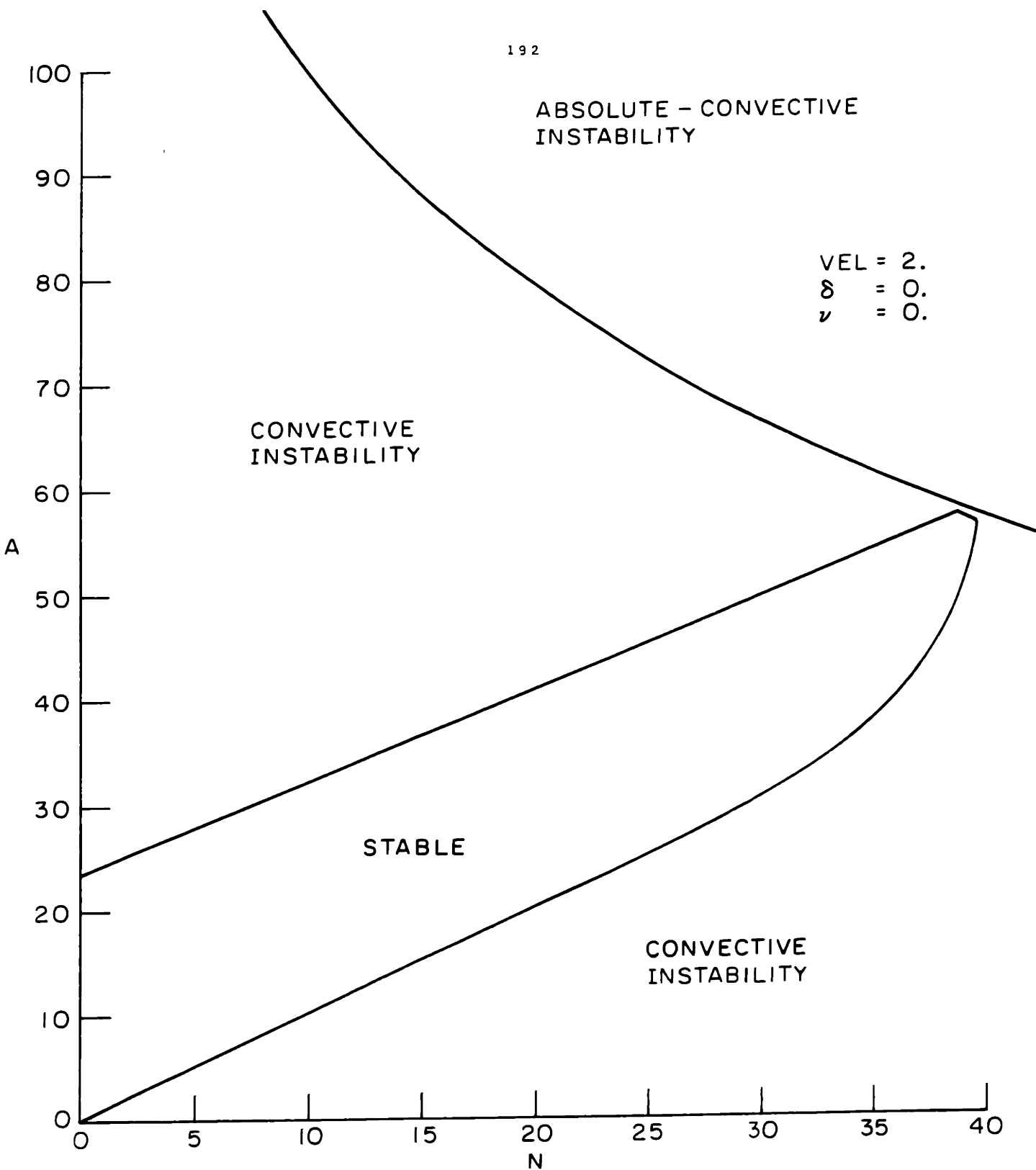


Figure 5.15 The regions of stable and unstable for the water jet as determined from the S-D dispersion equation. The types of instabilities are identified by using the modified Bers-Briggs criteria.

Discrete Spatial-Discrete Temporal Continuum Feedback

6.1 Introduction

For continuum feedback control systems which contain many feedback drivers and sensors, a time-sharing technique is attractive to generate the numerous control signals. It is explained in Chapters I and III that continuum feedback control systems are spatially discrete systems. The addition of a time multiplexed feedback system will make them also temporally discrete systems.

Thomas [1966] has analyzed the problem of a finite system with discrete temporal and spatial feedback. The system he studied is the same as the bounded string shown in Fig. 4.2, except that his driving voltages were generated on a discrete temporal basis. He described the deflections of the string with the normal modes of the undriven string. As the number of sampling stations became larger, the number of normal modes necessary to describe the system became too large for the method to be useful.

In Chapters II and III, it is shown that Z-transform theory is a useful tool for studying discrete temporal or discrete spatial feedback on a continuum. This technique is useful because the information concerning the string's deflection between the sampling times or sampling points is disregarded. In this chapter, the Z-transform is extended to the case of an infinite continuum, driven by a discrete temporal-discrete spatial feedback system. By ignoring the information about the string's deflection between sampling locations and times, a useful description of the system is made.

The system studied in this chapter is shown in Fig. 6.1. This system is the familiar string, driven by a series of electrodes which each affect a section of the string. For simplicity, only the electrodes on one side of the string are shown. The driving electrodes provide the same discrete spatial force that is considered in Chapter III, and is shown in Figure 3.2. The difference between this system and the one studied in Chapter III is the discrete temporal nature of the voltage applied to the electrodes.

The individual control voltages are adjusted on a discrete-time basis. The time interval between adjustments of a control voltage is t_0 seconds. The electrode is also broken into sections of J segments. The control voltages in this section are adjusted in a sequential manner, from left to right. When the last control segment in a section has been adjusted, the feedback returns to the first segment. With this type of sampling the electrode which drives the section of string for $-L/2 < x < L/2$ is adjusted at $t = t_0, 2t_0, 3t_0, \dots$. The electrode segment which drives the section of string for $nL - L/2 < x < nL + L/2$ is then adjusted at the times $t = t_0 + nt_0/J, 2t_0 + nt_0/J, 2t_0 + nt_0/J, \dots$. The form of the driving voltage that exists on the electrode segment for $nL - L/2 < x < nL + L/2$ is shown in Fig. 6.2, on the next page.

The reason for breaking up the control into sections of J segments is to make this infinite control system appear as an infinite number of finite control systems placed end to end. A real system would consist of only J segments, and the control system would adjust the control segments from left to right, and then repeat the process. If one were to analyze this finite system, it would be necessary to use normal modes and to consider

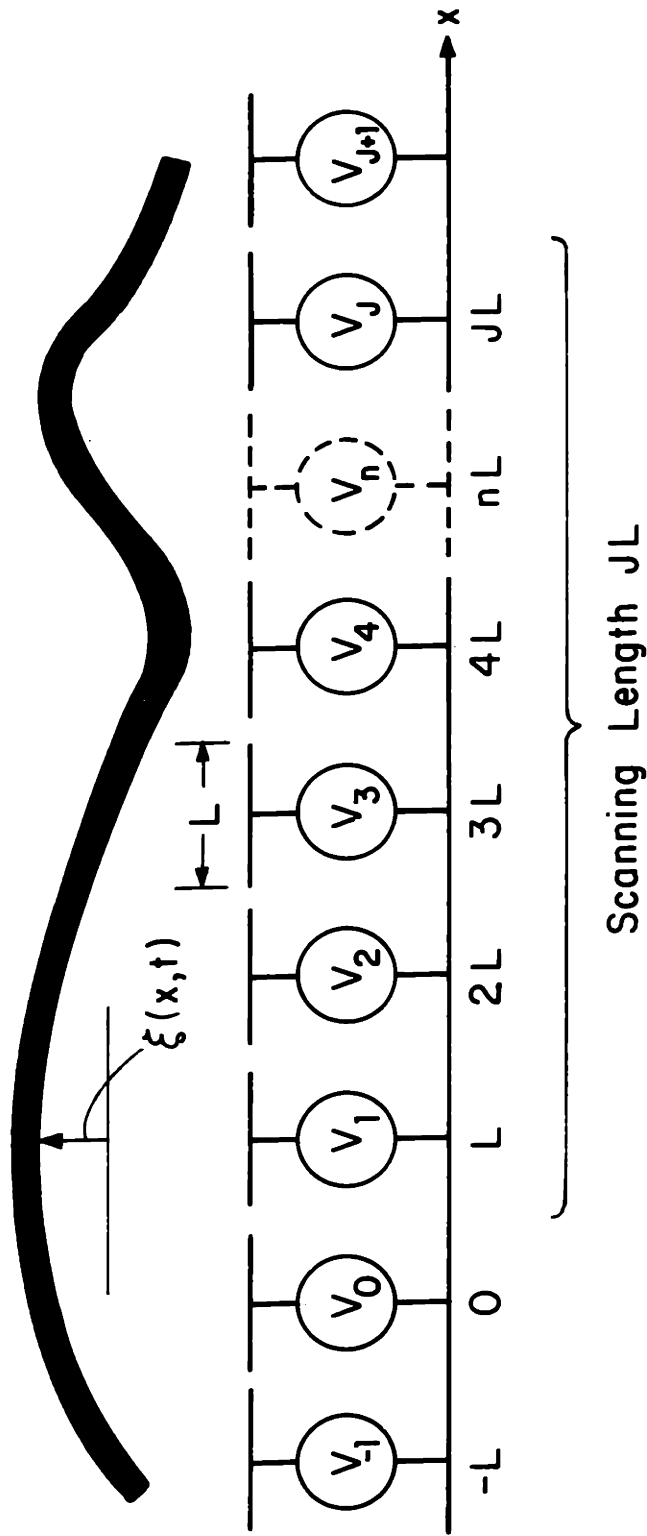


Figure 6.1 The string is driven by an electrode structure which produces a spatially and temporally discrete force.

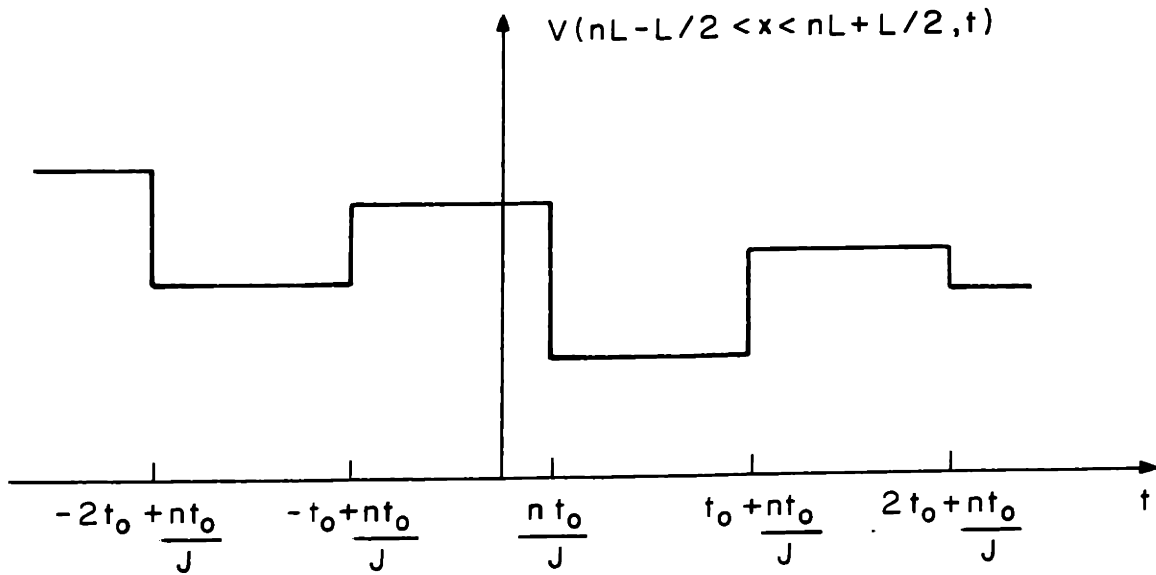


Figure 6.2

Discrete temporal voltage supplied to a Driving
Electrode

boundary conditions. By placing an infinite number of these finite systems together, the boundaries are moved to infinity. The boundary conditions can now be ignored, and a Fourier Integral representation for the spatial displacement can be used.

The motivation for this type of spatial and temporal sampling is the common television system. The intensity of a picture, seen by a television camera, is a function of space and time. The television camera measures the intensity of the picture on horizontal lines (spatial sampling) in a sequential manner (temporal sampling). The control system here can be thought of as a simplified television system that measures certain points on a line in a sequential manner.

6.2 Spatially and Temporally Sampled Signals

Detection Scheme: Spatial and Temporal Sampling

Similar to the case studied in Chapter III, the control system studied here measures or "spatially samples" the deflection of the string only at the center of each electrode. With the addition of a digital computer or other temporally discrete device to the feedback system, these measurements are made on a discrete time basis. That is, the "spatially sampled" output is "temporally sampled" by the control system. To simplify the analysis of the control system, the measurements of the deflection are made by scanning the sensors in the same way the driving voltages are adjusted. This means the value of the deflection at the point $x = nL$ is measured at the times $t = t_0 + nt_0/J, 2t_0 + nt_0/J, \dots$.

The measuring system provides no information about the deflection, except at the sampling points in space and time. This sampled output can be thought of as a grid of impulses in the x - t plane. At points in space and time other than the sampling points, the measured deflection is zero. At the sampling points, the area of the impulse is the value of the deflection. The time and space sampled deflection $\xi^*(x,t)$, can be written as a product of the deflection and an impulse array in the x - t plane:

$$\xi^*(x,t) = \xi(x,t) \cdot \sum_{n=-\infty}^{\infty} \sum_{m=-\infty}^{\infty} u_0(x-nL, t - \frac{nt_0}{J} - mt_0) \quad (6.1)$$

where J is the number of spatial samples in a repeat length.

It is convenient to define the impulse array in Eq. (6.1) as the sampling function, $i^*(x,t)$. Thus,

$$i^*(x,t) = \sum_{n=-\infty}^{\infty} \sum_{m=-\infty}^{\infty} u_0(x-nL, t - \frac{nt_0}{J} - mt_0) \quad (6.2)$$

The temporal and spatial sampling process can be represented by the network shown in Fig. 6.3. The spatially and temporally continuous function, $\xi(x,t)$, is multiplied by the sampling function, $i^*(x,t)$, to produce the sampled output, $\xi^{**}(x,t)$. In Fig. 6.3, the impulse arrays are drawn for a repeat length (J) equal to four.

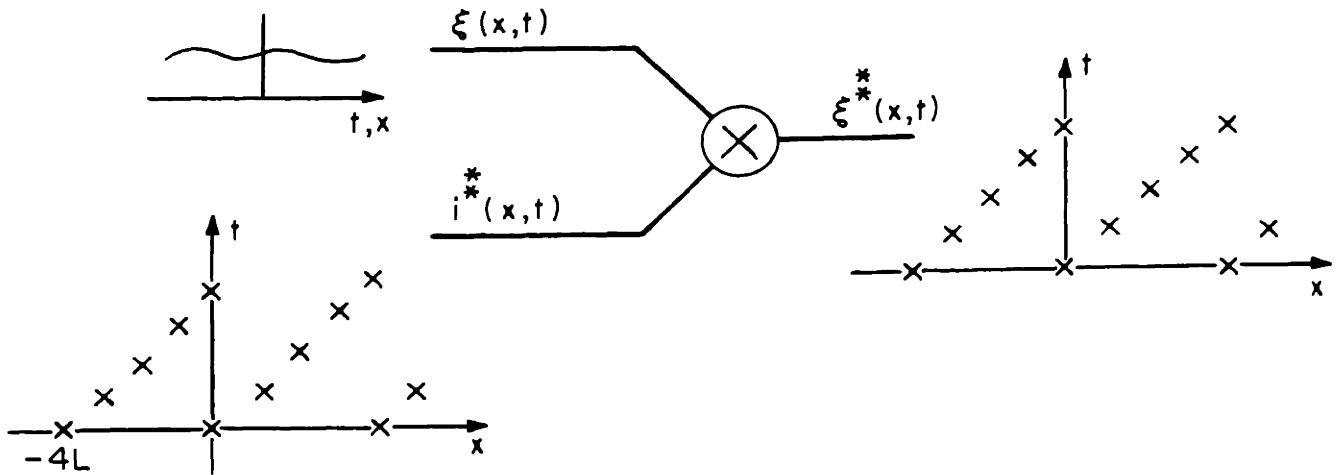


Figure 6.3

The detected signal is produced by multiplying the continuous signal by an impulse array.

Transform of the Sampling Function

The transform of the sampling function is derived in this section. This transform is used in the following sections to calculate the transform of the space- and time-sampled deflection.

The first step for finding the transform is to break up the sampling function into two convolved functions. In Fig. 6.3, the sampling function is seen to be a series of diagonal lines of impulses that are repeated on

the t - axis. Thus, the sampling function can be generated by convolving the diagonal line of impulses with an impulse train along the t - axis.

$$i^*(x, t) = \sum_{m=-\infty}^{\infty} u_0(x - mL, t - m \frac{t_0}{J}) \otimes \sum_{n=-\infty}^{\infty} u_0(x, t - nt_0) \quad (6.3)$$

where \otimes stands for convolution in x and t space.

The transform of the sampling function is the product of the transforms of the two terms on the right of Eq. (6.3). These transforms are

$$\sum_{n=-\infty}^{\infty} u_0(x, t - nt_0) \leftrightarrow \frac{2\pi j}{t_0} \sum_{n=-\infty}^{\infty} u_0(s - \frac{2n\pi j}{t_0}) \quad (6.4)$$

$$\sum_{m=-\infty}^{\infty} u_0(x - mL, t - m \frac{t_0}{J}) \leftrightarrow \frac{2\pi L J j}{t_0} \sum_{m=-\infty}^{\infty} u_0(s \frac{t_0}{J} + jkL + m2\pi j) \quad (6.5)$$

The transform given in Eq. (6.4) is found in Mason and Zimmerman [pg. 262]. The transform in Eq. (6.5) is shown to be correct by taking the inverse transform to recover the original time function. The inversion is accomplished by first integrating on the wavenumber, k .

$$\begin{aligned} & \frac{2\pi L J j}{t_0} \int_{-\infty}^{\infty} \int_{-j^{\infty} + \sigma}^{j^{\infty} + \sigma} \sum_{m=-\infty}^{\infty} u_0(s \frac{t_0}{J} + jkL + j2\pi m) e^{st} e^{jkx} \frac{ds}{2\pi j} \frac{dk}{2\pi} \quad (6.6) \\ & = \frac{J}{t_0} \sum_{m=-\infty}^{\infty} \int_{-j^{\infty} + \sigma}^{j^{\infty} + \sigma} e^{s(t - \frac{t_0 x}{JL})} e^{-j \frac{2\pi m x}{L}} \frac{ds}{2\pi j} \end{aligned}$$

The right-hand side of (6.6) can be factored to give

$$\frac{J}{t_0} \sum_{m=-\infty}^{\infty} e^{-j \frac{2\pi m x}{L}} \int_{-j^{\infty} + \sigma}^{j^{\infty} + \sigma} e^{s(t - \frac{t_0}{JL} x)} \frac{ds}{2\pi j} \quad (6.7)$$

Both of the terms in Eq. (6.7) can be put into a different form:

$$\sum_{m=-\infty}^{\infty} e^{-j \frac{2m\pi x}{L}} = L \sum_{m=-\infty}^{\infty} u_0(x - mL) \quad (6.8)$$

$$\int_{-j\infty + \sigma}^{j\infty + \sigma} e^{s(t - \frac{t_0}{JL} x)} \frac{ds}{2\pi j} = u_0(t - \frac{t_0 x}{JL}) \quad (6.9)$$

With Eqs. (6.7), (6.8) and (6.9), the right side of (6.6) becomes

$$\begin{aligned} \frac{J}{t_0} \sum_{m=-\infty}^{\infty} \int_{-j\infty + \sigma}^{j\infty + \sigma} e^{s(t - \frac{t_0 x}{JL})} e^{-j \frac{2m\pi x}{L}} \frac{ds}{2\pi j} = \\ \frac{JL}{t_0} \sum_{m=-\infty}^{\infty} u_0(x - mL) u_0(t - \frac{t_0 x}{JL}) \end{aligned} \quad (6.10)$$

In the x - t plane, $u_0(x - mL)$ and $u_0(t - t_0 x/JL)$ are impulse sheets. They are zero everywhere except along the lines represented by their arguments. The product of two impulse sheets is a two-dimensional impulse at the point of intersection. The right side of Eq. (6.10) can thus be written as

$$\frac{JL}{t_0} \sum_{m=-\infty}^{\infty} u_0(x - mL) u_0(t - t_0 x/JL) = \sum_{m=-\infty}^{\infty} u_0(t - \frac{mt_0}{J}, x - mL) \quad (6.11)$$

The original time function has been recovered from the transform in Eq. (6.5) and the transform is therefore correct.

The transform of the sampling function is the product of the transforms in Eqs. (6.4) and (6.5); it is

$$I^*(s, k) = \frac{(2\pi)^2 L J j^2}{t_0^2} \sum_{m=-\infty}^{\infty} u_0\left(s \frac{t_0}{J} + jkL + m2\pi j\right) \cdot \sum_{n=-\infty}^{\infty} u_0\left(s - \frac{2nj\pi}{t_0}\right) \quad (6.12)$$

Equation (6.12) can be put into a more compact form:

$$I^*(s, k) = \frac{(2\pi)^2 j}{t_0 L} \sum_{n=-\infty}^{\infty} \sum_{m=-\infty}^{\infty} u_0\left(s - \frac{2mj\pi}{t_0}, k + \frac{2n\pi}{L} + \frac{2m\pi}{JL}\right) \quad (6.13)$$

The transform of the sampling function is therefore a two-dimensional impulse array in the $s - k$ plane. This array shows immediately one of the effects that the scanning has on the system. When the deflection is sampled only in time, the transform of the deflection is periodic on the s axis, with a period of $2\pi j/t_0$. When the sampling is done only in space, the deflection's transform is periodic with a period of $2\pi/L$ on the k axis. When the system is sampled in time and space, both of the previous periodicities still occur. However, a new period of $2\pi/JL$ occurs in the k -direction; this new periodicity is a result of the scanning method used for sampling. This scanning length is JL and this causes the transform to have a period of $2\pi/JL$.

Transform of the Space- and Time-Sampled Deflection

The space- and time-sampled function $\xi^*(x,t)$, is the product of the continuous deflection and the sampling function. The transform of the sampled deflection is therefore the convolution of the transforms of $\xi(x,t)$ and $i^*(x,t)$,

$$\Xi^*(s,k) = \Xi(s,k) \otimes I^*(s,k) \quad (6.14)$$

where \otimes represents convolution in k and s space.

Equation (6.13) shows that the transform $I^*(s,k)$ is an impulse array in the s - k plane. Thus, the convolution to find Ξ^* can be done by observation, and the result is

$$\Xi^*(s,k) = \frac{1}{t_0 L} \sum_{n=-\infty}^{\infty} \sum_{m=-\infty}^{\infty} \left(s - \frac{2mj\pi}{t_0}, k + \frac{2n\pi}{L} + \frac{2m\pi}{JL} \right). \quad (6.15)$$

An alternate expression for Ξ^* is

$$\Xi^*(s,k) = \frac{1}{t_0 L} \sum_{n=-\infty}^{\infty} \sum_{m=-\infty}^{\infty} \left(s - \frac{2mj\pi}{t_0} + \frac{2nj\pi J}{t_0}, k + \frac{2m\pi}{JL} \right) \quad (6.16)$$

This transform is a periodic function in the k - s plane. The transform has a period of $2\pi/JL$ in the k plane, and of $2\pi/t_0$ in the s - plane.

It is shown in Chapter 2 that a transform that is periodic in s can be written in closed form by using Z transforms. That is, the transform of a temporally sampled function has two forms.

$$\Xi^*(k,s) = \frac{1}{t_0} \sum_{n=-\infty}^{\infty} \left(k, s + \frac{2n\pi j}{t_0} \right) = \Xi(k,Z) \quad (6.17)$$

where $*$ means temporal sampling with a period of t_0 .

In Chapter 3, it is shown that a transform which is periodic on the k axis can be written in closed form by using the discrete spatial wave-number D . Thus, the transform of a spatially sampled function can be expressed in two ways.

$$\Xi^*(k,s) = \frac{1}{L} \sum_{m=-\infty}^{\infty} \Xi(k + \frac{2m\pi}{L}, s) = \Xi(D,s) \quad (6.18)$$

where the * refers to spatial sampling with a period of L .

The techniques developed in Chapters 2 and 3 can also be used to get the transform of the space- and time-sampled function into a closed form for either s or k . The summation over the variable n in Eq. (6.15) can easily be put into closed form by using Eq. (6.18). For one value of m , the summation over n is

$$\begin{aligned} \frac{1}{t_0 L} \sum_{n=-\infty}^{\infty} \Xi(k + \frac{2m\pi}{JL} + \frac{2n\pi}{L}, s - \frac{j2m\pi}{t_0}) \\ = \frac{1}{t_0} \Xi(D e^{-j\frac{2m\pi}{J}}, s - \frac{2mj\pi}{t_0}) \end{aligned} \quad (6.19)$$

The variable D in Eq. (6.19) is defined as

$$D = e^{-jkL} \quad (6.20)$$

This definition is slightly different from that given by Eq. (3.11) because the length L has not been normalized to 1.

In a similar manner, Eq. (6.17) can be used to put the summation over n in (6.16) into closed form. For one value of m , the summation over n is

$$\begin{aligned} \frac{1}{t_0 L} \sum_{n=-\infty}^{\infty} \Xi(k + \frac{2m\pi}{JL}, s - \frac{2mj\pi}{t_0} + \frac{2nj\pi J}{t_0}) \\ = \frac{1}{LJ} \Xi(k + \frac{2m\pi}{JL}, z e^{\frac{j2m\pi}{J}}) \end{aligned} \quad (6.21)$$

The variable Z in Eq. (6.21) is defined as

$$Z = e^{-st_0/J} \quad (6.22)$$

This definition for Z is different from that given by Eq. (2.12) because the sampling time, t_0/J , has not been normalized to 1.

With Eqs. (6.19) and (6.21), the two forms of the transform of the space- and time-sampled functions, Eqs. (6.15) and (6.16), can be written as

$$\Xi^*(k, s) = \frac{1}{t_0} \sum_{m=-\infty}^{\infty} \Xi(De^{j\frac{2m\pi}{J}}, s - \frac{2mj\pi}{t_0}) \quad (6.23)$$

and

$$\Xi^*(k, s) = \frac{1}{JK} \sum_{m=-\infty}^{\infty} \Xi(k + \frac{2m\pi}{JL}, Ze^{j\frac{2m\pi}{J}}) \quad (6.24)$$

The transform of the sampled function is now a series only in terms of one variable, s or k . The series in the other variable has been put into closed form by using the discrete variables D and Z .

The transforms in Eqs. (6.23) and (6.24) are still periodic in one variable and appear as if they can be put into a closed form. Unfortunately, the Z transform method, which has been used to obtain closed-form transforms, does not work on the transforms in (6.23) and (6.24). For example, the periodicity in s of the transform given by Eq. (6.23) can be removed with Eqs. (2.10) and (2.11). The modified form of the transform is

$$\frac{1}{t_0} \sum_{m=-\infty}^{\infty} \Xi(De^{j\frac{2m\pi}{J}}, s - \frac{2mj\pi}{t_0}) = \int_{\text{Poles of } \Xi} \frac{\Xi(De^{j\frac{(s-p)t_0}{J}}, p)}{1 - e^{-(s-p)t}} \quad (6.25)$$

If the function Ξ has a finite number of poles in the p plane, the right

side of Eq. (6.25) yields a closed-form transform for the space- and time-sampled function. However, for the case of the string, $\Xi(\text{Dexp}[-(s-p)t_0/J], p)$ is a transcendental function of p , and consequently there are an infinite number of poles. The summation on the right side of Eq. (6.25) consists of an infinite number of terms and a transform in closed form is not achieved. By using a similar argument, it can be seen that the transform given by (6.24) is also not reducible to closed form for the case of the string.

6.3 The Open-Loop Transfer Function

The Electrode as a Spatial and Temporal Sample-and-Hold Filter

The driving electrodes and their associated electronic circuitry are a combination of the spatial sample-and-hold filter and the temporal sample-and-hold filter which were discussed in Chapters 2 and 3. At the sampling times, a pulse is fed to the electrode segment's electronic circuits. The voltage on the segment is then updated to a value proportional to the amplitude of the input pulse. Between the sampling times, the voltage on the electrode, and hence the force exerted on the string, is constant. The signal applied to the electrode segment can be considered to exist at only one point in space, the point where the signal lead is attached to the segment. The electrode segment accepts this signal and produces a spatially constant force to the adjacent section of the string. Each electrode segment, with its associated electronic circuitry, may be thought of as a sample-and-hold filter in space and time. The response of an electrode segment in space and time to an impulse at the x - t origin is shown in Fig. 6.4.

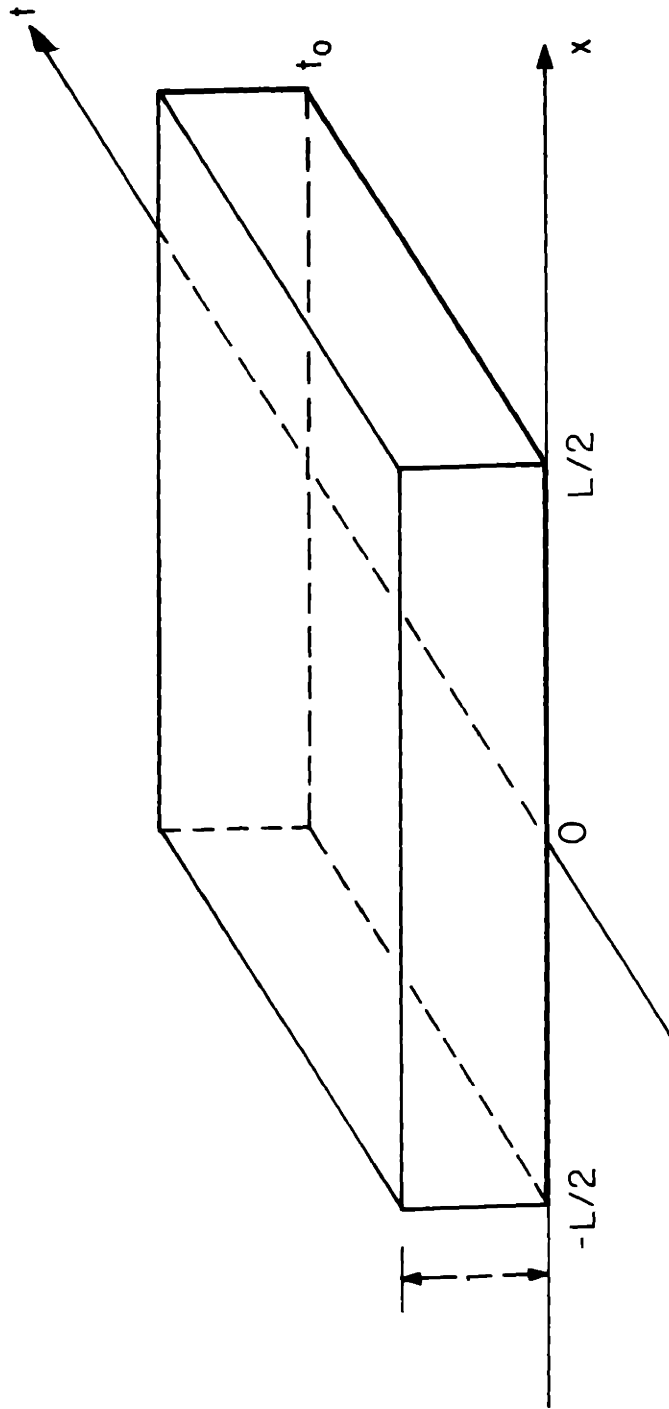


Figure 6.4 The electrode segment accepts an impulse at the sampling instant, and produces a constant force in both space and time.

The discrete temporal and spatial force applied to the string by the electrode segments is generated by driving the filter shown in Fig. 6.4 with an array of impulses in the x - t plane. The impulses of this array have the same locations in the x - t plane as those of the sampling function. The area of each impulse is the same as the force applied to a segment of the string between sampling times. This process of generating the driving force $f(x,t)$ is illustrated in Fig. 6.5.

Transfer Function of a Spatially Discrete System

The string and its driving electrodes can be thought of as a system which accepts a spatially and temporally discrete input and produces a spatially and temporally continuous output. The control system then measures or 'spatially and temporally samples' the deflection of the string. The system, as seen by the control system, is illustrated in Fig. 6.6. The signals generated by the control system are pictured as the impulse array $u^*(x,t)$. The electrodes are driven by this array, and generate the spatially and temporally discrete driving function $f(x,t)$. The force drives the string, and produces the spatially and temporally continuous deflection, $\xi(x,t)$. The detection system samples the deflection in space and time to obtain the impulse array, $\xi^*(x,t)$.

In Chapters 2 and 3, a transfer function was made which related the sampled output to the sampled input for space or time-sampled systems. The same arguments can be used with some modifications to produce a transfer function for a space- and time-sampled system.

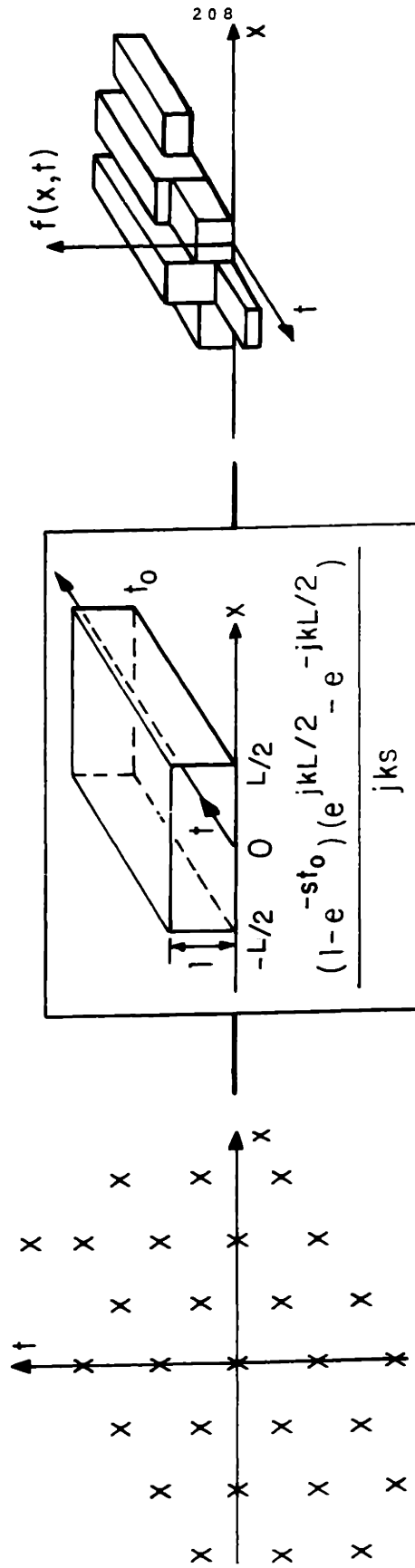


Figure 6.5 The force applied to the string is produced by driving the spatial and temporal sample-and-hold filter with an impulse array.

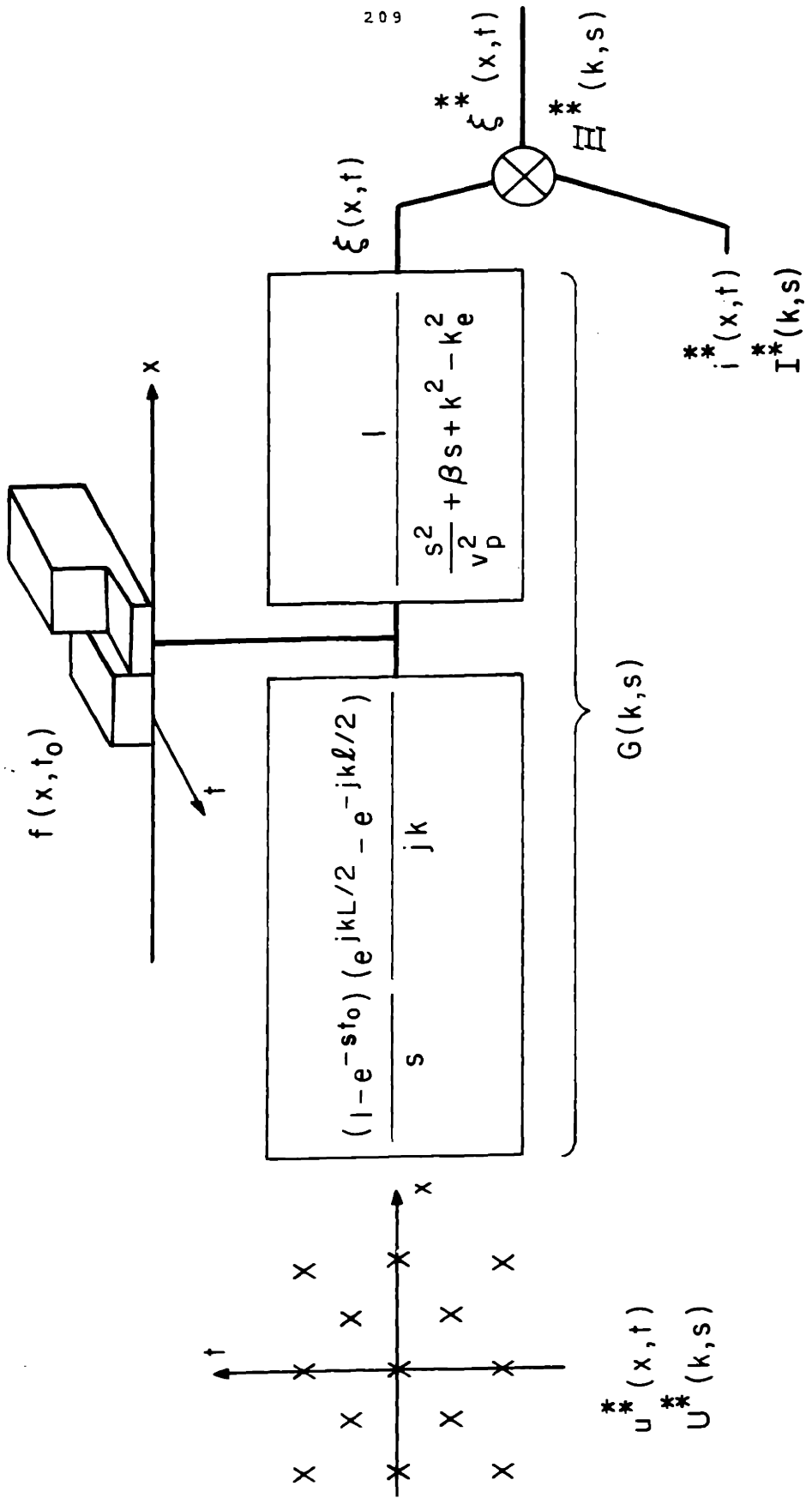


Figure 6.6 The electrode segments, string, and sensors are a system which accepts a spatially and temporally sampled input and produces a spatially and temporally sampled output.

In Fig. 6.6, the transform of the continuous deflection is related to the transform of the sampled input by

$$\Xi(k,s) = U^*(k,s)G(k,s) \quad (6.26)$$

From Eqs. (6.15) and (6.26), the transform of the sampled deflection is

$$\begin{aligned} \Xi^*(k,s) &= \frac{1}{t_0 L} \sum_{n=-\infty}^{\infty} \sum_{m=-\infty}^{\infty} U^*(k + \frac{2n\pi}{L} + \frac{2m\pi}{JL}, s - \frac{2mj\pi}{t_0}) \cdot \\ &G(k + \frac{2n\pi}{L} + \frac{2m\pi}{JL}, s - \frac{2mj\pi}{t_0}) \quad (6.27) \end{aligned}$$

The input, $U^*(x,t)$ is already a sampled function and its transform must obey the equation:

$$U^*(k + \frac{2n\pi}{L} + \frac{2m\pi}{JL}, s - \frac{2mj\pi}{t_0}) = U^*(k,s) \quad (6.28)$$

With Eq. (6.28), the transform of the drive can be brought outside of the summation signs and the relationship between the sampled input and sampled output becomes

$$\Xi^*(k,s) = U^*(k,s) \frac{1}{t_0 L} \sum_{n=-\infty}^{\infty} \sum_{m=-\infty}^{\infty} G(k + \frac{2n\pi}{L} + \frac{2m\pi}{JL}, s - \frac{2mj\pi}{t_0}) \quad (6.29)$$

From Eq. (6.29), the transfer function relating the spatially and temporally sampled input and output is the transform of the spatially and temporally sampled impulse response of the system. For this case, the impulse response means an impulse at the origin of the $x-t$ plane. With this discrete transfer function, the system can be represented by

a simple block diagram similar to those in Figs. 2.8 and 3.9.

Evaluation of the Spatially and Temporally Discrete Transfer Function

From Fig. 6.6, the continuous transfer function of the system is the product of the transfer functions of the string and the electrodes. This transfer function is

$$G(k,s) = \left[\begin{array}{c} -st_0 \\ \frac{1-e}{s} \end{array} \right] \left[\begin{array}{cc} jkL/2 & -jkL/2 \\ \frac{e}{jk} & -e \end{array} \right] \left[\begin{array}{c} 1 \\ \frac{1}{v_p^2} s^2 + \beta s + k^2 - k_c^2 \end{array} \right] \quad (6.30)$$

To simplify this transfer function, the length L is normalized to 1 by defining the following dimensionless variables.

$$K = kL \quad (6.31a)$$

$$S = Ls/v_p \quad (6.31b)$$

$$N = k_c^2 L^2 \quad (6.31c)$$

$$T = t_0 v_p / L \quad (6.31d)$$

$$\delta = \beta L v_p \quad (6.31e)$$

With these dimensionless variables, the continuous transfer function becomes:

$$G(K,S) = \left[\begin{array}{c} 1 - e^{-ST} \\ S \end{array} \right] \left[\begin{array}{cc} jK/2 & -jK/2 \\ \frac{e}{jK} & -e \end{array} \right] \left[\begin{array}{c} 1 \\ S^2 + \delta S + K^2 - N \end{array} \right] \quad (6.32)$$

The transfer function for the spatially and temporally sampled system is found by substituting Eq. (6.32) into (6.29). The transfer function produced in this manner is a series in terms of both K and S . The two desired forms of the transfer function use the discrete variables Z and D and are consequently a series in terms of only one variable, K or S .

These two expressions for the spatially and temporally sampled transfer function are obtained by plugging Eq. (6.32) into Eqs. (6.23) and (6.24). The final forms of the discrete transfer function are put into a more compact expression by defining the two functions:

$$H_1(K, S) = \left[\frac{1 - e^{-ST}}{S} \right] \left[\frac{1}{S^2 + \delta S + K^2 - N} \right] \quad (6.33)$$

and

$$H_2(K, S) = \left[\frac{e^{jK/2} - e^{-jK/2}}{jK} \right] \left[\frac{1}{S^2 + \delta S + K^2 - N} \right] \quad (6.34)$$

The function $H_1(K, S)$ is almost identical to the continuous transfer function of the temporally discrete system that was studied in Chapter 2. This function contains the portion of $G(K, S)$ which is a function of S . The function $H_2(K, S)$ is identical to the continuous transfer function of the spatially discrete system studied in Chapter 3. $H_2(K, S)$ contains that portion of $G(K, S)$ which is a function of K .

Substituting Eqs. (6.32) and (6.33) into (6.24) gives, for one form of the discrete transfer function:

$$G^*(K, S) = \frac{1}{J} \sum_{n=-\infty}^{\infty} \frac{2 \sin(K/2 + \frac{n\pi}{J})}{K + \frac{2n\pi}{J}} H_1 \left(Ze^{j(2n\pi/J)}, K + \frac{2n\pi}{J} \right) \quad (6.35)$$

where

$$H_1(Z, K) = \frac{(1-Z^J) \{-2W + Ze^{-\delta/2} [-\delta \sinh W + 2W \cosh W]\}}{2W(K^2 - N) [1 - 2Ze^{-\delta/2} \cosh W + Z^2 e^{-\delta}]} \quad (6.36)$$

$$+ \frac{2W[1 - 2Ze^{-\delta/2} \cosh W + e^{-\delta} Z^2] (1-Z^J)}{2W(K^2 - N) [1 - 2Ze^{-\delta/2} \cosh W + Z^2 e^{-\delta}] (1-Z)}$$

$$W = [(\delta/2)^2 - K^2 + N]^{1/2} \quad (6.37)$$

$$Z = e^{-ST/J} \quad (6.38)$$

An expression almost identical to Eq. (6.36) is derived in Chapter 2 and is given by Eq. (2.37). $H_1(Z,K)$ can be deduced from Eq. (2.37) by comparing Eq. (6.38) to (2.12) and Eq. (6.33) to (2.30).

The other form of the spatially and temporally discrete transfer function is found by substituting Eq. (6.34) and (6.32) into (6.23). It is:

$$G^*(D,S) = \frac{1 - e^{-ST}}{T} \sum_{n=-\infty}^{\infty} \frac{H \left(De^{j\frac{2n\pi}{J}}, S + j\frac{2n\pi}{T} \right)}{\left(S + \frac{j2n\pi}{T} \right)} \quad (6.39)$$

The function $H_2(D,S)$ is derived in Chapter 3 and is given in Eq. (3.47).

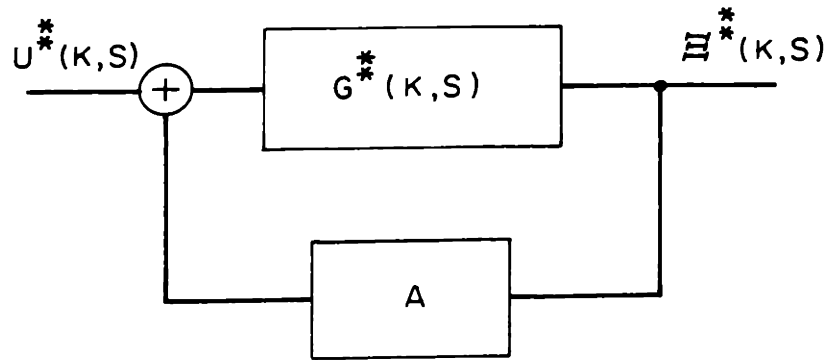
The discrete transfer function which describes the driving electrodes and the string as seen by the control system has been derived in two forms. One form gives the transfer function as a closed form in the discrete spatial wavenumber D and a series in S . The other expression is a closed form in terms of the discrete temporal frequency, Z , and a series in terms of the spatial wavenumber, K . These expressions are equivalent, since both can be put into the same series in terms of S and K .

6.4 Closed-Loop System

Closed-Loop Transfer Function

To stabilize the string, a control signal must be generated from the spatially and temporally sampled deflection. One possible control scheme is to multiply the measured deflection by a negative gain and feed the resulting signal to the electrodes driving the string. At the sampling time for a given electrode segment pair, the voltage on the segments

is adjusted. The new value of voltage produces a force proportional to the deflection of the string at the center of the electrode segments and with a polarity that drives the measured deflection toward zero. The driving force is held constant until the next sampling time. With this kind of feedback, the entire system can be represented by the feedback loop in Fig. 6.7.



A servo-loop representation of the string with spatially and temporally discrete feedback.

Figure 6.7

The feedback system probably can be improved by generating a more complicated feedback signal. The measured deflection can be filtered in both a discrete spatial and a discrete temporal manner. However, this chapter is concerned only with presenting a method for analyzing a spatially and temporally discrete system, and thus the simplest case of feedback is considered.

The transfer function for the closed-loop system of Fig. 6.7 is

$$\frac{\Xi^*(K, S)}{U^*(K, S)} = \frac{G^*(K, S)}{1 + A^*G(K, S)} \quad (6.40)$$

It should be remembered that this transfer function relates the spatially and temporally sampled output to the spatially and temporally discrete input. From this transfer function, only the value of deflection at the sampling points in space and time can be determined.

The D-S and K-Z Dispersion Equations

The stability of the measured deflection is determined from the natural frequencies of the closed-loop system. These natural frequencies are found by setting the denominator of the closed-loop transfer function to zero. From Eq. (6.40), this dispersion equation is

$$1 + A^*G(K, S) = 0 \quad (6.41)$$

There are three forms that this dispersion equation can have. It can be an infinite series in terms of both S and K; it can be in closed form in terms of D and a series in S; and it can be in closed form for Z and a series in terms of K.

To obtain useful numerical results from the dispersion equation, the series must be truncated, so that only a finite number of terms exists. If the dispersion equation is a series in terms of S and a series in terms of K, then both series must be truncated before numerical calculations can be made. A decision must be made as to how many terms in each series must be used to obtain an accurate answer. If the dispersion equation is in terms of Z and K, only the series for the variable K must be truncated; the variable Z has put the series for S into closed form. When the dispersion equation is in terms of D and S, only the series

for the variable S must be truncated; the variable D has put the series for K into closed form. It is therefore desirable to use a form of $G^*(K,S)$ that is a closed form in terms of either Z or D because there is less chance of truncation error than with the double series.

Stability Criterion

The stability criterion that is used on this system is the same as that used for any continuum system. From the dispersion equation, the values of S are found for all real values of K . If the real part of S is greater than zero for any value of K on the real axis, then the system is unstable. If there are no values of S with a positive real part for K on the real axis, then the system is stable. The same criterion is adapted to Z - K dispersion equations in Chapter 2, and it is adapted to D - S dispersion equations in Chapter 3. If a Z - K dispersion equation is studied, values of Z inside the unit circle for real K indicate the presence of an instability. If a D - S equation is analyzed, a positive real value of S for a value of D on the unit circle designates the system as unstable.

The spatially and temporally sampled system studied here can be described by a S - K , Z - K or D - S dispersion equation. The form of the dispersion equation that is easiest to use for numerical calculations is picked and the corresponding stability criterion applied.

Results of the Stability Analysis

The form of the dispersion equation that is most convenient for numerical stability calculations is the Z-K form. The desired form of the equation is obtained by substituting Eq. (6.35) into (6.41). The resulting dispersion equation is a polynomial in terms of Z whose coefficients are complicated functions of K. The highest power of Z in this equation depends on the number of terms in the series for $G^*(K, Z)$ that are used. If the terms in the summation of Eq. (6.35) corresponding to $n = -m, -(m-1), \dots, 0, 1, 2, \dots, m$ are used, the highest term in the resulting dispersion equation is Z^{4m+J+1} . For stability studies, each of the $4m+J+1$ roots must be found.

If the K-S form of the function $G^*(K, S)$ is used, the dispersion equation is transcendental in both S and K. This form is not used, because finding the roots in S of this transcendental equation is more difficult than finding the roots in Z of the polynomial form of the dispersion equation.

The D-S form of the dispersion equation, obtained by using the form of $G^*(K, S)$ given by Eq. (6.39), is useful for determining the type of instability a system may have. After the series in Eq. (6.39) is truncated, a dispersion equation which is a polynomial in D is achieved. With this equation, the modified form of the Bers-Briggs criterion can be used to determine the existence and nature of instabilities. For the case of the stationary string, there is no possibility of a convective instability. Therefore, there is no need to use the D-S dispersion equation and the modified Bers-Briggs criterion.

The roots of Z for the dispersion equation that results when Eq. (6.35) is substituted into (6.41) have been found for all real values of K . The regions of stable operation are shown in Figs. 6.8, 6.9 and 6.10.

For the cases shown in Figs. 6.8 and 6.9, the number of electrode segments in a section, J , is picked to be one. For this situation, the control voltage on all of the electrode segments is adjusted at the same time. This situation is not realistic, because the advantages of a time-sampled control system are lost unless different electrodes are adjusted at different points in time. The reason for doing this case first is that the numerical calculations are easiest when $J = 1$.

From Eq. (6.35), it can be seen that the open-loop transfer function is an infinite series and that the magnitude of the terms decreases as $|n|$ increases. This suggests that the series in Eq. (6.35) can be truncated for some value of $|n|$ and an accurate model of the system can still be obtained. The numerical solution of the dispersion equation shows this assumption to be correct. The data in Figs. 6.8 and 6.9 are found by using only the three terms $n = -1, 0, 1$. Using more terms in the series made no significant change in the calculated stability region.

There are four regions of stability plotted for Gain (A) versus electrical pressure (N) in Figs. 6.8 and 6.9. Figure 6.8 presents the stable regions for a normalized sampling time (T) of 1 and damping constants (δ) of 2 and 4. Figure 6.9 presents the stable regions for a faster sampling rate, $T = .5$, with the same values of damping. In both

$$T = 1.0$$
$$J = 1.0$$

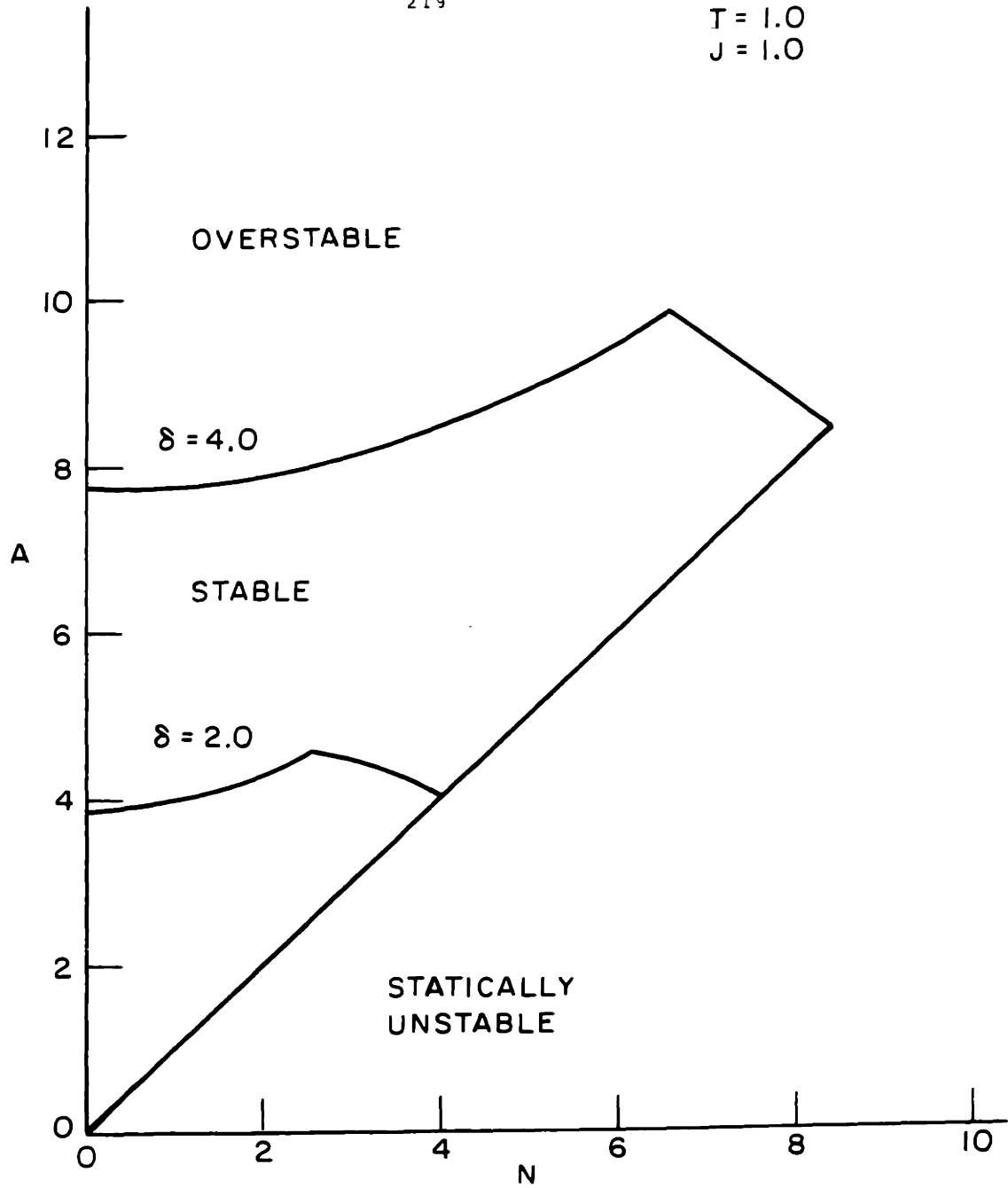


Figure 6.8 The region of stable operation for the spatially and temporally discrete system with a scanning length of one.

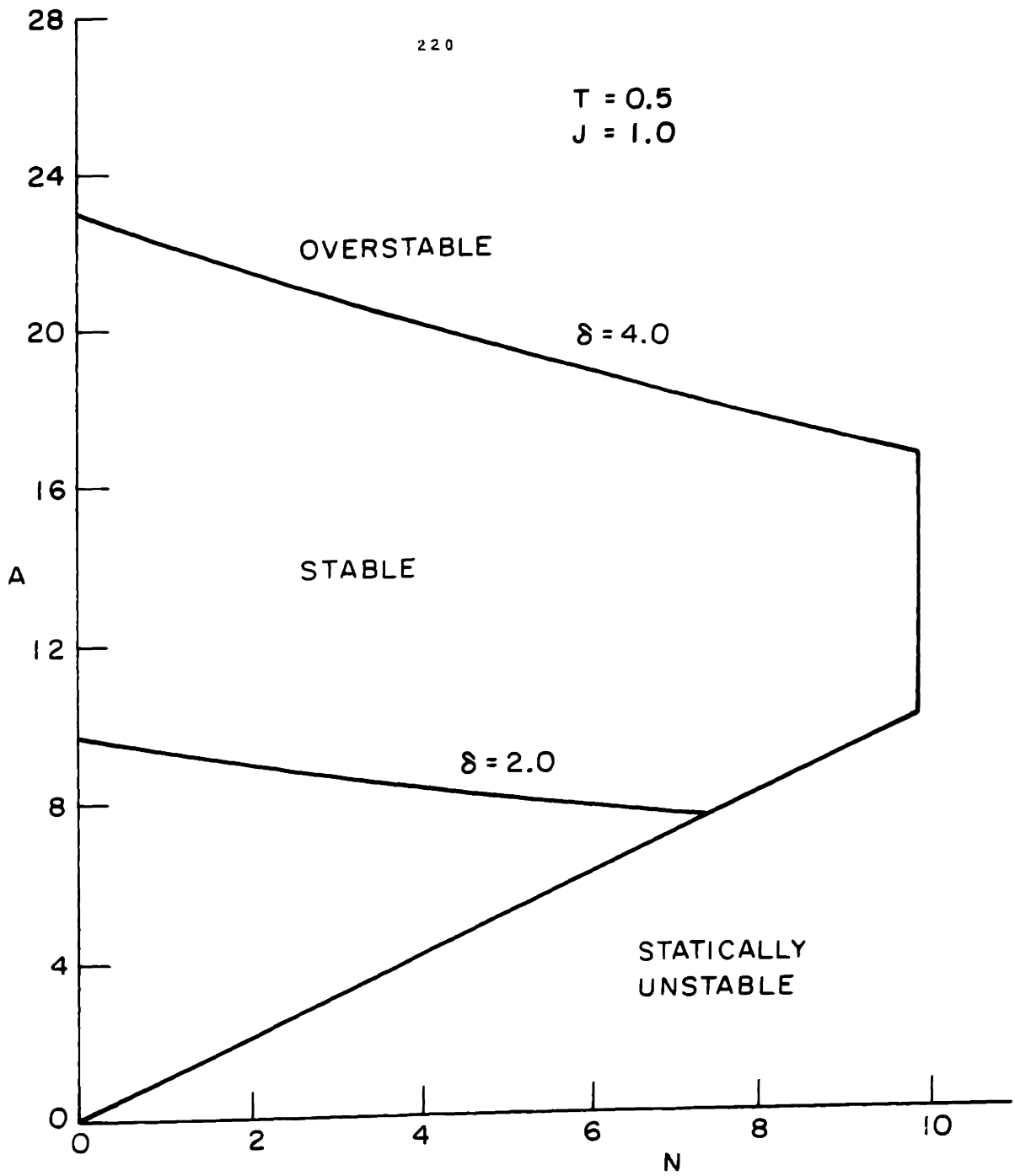


Figure 6.9 A stability plot for the spatially and temporally discrete system, showing the effect of increasing the sampling rate.

figures, the stable region is bounded from below by the line $A = N$. This line represents the minimum gain necessary to stop the absolute instability that occurs when there is no feedback. This same boundary was found in Chapter 2 for a temporally sampled system, and in Chapter 3 for a spatially sampled system. This instability occurs for long spatial wavelengths, $K \approx 0$, and appears at the discrete temporal frequency $Z = 1$.

When the gain is increased above a certain value, the system is characterized by growing oscillations, which are referred to as an over-stability. This instability also was observed in Chapters 2 and 3 when the feedback was only spatially or temporally sampled. These growing oscillations are caused by the feedback electrodes applying a force with the wrong spatial or temporal phase to a certain mode of the string.

Comparison of Fig. 6.9 with 6.8 shows that one method of increasing the maximum gain for stable operation is to decrease the sampling time. In Fig. 6.9, with $T = .5$, the maximum gains for stability are almost twice as large as those with $T = 1$ shown in Fig. 6.8. This effect of increasing the maximum gain by increasing the temporal sampling rate was also found in Chapter 2. The reason for this effect is that when the string displacement is sampled more often in time, the control system will apply a force of the wrong sign to fewer modes.

Figures 6.8 and 6.9 both show that the system is less apt to be overstable if the damping is increased. Since over-stability is caused by the control system pumping energy into a mode, providing a method to dissipate this energy will make the system more stable. In Fig. 6.9, the stable region of operation for $\delta = 4$ is bounded on the right by the line $N = \pi^2$. This limitation is caused by the spatial sampling. Whenever $N = \pi^2$, a disturbance with a normalized wavelength of two is unstable.

The string is sampled every unit length, so this wavelength is sampled exactly twice. As a consequence of the sampling theorem, the feedback system cannot detect this particular mode; it therefore cannot control this mode.

In Figure 6.10, the stable region for a system with a sampling length J of two is given. For this value of J , the control system adjusts the voltage on adjacent electrode segments in an alternating manner. This system does not represent an efficient time-sampled system because every other electrode segment is adjusted at the same time. This case is presented because it illustrates the effects that increasing the sampling length may have.

For the case of $J = 2$, it is necessary to use five terms ($n = -2, -1, 0, 1, 2$) in the series of Eq. (6.35) to obtain accurate results. For a given center wavenumber K , the extreme values used for the wavenumber are $K \pm 2\pi$. These values occur for $n = \pm 2$. This spread in the values of wavenumber that is needed for accuracy for $J = 2$ has the same width as for $J = 1$. The difference between the two cases is that, with the longer sampling length $J = 2$, the wavenumbers $K \pm \pi$ must also be considered. This result indicates that, as the number of segments in a sampling length increases, the spread in wavenumbers that must be considered for accuracy does not increase, but the number of intermediate wavenumbers increases.

The difference between sampling at all sensors at the same time and scanning the sensors can be seen by comparing Figs. 6.8 and 6.10. The only significant effect of the scanning is to decrease the tendency for overstability. The upper boundary between the stable and overstable

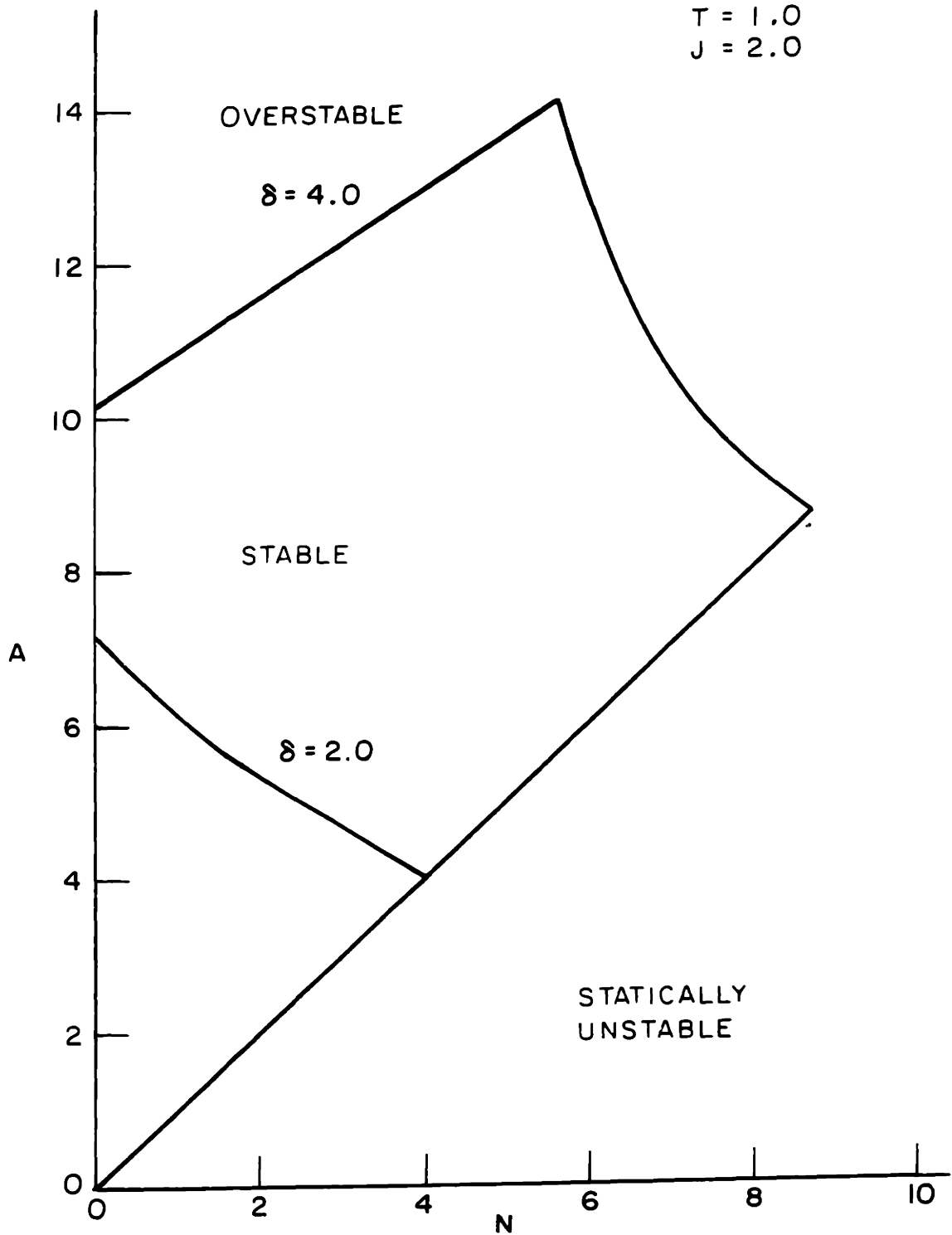


Figure 6.10 The region of stable operation for the spatially and temporally discrete system for a scanning length of two.

areas is increased for $\delta = 2$ and 4.

When the feedback signal is changed at every electrode segment simultaneously, certain modes can be pumped by the feedback. When the feedback signal is changed at different times on adjacent electrodes, a different set of modes will be pumped. Figures 6.8 and 6.10 show that, for $T = 1$, the modes driven by the feedback for $J = 2$ are more difficult to drive overstable than those driven by the feedback for $J = 1$. These results may indicate that increasing J forces the over stability to modes of shorter wavelength and the necessary gain for over stability is increased. However, the data presented here are not sufficient to justify this assumption.

Numerical calculations to determine the stability of systems with larger values of J were not done. The work presented here shows the order of the dispersion equation which accurately describes the system grows linearly with the value of J . This dispersion equation therefore remains solvable by digital computer as J is increased. However, the time needed to find all the roots of the dispersion ^{equation} is long. Since the purpose of this chapter was merely to present a method of analyzing a large temporally and spatially sampled system, further calculations are not necessary.

6.5 Summary

By using the Z-transform techniques that were developed in Chapters 2 and 3, a usable transfer function can be generated for a spatially and temporally discrete system. This transfer function is initially expressed as a double series in terms of S and K . By using Z transforms, one of the series can be put into closed form and the transfer function

can be written as an expression in S and D , or Z and K .

A closed-loop transfer function can be generated when spatially and temporally discrete feedback is applied to the continuum. From the poles of the closed-loop transfer function, a dispersion equation can be derived. The dispersion equation can be an expression that is a double series in S and K , a closed form in D , and a series in $S \dots$ or a closed form in Z and a series in K . The stability of the closed-loop system can be determined from this dispersion equation.

The stability of the string with spatially and temporally discrete feedback was studied in detail. The D - S form of the dispersion equation was found to be the easiest form to use for numerical calculations. To obtain accurate results for a system with a scanning length of J , it was necessary to use $2J + 1$ terms in the series of the open-loop transfer function. The dispersion equation that resulted from the $2J + 1$ terms was a polynomial in S of order $5J + 1$.

The numerical calculations produced effects that had been seen in Chapters 2 and 3 when either spatial or temporal discreteness was studied. The stable region had a right-hand boundary that was caused by the failure of the spatial sampling to detect certain modes. With no damping, the system was overstable for any finite gain, because the temporal discreteness caused certain modes to be pumped by the feedback. By adding damping to the system, the gain necessary for over-stability was increased.

It must be remembered that any physical system will not be infinite, but will be one scanning length long. The analysis in this chapter

was done for an infinite system, so that boundary conditions could be ignored. If the actual system has only a few feedback electrodes (small J), the boundary conditions will be important and the method of analysis presented in this chapter is inaccurate. For these small systems, the normal mode analysis developed by Thomas must be used. As the number of electrodes in a scanning length is increased, the boundary conditions become less important. It is for these systems with a larger number of feedback drives that the method shown in this chapter is valid.

7.1 Introduction

The objective of the experimental portion of this thesis is to build a spatially and temporally discrete feedback control system which controls a continuum instability. The purpose of the apparatus is to have a system which demonstrates how a large number of feedback stations can be controlled using a single amplifier on a time-multiplexed basis.

A general block diagram of the desired continuum control system is given in Fig. 1.3. The deflection of the continuum is sampled in space and time by a scanning device. The output of the scanner is amplified and the switching system applies the amplified signal to the proper point on the surface of the continuum. A synchronizing network is used to coordinate the scanning and switching circuits so that the feedback signal is applied to the proper location on the continuum.

This system is in many ways similar to a television system. In a television system, an image, which is a continuum of light intensity, is scanned by the television camera, which scans discrete lines on the image and repeats these scans at regular time intervals. The output of the camera is sent to a receiver which applies the signal to the face of a cathode ray tube. The receiver is synchronized to the camera, so that the image is reproduced on the cathode ray tube. The fundamental difference between the experimental setup and a television system is that the latter is open loop, and the experimental apparatus is closed loop.

In designing an experiment, there are the conflicting requirements of making the apparatus as simple as possible, while having it conform to the model set forth theoretically. A good device for linearly measuring the deflection at the sampling points is relatively difficult to construct. If, instead, the deflection is measured by a nonlinear method... a bang-bang feedback signal ... the system is considerably simplified. Although the theoretical developments in Chapter VI can not be quantitatively tested on such an apparatus, useful experience concerning the development of spatially and temporally sampled control systems is obtained. This alternative of a simplified "on-off" type of feedback is used in the experiments to be described, and hence no attempt is made to quantitatively compare theory and experiment.

7.2 Apparatus

The Continuum Instability

The continuum instability which is controlled is of the Rayleigh-Taylor type. This is the instability which occurs when a heavy fluid is supported against gravity by a lighter fluid. The interface between the two fluids is unstable, and the heavier fluid falls to the bottom of the container. The theory for this instability is presented in Chandrasekhar [Chapter 10]. This particular instability is picked for several reasons. The mathematical description of the Rayleigh-Taylor instability is similar to that of some magnetohydrodynamic instabilities which occur in plasma confinement experiments.

Learning to control the Rayleigh-Taylor instability provides information which is useful for attempts to control plasma instabilities.

It is also convenient to have an interface between two fluids which can be sensed optically. If one liquid is opaque and other transparent, the interface can be detected by a photodiode or other light detector.

The tank which holds the liquid is shown in Fig. 7.1. It consists of two four-inch square glass plates separated by a gasket of teflon .020" thick. The teflon gasket seals three sides of the tank. One side is left open for cleaning and filling the vessel.

The liquid-air interface is driven by an electric field which is tangential to the interface. The explanation of this force is given by Woodson and Melcher [Chapter 8]. To generate the electric field, the inside surfaces of the glass are coated with a transparent conductor which serves as an electrode. The transparent coating is tin oxide doped with antimony for better conductivity. One glass plate is covered completely with the tin oxide and serves as a ground plane. The other plate has 16 vertical strips four mm. wide which are separated by a gap of one mm. By placing a voltage between the strip electrodes and the ground plane, the electrical field tangential to the fluid surface is generated. The voltages on the strip electrodes can be adjusted independently, and thus a control force can be applied to each of the 16 segments of the liquid-air interface.

The liquid used in the tank is transformer oil, manufactured by General Electric Corporation. It has a very high resistance, and does not allow any significant current to flow between the electrodes. The oil is dyed dark green with copper naphthalene to make the oil-air interface easier to detect.

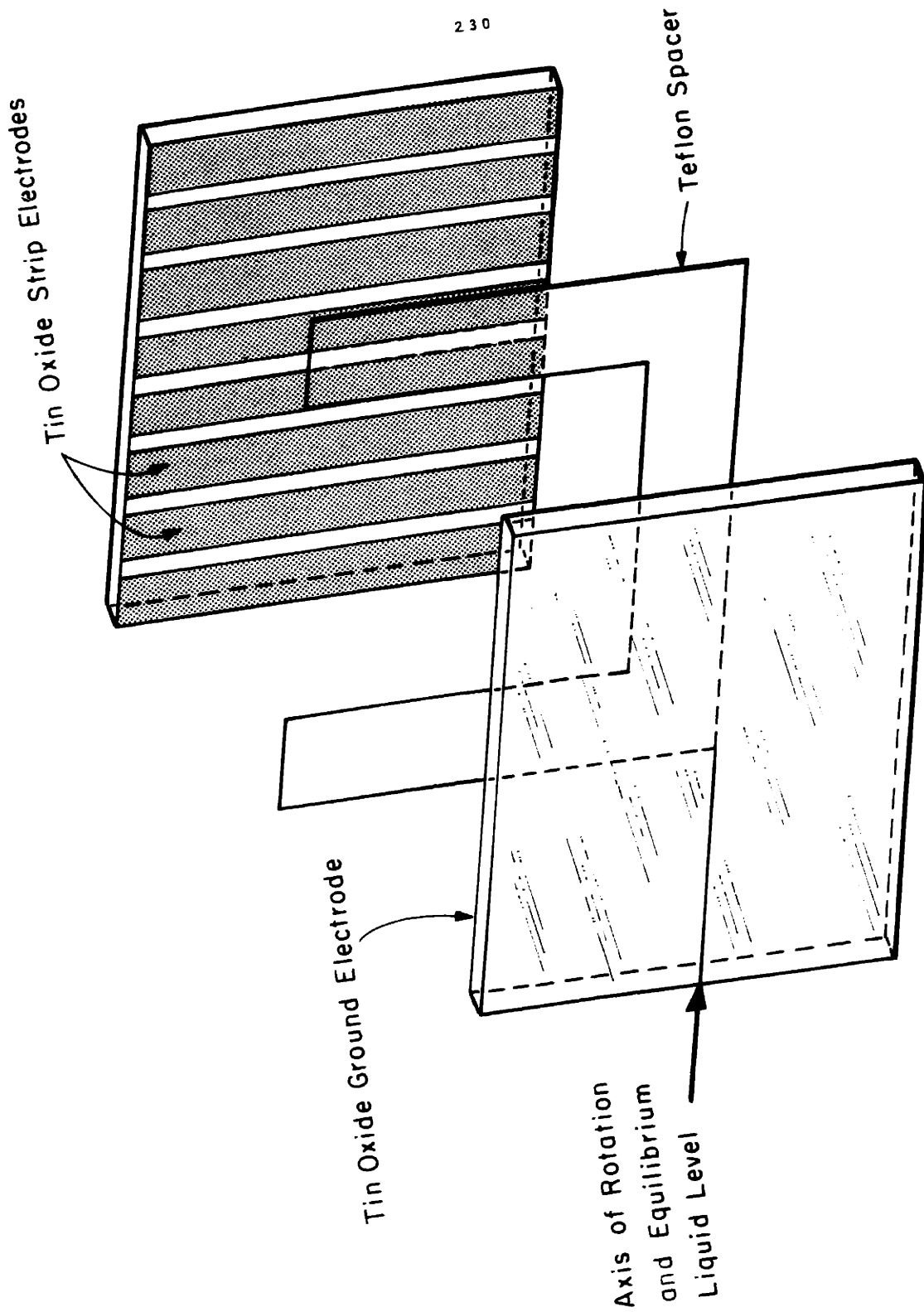


Figure 7.1 A breakdown drawing of the tank showing the strip electrodes which apply a spatially discrete voltage to the liquid-air interface.

The tank is mounted so that it can rotate about a horizontal axis which passes along the equilibrium fluid surface. By rotating the tank on this axis, the component of gravity perpendicular to the fluid surface can be varied. The tank is filled with its open end on top and the fluid collects in the bottom. The component of gravity perpendicular to the surface points from the air into the liquid: a stable configuration. If the tank is rotated more than 90° , the gravity vector will point from the fluid into the air.

This latter configuration is unstable without feedback. By changing the angle of the tank, the magnitude of the perpendicular gravity vector is changed, and the growth rate of the instability affected. The dimensions of the tank force the instability of the liquid surface to occur in only two dimensions: a plane parallel to the axis of rotation. The surface perpendicular to the axis of rotation is only .020" wide and the surface tension keeps the interfacial deflections that vary in that direction stable.

The Cathode Ray Tube Amplifier and Switching Network

The block diagram of the system, Fig. 1.3, shows the system being operated with one amplifier. Its output is shared by all of the feedback electrodes on a time-multiplexed basis. A switching network between the amplifier and driver electrodes performs the time-sharing operation.

The amplifier and switching circuit are combined into a single device by modifying a cathode ray tube. A schematic diagram of the modified CRT and its connections to the liquid tank is shown in Fig. 7.2. An electron gun and its deflection plates were removed from a Dumont 5ADP

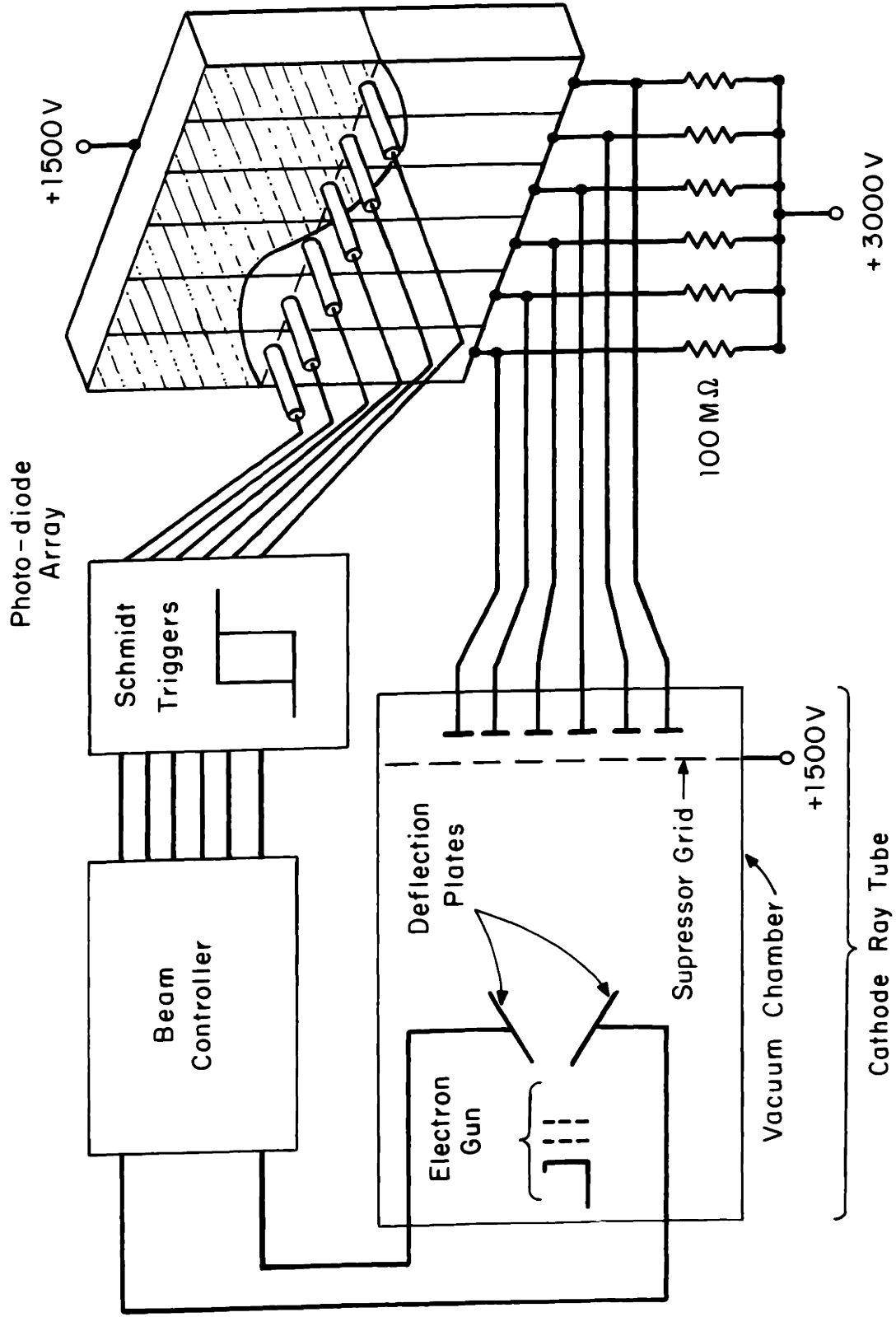


Fig. 7.2 A schematic drawing showing the connections of the CRT to the control electrodes and the level detectors.

cathode ray tube and mounted in a vacuum chamber which is made from a glass pipe, six inches in diameter and 18 inches long.

The ends of the glass pipe are sealed with brass plates. The electron gun is mounted on one brass plate (the back one) and the electron beam is pointed toward the other brass plate (the face plate). The electrical connections for the electron gun are made with insulating feed-throughs on the back plate. The face plate supports 16 targets. Each of these is mounted on a nickel wire which goes through a covar-glass feedthrough and out of the vacuum system. Hence, each target is insulated from the brass end plate and from the other targets. The array of targets is covered by a suppressor grid which is mounted on the brass face plate and is at the same voltage as the face plate.

The suppressor grid is needed on the CRT to suppress secondary emission. When the electron beam hits a target, many electrons are dislodged from the target by the energy in the beam. If there is no suppressor grid, the dislodged electrons drift away and are collected by the anode on the wall of the tube. The result is a loss of electrons and the current from the target is smaller than the electron beam current. When the suppressor grid is placed near the targets, the dislodged or secondary emission electrons are returned to the target by the field between the suppressor grid and the target. The current that can be drawn from the target is then the same as the beam current.

It is possible to vary the beam current by varying voltage on the first grid of the electron gun. The current drawn from any target can

be regulated by varying the grid voltage.

The targets on the face plate are located in two horizontal rows of eight targets each. The electron beam can be aimed to hit any target by putting the proper voltages on the deflection plates. The beam is focused to a small point and hits only one target at a given time.

The net result of the CRT with the 16 targets is a device which is both a switch and an amplifier. The electron gun and one target constitute a tetrode tube. By connecting a load resistor to the target (which is the tetrode anode), an amplifier can be made. Varying the first grid voltage varies the beam current and the voltage drop across the load resistor. The deflection plates allow the beam to be switched from one target to another. Switching the beam is equivalent to turning one tetrode off and turning another one on.

Although the CRT is capable of being operated as a linear amplifier, it is not used in that manner for the nonlinear form of feedback which is of interest here. The sensing circuits for the interface position produce only binary signals and there is no analog information available for modulating the CRT beam current. The beam current is adjusted to its maximum value and this intense beam is shifted to the desired target.

During operation, the voltage changes on the 100 Megohm resistors are found to be limited to 1500 volts. This limit is caused by secondary emission of electrons from the targets. The no-current voltage on the target is 3000 volts and the voltage of the suppressor grid 1500 volts. If the beam current were large enough, the voltage drop on the 100 Megohm resistor would reduce the target to 1500 volts. Once the

target reached the potential of the suppressor grid, the electrons generated by secondary emission would be able to leave the target. Any attempt to further increase the current to the target results only in more electrons leaving the target by secondary emission.

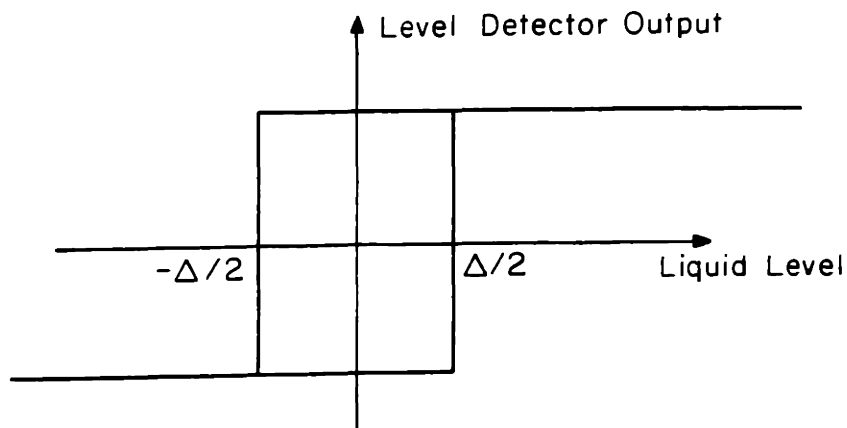
An unexpected effect is found to occur when the beam current is removed from a target. The voltage across the liquid interface should decay with a time constant of about 30 milliseconds. This time constant is due to the capacitance of the driving electrode in the tank and the 100 Megohm load resistor. The actual decay time for the voltage is found to be less than a millisecond. If the CRT beam is turned off, and the driving electrode is put at 1500 volts by an external battery, the time constant is about 30 milliseconds. A possible explanation for this dependence of the time constant on the beam current is the presence of gas in the vacuum chamber. The electron beam ionizes the gas, and the ions collect on the target after the beam is removed from it. The ions place a positive charge on the target and discharge the capacitance of the tank. When the electron beam is off, the ions are not present, and the tank capacitance discharges through the 100 Megohm resistor.

The Spatial Sampling System

The theory developed in Chapter VI assumes the magnitude of the deflection can be measured at regularly spaced intervals in space. To perform this measurement, some type of light detectors must be placed along the equilibrium surface of the liquid in the tank. As the surface moves up and down, the signals from the light detectors change, depending on the portion of the detector masked by the liquid. The output of the detectors might be an analog signal proportional to the position of the surface. This technique is not used. Rather, a simple

binary sensing system is used to measure the position of the oil-air interface. Inexpensive photodiodes, about 2 mm in diameter, are positioned along the side of the tank. These detectors are located at the air-oil interface and one is positioned at the center of each driving electrode. The diodes are made for digital applications; their sensitivity varies greatly and their output is not a linear function of the input light. The signal from each diode is fed to a Schmidt trigger circuit which acts as a level detector and produces a binary signal which indicates whether or not the diode is exposed to light. The signal obtained from the Schmidt triggers is thus a bang-bang type of signal.

A characteristic of Schmidt triggers and level detectors is that they exhibit hysteresis. The output of one trigger as a function of the liquid is shown in Fig. 7.3.



The output of the level detector exhibits hysteresis

Figure 7.3

Due to the nature of the triggers and the variation in sensitivity of

the light diodes, the width of the hysteresis is approximately 2 mm of interfacial deflection. This means that the interface can move 2 mm. about its equilibrium position and the signal from the detectors will show no change.

The hysteresis of the sensing circuits is a large factor in limiting the capabilities of the entire control system. Due to the uncertainty about the true location of the interface, it could move approximately one millimeter before a control signal is initiated to restore it to equilibrium. The distance the interface moves before the change is detected is an important parameter which establishes the minimum gain needed by the circuit. If very small excursions from equilibrium can be detected, only a small force is required to move the surface back to equilibrium. If the deflection is large before it is detected, a large force is required to restore the surface to equilibrium. The hysteresis of the Schmidt triggers used in the experiment is so large that, for some conditions, the available gain is not large enough to move the surface back to equilibrium.

The Synchronizing Network

A device is constructed from binary integrated circuits for temporarily sampling the diode detector outputs and deflecting the electron gun. Only a general description of the operation of the synchronizing network is presented here; the actual logic design of the network is not of general interest.

The general mode of operation of the synchronizing network is as follows. The photodiodes are checked in a sequential manner, from left to right across the tank. When the network finds a diode that is

exposed to light, it stops checking and waits for a clock pulse. When the clock pulse occurs, the beam is switched to the electrode at the position of the uncovered diode. The electric field puts a force on the surface which restores the surface to a position in front of the diode.

While the beam is maintaining a voltage on the electrode, the synchronizing network resumes its search for an uncovered diode. When the next clock pulse occurs, the beam goes to the next electrode, where the adjacent fluid needs to be pulled back to a position in front of the diode. Since the electric field can exert a force on the liquid surface only in the direction from the liquid into the air, the electrodes (which correspond to detector diodes covered by the liquid) receive no charge from the electron beam.

The synchronizing network constructed in this manner better utilizes the available current from the electron beam. It is more straightforward to step the beam sequentially across the targets. If a diode indicated the electrode needed charge, the beam would be turned on; if the diode was obscured from the light by the liquid, the beam would be turned off. It seemed that the system could be improved by not turning off the beam. If an electrode needed no charge, the beam would be immediately switched to charge an electrode that did need the charge.

7.3 Operation of the Apparatus

Experimental Results

In the first experiment for stabilizing the liquid, only a short liquid interface is used. The teflon spacer is made wide enough to fill most of the volume between the two glass plates. The area left in the

spacer for liquid is as wide as four of the strip electrodes. The surface of the liquid is thus .8 inches wide. Four points on the surface are sampled and four of the strip electrodes used to control the deflections.

For this first experiment, the control system can stabilize the surface until the tank is rotated 150° (60° past horizontal) from its initial position. For rotations greater than this angle, the surface is unstable. The shape of the unstable surface is similar to that shown in Fig. 7.4. The liquid under one electrode strip falls while the surface under the other three strips moves upward.

With the liquid cavity as wide as eight electrode strips, the surface is 1.6 inches long and sampled in eight places with eight electrodes used to control the surface. For this second experiment, the control system stabilizes the surface for tank rotations less than 120° (30° past horizontal). For greater rotations, the surface is unstable. Similar to the case of four feedback stations, the shape of the surface as it becomes unstable is the same as that shown in Fig. 7.4. The liquid under one electrode strip falls and the surface under the other seven move upward.

Explanation of Results

The limited performance of the control system can be attributed to two components of the system. The hysteresis of the interface detectors and the limited voltage swing available on the output of the CRT.

The switching circuit did not apply a restoring force to the electrodes on a regular basis. If an electrode did not need to be charged,

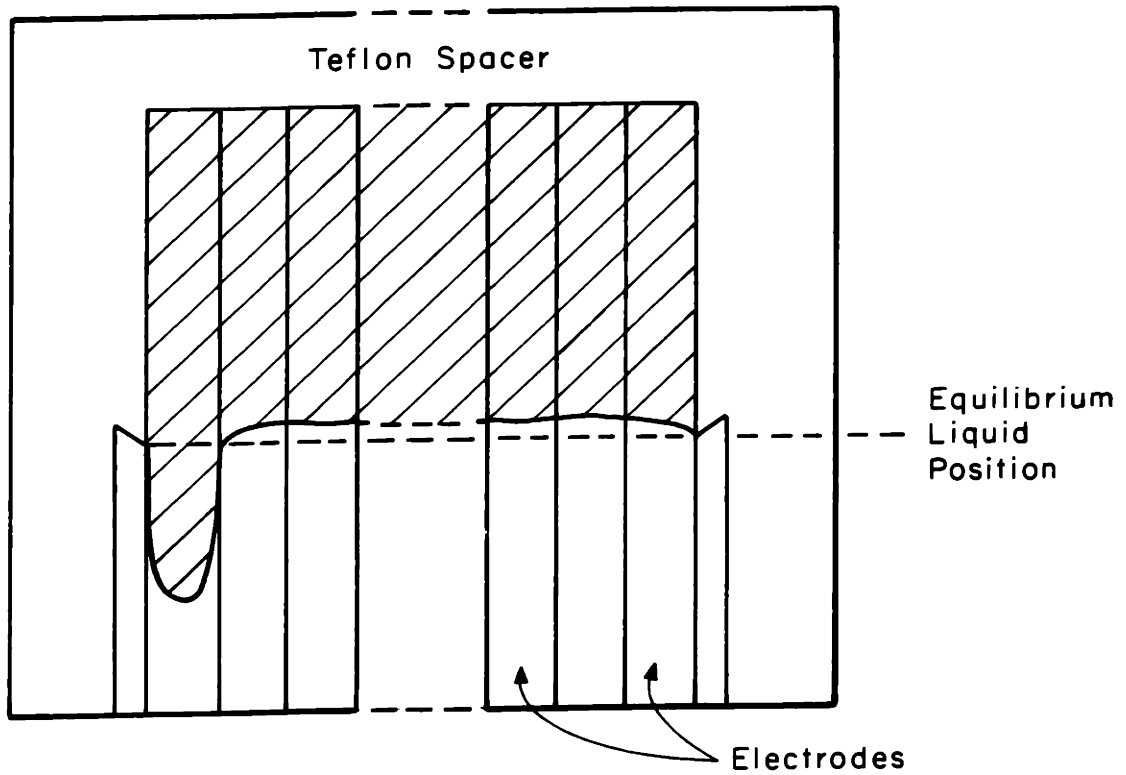


Figure 7.4 The liquid surface goes unstable with the liquid falling under one electrode and rising under the remaining electrodes.

the electron beam skipped it and went to the next electrode which needed the charge; if only a few other electrodes needed charge, the beam could soon return to the initial electrode. If many other electrodes needed charge, it would be a longer time before the beam could return. The result is that the time average force exerted by an electrode depends on how many other electrodes are being charged.

From Fig. 7.4, it can be seen that the mode which goes unstable is the one which makes the least gain available to the feedback electrodes. The liquid surface moves so that all the electrodes but one are charged by the electron beam. The liquid interface defeats the logic in the switching network and forces the beam to move sequentially from one electrode to the next. Only one electrode, the leftmost one in Fig. 7.4, does not receive charge from the beam.

In both experiments, the circuitry is fixed so that during every cycle the beam hits one of the 16 targets which is unused. This unused target is hit so that whenever the fluid interface is flat, and no electrode needs charge, the beam goes to the unused target. When the unused target is considered, the beam is shared by four electrodes as the four-station experiment goes unstable. As the eight-station experiment goes unstable, eight electrodes are sharing the electron beam. The angle of rotation where the instabilities occur can be predicted approximately from the hysteresis of the detector and the maximum voltage charge available on the targets of the cathode ray tube, using the following facts.

While the tank is not rotated (liquid on the bottom), one of the electrode strips is charged to 1500 volts with respect to the ground

plane electrode. The surface of the liquid in the region between the electrodes is raised vertically about eight millimeters. This is the maximum deflection that the CRT can cause if its beam is pointed at the corresponding target continuously. If the electron beam is being time-shared among four or eight targets, the maximum deflection of the surface that can be induced is one fourth, or one eighth, the maximum deflection when one electrode is charged.

For the feedback system to be effective, the deflection of the surface which the feedback can make must be as large as the hysteresis band of the detector. Otherwise, by the time the detector has noticed a perturbation from equilibrium, the perturbation can be too large for the feedback force to check its growth.

When there are feedback stations, the maximum vertical deflection from the control system is one millimeter. If the surface is rotated 60° from horizontal, the deflection of the surface is 2 mm for a one mm vertical deflection. The 2 mm deflection is equal to the hysteresis of the detector and thus the surface cannot be stabilized for rotations which make the surface have less than a 60° angle with horizontal. This rough number agrees with the observed value.

The same argument can be used for the control system when only four electrodes are used. The feedback can make a 2 mm vertical deflection and thus the surface can be stable with a tank rotation of 180° . The tank is at about 150° when the instability occurs. The 30° error makes only a 13% change in the gravity component perpendicular to the surface. This discrepancy is not too large, considering the rough calculations used.

7.4 Summary

For the experimental portion of the thesis, a continuum feedback control system was constructed which is capable of levitating a liquid by stabilizing the Rayleigh-Taylor instability. Although the control system is not capable of stabilizing a large continuum surface, the experimental results indicate a large-scale system using a time-multiplexing can be built.

The experiment illustrates some problems which are encountered in nonlinear continuum feedback control systems. The dependence of the time average force on the shape of the surface deflection and the hysteresis of the detectors are two nonlinear phenomena that influenced the operation of the control system.

CHAPTER VIII

SUMMARY AND SUGGESTIONS FOR FURTHER RESEARCH

8.1 Summary

In Chapter 2, the Z transform, which has been used to describe discrete time, lumped-parameter systems, is applied to discrete time, continuum systems. With Z transforms, a time-sampled continuum is described by a closed-form transfer function in terms of the wavenumber, K, and the discrete temporal frequency, Z. When discrete time, spatially continuous feedback is applied to the continuum, a closed-loop transfer function is generated by use of conventional servo theory. A dispersion equation in terms of Z and K is obtained in closed form from the poles of the closed-loop transfer function and the stability of the closed-loop system is determined from this dispersion equation.

The case of the string with discrete temporal feedback is analyzed in detail. It is found that increasing the feedback gain can stabilize the system, but that too much gain drives the string overstable. The maximum gain that can be used before overstability results depends on the damping applied to the string. When there is no damping, any non-zero gain drives the string overstable. This overstability occurs because there is a wavenumber which corresponds to oscillations at twice the sampling frequency. The control system pumps this mode, and the system becomes overstable.

In Chapter 3, the Z transform is adapted to describe spatially discrete systems. With this transform, a spatially sampled continuum is described by a closed-form transfer function in terms of the discrete spatial wavenumber D, and the frequency S.

Spatially discrete feedback is applied to the system and a closed-loop transfer function is generated. The dispersion equation of the system in terms of S and D is found from the closed-loop transfer function and the stability of the spatially discrete system is determined from this equation.

The stability of the infinite string with spatially discrete feedback is studied in detail. Similar to temporally discrete feedback, the spatially discrete feedback can drive the string overstable if high values of gain are used. The addition of damping reduces the tendency for overstability.

The Z transform technique is compared with wave train analysis used by Melcher. The dispersion equation obtained with the Z transforms is a closed-form expression in terms of S (or ω) and D , while the dispersion equation obtained from the wave train analysis is an infinite series in terms of S and K . To do calculations with Melcher's dispersion equation, the series must be truncated, and there is the possibility of truncation error. The dispersion equation obtained from the Z transform method is in closed form, and there is no possibility of truncation error.

In Chapter 4, three methods for describing a spatially sampled continuum system with boundaries are compared. These three methods are: the matrix approach used by Gould, the theory of normal modes used by Melcher, and the Z transform.

The matrix approach considers the measured, or "sampled", deflections of the system as the outputs and signals to the drivers as the inputs. This view of a continuum system results in a model with a finite number of coupled inputs and outputs. By the proper transformation, the normal coordinates of this system can be found. With these, the system can be made into a finite number of independent, single-input, single-output systems.

The Z transform method also considers the sampled deflection as the output. By using Fourier integral techniques, the discrete normal modes of the system are found. These modes are not coupled by the feedback. The total system can then be modeled by a finite sum of uncoupled feedback loops, one for every discrete normal mode. These discrete normal modes are the same as the normal coordinates found by Gould's method.

Melcher has modeled the bounded system by the normal modes of the system without feedback. This analysis considers the continuous deflection of the system as the output; by this approach, the output has an infinite number of degrees of freedom, and therefore an infinite number of modes are required to describe the system. By the proper mathematical manipulations, the information about the deflection between the sampling points can be dropped from Melcher's analysis, which then gives the same closed loop normal modes that can be obtained from the Z transform method, or from Gould's matrix method.

The easiest method of determining if a spatially discrete system is unstable is to use Gould's method or the Z transform. Both methods provide the same set of independent feedback loops which represent the total system. By checking the stability of each of these loops, the total system stability can be found.

Melcher's normal-mode approach is more complicated than the other two, because it provides information about the entire deflection of the string. This method is useful when the deflection at every point of the string must be determined. With any spatially sampled system, there is a chance that the instability is not detected by the control system. With Melcher's normal-mode method and with the Z transform method, any possible unobservable disturbances are easily identified. These unobserved modes can be

checked, and the stability of the entire system can be determined.

If Green's functions are used to derive a matrix description of the system, it is not apparent how the unobserved disturbances can be detected. Thus, for systems which may contain unobservable instabilities, the Z transform and modal methods are probably the best methods to use.

In Chapter 5, criteria for determining the existence and type of instabilities on a spatially discrete system are developed. These criteria make it possible to determine if the system is stable, or if it exhibits an absolute instability, a convective instability, or a convective-absolute instability.

Bers and Briggs have previously derived stability criteria which are used to investigate the stability of spatially continuous systems. Their criteria are applied to the ω - k dispersion equation for the system. The criteria presented here are derived by modifying the Bers-Briggs criteria so they can be applied to spatially discrete systems described by an S-D dispersion equation. For an example, the criteria are applied to the string driven by a spatially discrete feedback system. It is shown that, with the proper values of gain, damping, and convection, the string can exhibit any of the three possible types of instability.

In Chapter 6, the Z transform techniques that are developed in Chapters 2 and 3 are used to construct a transfer function for a spatially and temporally discrete system. This transfer function is initially expressed as a double series in terms of S and K. By using Z transforms, one of the series can be put into closed form, and the transfer function can be written as an expression in S and D, or Z and K.

A closed-loop transfer function can be generated when spatially and temporally discrete feedback is applied to the continuum. From the poles of the closed loop transfer function, a dispersion equation can be derived which can be an expression that is a double series in S and K , a closed form in D , and a series in S , or a closed form in Z and a series in K . The stability of the closed-loop system can be determined from this dispersion equation.

The stability of the string with spatially and temporally discrete feedback was studied in detail. The D - S form of the dispersion equation was found to be the easiest form to use for numerical calculations. To obtain accurate results for a system with a scanning length of J , it was necessary to use $2J + 1$ terms in the series of the open-loop transfer function. The dispersion equation that resulted from the $2J + 1$ terms was a polynomial in S of order $5J + 1$.

The numerical calculations produced effects that had been seen in Chapters 2 and 3 when either spatial or temporal discreteness was studied. The stable region had a right-hand boundary that was caused by the failure of the spatial sampling to detect certain modes. With no damping, the system was overstable for any finite gain, because the temporal discreteness caused certain modes to be pumped by the feedback. By adding damping to the system, the gain necessary for overstability was increased.

Chapter 7 describes the experimental portion of the thesis, where a continuum feedback control system is constructed which is capable of levitating a liquid by stabilizing the Rayleigh-Taylor instability. Although the control system is not capable of stabilizing a large

continuum surface, the experimental results indicate a large-scale system using time multiplexing can be built.

The experiment illustrates some problems which are encountered in nonlinear continuum feedback control systems. The dependence of the time average force on the shape of the surface deflection and the hysteresis of the detectors are two nonlinear phenomena that influenced the operation of the control system.

8.2 Suggestions for Further Research

The work in this thesis has been limited to a study of the string model, a quasi-one-dimensional system. Although the analysis has wide applicability, there are many situations in which the techniques presented here need more development. For instance, the control of a liquid surface would require a two-dimensional array of feedback electrodes. The Z transforms presented in this thesis are for discreteness in only one spatial dimension. In some instances, the spacing between the feedback electrodes and the continuum may not be small compared to the width of the electrode. The long-wave limit used in this thesis is not appropriate for these situations. In some plasma experiments, it is convenient to measure the average deflection adjacent to an electrode; all of the cases studied here have measured the deflection at one point in the center of the electrode.

An outline for extending the techniques in this thesis to deal with these situations is presented in this section and suggestions are made for improving the experimental portion of the thesis.

Removing the Long-Wave Limit

In this thesis, the force applied to the string is derived by using the long-wave limit. With this limit, it is assumed that the deflections on the string are small compared to the wavelength of the deflection. When this assumption is used, the electric field is assumed to be uniform as the observer moves between the string and the electrode. The electric field is then given by

$$E = \frac{V_o + v_d}{d - \xi} \quad (8.1)$$

which is linearized to give

$$E = \frac{V_o}{d} + \frac{V_o}{d^2} \xi + \frac{v_d}{d} \quad (8.2)$$

By considering the E field from the other electrode and using the Maxwell stress tensor, the stress on the string is found to be

$$\tau = \frac{2\epsilon_o V_o^2}{d^3} \xi + \frac{2\epsilon_o V_o v_d}{d^2} \quad (8.3)$$

A more thorough analysis includes the two-dimensional aspects of the field. Both the field variations along the string and between the string and the electrodes are considered. The method for finding the two-dimensional field is given by Melcher (MIT Press, Chapter 3), and the resulting perpendicular, linearized field is

$$E = \frac{V_o}{d} + \xi \frac{V_o}{d} k \coth kd + \frac{k v_d}{\sinh kd} \quad (8.4)$$

By using the Maxwell stress tensor, the stress of electrical origin on the string can be calculated from Eq. (8.4). With this value of stress, the equation of motion for transverse deflections on the string is

$$\begin{aligned} R \frac{D^2 \xi}{Dt^2} = & \gamma \frac{\partial^2 \xi}{\partial x^2} - \alpha' \frac{D\xi}{Dt} - \beta' \frac{\partial \xi}{\partial t} + \frac{2\epsilon_o V_o^2 k \cosh kd}{d^2 \sinh kd} \\ & + \frac{2\epsilon_o V_o}{d} \frac{k v_d}{\sinh kd} \quad (8.5) \end{aligned}$$

This equation is more inclusive than Eq. (1.4), the equation of motion used earlier in this thesis. It shows that for short wavelengths, the coupling of the feedback voltage decreases, and the unstabilizing effect of the bias voltage is increased.

By taking the Fourier-LaPlace transform of Eq. (8.5) and using the normalized variables given in Eqs. (5.34a) to (5.34g), the transfer function

relating the deflection to the driving voltage can be found to be

$$G(K, S) = \left[\frac{e^{jK/2} - e^{-jK/2}}{jK} \right] \cdot \left[\frac{K \frac{d}{L}}{\sinh(K \frac{d}{L})} \right] \cdot \left[\frac{1}{S^2 + K^2(1-U^2) + K(2US_j + \nu U_j) + \delta S + \nu S - \frac{NKd \coth[K(d/L)]}{L}} \right] \quad (8.6)$$

The transfer function given by Eq. (8.6) is separated into three terms. The first and third terms have been identified in Chapter 3 and are the transfer functions of the driving electrode and the string. The second term is the transfer function of the space between the driving electrode and the string.

With this continuous transfer function, the spatially discrete transfer function can be generated. The problem that occurs is that the poles of the transfer function in K cannot be found analytically. The transcendental nature of the transfer function makes it necessary to find the roots of K numerically. Once these roots are found, Eq. (3.41) is used to obtain the discrete transfer function. The discrete transfer function thus obtained has a denominator which is a second-order polynomial in D . The coefficients of the polynomial are tabulated numerical values which must be calculated for each value of δ , ν , N , S and d/L .

When feedback is applied to the spatially discrete system, the modified Bers-Briggs criteria must be used to determine if the system is stable. The values of the coefficients of D in the open-loop transfer function must be found for values of S in the right-half S plane. Once these coefficients are determined, the trajectories of the poles in D of the

closed-loop system can be plotted as the real part of S is decreased. From these trajectories, the stability of the system can be determined.

Average Deflection Feedback

In this thesis, the feedback signal is generated by sensing the deflection of the string at the center of the feedback electrode. This type of sensing is used because of its mathematical simplicity. In more practical situations, it may be preferable to sense the spatially averaged deflection of the continuum over the electrode, and not the deflection at the center of the electrode. In an experiment performed by Melcher and Warren [November 1966] and in numerous plasma experiments, the capacitance between the continuum and the feedback electrode is measured. From the capacitance, the spatial average deflection of the continuum adjacent to the electrode is obtained. The measurement of the average deflection is then used to generate the feedback signal.

The examples presented in this thesis can be modified to use a feedback signal proportional to the average deflection in the following manner. The variable $\bar{\xi}(x,t)$ is defined as

$$\bar{\xi}(x,t) = \frac{1}{L} \int_{-L/2}^{L/2} \xi(x+y,t) dy \quad . \quad (8.7)$$

This quantity is the average deflection for a length L centered at the point x . The transform of $\bar{\xi}(x,t)$ can be generated by multiplying the transform of the deflection by the proper spatial filter. The filter can be deduced from Eq. (8.7), and the transform of $\bar{\xi}(x,t)$ is

$$\bar{\Xi}(k,s) = \left[\frac{e^{jkL/2} - e^{-jkL/2}}{jkL} \right] \Xi(k,s) \quad (8.8)$$

When $\bar{\xi}$ is sampled by the spatial impulse train used in Chapter 3, the result is an impulse train whose amplitudes are the average deflections above each driving electrode.

With the filter given in Eq. (8.8), the analysis in this thesis can be modified to use the sampled average deflection for feedback. For example, in the case of the stationary string, the continuous transfer function which relates the average deflection to the excitation is found by adding the filter in Eq. (8.8) to the transfer function given in (3.42). The result is

$$G(K,S) = \left[\frac{e^{jK/2} - e^{-jK/2}}{jK} \right] \left[\frac{1}{S^2 + \delta S + K^2 - N} \right] \left[\frac{e^{jK/2} - e^{-jK/2}}{jK} \right]$$

electrode as driver
string
electrode as sensor

By using the techniques given in Chapter 3, the spatially discrete transfer function, relating the sampled averaged deflection to the sampled input, can be generated from Eq. (8.9). The desired closed-loop dispersion equation is then obtained by placing this transfer function into a servo-loop similar to Fig. 3.11.

If the analysis does not use the long-wave limit, then the spatial filter in Eq. (8.8) is not sufficient. Another term must be added to include the effect of the space between the sensing electrode and the string. By multiplying the filter of Eq. (8.3) by the second term on the right of Eq. (8.6), the correction for the string-electrode spacing is made.

Extension to Two-Dimensional Surfaces

Melcher [October, 1966] and Melcher and Warren [November, 1966] have studied the control of a two-dimensional liquid surface. To drive this surface, an array of rectangular electrodes is used. The driving force is thus discrete in both directions in the plane of the surface. The surface deflection is sensed at the center of each driving electrode. The measured deflection is therefore a two-dimensional impulse array.

In his analysis, Melcher uses a wave-train approach. Because the system is discrete in two dimensions, x and y , the dispersion equation which he derives is a series in both k_x and k_y . The Z transforms, shown in Chapter 3, can be used to achieve a closed-form transfer function for a system which is discrete in one dimension; in Chapter 6 a spatially and temporally discrete system is studied and it is found that the Z transform can produce a closed-form transfer function for only S or only K ; the other variable, K or S , remains in series form.

When Z transforms are applied to a system which is sampled in two dimensions, a problem occurs which is similar to the problem with space and time sampling. Only one of the series, in k_x or k_y , can be put into closed form; the other series cannot. The Z transform, as presented here, can be applied to the two-dimensional sampling. It is useful because it makes the dispersion equation a series in one variable instead of two. The Z transform would be more useful if both series could be put into closed form. A significant project would be to develop a modification of the Z transform which gives transfer functions in closed form for systems that are discrete in two dimensions.

Suggestions for Experimental Research

The experimental portion of this thesis cannot be compared directly

to the theoretical part, because the level detectors used in the experiment cause the feedback signal to be nonlinear; the theoretical work considers only linear feedback signals. An experiment that can be compared to the linear theory can be made by constructing a linear, spatially-discrete, level detector. There are many ways of building the linear level detectors, two of which are outlined here.

The first method is to use a television camera to detect the surface of the liquid in the tank, which is a dark green color and can be detected optically. The television camera is fixed to scan the image of the tank along vertical lines located in the center of each electrode strip. As the camera scan moves from the liquid across the liquid-air interface, the video output will change. Plotted versus time, the video output for one scan will resemble the plot in Fig. 8.1

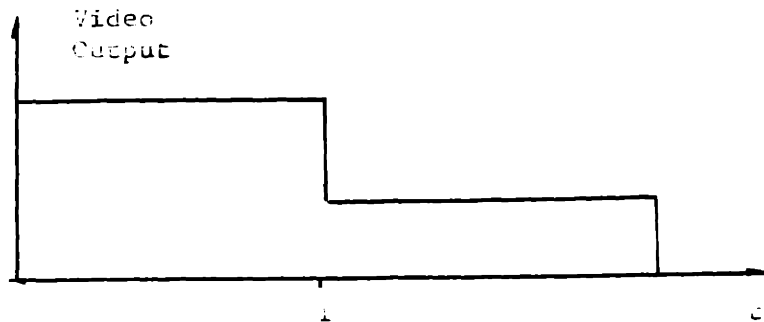


Fig. 8.1 The discontinuity in the video signal determines the location of the liquid-air interface.

The signal is low as the camera scans down the side of the tank and sees the dark liquid. At the liquid-air interface, the signal jumps to a high level because of the light coming through the transparent tank. By

measuring the time from the beginning of the scan to the jump in the signal, the distance of the interface from the origin of the scan can be computed. The distance measurement is used to modulate the CRT beam and a feedback voltage proportional to the deflection of the interface is applied to the proper feedback electrode. To maintain a constant gain as a function of the angle of tank rotation, it is necessary to attach the camera to the tank so that the tank and the camera are rotated as a unit.

Another method of linearly measuring the position of the interface is to use an oscilloscope and a light-sensing diode. The liquid tank is mounted flat on the face of the oscilloscope. A signal is applied to the oscilloscope, causing the beam to trace out vertical lines down the center of each feedback electrode on the tank. The light-sensing diode is mounted so that it picks up light from the oscilloscope beam, which is transmitted through the tank. When the liquid is between the oscilloscope beam and the diode, the latter gives a low signal. When the beam is scanned vertically, a signal similar to Fig. 8.1 is obtained from the light diode.

The time from the start of the scan to the jump in the diode signal is proportional to the distance of the liquid-air interface from the point where the scan started. The time measurement is used to modulate the beam of the CRT and a feedback voltage, proportional to the deflection of the interface, is applied to the proper electrode.

REFERENCES

- Athans, M., "Control of Distributed Parameter Systems", A.S.M.E. Publication, Control, August, 1969.
- Benjamin, T. B., "Effects of a Flexible Boundary on Hydrodynamic Stability", J. of Fluid Mechanics, 9, Dec., 1960, pp. 513-532.
- Bers, A., and Briggs, R. J., "Criteria for Determining Absolute Instabilities and Distinguishing between Amplifying and Evanescent Waves", QPR No. 71, M.I.T., Cambridge, Mass., October, 1963, pp. 122-137.
- Birdsall, C. K., Brewer, G. R., and Haeff, V. V., "The Resistive-Wall Amplifier", Proceedings of the I.R.E., 41, pp. 865-875.
- Briggs, R. J., Electron-Stream Interaction with Plasmas, The M.I.T. Press, Cambridge, Mass., 1964.
- Butkovsky, A. G., Egorov, A. I., and Lurie, K. A., "Optimal Control of Distributed Systems" (A Survey of Soviet Publications), S.I.A.M. Journal on Control, 6, #3, August, 1968, pp. 437-477.
- Carlye, D. C., "Passive Feedback Stabilization", Feedback and Dynamic Control of Plasmas, Proc. of the A.I.P. Conference, Princeton, N. J., June, 1970, published by A.I.P., New York, 1970, #1, pp. 138-141.
- Cassedy, E. S., and Oliner, A. A., "Dispersion Relations in Time-Space Periodic Media: Part I. Stable Interactions", Proc. of the I.E.E.E., 51, October 1963, pp. 1342-1359.
- Cassedy, E. S., "Dispersion Relations in Time-Space Periodic Media: Part II. Unstable Media", Proc. of the I.E.E.E., 55, #7, July, 1967, pp. 1154-1168.
- Cassedy, E. S., and Evans, C. R., "A Note on Optical Parametric Backward-Wave Instabilities", Proc. of the I.E.E.E., 58, #1, January 1970, pp. 164-165.

References (continued)

- Chandrasekhar, S., Hydrodynamic and Hydromagnetic Stability, Oxford Press, London, 1961.
- Crowley, J. M., "The Stabilization of a Spatially Growing Wave by Feedback", Ph.D. Thesis, Department of Electrical Engineering, M.I.T., 1965.
- Crowley, J. M., "Stabilization of a Spatially Growing Wave by Feedback", Phys. of Fluids, 10, #6, June, 1967, pp. 1170-1177.
- Crowley, J. M., "Feedback Control of Plasma Flutes with Finite Enforcer Electrodes", Phys. of Fluids, 14, #6, June, 1971.
- DeRusso, P. M., Roy, R. J., and Close, C. M., State Variables for Engineers, John Wiley & Sons, Inc., New York, 1965.
- Desalu, A. A., "Optimal Control of a Regenerative Chemical Process", S. M. Thesis, Dept. of Electrical Engineering, M.I.T., 1968, ESLTM-358.
- Dressler, J. L., "Videotype Sampling in the Feedback Stabilization of Electromechanical Equilibria", Feedback and Dynamic Control of Plasmas, Proc. of the American Institute of Physics Conference, Princeton, N.J., June 1970, pub. by A.I.P., New York, 1970, No. 1, pp. 60-67.
- Gould, L. A., Chemical Process Control: Theory and Applications, Addison-Wesley Publishing Co., Inc., Reading, Mass., 1969.
- Heller, W. G., "On the Feedback Stabilization of a Distributed Parametric System by Scanning", Ph.D. Dissertation, Department of Electrical Engineering, Univ. of Pennsylvania, 1971.
- Hildebrand, F. B., Methods of Applied Mathematics, Prentice-Hall Inc., Englewood Cliffs, N. J., 1952.
- Jefferis, R. P., "Feedback Control of the Buckling Instability in an Axially Compressed Thin Elastic Beam", Ph.D. Thesis, in Electrical Engineering, Dept. of Arts and Sciences, University of Pennsylvania, 1968.

References (continued)

- Jury, E. J., Theory and Application of the Z Transform Method, John Wiley & Sons., Inc., New York, 1964.
- Komkov, V., "The Optimal Control of a Transverse Vibration of a Beam", S.I.A.M. Journal on Control, 6, #3, August 1968, pp. 401-421.
- Kr amer, M. O., "Boundary Layer Stabilization by Distributed Damping", Journal of the Amer. Soc. of Nav. Engrs., 72, February 1960, pp. 25-33.
- Laslett, L. J., and Neil, V. K., and Sessler, A. M., "Transverse Resistive Instabilities of Intense Coasting Beams in Particle Accelerators", Lawrence Rad. Lab., The Review of Scientific Instr, 36, #4, April 1965, pp. 436-448.
- Mason, S. J., and Zimmermann, H. I., Electronic Circuits, Signals and Systems, John Wiley & Sons., Inc., New York, 1960.
- Melcher, J. R., "An Experiment to Stabilize an Electromechanical Continuum", I.E.E.E. Trans. on Automatic Control, AC-10, #4, October, 1965, pp. 466-469.
- Melcher, J. R., "Control of a Continuum Electromechanical Instability", Proc. I.E.E.E., 53, #5, May 1965, pp. 460-473.
- Melcher, J. R., "Continuum Feedback Instabilities on an Infinite Fluid Interface", Phys. of Fluids, 9, #10, October, 1966, pp. 1973-1982.
- Melcher, J. R., and Warren, E. P., "Continuum Feedback Control of a Rayleigh-Taylor Type Instability", Phys. of Fluids, 9, # 11, November 1966, pp. 2085-2094.
- Melcher, J. R., Field-Coupled Surface Waves, M.I.T. Press, Cambridge, Mass., 1963.

References (continued)

- Millner, A. R., and Parker, R. R., "Nonlinear Stabilization of a Continuum", Feedback and Dynamic Control of Plasmas, Proc. of the American Inst. of Physics Conference, Princeton, N.J., June 1970, pub. by A.I.P., New York, 1970, #1, pp. 38-53.
- Morse, P. M., and Feshbach, H., Methods of Theoretical Physics, McGraw-Hill Book Co., New York, 1953.
- Murray, M. A., "The Modal Analysis and Synthesis of Linear Distributed Control Systems", Sc.D. Thesis, Dept. of Electrical Engineering, M.I.T., June 1965.
- Neil, V. K., and Sessler, A. M., "Longitudinal Resistive Instabilities of Intense Coasting Beams in Particle Accelerators", Lawrence Rad. Lab., Review of Scientific Instr., 36, #4, April 1965, pp. 429-436.
- Parker, R. R., and Thomassen, K. I., "Feedback Stabilization of a Drift Type Instability", Phys. Review Letters, 22, 1969, pp. 1171-1173.
- Robinson, A. C., "A Survey of Optimal Control of Distributed Parameter Systems", ARL 69-0177, Aerospace Research Labs., November 1969.
- Rose, D. J., and Clark, M., Plasmas and Controlled Fusion, M.I.T. Press, Cambridge, Mass., 1961.
- Schlaepfer, F. M., "Modal Control of an Ammonia Reactor", M.S. Thesis, Dept. of Electrical Engineering, M.I.T., December 1966, ESL-R-293.
- Schlaepfer, F. M., "Set Theoretic Estimation of Distributed Parameter Systems", Ph.D. Thesis, Dept. of Electrical Engineering, M.I.T., January 1970, ESL-R-413.
- Shortley, G., and Williams, D., Elements of Physics, Prentice-Hall Inc., Englewood Cliffs, N. J., 1953.
- Sturrock, P. A., "Kinematics of Growing Waves", Physical Review, 112, #5, December 1958, pp. 1488-1503.

References (continued)

- Sturrock, P. A., "In What Sense do Slow Waves Carry Negative Energy?", J. Applied Phys., 31, 1960, pp. 2052-2056.
- Thomas, R. H., "Temporally Sampled Distributed Parameter Feedback Systems", Center for Space Research, TR-67-2, 1967. Also: "Stability of a Distributed Parameter System Controlled by Spatially and Temporally Sampled Feedback", S. M. Thesis, Dept. of Electrical Engineering, M.I.T., September 1966.
- Thomassen, K. I., "Feedback Stabilization in Plasmas", Nuclear Fusion, 11, 1971, p. 175.
- Truxal, J. G., Automatic Feedback Control System Synthesis, McGraw-Hill Book Co., Inc., New York, 1955.
- Wang, P. K. C., "Optimal Control of a Class of Linear Symmetric Hyperbolic Systems and Applications to Plasma Confinement", School of Engineering and Applied Science, Univ. of California, Los Angeles, Ca., Report No. 69-15, March, 1969.
- Wang, P. K. C., "Control of a Distributed Parameter System with a Free Boundary", Univ. of Southern Calif. School of Engineering, Electronic Sciences Laboratory, USCEE Report 189, March, 1967.
- Wang, P. K. C., "Theory of Stability and Control of Distributed Parameter Systems" (a bibliography), Int. Journal of Control, 7, 1968, pp. 101-116.
- Wang, P. K. C., "Feedback Stabilization of Distributive Systems with Applications to Plasma Stabilization", presented at International Union of Theoretical and Applied Mechanics Symposium on Instability of Continuous Systems, Karlsruhe, Germany, Sept. 8-12, 1969.
- Wang, P. K. C., and Janos, W. A., "A Control-Theoretic Approach to the Plasma Confinement Problem", School of Engineering & Applied Science, Univ. of California, Los Angeles, Ca., Report 69-17, April, 1969,

References (continued)

- Wiberg, D. M., "Optimal Feedback Control of Spatial Xenon Oscillations in a Nuclear Reactor", Ph.D. Dissertation, California Institute of Technology, Pasadena, 1965.
- Woodson, H. H., and Melcher, J. R., Electromechanical Dynamics, John Wiley & Sons., Inc., New York, 1968.

BIOGRAPHY

John L. Dressler was born in Chillicothe, Ohio, on October 21, 1942. He attended public schools and graduated from Chillicothe High School in 1960. He received his S.B. degree in 1964, S.M. degree in 1966, and E.E. degree in 1967 from M.I.T. From 1964 to 1965, he was employed as a Research Engineer by Autometrics, a Division of the North American Rockwell Corporation. From 1966 to 1967, he was a teaching assistant in the Department of Electrical Engineering at M.I.T. From 1967 to 1969, he was supported by a fellowship from the Atomic Energy Commission. He is now employed as a Senior Research Engineer at the Mead Central Research Laboratory in Chillicothe, Ohio.